

**University of Alberta**

**Influence of Polymerization Conditions on Activities and Product Properties of  
Polymer Supported  $(n\text{-BuCp})_2\text{ZrCl}_2/\text{MAO}$  Catalysts**

by

**Tariq M. Mannan**



A thesis submitted to the Faculty of Graduate Studies and Research  
in partial fulfillment of the requirements for the degree of  
**Doctor of Philosophy in Chemical Engineering**

**Department of Chemical and Materials Engineering**

Edmonton, Alberta

Spring 2006



Library and  
Archives Canada

Bibliothèque et  
Archives Canada

Published Heritage  
Branch

Direction du  
Patrimoine de l'édition

395 Wellington Street  
Ottawa ON K1A 0N4  
Canada

395, rue Wellington  
Ottawa ON K1A 0N4  
Canada

*Your file* *Votre référence*

*ISBN: 0-494-14017-8*

*Our file* *Notre référence*

*ISBN: 0-494-14017-8*

#### NOTICE:

The author has granted a non-exclusive license allowing Library and Archives Canada to reproduce, publish, archive, preserve, conserve, communicate to the public by telecommunication or on the Internet, loan, distribute and sell theses worldwide, for commercial or non-commercial purposes, in microform, paper, electronic and/or any other formats.

The author retains copyright ownership and moral rights in this thesis. Neither the thesis nor substantial extracts from it may be printed or otherwise reproduced without the author's permission.

#### AVIS:

L'auteur a accordé une licence non exclusive permettant à la Bibliothèque et Archives Canada de reproduire, publier, archiver, sauvegarder, conserver, transmettre au public par télécommunication ou par l'Internet, prêter, distribuer et vendre des thèses partout dans le monde, à des fins commerciales ou autres, sur support microforme, papier, électronique et/ou autres formats.

L'auteur conserve la propriété du droit d'auteur et des droits moraux qui protègent cette thèse. Ni la thèse ni des extraits substantiels de celle-ci ne doivent être imprimés ou autrement reproduits sans son autorisation.

---

In compliance with the Canadian Privacy Act some supporting forms may have been removed from this thesis.

Conformément à la loi canadienne sur la protection de la vie privée, quelques formulaires secondaires ont été enlevés de cette thèse.

While these forms may be included in the document page count, their removal does not represent any loss of content from the thesis.

Bien que ces formulaires aient inclus dans la pagination, il n'y aura aucun contenu manquant.

  
**Canada**

In loving memory of my father,

Dr. Md. Abdul Mannan

## Abstract

A novel laboratory-scale gas-phase polymerization reactor system with improved temperature control was designed, constructed and used to study the kinetics of polymer-supported bis(*n*-butylcyclopentadienyl)zirconium dichloride and methyl aluminoxane (MAO) catalysts. The 2 L stainless steel reactor was cooled by flow of proportioned amounts of hot and cold oil coming from a single partitioned heating bath, through drilled bores in the reactor walls. Static mixers in the coolant channels ensured good heat transfer. Control of the bulk gas temperature in the reactor to  $\pm 0.2^\circ\text{C}$  during polymerization at rates up to  $0.04 \text{ mol-C}_2\text{H}_4 / \text{min}$  was achieved with this novel design. An online GC connected via a modified metering-valve with zero volume in the high pressure side was used to analyze the head-space gas composition. A mini-reactor with Pyrex windows built from a Swagelok Tee, interfaced with a video microscope was used to observe the growth of catalyst/polymer particles during polymerization.

Twenty two batches of supported metallocene catalysts, with aluminum and zirconium from 12.9 to 21.2 and 0.12 to 0.35 mass%, respectively and Al:Zr ratio of 168 to 482, were prepared by contacting MAO solution with the carrier, followed by the addition of the metallocene solution and then drying under vacuum to obtain free flowing solid catalysts. Both in-house and commercial organic polymeric porous supports of size range from 5 to 850  $\mu\text{m}$  were used.

The supported catalysts were active for both ethylene homopolymerization and ethylene/1-hexene copolymerization in temperature range 60 to  $100^\circ\text{C}$  and ethylene pressure range 0.34 to 2.07 MPa. Except for the 5  $\mu\text{m}$  sized catalysts, all catalysts had in

general much higher copolymerization activity [up to 37,000 kg-PE/(mol-Zr)·h] than homopolymerization activity [up to 21,000 kg-PE/(mol-Zr)·h]. However, the highest activity was shown by the 5  $\mu\text{m}$  sized supported catalysts that had both high homo- and co-polymerization activity [up to 189,000 and 78,000 kg-PE/(mol-Zr)·h respectively]. The catalyst activities depended on the polymerization temperature, concentrations of comonomer and scavengers, ethylene pressure, and size of support particles. In the larger-sized lower activity supported catalysts, the catalyst particles fragmented in layers during copolymerization and resulted in formation of concentric shells of polymer while during homopolymerization polymer grew outward from the unfragmented catalyst cores. The shapes of the support particles were replicated during polymerization.

The molar masses of the copolymers ( $M_w$  range 50 to 175 kg/mol) were significantly less than that of the homopolymers ( $M_w$  range 130 to 265 kg/mol). The short chain branching (SCB) increased with increase in initial concentration of 1-hexene. Both molar masses and SCB depended on polymerization time and radial position in the polymer particle.

## Acknowledgements

It was my privilege to have worked under the supervision Professor Sieghard E. Wanke and Professor David T. Lynch. I am forever indebted for their erudite guidance and support and their patient perseverance throughout the course of this project.

I would like to express my heartfelt thanks to the technical staff of the department: Bob Smith, Bob Scott, and James Mackinnon at the machine shop for the reactor fabrication, Naiyu Bu for molar mass measurements, Andrée Koenig for helping with the gas chromatograph, Christina Barker for scanning electron microscopy, Walter Boddez and Richard Cooper for setting up the instrumentation/data acquisition hardware, Jack Gibeau for his assistance on Opto22/LabView interfacing, Dr. Naihong Li for preparing the in-house polymeric supports, and last but not least Dr. Leu Ahdong for pore volume and surface area measurements. My work here has been very pleasant and memorable thanks to my friends and colleagues in the department, especially Hassan Hammawa and Dr. Long Wu who were always there for any discussion.

I would express my gratitude to BUET-CIDA Institutional Linkage Program for supporting me financially during the Ph.D. program and FGSR for awarding me other scholarships. I would also like to thank NOVA Chemicals for financially supporting the research project and for supplying the metallocene catalyst and 1-hexene.

And finally I would like to thank my family members for their constant encouragement, help, and understanding specially my wife, Rumana who had to endure the most during the past few years!

# Table of Contents

Abstract	
Acknowledgements	
Contents	
List of Tables	
List of Figures	
List of Abbreviations	
<b>1. Introduction</b>	<b>1</b>
1.1 History of Polyolefin Production	1
1.2 Classification of PE Resins	3
1.3 Polyolefin Synthesis Technologies	4
1.4 Challenges in Polyolefin Research	7
1.5 Objectives of the Current Research	8
<b>2. Literature Review</b>	<b>11</b>
2.1 Metallocene Catalyst	11
2.2 Aluminoxane Cocatalyst	13
2.3 Supported Metallocene Catalysts	17
2.4 Organic Polymeric Supports	20
2.5 Laboratory-Scale Gas-Phase Polymerization Reactor Systems	22
2.6 In-Situ and Ex-Situ Observation of Particle growth during Polymerization	24
2.7 Effects of Polymerization Conditions	26
2.7.1 Effects of Alkyl Aluminum	26

2.7.2 Effects of Polymerization Temperature	27
2.7.3 Effects of Ethylene Pressure	28
2.7.4 Effects of Comonomer	28
<b>3. Reactor Design and Experimental Details</b>	<b>30</b>
3.1 Gas Phase Polymerization Reactor System	30
3.1.1 Description of Novel Reactor System for Olefin Polymerization	31
3.1.2 The Gas-Phase Analysis System	41
3.2 Micro-Reactor for Observation of Polymer Growth	43
3.3 Catalyst Preparation	44
3.4 Polymerization Procedure	45
3.5 Characterization of Supports, Catalysts, and Products	48
3.5.1 Surface Area Determination	48
3.5.2 Scanning Electron Microscopy	48
3.5.3 Instrumental Neutron Activation Analysis	49
3.5.4 Molar Masses of Polymer Products	49
3.5.5 Temperature Rising Elution Fractionation	50
<b>4. Supports and Catalysts</b>	<b>52</b>
4.1 Supports used for Catalyst Preparation	53
4.2 Prepared Supported Catalysts	56
<b>5. Exploratory Experiments</b>	<b>65</b>
5.1 Test Runs and Gas Phase Temperature Control	65
5.2 Effect of Scavenger on Activity Profiles	74

5.3 Effect of Temperature on Activity Profiles	83
5.4 Effect of Ethylene Pressure on Activity Profiles	94
5.5 Effect of Nitrogen on Activity Profiles	100
5.6 Effect of Catalyst Amount on Activity Profiles	103
5.7 Summary of Observation from Exploratory Experiments	108
<b>6. Imaging of Growing Polymer Particles</b>	<b>110</b>
6.1 Micro-Reactor Operation Procedure	111
6.2 In Situ Video Imaging of Growing Particle	114
6.3 Ex Situ SEM Imaging of Growing Polymer Particles	117
6.3.1 Growth of Polymer Particles during Copolymerization	119
6.3.2 Growth of Polymer Particles during Homopolymerization	137
6.4 Summary of Observations from Imaging of Growing Particles	143
<b>7. Effect of Comonomer on Ethylene Polymerization</b>	<b>145</b>
7.1 Effect of 1-Hexene on Ethylene Polymerization	145
7.2 Control of Concentration of 1-Hexene during Polymerization	161
7.3 Effect of n-Heptane during Polymerization	168
7.4 Temperature Rising Elution Fractionation (TREF) Analysis	171
7.5 Summary of Effects of Comonomer 1-Hexene	185
<b>8. Effect of Catalyst Size on Polymerization Activity</b>	<b>187</b>
8.1 Activity Profiles of Catalysts Supported on 5 $\mu$ m Porous Particles	187
8.2 Effect of Catalyst Particle Size on Polymerization Activity	192
8.3 Summary of Effects of Catalyst Size on Polymerization Activity	200

<b>9. Conclusions and Recommendations for Future Work</b>	<b>202</b>
9.1 Summary and Conclusions	202
9.2 Recommendations for Future Work	207
<b>References</b>	<b>209</b>
<b>Appendix A</b>	<b>220</b>
<b>Appendix B</b>	<b>225</b>

## List of Tables

Table 1.1	Commercial classification of PE resins	3
Table 1.2	PE production utilizing catalytic low pressure technologies	6
Table 2.1	Organic polymer-supports for metallocene catalysts mentioned in the literature	21
Table 4.1	Description of supports used for making catalysts	54
Table 4.2	Catalyst batches and their composition	56
Table 4.3	Elemental analysis of probe positions showing normalized mass percentage	60
Table 5.1	Initial polymerization conditions of test runs	67
Table 5.2	Experiments to compare gas phase temperature control during polymerization	70
Table 5.3	Initial conditions of runs to determine effect of TIBA (tri-isobutyl aluminum) on polymerization using Catalyst TM01	74
Table 5.4	Experiments to determine effect of TEA (triethyl aluminum) on polymerization using Catalyst TM01 at 80°C	76
Table 5.5	Experiments to determine the effect of TIBA (tri-isobutyl aluminum) on homopolymerization using Catalyst TM02	79
Table 5.6	Polymerization runs using Catalyst TM11 to study effect of gas phase temperature on activity profiles	83
Table 5.7	Polymerization runs using Catalyst TM17 to study effect of gas phase temperature on activity profiles	88

Table 5.8	Polymerization runs using Catalyst TM10 to study effect of ethylene pressure on activity profiles	94
Table 5.9	Experiments using Catalyst TM10 to study effect of nitrogen pressure on activity profiles during ethylene polymerization at 80°C	100
Table 5.10	Experiments using Catalyst TM10 to study effect of amount of catalyst on activity profiles during ethylene polymerization at 80°C	103
Table 5.11	Experiments using Catalyst TM11 to study effect of amount of catalyst on activity profiles during ethylene polymerization	106
Table 6.1	Polymerization runs used for ex-situ SEM study of growing polymer particles	118
Table 7.1	Experiments to study effect of initial concentration of 1-hexene on polymerization using Catalyst TM08	146
Table 7.2	Experiments to study effect of initial concentration of 1-hexene on polymerization using Catalyst TM08 after coolant reservoir modification	148
Table 7.3	Experiments to study effect of initial concentration of 1-hexene on polymerization using Catalyst TM11 with circulation of coolant oil at 80°C to reactor	151
Table 7.4	Effect of initial concentration of 1-hexene on polymer product molar masses	154
Table 7.5	Experiments to study effect of initial concentration of 1-hexene and ethylene pressure on polymerization at 80°C using Catalyst TM17	157

Table 7.6	Experiments to determine change and control the concentration of 1-hexene during polymerization at 80°C using Catalyst TM13	162
Table 7.7	Experiments to study effect of controlling the concentration of 1-hexene during polymerization at 80°C using Catalyst TM17	164
Table 7.8	Experiments to study effect of addition of <i>n</i> -heptane during homopolymerization at 80oC using Catalyst TM15	168
Table 7.9	TM11 catalyzed polymerization runs having various initial concentration of 1-hexene used for TREF analyses	172
Table 7.10	Polymerization runs carried out using Catalyst TM12 at 80°C analyzed to determine effect of polymerization time on TREF profiles of product	174
Table 8.1	Polymerization conditions and product properties of runs using very high activity Catalyst TM14 supported on 5µm porous particles	188
Table 8.2	Polymerization conditions and product properties of runs to determine the effects of catalyst particle size on polymerization	194
Table 8.3	Polymerization conditions and product properties of runs to determine the effects of catalyst particle size and gas phase temperature on polymerization	196
Table A1	Detailed description of catalyst preparation conditions	221
Table A2	Composition of supported catalysts	223
Table A3	Carriers used for supporting catalysts	224
Table B1	Summary of polymerization run conditions	226

## List of Figures

Figure 2.1	Some classes of metallocene used for olefin polymerization	12
Figure 2.1	Proposed structures for MAO showing (1) linear chains, (2) cyclic rings, containing three coordinate Al centres in two-dimensional structures, and (3) three-dimensional cage-like structures containing four coordinate Al centers	14
Figure 3.1	Schematic of Reactor Body and Top Flange Construction	32
Figure 3.2	Schematic of Assembled Reactor: A) Radial Thermocouples not shown, B) Position of Radial Thermocouples	33
Figure 3.3	Schematic of Reactor System	35
Figure 3.4	Photographs of (A) the impeller system and (B) impellers in action inside Plexiglas replica of reactor	36
Figure 3.5	Data gathered during a typical polymerization run shown graphically giving (A) ethylene flowrate into reactor, (B) temperature at different locations in the reactor, (C) circulating coolant oil temperature at different locations, and (D) reactor gas pressure	40
Figure 3.6	Schematic of Micro-Reactor	43
Figure 4.1	SEM images of supports of different sizes used for catalyst preparation – (A) 5 $\mu\text{m}$ PS/DVB-1; (B) 75-90 $\mu\text{m}$ HS-R6; (C) 125-15 $\mu\text{m}$ HS-R5; (D) 180-250 $\mu\text{m}$ HS-R3; (E) 250-300 $\mu\text{m}$ HS-R2; and (F) 600-850 $\mu\text{m}$ HS-R1	55

Figure 4.2	SEM images of catalyst TM20; (A) low magnification showing the uniform distribution of particle sizes; (B) higher magnification showing the catalyst particles having mainly uniform morphologies similar to support (HS-R6); (C) individual catalyst particle having relatively smooth surface; (D) individual particle having flaky surface	57
Figure 4.3	(A) Cut TM19B particle for determining distribution of metal showing line-scanning position; (B) EDX linescan for aluminum; (C) EDX linescan for zirconium	59
Figure 4.4	Fragmented TM19A particle for EDX probe analysis showing probe positions	60
Figure 4.5	Plot of measured Al and Zr concentration versus estimated Al and Zr concentration in prepared catalysts	62
Figure 4.6	(A) Aluminum and (B) zirconium concentrations in catalysts, calculated from amounts of reagents used and measured using instrumental neutron activation analysis	63
Figure 5.1	Effect of controller tuning on reaction profiles. Polymerization data from test runs using Catalyst JM29 showing (A) rate of ethylene flow into reactor, (B) reactor gas pressure, and (C) bulk gas temperature	66
Figure 5.2	Effect of high activity on reaction profiles. Polymerization data from test runs using Catalysts JM38 and JM29 showing (A) rate of ethylene flow into reactor, (B) reactor gas pressure, and (C) gas temperature	69

Figure 5.3	Comparison of gas phase temperature control during polymerization under various modes of operation showing (A) activity profiles, and (B) the corresponding temperature profiles	71
Figure 5.4	Effect of TIBA (tri-isobutyl aluminum) on polymerization profiles (A) activity measured from flow rate of ethylene into reactor, (B) gas phase temperature, and (C) gas pressure	75
Figure 5.5	Effect of TEA (triethyl aluminum) on polymerization profiles (A) activity measured from flow rate of ethylene into reactor, (B) gas phase temperature, and (C) gas pressure	77
Figure 5.6	Effect of TIBA on gas phase homopolymerization using Catalyst TM02 showing (A) activity profiles, and (B) temperature profiles	80
Figure 5.7	Effect of scavenger TIBA (tri-isobutyl aluminum) on PE molar masses, Mn and Mw, and time averaged gas phase temperature, T	82
Figure 5.8	Effect of temperature on gas phase polymerization of ethylene and 1-hexene using Catalyst TM11 showing (A) activity profiles, and (B) temperature profiles	84
Figure 5.9	SEM images of polymer particles showing effect of gas phase polymerization temperature on outer morphologies at (A) 70°C (Run # 105TM), (B) 80°C (Run # 101TM), and (C) 90°C (Run # 104TM) using Catalyst TM11	86

Figure 5.10	SEM images of polymer particles showing effect of gas phase polymerization temperature on inner morphologies at (A) 70°C (Run # 105TM), (B) 80°C (Run # 101TM), and (C) 90°C (Run # 104TM) using Catalyst TM11	87
Figure 5.11	Effect of temperature on gas phase polymerization of ethylene and 1-hexene using Catalyst TM17 showing (A) activity profiles, and (B) temperature profiles	90
Figure 5.12	SEM images of polymer particles showing effect of gas phase polymerization temperature on outer morphologies at (A) 60°C (Run # 197TM), (B) 80°C (Run # 192TM), (C) 90°C (Run # 194TM), and (D) 100°C (Run # 196TM) using Catalyst TM17	91
Figure 5.13	SEM images of polymer particles showing effect of gas phase polymerization temperature on inner morphologies at (A) 60°C (Run # 197TM), (B) 80°C (Run # 192TM), (C) 90°C (Run # 194TM), and (D) 100°C (Run # 196TM) using Catalyst TM17	92
Figure 5.14	Effect of polymerization temperature on product polymer molar mass	93
Figure 5.15	Effect of ethylene pressure on gas phase copolymerization using Catalyst TM10 showing (A) activity profiles, and (B) temperature profiles	95
Figure 5.16	SEM images of polymer particles showing effect of gas phase pressure on outer morphologies at (A) 0.70 MPa (Run # 74TM), (B) 1.05 MPa (Run # 76TM), (C) 1.39 MPa (Run # 78TM), (D) 1.74 MPa (Run #	97

77TM), and (E) 2.06 MPa (Run # 75TM) produced by polymerization at 80°C using Catalyst TM10

Figure 5.17 SEM images of polymer particles showing effect of gas phase pressure on inner morphologies at (A) 0.70 MPa (Run # 74TM), (B) 1.05 MPa (Run # 76TM), (C) 1.39 MPa (Run # 78TM), (D) 1.74 MPa (Run # 77TM), and (E) 2.06 MPa (Run # 75TM) produced by polymerization at 80°C using Catalyst TM10 98

Figure 5.18 Effect of ethylene concentration on product polymer molar masses 99

Figure 5.19 Effect of presence of nitrogen on gas phase copolymerization using Catalyst TM10 showing (A) activity profiles, and (B) temperature profiles 101

Figure 5.20 Effect of amount of catalyst used on gas phase copolymerization using Catalyst TM10 showing (A) activity profiles, (B) activity profiles per mole of zirconium, and (C) temperature profiles with PID temperature controller switched on 104

Figure 5.21 Effect of amount of catalyst used on gas phase copolymerization using Catalyst TM11 showing (A) activity profiles, (B) activity profiles per mole of zirconium, and (C) temperature profiles with coolant oil at 80°C circulating in reactor channels 107

Figure 6.1 Growth of Catalyst TM15 (600–850 μm support size range) particles and fragments on 250 μm sieve during polymerization from (A) immediately after gas entry into micro-reactor to (F) 30 minutes later 112

Figure 6.2	Growth of Catalyst TM22 (300-350 $\mu\text{m}$ support size range) particles and fragments during polymerization from (A) immediately after gas entry into micro-reactor to (F) 7 minutes later. Black scale markings are approximately 1 mm apart	113
Figure 6.3	SEM of copolymerization of Catalyst TM20 at low (I) and high (II) magnifications for runs of different lengths – (A) catalyst particles; (B) 2 min polymerization; (C) 4 min polymerization; (D) 10 min polymerization; (E) 15 min polymerization; (F) 60 min polymerization	120
Figure 6.4	Activity and bulk gas temperature profiles of copolymerization of ethylene and 1-hexene at 80°C for runs of various lengths using Catalyst TM20	122
Figure 6.5	SEM of development of internal structure of particles during copolymerization with (A) Catalyst TM20 at 80°C after (B) 10 minutes, and (C) 60 minutes taken at low (I) and high (II) magnification	124
Figure 6.6	Development of molar masses and polydispersities with time during ethylene/1-hexene copolymerization at 80°C using Catalyst TM20	126
Figure 6.7	Activity and bulk gas temperature profiles of copolymerization of ethylene and 1-hexene with Catalyst TM22 at 80°C	128
Figure 6.8	Activity and bulk gas temperature profiles of copolymerization of ethylene and 1-hexene with Catalyst TM22 at 70°C	129

- Figure 6.9 SEM of polymer particles produced by copolymerization at 80°C with Catalyst TM22 for (A) 2 minutes, (B) 4 minutes, (C) 10 minutes, (D) 15 minutes, and (E) 60 minutes at low (I) and high magnification showing whole (II) and cut (III) particles 131
- Figure 6.10 SEM of polymer particles produced by copolymerization at 70°C with Catalyst TM22 for (A) 2 minutes, (B) 4 minutes, (C) 10 minutes, (D) 15 minutes, and (E) 60 minutes at low (I) and high magnification showing whole (II) and cut (III) particles 132
- Figure 6.11 SEM showing formation of shells by catalyst/polymer breaking away from surface of catalyst core after (A) 2 min, (B) 4 minutes, (C) 10 minutes, and (D) 15 minutes of copolymerization at 80°C with Catalyst TM22 134
- Figure 6.12 SEM showing formation of shells by catalyst/polymer breaking away from surface of catalyst core after (A) 2 min, (B) 4 minutes, (C) 10 minutes, and (D) 15 minutes of copolymerization at 70°C with Catalyst TM22 135
- Figure 6.13 Development of molar masses and polydispersities with time during ethylene/1-hexene copolymerization at 80°C using Catalyst TM22 136
- Figure 6.14 Development of molar masses and polydispersities with time during ethylene/1-hexene copolymerization at 70°C using Catalyst TM22 136
- Figure 6.15 Activity and bulk gas temperature profiles of homopolymerization of ethylene using Catalyst TM22 at 80°C 138

Figure 6.16	Homopolymerization with (A) Catalyst TM22 showing result of polymerization for (B) 2 minutes, (C) 10 minutes, and (D) 30 minutes at low, (I), and high, (II) and (III), magnifications for whole and cut particles	139
Figure 6.17	SEM of homopolymer particles showing radial growth of polymer outwards from catalyst core after (A) 2 minutes, (B) 15 minutes, and (C) 30 minutes of polymerization	141
Figure 6.18	Development of molar masses and polydispersities with time during ethylene homopolymerization at 80°C using Catalyst TM22	142
Figure 7.1	Effect of varying initial concentration of 1-hexene on polymerization using Catalyst TM08 showing (A) the activity profiles, and (B) the corresponding gas phase temperature profiles	147
Figure 7.2	Effect of varying initial concentration of 1-hexene on polymerization using Catalyst TM08 showing (A) the activity profiles, and (B) the corresponding gas phase temperature profiles after coolant reservoir modification	149
Figure 7.3	Effect of varying initial concentration of 1-hexene on polymerization using Catalyst TM11 showing (A) the activity profiles, and (B) the corresponding gas phase temperature profiles with circulation of coolant oil at 80°C to reactor	152
Figure 7.4	Effect of varying initial concentration of 1-hexene on PE molar masses, $M_n$ and $M_w$ , and time averaged gas phase temperature, T	154

Figure 7.5	SEM images of copolymer particles from Run 90TM showing (A) whole and (B) cut particles; and homopolymer particles from Run 91TM showing (C) whole and (D) cut particles at increasing magnification	156
Figure 7.6	Effect of varying initial concentration of 1-hexene and ethylene pressure on polymerization using Catalyst TM17 showing (A) activity profiles, (B) activity profiles normalized with respect to total pressure, and (C) gas phase temperature profiles	158
Figure 7.7	Effect of varying initial concentration of 1-hexene and ethylene pressure on PE molar masses, Mn and Mw during polymerization at 80°C using Catalyst TM17	160
Figure 7.8	Experiments to study variation of concentration of 1-hexene during polymerization using Catalyst TM13 at 80°C showing (A) activity profiles, (B) gas phase concentration of 1-hexene, and (C) gas phase temperature profiles	163
Figure 7.9	Effect of continuous injection of 1-hexene during polymerization at 1.4 MPa using Catalyst TM17 at 80°C showing (A) activity profiles, (B) concentration of 1-hexene, and (C) temperature profiles	165
Figure 7.10	Effect of continuous injection of 1-hexene during polymerization at 2.1 MPa using Catalyst TM17 at 80°C showing (A) activity profiles, (B) concentration of 1-hexene, and (C) temperature profiles	166

Figure 7.11	Effect of addition of <i>n</i> -heptane during homopolymerization at 1.4 MPa and 80°C using Catalyst TM15 showing (A) activity profiles, and (B) temperature profiles and compared to activity during copolymerization with 1-hexene (secondary Y-axis)	169
Figure 7.12	TREF profiles of homopolymer and copolymers formed from different initial concentration of 1-hexene	173
Figure 7.13	Catalyst TM12 catalyzed polymerization runs of various durations showing (A) activity profiles, (B) temperature profiles, and (C) pressure profiles	175
Figure 7.14	Effect of polymerization time on molar masses and polydispersity of copolymers catalyzed by Catalyst TM12 at 80°C	177
Figure 7.15	Effect of polymerization time on TREF profiles of copolymers showing elution curves for run of (A) 5, (B) 9, (C) 15, (D) 30, and (E) 60 minutes duration	179
Figure 7.16	Run TM166 using Catalyst TM15 showing (A) activity, (B) gas phase temperature, and (C) pressure profiles	180
Figure 7.17	Image of a typical cut polymer particle from Run TM166 formed by superimposition of 4 SEM images	181
Figure 7.18	Variation of molar masses with radial distance in polymer particles	182
Figure 7.19	Variation of short chain branching with radial distance in a polymer particle	183

Figure 8.1	Polymerization runs using Catalyst TM14 showing (A) activity profiles, (B) gas phase temperature profiles, and (C) pressure profiles and concentration of 1-hexene	189
Figure 8.2	SEM images of polymer particles from (A) ethylene homopolymerization run 146TM and (B) ethylene/1-hexene copolymerization run 147TM using Catalyst TM14 taken at low (I) to high (III) magnifications	191
Figure 8.3	SEM image of Catalyst TM19 showing sizes of small (TM19A) and large (TM19B) particles	192
Figure 8.4	Effect of catalyst particle size on polymerization runs showing (A) activity profiles, (B) gas phase temperature profiles, and (C) pressure profiles	195
Figure 8.5	Effect of temperature on polymerization runs with different size catalysts showing (A) activity, (B) gas phase temperature, and (C) pressure profiles	197
Figure 8.6	SEM images of Catalyst TM19 polymerized (I) small and (II) large particles, produced at 80°C, Run 214TM (A, B) and 70°C, Run 217T (C, D) showing whole (A, C) and cut (B, D) particles	199

## List of Abbreviations

AA	acrylic acid
ASTM	American Society for Testing and Materials
BET	Brunauer Emmett Teller
BJH	Barret Joyner Halenda
BSE	back scattered electron
CA	catalyst injector
CSTR	continuous-stirred-tank reactor
DC	direct current
DSC	differential scanning calorimetry
DVB	divinylbenzene
EA	ethylacrylate
EDX	energy dispersive X-ray analysis
F	filter
GC	gas chromatograph
GP	gas purifiers
GPC	gel permeation chromatograph
HDPE	high-density polyethylene
HEMA	2-hydroxyethylmethacrylate
HS	HayeSep
INAA	instrumental neutron activation analysis
IR	infrared

LDPE	low density polyethylene
LLDPE	linear low-density polyethylene
MAO	methylaluminoxane
MDPE	medium density polyethylene
MF	mass flow meter
MFI	melt flow index
MMAO-4	modified methylaluminoxane type-4
MMD	molar mass distribution
M <sub>n</sub>	number averaged molar mass
MP	metering pump
MS	Magnedrive stirrer
M <sub>w</sub>	weight averaged molar mass
NAA	neutron activation analysis
NMR	nuclear magnetic resonance (analysis)
NVP	<i>n</i> -vinyl-2-pyrrolidinone
P	centrifugal pump
P <sub>d</sub>	polydispersity
PE	polyethylene
PG	pressure gage
PID	proportional integral differential
PR	pressure regulator
PS	polystyrene
PT	pressure transducer

SCBD	short chain branching distribution
SEC	size exclusion chromatography
SEM	scanning electron microscopy
SLOWPOKE	Safe LOW POver Kritical Experiment
SP	syringe pump
STP	standard temperature and pressure
STY	styrene
SY	syringe injection port
TEA	triethylaluminum
Ti	thermocouple i
TIBA	triisobutylaluminum
TMA	trimethylaluminum
TNOA	tri- <i>n</i> -octylaluminum
TREF	temperature rising elution fractionation
V	vent
VLDPE	very low density polyethylene

# 1. Introduction

Polyethylene (PE) resins are commodity plastics used ubiquitously in our lives. Based on 2001 data, over 50 million tons of PE was consumed worldwide (Schumacher and Borruso, 2002). The resins are essentially linear polymers with ethylene molecules as the main building block, although most PE molecules also contain branches in their chains. A wide variety of PE resins are produced industrially with differing molar masses, origins and types of branching, and uniformity of branching distribution. In contrast to other materials, PE combines several ecological and economic benefits. They are produced from cheap and easily available monomers such as ethylene in low-cost, energy-saving, and non-polluting processes and can be recycled after use. Moreover as their properties can be tailored using modern catalysts and process technologies they can be used in producing simple shopping bags and food wrappers to heavy-duty crates and even armor plating for bullet-proof vests.

## 1.1 History of Polyolefin Production (Kissin, 2000):

In 1898, von Pechmann first synthesized polymer with a polymethylene structure from diazomethane. Since then four milestones are significant in the history of PE as commercial plastics.

First, in 1935, Perrin discovered at ICI laboratories that ethylene could be polymerized under high pressure into a solid semicrystalline material. This led to the manufacture of low density PE (LDPE), which began in the United Kingdom in 1938 and in the United States in 1943. The polymerization reaction proceeds by free-radical

mechanism in supercritical ethylene at high pressures of around 60-350 MPa (10,000-50,000 psi) and temperatures of 200-350 °C. Copolymerization with  $\alpha$ -olefins and other polar monomers, such as vinyl acetate is possible.

Second, in the early 1950s, Hogan and Bank at Phillips Petroleum Company discovered that chromium oxides supported on silica (Phillips catalysts) polymerized ethylene under more moderate conditions: at a pressure of 3–4 MPa (435-580 psi) and temperature of 70-100°C. This produced PE molecules that are linear and highly crystalline with much higher density; such resins are known as high density polyethylene (HDPE).

Third, in 1953, Ziegler in Germany discovered that ethylene could be polymerized under milder conditions, that is at atmospheric pressure and temperatures of 50-100°C, in presence of catalyst systems containing titanium halides and alkylaluminum compounds (Ziegler catalysts). These versatile catalysts could easily copolymerize ethylene and  $\alpha$ -olefins with vinyl double bonds. Depending on the amount of  $\alpha$ -olefin in the copolymerization reaction, these polymers can range from highly crystalline to completely amorphous. Natta, in Italy, used Ziegler's catalysts to synthesize polypropylene with high selectivity to the isotactic polypropylene. These catalysts, based on titanium halides and aluminum alkyls are therefore commonly known as Ziegler-Natta catalysts.

Finally, in 1976, a new family of catalysts for ethylene polymerization was discovered by Kaminsky and Sinn in Germany. Comprising of two components: a metallocene complex, usually a zirconocene, and an organoaluminum compound, methylaluminoxane (MAO), these catalysts and their various modifications enabled

synthesis of ethylene copolymers with a high degree of branching uniformity. The resins produced have very different properties from common PE resins in terms of performance and application.

## 1.2 Classification of PE Resins

Commercially the PE resins are classified according to two parameters that can be easily measured: the resin density and its melt index. Although this cannot distinguish between the structures and properties of various resins, it provides a simple means for a basic differentiation of the PE resins. Some of the common polyethylene resins used industrially are given in Table 1.1.

Table 1.1: Commercial classification of PE resins (Enderle, 2001 and Kissin, 2000)

Designation	Acronym	Density (g/cm <sup>3</sup> )	Melt Temperature (°C)
High density polyethylene	HDPE	0.940 – 0.970	128 - 136
Medium density polyethylene	MDPE	0.930 – 0.940	120 - 130
Linear low density polyethylene	LLDPE	0.915 – 0.925	120 - 130
Low density polyethylene	LDPE	0.910 – 0.940	105 - 115

A more comprehensive characterization of PE would include composition, molar mass, distributed branch content and branching distribution. The branch content of ethylene copolymers is usually measured by <sup>13</sup>C-NMR, <sup>1</sup>H-NMR, or IR techniques.

Molar masses of polymers are characterized by the weight-average molecular mass,  $M_w$ , and the number-average molecular mass,  $M_n$ . The molar mass distribution of polymers (MMD) is usually represented as  $M_w/M_n$ , which is also known as polydispersity

(Pd). The  $M_w$  and  $M_n$  values of PE resins are measured by high temperature size exclusion chromatography (SEC), which is also known as gel permeation chromatography (GPC).

The branching distributions of ethylene copolymers are measured by either temperature-rising elution fractionation (TREF) or, semi-quantitatively, by differential scanning calorimetry (DSC). This represents relative contribution of macromolecules of different comonomer contents to a given resin.

### 1.3 Polyolefin Synthesis Technologies

PE production technologies can be classified into four broad groups:

- A) Polymerization in Supercritical Ethylene,
- B) Polymerization in Suspension (Slurry),
- C) Polymerization in Solution, and
- D) Polymerization in the Gas Phase.

As discussed earlier, LDPE can be produced under high ethylene pressure. At present two high pressure processes can be recognized: the autoclave and tubular reactors. Oxygen and/or organic peroxides are used as initiators for the free radical polymerization. Molar mass can be controlled by adding chain transfer agents such as saturated hydrocarbons,  $\alpha$ -olefins, ketones, or aldehydes to the reaction mixture (Whiteley et al. (2002)). Under polymerization conditions the polymer is dissolved in the supercritical ethylene resulting in a one-phase reaction mixture. The polymer produced is separated from unreacted monomer by reducing the pressure in two stages. The unreacted monomer is recycled, while the polymer is extruded, pelletized, degassed, and transferred

to storage silos. The reaction pressure and temperature are typically in the range 150 – 200 MPa and 180 – 290°C, respectively for the autoclave process and 200 – 350 MPa and 140 – 190°C, respectively for a tubular reactor. Such high pressures require very specialized technology and the capital cost for these plants is very high.

The catalytic processes include the slurry, solution, and gas-phase processes. Hydrocarbon diluents can be used to suspend PE particles and can be used for suspension (slurry) polymerization. This polymerization technology is the oldest used for HDPE production and accounts for nearly 66% of all HDPE produced worldwide (Enderle, 2001). A number of processes based on stirred tank or tubular flow reactors at present employ suspension polymerization. Depending on particular process, the operating pressures of 1 - 4.5 MPa (150 – 700 psi) and temperatures of 70 – 110°C are used.

It has been found that saturated C<sub>6</sub> – C<sub>9</sub> hydrocarbons above 120 – 130°C dissolves polyethylene and can be used as a medium for polymerization. However, as the viscosity of the HDPE solutions rapidly increases with molecular weight, solution polymerization is primarily employed for production of low molecular weight resins. Typical pressures and temperatures for such processes are 5 – 10 MPa (725 – 1450 psi) and 150 – 200°C respectively. The advantage of the solution process is that low residence times can be used due to the higher rates of polymerization at elevated temperatures. In both slurry and solution polymerization the diluent / solvent must be removed from the product at the end of the process and recycled.

Union Carbide first introduced the Unipol gas-phase polymerization process in 1968 in which polymerization takes place under mild operating conditions. The Unipol process operates as a fluidized bed in which the polymer particles grow as polymerization

proceeds. Other gas-phase processes use mechanical stirrers to suspend the growing particles. During polymerization the solid catalyst particles are fed continuously as a powder and the product, which contains the catalyst particles, is removed intermittently from the reactor. The temperature of the reactor must be kept below 110°C to prevent the PE particles from agglomerating and sticking to reactor walls. Typical operating pressure is about 2 MPa (300 psi). Gas-phase processes account for over 20% of the world PE capacity. The technology is economical and flexible; it can accommodate a large variety of solid and supported catalysts capable of ethylene polymerization at relatively low pressure. Moreover, the capital investment for such process is much lower than that for the other competing processes. Details of current industrial catalytic low pressure olefin polymerization processes are summarized in Table 1.2 below.

Table 1.2: PE production utilizing catalytic low pressure technologies (Enderle, 2001).

	Solution Process	Slurry Process	Gas Phase Process
Products	HDPE, MDPE, LLDPE, VLDPE	HDPE, MDPE	HDPE, MDPE, LLDPE, VLDPE
Density Range	Full	Limited	Full
MFI Range*	Limited	Full	Full
Catalyst System	Ti, V-comp. Metallocenes	Supported Ti, Cr-comp.	Supported Ti, Cr-comp.
Cocatalyst	TEA, TIBA**	TEA, TIBA**	TEA, TIBA**
Reactor Type	CSTR <sup>+</sup>	CSTR <sup>+</sup> , loop reactor	Fluidized & stirred- bed reactor
Pressure (MPa)	1 – 14	1 – 7	2
Temperature (°C)	140 – 300	70 – 110	80 – 110
Residence time(min)	1 – 5	30 – 180	60 – 180
Diluent/Solvent	<i>n</i> -hexane, cyclohexane	hexane, isobutane	

\*MFI = Melt Flow Index (indication of  $M_w$ )

\*\*TEA: triethylaluminum. TIBA: triisobutylaluminum. <sup>+</sup>CSTR: continuous-stirred-tank reactor

#### 1.4 Challenges in Polyolefin Research

Unlike many common chemical products, polymer molecules cannot be easily separated from each other. While blending of different grades of polyolefins may produce the desired product, it is more economical to produce polymers with the required specification in the reactor. As the properties of the polyethylene produced depends on reactor operating conditions it is essential to be able to control them precisely. Moreover, how these various parameters affect the activity profiles during polymerization and the product polymer properties needs to be studied.

Olefin polymerization is a highly exothermic reaction, with heats of polymerization in the order of 100 kJ/mol. Thus, significant temperature increase can occur during polymerization, e.g. the adiabatic temperature rise during gas-phase polymerization for 1% conversion of ethylene to polyethylene in a batch reactor is about 16°C. Large increase in temperature degrades the product and deactivates the catalyst. Heat removal is thus a key factor especially in gas-phase polymerization. While commercial processes employ limited conversion per pass so that the heat of reaction is absorbed by the cool reactants, this remains a significant problem for laboratory scale semi-batch gas phase processes. Thus most laboratory polymerization studies in literature use slurry processes. However, catalyst behavior in slurry processes is significantly different than the gas-phase polymerization.

The catalysts used for ethylene polymerization such as Ziegler-Natta and metallocene catalysts and their cocatalysts are highly sensitive and pyrophoric. Therefore, an inert atmosphere free of oxygen and moisture is required for preparing, handling and transporting them. The catalyst must be supported on a carrier for use in gas phase

polymerization reactor. Moreover, the reactor itself must be free of such contaminants so that the catalysts are not deactivated inside the reactor. This requires special procedural consideration for laboratory scale reactor operation.

### 1.5 Objectives of the Current Research

The objectives of this research work can be enumerated as follows:

1. Design a laboratory-scale gas-phase polymerization reactor with better gas-phase temperature control than that present in our laboratory.
2. Design a micro-reactor to observe catalyst particle growth during polymerization.
3. Prepare active organic-polymer supported metallocene catalysts.
4. Determine effects of parameters such as scavenger concentration, temperature, pressure, inert gas concentration, and catalyst amounts on activity profiles and product properties.
5. Observe development of product particle morphologies and its effects on activity profiles.
6. Determine effects of concentration of the comonomer 1-hexene on activity profiles and product properties.
7. Determine effects of catalyst particle size on activity profiles.

The chapters in this thesis have been arranged in the same order as the objectives. The literature on metallocene catalysts and aluminoxane cocatalysts and gas-phase olefin polymerization using these catalytic systems is reviewed in Chapter 2. In Chapter 3, details of a novel gas phase laboratory scale olefin polymerization reactor with excellent

temperature control are given. This includes description of the reactor temperature controller system and gas phase analysis procedure. Further a micro-reactor for observing polymer growth that can be used in conjunction with the main reactor is described. Experimental procedures and methods used for preparing supported catalysts and characterizing catalysts and polymer products are also discussed.

The future of metallocene/MAO catalyst systems for olefin polymerization has looked very promising since its discovery by Kaminsky in 1976. Although low activities of the system dampened its initial growth, high activity metallocene catalysts are now available. Although Mitsui in Japan operates a large fluidized bed reactor using a silica supported metallocene catalyst, at present, industrial use of the metallocene catalysts is mainly limited to solution polymerization where high ratio of cocatalyst is required. This is expensive and leaves undesirable amounts of ash in the PE product. The development of better supported metallocene catalyst with the reduction of cocatalyst ratio and use of organic supports have raised hopes of making metallocene based gas-phase commercial ethylene polymerization more attractive. Moreover, the existing gas phase polymerization plants provide huge potential for using such supported catalysts. In Chapter 4, details about supports used and the catalysts made are given.

The metallocene catalysts are single site catalysts and the product PE has a much narrower molecular weight distribution than that produced by Ziegler catalysts. While such narrow polydispersity is desirable to obtain some specific properties in the polymer product, it also gives rise to processing difficulties. However, as the molecular weight distribution also depends on the conditions during polymerization, in theory it should be possible to control this by manipulating the reactor operating parameters. Thus, scope

exists for detailed study of how the polymer properties depend on the polymerization conditions. In Chapter 5, exploratory experiments to determine the efficacy of the reactor system in gas phase temperature during polymerization are described. Moreover, the effects of various operating parameters such as scavenger concentration, gas phase temperature, ethylene pressure, inert gas concentration, and amount of catalyst used are presented.

Observations of growth of individual catalyst/polymer particles using the micro-reactor during ethylene/1-hexene copolymerization are discussed in Chapter 6. Further, ex-situ observations of internal and external particle growth during both homo- and copolymerization using SEM are described and discussed in this chapter.

Presence of an  $\alpha$ -olefin comonomer can profoundly effect ethylene polymerization activity. In Chapter 7 details of effects of presence of a 1-hexene comonomer during ethylene polymerization and controlling the concentration of 1-hexene during the polymerization using a GC for headspace gas analysis are given. The effect of presence of small amounts of an inert hydrocarbon, n-heptane during ethylene homopolymerization and the use of TREF analysis for determining short chain branching in copolymer resins are also presented.

In Chapter 8 the effect of catalyst particle size on polymerization activity is given. Results from runs using catalyst supported on very small 5  $\mu\text{m}$  particles and catalysts of different size ranges prepared together are discussed. And finally a summary of the results obtained during the course of this work and recommendation for future work are presented in Chapter 9.

## 2. Literature Review

Since the discovery of highly active metallocene-aluminoxane catalyst system for olefin polymerization by Kaminsky and Sinn in their laboratory in Germany over 25 years ago over 10,000 articles and more than 4000 patents have been published on the subject of polymerization with these single site catalysts (Kaminsky, 2004). Thus a comprehensive review of all available literature is beyond the scope of this work and only some of the topics pertinent to this work will be covered in this chapter. However, a number of review papers have been published, which covers a broad spectrum of relevant material, such as those by G. G. Hlatky (2000), E. Y. X. Chen and T. J. Marks (2000), M. R. Ribeiro, A. Deffieux and M. F. Portela (1997), A. E. Hamielec and J. B. P. Soares (1996), W. Kaminsky (1996), J. Huang and G. L. Rempel (1995), S. S. Reddy and S. Sivaram (1995), and J. B. P. Soares and A. E. Hamielec (1995).

### 2.1 Metallocene Catalyst

Metallocene catalysts, also known as single-site catalysts, can be defined as organometallic coordination compounds in which two cyclopentadienyl rings are  $\pi$ -bonded to a central transition metal atom usually titanium, zirconium, or hafnium. The rings play a vital role in the polymerization activity of the metallocene catalyst (Hlatky, 1999). By varying the substituents on the rings, changing the central metal atom or bridging the two rings a large number of different catalysts can be synthesized that can tailor polyolefins of different properties. During classical Ziegler-Natta catalysis the polymerization takes place on dislocations and edges of the surface of solid  $\text{TiCl}_3$  or

mixtures of  $\text{MgCl}_2/\text{TiCl}_4$  catalysts. Thus, many different catalytic sites exist and the resulting polymers have broad molecular weight distributions. In contrast to classical Ziegler-Natta catalysis, metallocene catalysts are soluble in hydrocarbons and polymerization in these single-site catalyst takes place at a defined transition metal centre that allows precise control of the monomer insertion and other steps, thus enabling control over polymer tacticity, molecular weight, and molecular weight distribution more efficiently (Kaminsky, 2001). The product polymer from homogeneous polymerization using metallocene catalyst has a Schultz-Flory distribution of molecular weights with polydispersity of about 2. In Figure 2.1 some typical classes of metallocene catalysts used for olefin polymerization are shown.

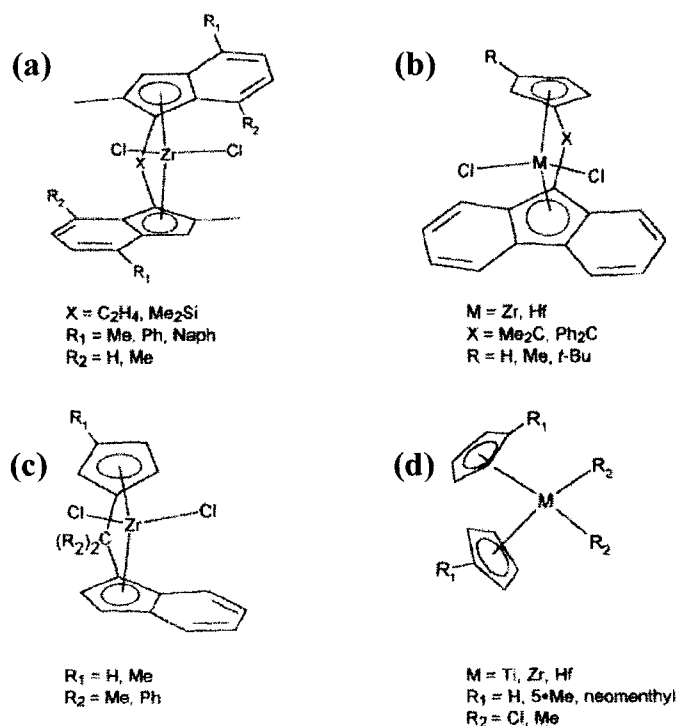


Figure 2.1: Some classes of metallocene used for olefin polymerization (Kaminsky, 1996). [Type (d) metallocene with  $R_1 = n\text{-C}_4\text{H}_9$ , and  $R_2 = \text{Cl}$  was used in this thesis work.]

## 2.2 Aluminoxane Cocatalyst

The structure of metallocenes was elucidated in the early 1950's and their use in combination with alkyl aluminums as catalysts for olefin polymerization followed soon thereafter. However, the activities of these catalysts were poor and use of these catalysts was mainly limited to mechanistic studies of olefin polymerization, which was simpler with a homogeneous catalyst than a heterogeneous Ziegler-Natta system (Kaminsky, 2001). The situation changed dramatically with the discovery and application of methylaluminoxane (MAO) by Kaminsky and Sinn as a cocatalyst in 1977 (Kaminsky, 1998). The catalytic activity of metallocene was enhanced by a factor of 10,000 in presence of MAO and the resulting catalyst system had activities 10-100 times higher than the most active classical Ziegler-Natta catalysts.

Methylaluminoxane (MAO) is prepared by the controlled hydrolysis of trimethylaluminum (TMA) and is generally considered to be an oligomer of subunits  $[-Al(Me_3)-O-]_n$  where  $n \approx 5 - 10$  (Chen, 2000). Although MAO has been studied extensively its structure is not known exactly due to existence of multiple equilibria in its solution. Moreover, commercial MAO contains residual TMA which can be either "associated" or "free" resulting in variation of ratio of Me:Al. As vacuum-drying only removes the free TMA, the ratio of Me:Al cannot be easily reduced to less than 1.5 by evaporation of volatile components and the associated TMA must be removed chemically. The TMA has significant effect on the molar mass of the MAO and its activity as a cocatalyst (Tritto et al. 1997). It has been found that with increases in the amounts of free TMA to MAO both the catalyst activity and product polymer molar mass decreases. Thus various schemes have been used to denote the structure of MAO - from

linear chains for simplicity of representation to three-dimensional cage like structure as shown in Figure 2.2. Kaminsky (1998) reported that according to investigations by Sinn and Barron MAO consists of the repeating units of basic structure  $[Al_4O_3Me_6]$  in three-dimensional cage like structure as shown in Figure 2.2 (4). With empirical data from Raman and IR spectroscopy and theoretical consideration of MAO solutions, Ystenes et al. (2000) postulated the presence of a few  $Me_{18}Al_{12}O_9$  rigid cage structures containing bridging methyl groups on the cage surfaces that are labile and reactive.

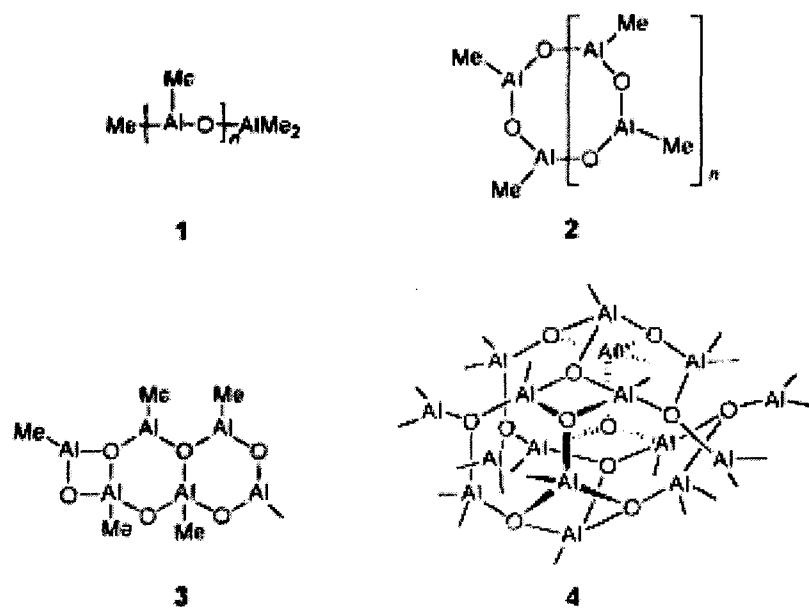


Figure 2.2: Proposed structures for MAO showing (1) linear chains, (2) cyclic rings, containing three coordinate Al centres in two-dimensional structures, and (3) three-dimensional cage-like structures containing four coordinate Al centres (Chen and Marks, 2000).

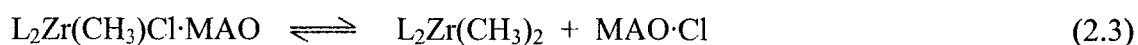
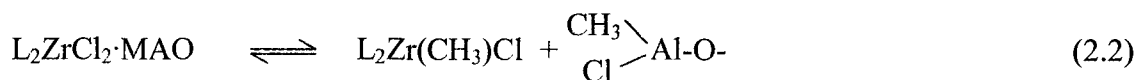
As conventional MAO has very low solubility in aliphatic solvents and poor shelf-life and other more soluble aluminoxanes such as ethylaluminumoxane and isobutylaluminumoxane have been tried as cocatalysts for metallocene; but their activities have been found to be less than that of MAO (Kaminsky and Steiger, 1988). However, modified methylaluminumoxanes (MMAO) having improved solution storage stability and solubility in aliphatic solvent, made from controlled hydrolysis of trimethylaluminum (TMA) and triisobutylaluminum (TIBA) is commercially available from Akzo-Noble and has reasonable co-catalytic activity. Other non-aluminum Lewis acid species, such as borates have also been used as cocatalyst (Britovsek et al., 1999) but these are more prone to poisoning (Hlatky, 2000) and MAO remains the cocatalyst of choice.

Although the role of MAO during polymerization is not understood completely, experimental evidence indicates that beside acting as an alkylating agent, MAO is involved in the formation of cationic active sites via a fast ligand exchange and in the stabilization of the anion and in the prevention of their deactivation by bimolecular processes, by stabilization of the active species and by scavenging impurities (Hamielec and Soares, 1996). The steps involved in the formation of active species by reaction with MAO with a zirconocene can be summarized as follows (Kaminsky, 2004, Hlatky, 2000 and, Chien and Razavi, 1988):

Complexation



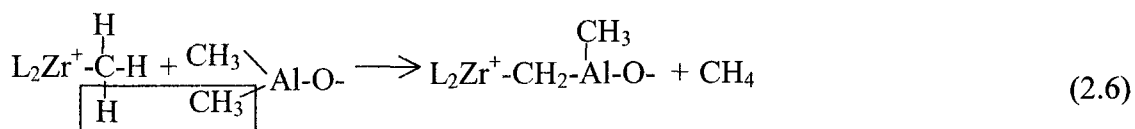
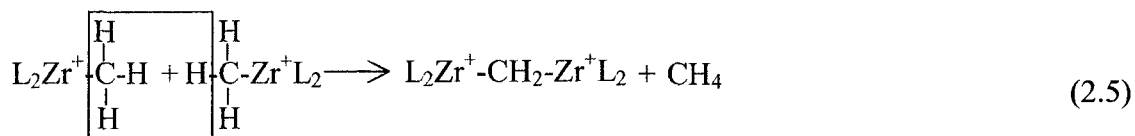
Methylation



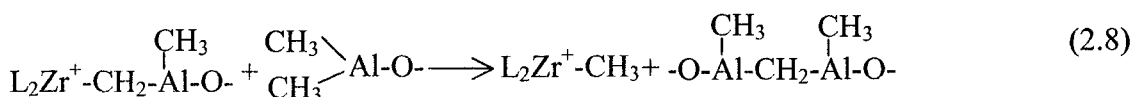
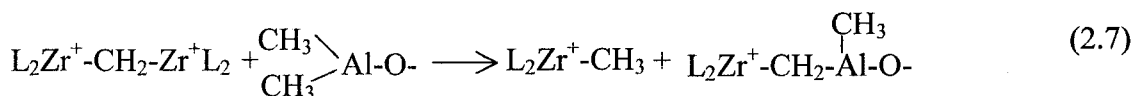
Activation



Deactivation



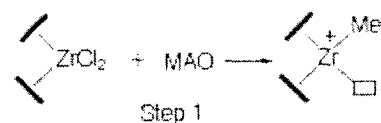
Reactivation



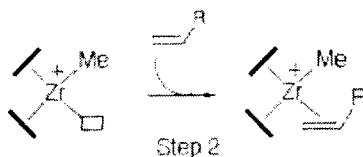
It has been postulated that the fast ligand exchange between the zirconium ion of the metallocene and MAO (eqn.2.2) takes place with the free TMA that is present in the MAO (Barron, 2000). The large excess of MAO required in homogeneous metallocene polymerization helps to reverse the binuclear deactivation (see equations 2.5 and 2.6) of the catalyst via equations 2.7 and 2.8 (Kaminsky, 2004).

As the essential role MAO plays in activating the metallocene has been explained the mechanism of olefin polymerization by zirconocene can now be represented by the following steps (Kaminsky, 1998):

Step 1: The cocatalyst MAO converts the zirconocene after complexation into the active species which has a free co-ordination position for the monomer and stabilizes the latter.

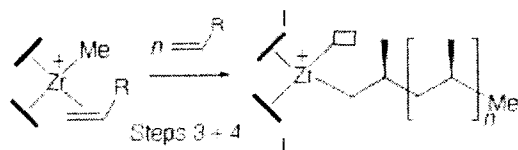


Step 2: the monomer (olefin) is allocated to the complex.



Step 3: insertion of the olefin into the zirconium-alkyl bond and provision of a new free co-ordination position.

Step 4: repetition of step 3, in a very short period of time, thus forming a polymer chain.



### 2.3 Supported Metallocene Catalysts

Although MAO is successful in promoting very high activity metallocene based homogeneous polymerization, there are some disadvantages. High concentration of the expensive cocatalyst MAO is required during solution polymerization that leaves high ash content ( $\text{Al}_2\text{O}_3$ ) in the product polymer. There are also inherent drawbacks to solution polymerization such as poor control over polymer morphology and reactor fouling and limitation on the molar masses of the product. Moreover, most current industrial production of polyolefins is based on heterogeneous systems and it would be uneconomical to convert the existing plants to homogeneous solution based systems. Thus development of supported metallocene aluminoxane catalysts is necessary for their use in existing gas-phase polymerization plants.

The literature shows three main ways by which metallocenes can be supported on carriers. These are as follows (Hlatky, 2000):

- 1) Direct immobilization of the metallocene on the support surface (direct heterogenization) followed by addition of aluminoxane or other cocatalyst. The metallocene is adsorbed on the surface by physisorption or chemisorption or covalently bonded to the support via a spacer and an anchor group. Variation of this method includes in situ synthesis of metallocene on the support.
- 2) Initial adsorption of the cocatalyst (aluminoxane) to the support, followed by adsorption of the metallocene (indirect heterogenization). Variation of this method includes in situ hydrolysis of alkyl aluminums on the surface to generate aluminoxane.
- 3) Contacting the aluminoxane and metallocene in solution before precipitating them onto the support. Variation includes vacuum impregnation where the activated catalyst solution is added to the support and kept under vacuum to improve penetration into the pores of the support; the slurry is dried under vacuum, by nitrogen purge or by spray drying to form a free-flowing solid finished product.

In supporting the metallocene directly onto the support surface first, as described in method (1) above, the nature of the metallocene can be significantly affected. Moreover, for surfaces such as silica much of the metallocene can be destroyed by interaction with surface  $-OH$  groups. Thus, the activity of these types of supported metallocene catalysts is much lower than that in the case of homogeneous systems and the molar mass distribution of the polymer produced is much broader ( $M_w/M_n = 5-10$ )

(Kaminsky and Winkelbach, 1999). If the metallocene is covalently bonded to the surface the nature of the active sites is changed. Often many cumbersome synthesis steps are required to immobilize the metallocene via covalent bonds to the support (Alt, 1999, 2001). However, in these types of supported catalysts there is very little leaching of the metallocene out of the supports during polymerization and fouling is prevented (Fink et al., 2000) and covalently bonded metallocene can be distributed evenly throughout the support and not just on the external surface (Roscoe et al., 2000).

The polymers obtained by catalysts made by the second method are very similar to those obtained in a homogeneous system. It is postulated that as the surface is essentially covered by aluminoxane the cationic metallocene species floats over the solid surface, much like in solution (Ribeiro et al., 1997). Each metallocene on the support forms an active site. Although the molar masses are similar to that of the homogeneous system, the activity is about half of that of the homogeneous system as one side of the metallocene is blocked by the support (Kaminsky and Winkelbach, 1999).

The third method produces most active supported catalysts as the process maximizes the number of active sites by activating the metallocene in solution, instead of carrying out the process with one or the other component in an immobilized state (Hlatky, 2000). The activity of the catalyst is however influenced by the concentration and viscosity of the organic solvent and the contact time.

An added benefit of heterogenation is that the bimolecular deactivation of the metallocene is greatly reduced due to the decreased mobility of the metallocene and aluminoxane species. Thus the high excess of MAO required to achieve good activity can be reduced from Al:Zr ratios of 3000-10000 (homogeneous) to 100-500 (heterogeneous)

(Kaminsky and Winkelbach, 1999). Moreover, supported metallocene complexes show good storage and thermal stability (dos Santos et al., 2001). Polymers produced by supported metallocenes in general have slightly broader polydispersities (2-5) than that corresponding to homogeneous systems (1-2) likely arising from probable formation of active sites differing in electronic and steric character from interactions between the metallocene and the support (Ribeiro et al., 1997).

#### 2.4 Organic Polymeric Supports

The literature shows that most of early supports used for heterogenation of metallocene catalysts were inorganic materials. The earliest and most commonly used support was silica; however, inorganic carriers such as alumina ( $\text{Al}_2\text{O}_3$ ), magnesium chloride, fluoride and oxide ( $\text{MgCl}_2$ ,  $\text{MgF}_2$ ,  $\text{MgO}$ ), calcium fluoride ( $\text{CaF}_2$ ) and zeolites have also been used as supports (Hlatky, 2000). However, these supports leave behind inorganic residues in the product polymers and often the nature of the metallocene is changed due to strong electrostatic interaction between the support and the metallocene. Moreover, fragmentation of rigid support particle may result in undesired morphology of product and in fines. In contrast, organic carriers for supporting metallocene catalysts provide a much closer analogue to the environment prevailing under homogeneous polymerizations. Moreover, organic supports are easy to prepare and low cost (Meng et al., 1999) and can be easily functionalized to satisfy certain requirements (Qin et al., 2003) and thus vary the catalytic performance at will. Organic supports leave lower inorganic residues in comparison to inorganic supports and the morphology of the polymer can be better controlled. An updated summary of the literature on organic polymeric supports is given in Table 2.1 based on Hammawa (2004).

Table 2.1 Organic polymer-supports for metallocene catalysts mentioned in the literature.

Support*	Catalyst	Key features and reference
Poly(STY/2%-DVB)	(Ind) <sub>2</sub> ZrCl <sub>2</sub> ; 0.02-0.20 mass% Zr	Very low activity due to support influence, Nishida et al. (1995).
Poly(STY/2%-DVB)	<i>rac</i> -Ph <sub>2</sub> Si(Ind) <sub>2</sub> ZrCl <sub>2</sub>	<i>rac</i> -Ph <sub>2</sub> Si(Ind) <sub>2</sub> tethered to support by phenyl spacer, catalyst activated by MAO prior to polymerization, Hong et al. (1998a)
Poly(STY/2%-DVB)	Cp <sub>2</sub> TiCl <sub>2</sub> ;	Tethering the titanocene with 17-atom long spacer produced catalyst resembling homogeneous one; Barrett and de Miguel (1998).
Polyethylene	[C <sub>13</sub> H <sub>8</sub> C(Me)(C <sub>4</sub> H <sub>7</sub> )C <sub>3</sub> H <sub>3</sub> Bu]ZrCl <sub>2</sub>	Metallocene catalysts with olefin/alkyne function were copolymerized with ethylene to form supported catalyst. Alt, 1999.
Poly(STY/acrylamide/ 5%-DVB)	Cp <sub>2</sub> ZrCl <sub>2</sub> /MAO	Some reactive functional groups of the support were inaccessible to MAO; Liu et al. (1999).
Crosslinked polystyrene	Cp <sub>2</sub> ZrCl <sub>2</sub> /MAO	Metallocene-attached soluble polymer was crosslinked by Diels-Alder reaction to form supported catalyst; Stork et al. (1999).
Cross-linked poly(styrene-co-4-vinylpyridine),	Cp <sub>2</sub> ZrCl <sub>2</sub>	Crosslink density and 4-vinylpyridine content of support increased activity per mole Zr; only the 4-vinylpyridine content increased the Al and Zr loading on catalyst; Meng et al. (1999).
Amine-functionalized poly(STY/1%-DVB)	(C <sub>5</sub> HMe <sub>4</sub> ) <sub>2</sub> HfMe <sub>2</sub> /[B(C <sub>6</sub> F <sub>5</sub> ) <sub>4</sub> <sup>-</sup> ]; 2.5-13.7 mass % Hf	Catalyst immobilized by coordination interaction between N on support and the Hf. Choice of diluent and polymerization condition critical in preventing catalyst leaching; Roscoe et al. (2000).
Reversibly cross-linked polystyrene	Me <sub>2</sub> Si(2-MeBenzInd) <sub>2</sub> ZrCl <sub>2</sub> /MAO	Reversibly (not DVB) crosslinked support improved catalyst fragmentation. Koch et al. 2000 and 2001.
Poly(4-vinylpyridine/ 2%-DVB)	Cp <sub>2</sub> ZrMe <sub>2</sub> /[B(C <sub>6</sub> F <sub>5</sub> ) <sub>4</sub> <sup>-</sup> ]; 0.76 mass % Zr	Use of functional monomer and higher crosslink density support improved catalyst immobilization over the work of Roscoe et al. above; Musikabhumma et al. (2000).
Poly(HEMA/DVB)	( <i>n</i> -BuCp) <sub>2</sub> ZrCl <sub>2</sub> /MAO	Porous support beads impregnated with MAO then metallocene; Zhou et al. 2003.
Poly(DVB/STY/EA/AA)	Cp <sub>2</sub> ZrCl <sub>2</sub> /MAO	Porous support beads impregnated with MAO then metallocene; Qin et al. (2003).
Chloromethylated Polystyrene	Cp <sub>2</sub> ZrCl <sub>2</sub> /MAO	Metallocene physically immobilized inside crosslinked polystyrene; Wang et al. (2005).

\* STY = styrene; EA = ethylacrylate; AA = acrylic acid; HEMA = 2-hydroxyethylmethacrylate

## 2.5 Laboratory-Scale Gas-Phase Polymerization Reactor Systems

Due to the very exothermic nature of ethylene polymerization and poor gas phase heat transfer coefficients, control of temperature during gas-phase polymerization in a laboratory-scale reactor is a very challenging issue. Thus most research on heterogeneous polymerization cited in the literature was done in slurry and not in gas phase systems. However, a few academic groups have been active in laboratory-scale gas-phase polymerization research.

Lynch and Wanke (1991) at the University of Alberta, Canada, described a 1L stainless steel gas-phase polymerization reactor that was immersed in a circulating oil-bath to control the temperature. However, the gas phase temperature cannot be rapidly controlled during very high activity polymerization runs and the temperature can rise significantly above the initial temperature (Zhou et al., 2003, Kumkaew et al., 2003). Ray and his group at the University of Wisconsin, USA have been using a 1L horizontal stainless reactor with an electrical heating jacket and coolant flowing through copper coils soldered on the outside of reactor for temperature control during gas-phase olefin polymerization (Han-Adebekun et al., 1997a). Although gas phase temperature could be controlled to  $\pm 0.5^{\circ}\text{C}$  of the desired temperature this could only be attained after more than 15 minutes of polymerization and initially there were significant oscillations in temperature. Weickert and Westerterp and their group at the Twente University of Technology, The Netherlands, have used a jacketed 1L glass reactor for gas phase polymerization (Samson et al., 1999). However, no data on temperature profiles during the polymerization runs were given. More recently, at Queen's University, Canada, Chung and Hsu (2002) described a stainless steel gas-phase polymerization reactor with

internal cooling coils and external electrical heating tapes for temperature control. It has been reported to control temperature to within  $\pm 0.5^\circ\text{C}$  but no temperature profiles during polymerization were given. Stirrers were used to agitate the catalyst bed in all these reactors.

As the polymerization catalysts are very sensitive to oxygen and moisture, they must be stored and handled in an inert atmosphere. Although dry glove-boxes are often used to store these catalysts, there are significant differences in the reported purity levels in these glove-boxes. For example, Jejelowo et al. (1991) found oxygen and moisture concentrations of about 2 ppm and 3 ppm respectively while Samson et al. (1999) reported concentrations that were less than 0.1 ppm for both. Another concern is the removal of the catalyst from the glove-box to the reactor. Although dry catalyst injection is the most suitable for gas-phase polymerization, problems with reproducibility arise with injection of small amounts of catalyst (Kunkeaw et al., 2003). Weickert et al. (1995) injected small quantities of catalyst into the reactor reliably as a suspension but the solvent needs to be removed by evacuation (Chung and Hsu, 2002) or purging (Samson et al., 1999). This can affect the acquisition of initial polymerization data and may also lead to loss of volatile Al alkyls (Samson et al., 1999).

Another concern during gas-phase polymerization is maintaining the concentration of the monomers. While for homopolymerization the ethylene concentration can be easily manipulated by controlling the total pressure in the reactor, for co-polymerization the concentration of the comonomer needs to be determined separately. Usually, the comonomer is added batchwise at the beginning of the polymerization run while the ethylene is fed continuously resulting in continuous

decrease in concentration of the comonomer during the run. This method can lead to variations in molar masses and composition with time of polymerization in the product polymer (Roscoe et al., 2000). One method to overcome this is to run the experiment for a very short time (Sun et al., 1994) on the assumption that the concentration of the comonomer will not change significantly during the interval. However, this method limits the freedom to run experiments for longer periods of time. Literature mentions the use of Fourier Transform Infra-Red (FTIR) Spectroscopy and Gas Chromatography (GC) to measure the concentration of monomers during polymerization. Han-Adebekun et al. (1997a) used FTIR spectroscopy in conjunction with running the reactor in “purge mode” to measure and control the composition of comonomer during polymerization. Liu (2002) used GC to determine the gas phase composition and estimated the amount of comonomer to inject during the polymerization run to maintain the composition based on GC readings from previous similar run in which the comonomer composition had been allowed to change.

## 2.6 In-Situ and Ex-Situ Observation of Particle Growth during Polymerization

With advances made in video-microscopy and electron microscopy techniques, literature cites methods for studying development of catalyst/polymer particles during polymerization. Oleshko et al. (2001) described in-situ video light-microscopy to study propylene polymerization using  $\text{TiCl}_4\text{-MgCl}_2$  Ziegler-Natta catalyst and used environmental transmission electron microscopy to further analyze the system (Oleshko et al., 2002). Initial nanoscale PP growth in the form of globules and continuous non-uniform polymer layers was observed. Zöllner and Reichert (2002) using video

microscopy to observe particle growth during polymerization in a mini-reactor found that individual catalyst particles start to polymerize under same conditions at different times. Temperature and pressure also influenced the particle activities. Further study of polymerizing catalyst particles in a mini-reactor using optical and infrared imaging by Pater et al. (2003) also found similar results. Further, the surface temperature of the individual particles determined by IR imaging depended on their sizes and polymerization rates and increased to a maximum before decreasing during the polymerization run. Knoke et al. (2003) studied growth of silica supported metallocene catalyst during polymerization using video-microscopy and observed formation of diffusion limiting polymer layer at the very onset of polymerization.

Steinmetz et al. (1997) used scanning electron microscopy (SEM) for ex-situ study of propylene growth on silica supported metallocene catalysts. Induction period observed at early polymerization stages were attributed to the formation of discrete polymer layer only on the outer surface of the catalyst particle. Further, the fragmentation of the catalyst particles during polymerization depended how the catalyst were prepared. Hong et al. (1998) also used SEM for ex-situ analysis of polyethylene particle growth during polymerization using metallocene catalysts supported on cross-linked polystyrene. Observation that fragmentation of the carrier only occurred in regions where the active species were present provided evidence that development of hydraulic forces by the growing polymer chain led to support breakup.

## 2.7 Effects of Polymerization Conditions

The activity of polymerization catalyst and product polymer properties not only depends on the catalyst types but also on condition and various operating parameters of the reactor such as pressure, temperature and concentration of scavengers and comonomers. In this last section of the literature review, effects of various parameters are covered.

### 2.7.1 Effects of Alkyl Aluminum

Alkyl aluminums have been used as cocatalysts for supported metallocene catalysts (Fink et al. (2000), Hlatky (2000), Pryzbyla et al. (1999), Ribeiro et al. (1997), Soga and Kaminaka (1993)) and as scavengers due to their very high affinity for moisture and oxygen. Thus any unreacted alkyl aluminum remaining in the reactor after scavenging will affect the catalyst activity and product polymer properties.

Kumkaew et al. (2002) reported that the activity and activity profiles of silica supported (*n*-BuCp)<sub>2</sub>ZrCl<sub>2</sub> catalyst was markedly influenced by the amount of TIBA added with increase in amounts of TIBA resulted in slower activation and broader activity profiles. Hammawa et al. (2004) found that the reduction in initial activity depended on Al:Zr ratio of the catalysts used and the type of alkyl aluminum used. The effectiveness of alkyl aluminums in inhibiting the initial polymerization activity followed the following trend: TEA > TIBA >> TNOA. Moreover, at high concentration of alkyl aluminum, formation of Lewis acid-base complex can render the metallocene inactive

(Barron, 2000). Thus an optimum amount of alkyl aluminum exists for a given polymerization run.

### 2.7.2 Effects of Polymerization Temperature

It has been found that increases in polymerization temperature increase the activity and reduce the time required to reach maximum activity (Chakravarti and Ray, 2001; Korber et al., 2001; Mortara, 2001; Xu et al., 2001; Wu et al., 1999; Hong et al., 1998a, Eskelinen and Seppälä, 1996; Pietikäinen and Seppälä, 1994). Moreover, there may be a large increase in activity as heterogeneous slurry polymerization system changes to homogenous solution polymerization system as the temperature rises due to decrease in diffusion limitations (Hong et al. 1998a). However, catalyst deactivation rates also increase with increases in temperature. This is probably due to the easier dissociation of the olefin-metallocene  $\pi$ -complex formed during polymerization (dos Santos et al., 2001) and possible dissociation of the MAO and release of TMA (Panchenko et al., 2001) with increase in temperature. Thus, there is an optimum polymerization temperature for a given catalytic system.

The polymerization temperature also affects the molar masses of the polymer. Generally the molar mass decreases with increase in temperature and the crystallinity increases. Meng et al. (1999) found that the molar masses of polymer made by supported metallocene catalysts were higher than that produced by unsupported catalyst and had a maximum at 50°C for the polymer made by the supported catalyst.

### 2.7.3 Effects of Ethylene Pressure

The monomer concentration in the amorphous part of the polymer surrounding the catalytic sites increase with increase in ethylene pressure. Samson et al. (1999) found that yield increases linearly with increase in pressure and from 5-10 bar the reaction is first order with respect to monomer concentration. However, at pressure greater than 20 bar deviations from this linearity occurs (Meier et al., 2001). At these high pressures and the corresponding high activities, it was speculated that catalyst particle temperature was much higher than the bulk temperature, which may have led to deactivation of the catalyst. Moreover, these deviations depended on the initial size of the catalyst particle with larger catalysts showing these deviations.

### 2.7.4 Effects of Comonomer

It is widely reported in literature that the presence of  $\alpha$ -olefin comonomers increases the activity of heterogeneous Ziegler-Natta and metallocene catalysts. This is known as the “comonomer effect”. This effect has been attributed to a number of reasons such as increase in monomer diffusivity through the copolymer due to decrease in crystallinity and molar mass of the polymer surrounding the active sites (Koivumäki and Seppälä, 1993, Chien and Nozaki, 1993), increase in fracturing rate of the catalyst (Wester and Ystenes, 1997), formation of new sites or reactivation of dormant ones (Pasquet and Spitz, 1993) and increase in propagation rate constant (Han et al., 1996). Laguna et al. (2003) found that the diffusion and permeability coefficients in polyolefin films increase with the temperature and comonomer contents in ethylene-1-hexene copolymers thus supporting the physical causes for the comonomer effect.

In homogeneous systems Chien and Nozaki (1993) found that addition of 1-hexene comonomer decreased the activity. This decrease was attributed to competition between 1-hexene and ethylene in  $\pi$ -complexation with the metallocene. However, Galland et al. (1999) observed that activity increased initially with increase in concentration of 1-hexene before decreasing in a homogeneous zirconocene system. The initial enhanced activity was attributed to higher solubility of the copolymer in the reaction medium allowing higher diffusion rates of the monomers onto the active sites. The lower activity at higher concentrations of 1-hexene was attributed to increase in comonomer content of the growing polymeric chain that led to a reduction in activity because of a decrease in propagation rate with the comonomer incorporation. Dos Santos et al. (2001) observed similar increase then decrease in activity with increase in concentration of the comonomer 1-hexene during ethylene polymerization using supported metallocene catalysts.

The crystallinity of the polymer is significantly reduced with even small amounts of comonomer incorporation as compared to ethylene homopolymer (dos Santos et al., 2001). Both the crystallinity and molar masses decrease monotonously with increases in comonomer content (Galland et al., 1999). The incorporation of comonomer in polymers produced by supported catalysts is less than that produced by the corresponding homogenous catalytic systems due to possible steric hindrance by the support surface reducing accessibility of the comonomer on to the active sites.

## 3. Reactor Design and Experimental Details

### 3.1 Gas Phase Polymerization Reactor System

The bulk of the research work consisted of preparation of supported metallocene catalysts, study of gas-phase polymerization of ethylene using these catalysts, and characterizations of the supports, catalysts and polyethylene resins produced. However, in view of the difficulties faced in controlling gas-phase temperature during polymerization, it was decided to build a novel gas-phase reactor with improved temperature control for carrying out the polymerization runs. The initial period of this research work therefore involved the fabrication and commissioning of the new reactor system; the reactor design, construction, and commissioning were done with another graduate student, Hassan Hammawa, of our group. In order to observe the growth of polymer particles during polymerization a micro-reactor with windows that can withstand normal gas-phase polymerization conditions was also built.

For catalyst preparation, both in-house and commercial organic supports were used. The surface area and pore volume measurements of these supports were determined using BET method. Scanning electron microscopy, SEM, was used to characterize visually the supports, catalysts and polymer particles. Energy dispersive X-ray spectroscopy, EDX, in combination with SEM was used to map the distribution of methylaluminoxane within the catalyst and polymer particles. Instrumental Neutron Activation Analysis, INAA was used to determine the zirconium and aluminum content of the catalysts. The product polyethylene resins were characterized using gel permeation

chromatography, GPC, also known as size exclusion chromatography, SEC, and by temperature rising elution fractionation, TREF, especially for copolymer resins.

### 3.1.1 Description of Novel Reactor System for Olefin Polymerization<sup>1</sup>

A 2-L reactor of 4.50-inch internal diameter and 5.75-inch external diameter, shown in Figure 3.1(A), was cut out of single cylindrical piece of type-316 stainless steel for integrity and robustness. The reactor had a torispherical bottom so that there were no sharp corners that could become dead spaces for solids. The reactor body was suspended from a top flange that also was fabricated from a single disk of type-316 stainless steel, shown in Figure 3.1 (B). The top flange was rigidly fixed to a support stand while the reactor body could be easily removed for cleaning. A Viton O-ring between the reactor body and the top flange ensured a leak-proof seal during operation when reactor body was tightly bolted to the top flange. The ports for feeding reactants, catalyst and co-catalyst into the reactor and venting or withdrawing gas from the reactor were concentrically arranged in the top flange as shown in Figure 3.1(B). These ports were drilled at an angle so that the valves and fittings at the top of these ports were pointing away from the central shaft and there was more space for ease of operability. The void volume of the assembled reactor was 2.27 L.

For the flow of heat transfer fluid 20, ¼ inch diameter channels were drilled through the wall of the reactor. These bores were distributed around the reactor as shown in Figures 3.1(A) and 3.2. As calculation indicated that the flows in these channels were

---

<sup>1</sup> Detailed description of the reactor system has been published; Mannan et al., *Canadian Journal of Chemical Engineering*, **82**, 371-381 (2004)

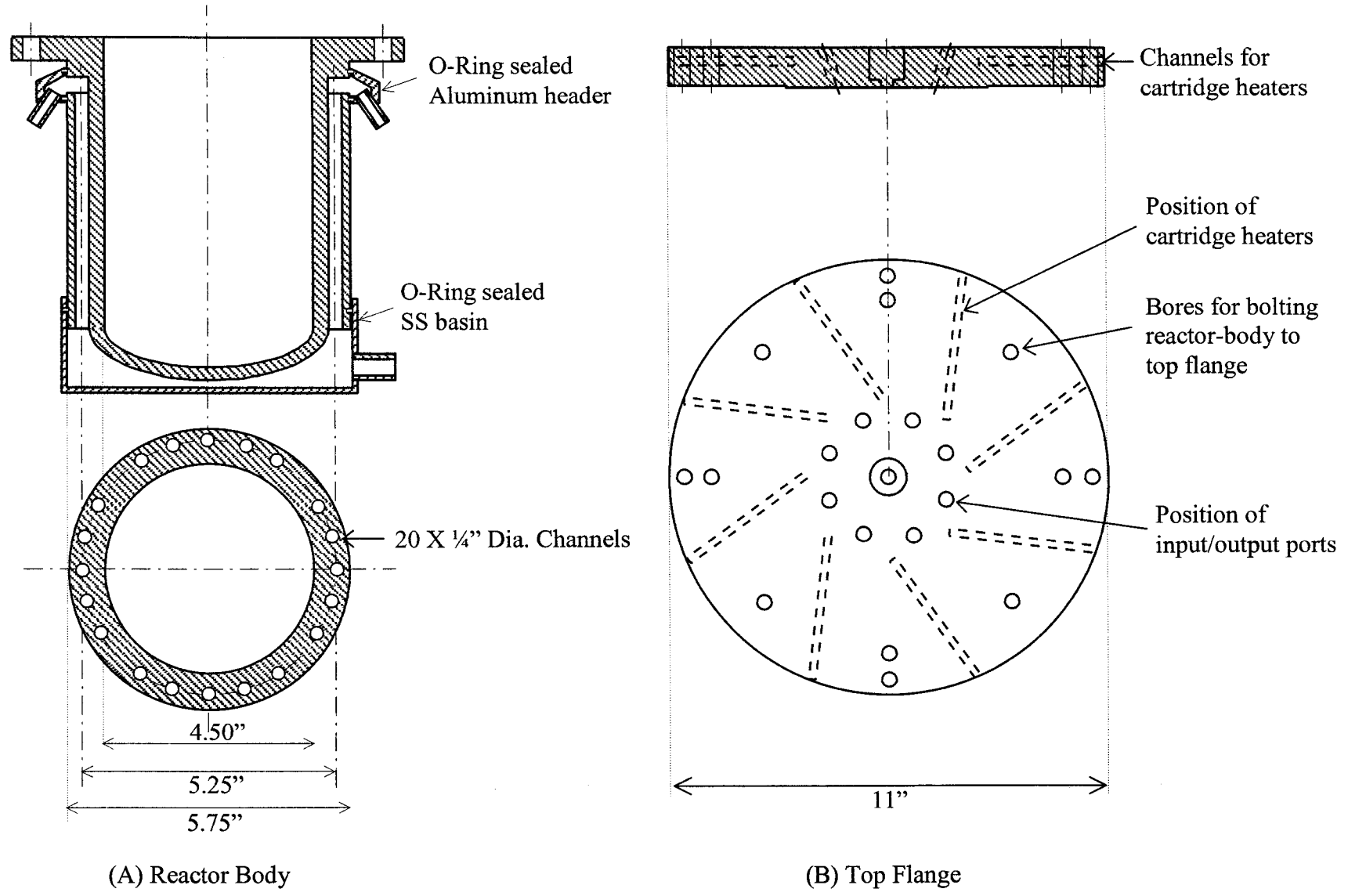


Figure 3.1 Schematic of Reactor Body and Top Flange Construction

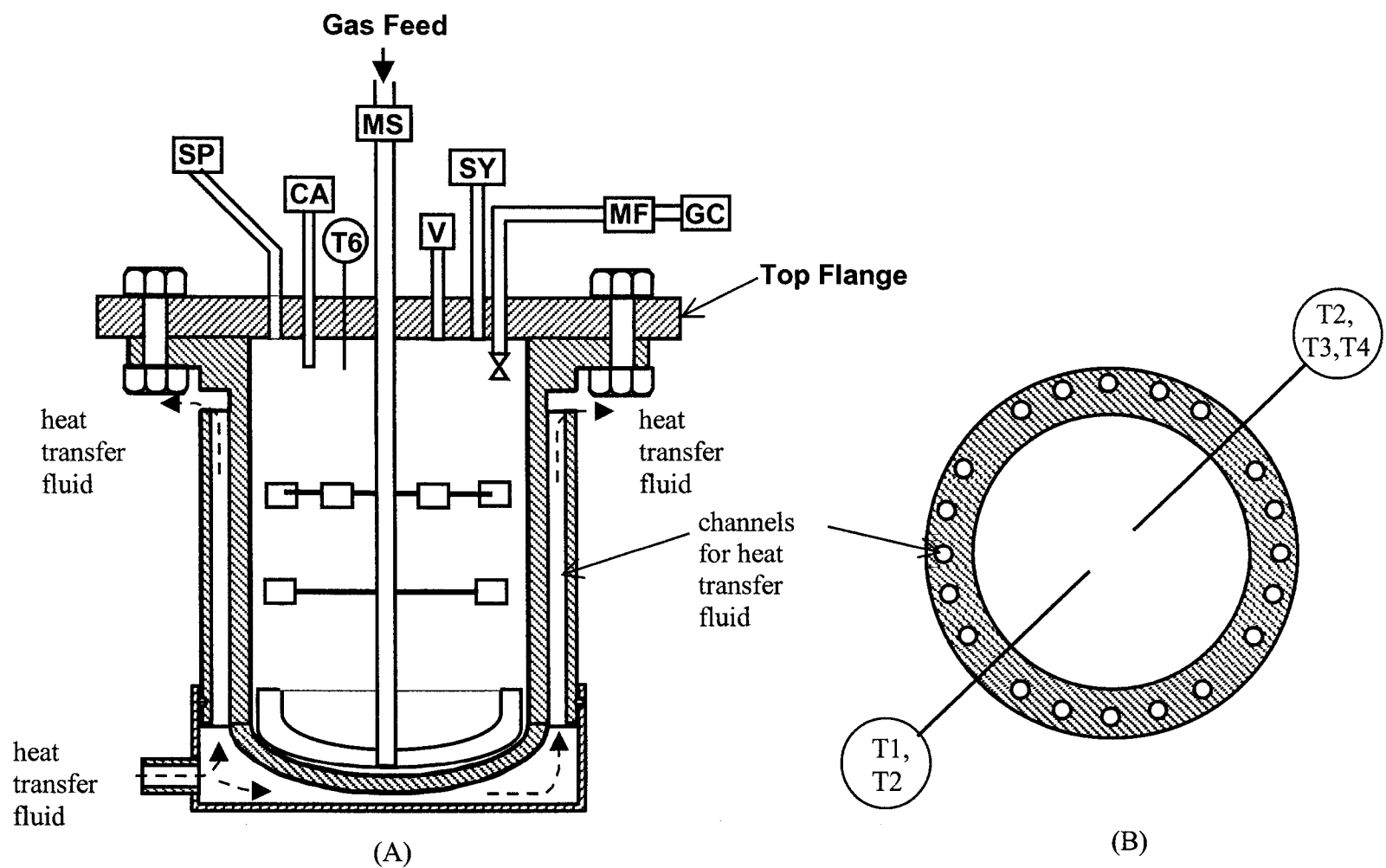


Figure 3.2. Schematic of Assembled Reactor: A) Radial Thermocouples not shown, B) Position of Radial Thermocouples (CA – catalyst injector; GC – gas chromatograph; MF – mass flow meter; MS – Magnedrive stirrer; SP – syringe pump; SY – syringe injection port;  $T_i$  – thermocouple  $i$  mounted as shown; V – vent)

in the laminar flow regimes, static mixers were later inserted to improve heat transfer from the reactor body to the fluid in the channels. These static mixers were custom built Kenics-type,  $\frac{1}{4}$  inch diameter, about 7.36 inch in length with an element length of 0.7 inch similar in design to those described by Pahl and Muschelknautz (1982). A stainless steel basin that was clamped to the bottom of the reactor body acted as a distributor for the channels as shown in Figures 3.1 and 3.2. The channels drained into an aluminum header that was clamped to the top of the reactor.

The top flange was heated by eight electrical cartridge heaters that were embedded in the flange as shown in Figure 3.1(B). Omega cartridge heaters,  $\frac{1}{4}$  inch diameter and 3.5 inch long (Model Number CSH-10350/120) were used. An independent temperature controller (Omron E5CK digital controller) was used to control the temperature of the top flange at the desired set point. This provides flexibility of use as the flange temperature could then be set at different value from that of the reactor.

Temperatures at various locations in the reactor were measured by eight thermocouples. Stainless steel sheathed  $\frac{1}{8}$  inch Type J thermocouples were used. Six thermocouples inside the reactor located as shown in Figures 3.2 and 3.3 were used to measure the gas phase temperature at different positions. This is important as the gas temperature can vary considerably with locations inside the reactor as reported by Lynch and Wanke (1991). Of the remaining two thermocouples one was used to measure the top flange temperature while the other was used to measure the temperature of the heat transfer fluid entering the feeder basin.

To ensure good mixing of the gases within the reactor a magnetically driven stirrer (Autoclave Engineers Magnedrive), driven by a variable speed DC motor was

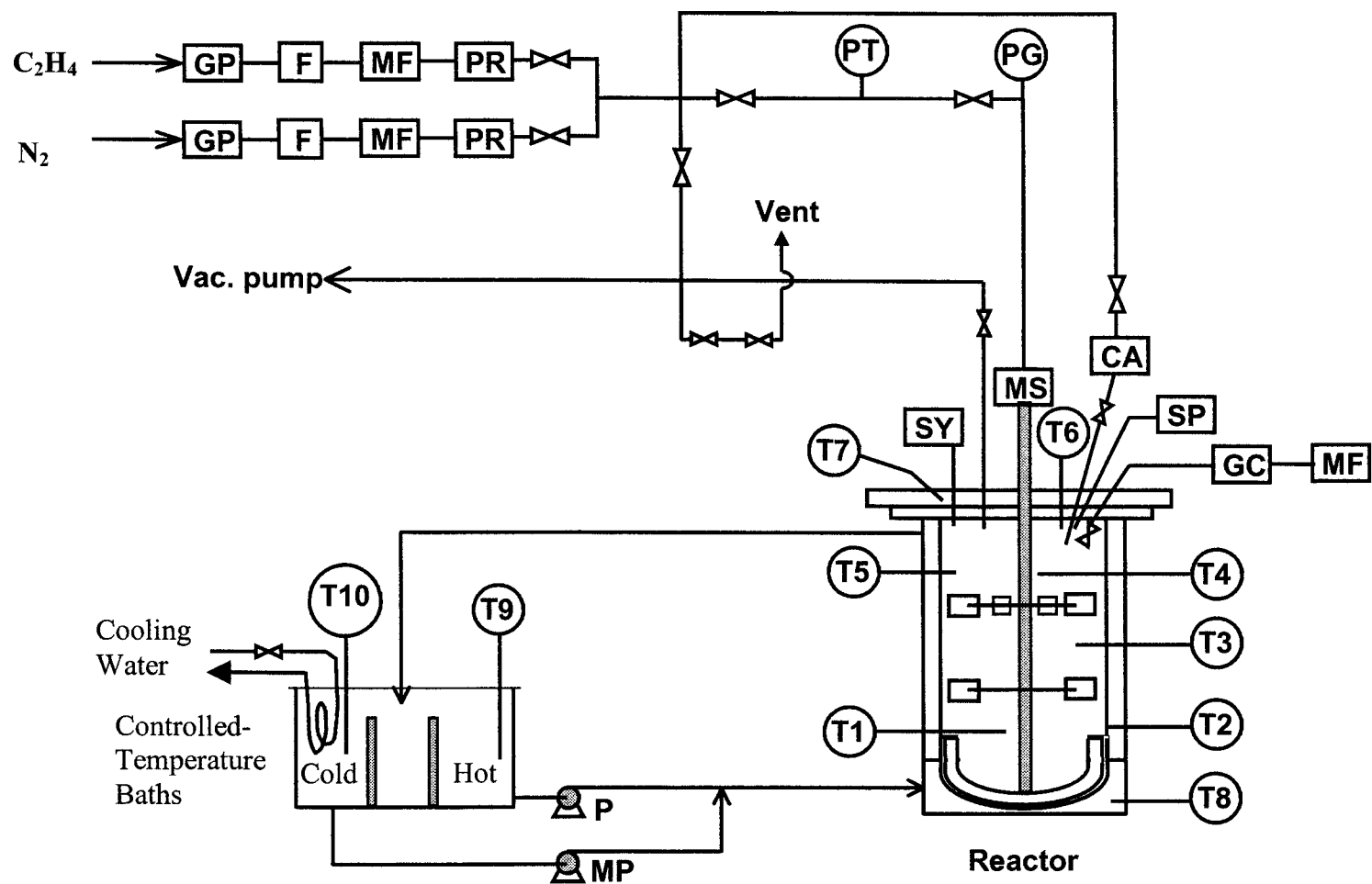


Figure 3.3. Schematic of Reactor System. (CA – catalyst injector; GC – gas chromatograph; GP – gas purifiers; F – filter 7  $\mu\text{m}$ ; MF – mass flow meter; MP – metering pump; MS – Magnedrive stirrer; P – centrifugal pump; PG – pressure gauge; PR – pressure regulator; PT – pressure transducer; SP – syringe pump; SY – syringe injection port;  $T_i$  – thermocouple  $i$  mounted as in figure 2; V – vent)

used. Various types of stirrers were evaluated. Using visual observation of polymer particles stirred in a Plexiglas replica of the reactor, the efficacy of these stirrers at different rotational speeds in agitating the solid particles was determined. The final configuration consisted of a pitched anchor-type stirrer attached to the bottom of the stirrer shaft and two variable-angle paddle-type stirring vanes attached towards the middle and top of the stirring shaft as shown in Figures 3.2, 3.3, and 3.4 (A). In Figure 3.4(B) photograph of the impellers in action in the Plexiglas replica of the reactor is shown. At stirrer speed above 300 rpm good mixing of solids was obtained with this configuration.

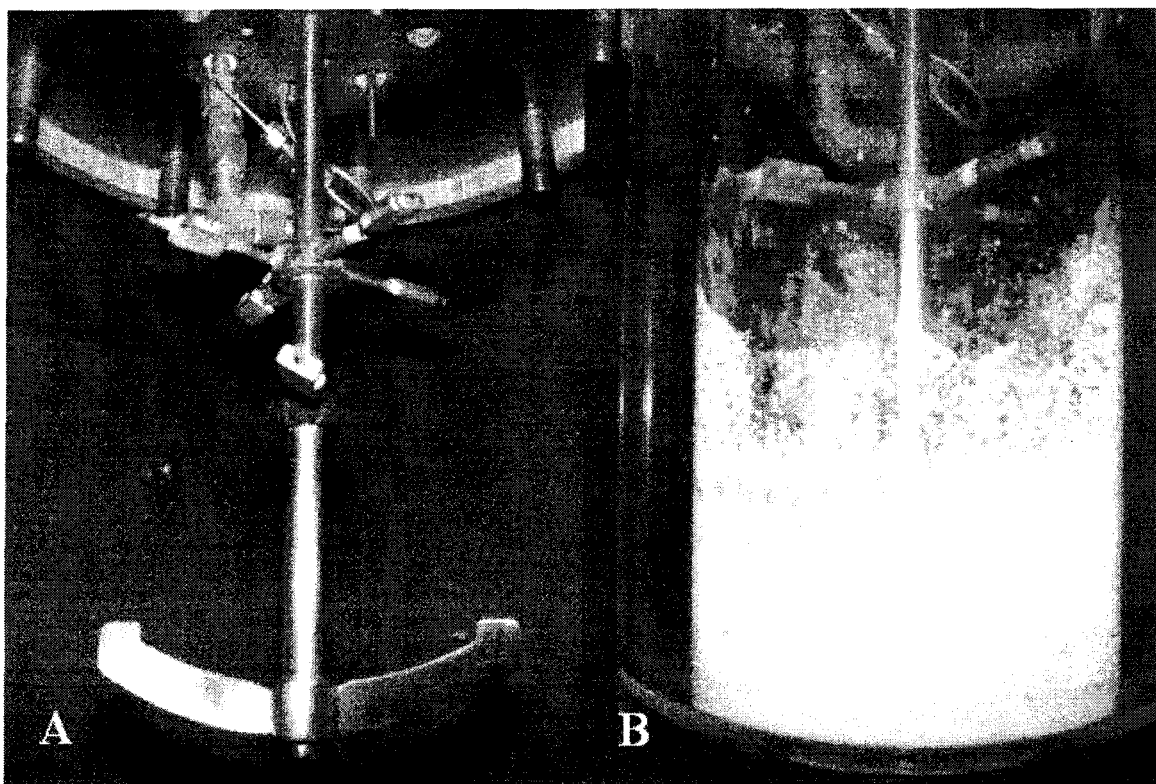


Figure 3.4: Photographs of (A) the impeller system and (B) impellers in action inside Plexiglas replica of reactor.

To minimize impurities from entering the reactor with the feed gases, gas purification trains consisting of Alltech High-Pressure Oxy-Traps and Gas-Drier columns and 7  $\mu\text{m}$  stainless steel filters (Swagelok, F-series) in series were used. Pressure regulators were used to control the flow of gases into the reactor. Ultra High Purity (UHP) Nitrogen from Praxair and Polymer Grade (PG) Ethylene from Praxair and Matheson were used for the experiments. The ethylene flow rate, regulated by a Tescom Non-Venting regulator, to the reactor was such that the pressure in the reactor remained constant at the preset value, usually about 200 psia (1.4 MPa) during polymerizations. For copolymerization runs an ISCO Model 500D high-pressure syringe pump was used to feed liquid 1-hexene into the reactor. This Polymer Grade 1-hexene was donated by NOVA Chemicals and used without further purification.

The catalyst holder/injector was made from two sets of stainless steel male and female Swagelok quick-connects with a Swagelok plug valve in-between. An airtight space was formed by closing the valves and connecting the two sets together. The whole assembly could easily be connected to the reactor system or removed and be loaded with catalyst inside a glove-box. This ensured that the catalyst did not come in contact with atmospheric oxygen or moisture during transfer from the glove-box to the reactor.

The temperature in the reactor was controlled by the flow of silicone oil (Dow Corning 200 Fluid, 50 centistokes) through the channels in the reactor wall. The temperature of the oil entering the channels in the reactor was controlled by mixing proportioned amounts of hot and cold silicone oil prior to the entry of the oil to the bottom of the reactor (see Figure 3.3 for flow circuit of silicone oil). The flow rate of the hot oil was usually constant at about 4 L/min. However, this flow rate could be varied

manually if required. The flow rate of the cold silicone oil was varied by a variable-speed metering-pump (Micropump Inc. Series 2200 magnetic drive gear pump, Model GD-M35 PVSE close-coupled to 0.5 hp, DC TEFC motor with a 4-20 mA remote signal speed control, Penta KB Power, Model KBPC-240D). A Personal Computer running a LabVIEW based PID controller program was used to control the speed of the metering pump; the output from Thermocouple 1 was the input to the PID controller. The flow varied from 0 L/min, for runs without PID temperature control, to as high as 8 L/min. Even at such high flow rates, the Reynolds numbers in the empty channels were less than 100; thus necessitating the insertion of the static mixers into the channels to improve heat transfer.

A modified Neslab high temperature bath (Model EX-251HT) was used as reservoirs for the hot and cold silicone oil. A 5.8 L insulated rectangular container was placed at one end of the 25 L cavity in the high-temperature bath; the top of the container was 55 mm lower than the top of the bath. The remaining space in the bath was divided into two compartments by the insertion of a 25 mm thick insulating divider; the central space, used as the return vessel of the silicone oil, had a volume of about 3.8 L. The other space, which had a volume of about 11 L, was the reservoir for the hot silicone oil. The fluid returning from the reactor flowed into the central space and overflowed from this compartment into the adjacent hot and cold fluid compartments. The hot fluid temperature was maintained at the desired level by the original heater-controller system of the Neslab temperature bath. For this research work the hot fluid temperature ranged from 70 to 110°C. The cold fluid reservoir was cooled with chilled water flowing through a cooling coil immersed in this compartment. The temperature of the cold fluid was

controlled with a 1.1 kW MGW Lauda immersion heater controller system (Type MS # G08019). The cold fluid temperature was between 50 and 65°C for most of the experiments performed.

The program used for reactor temperature control was also used for data acquisition. An OPTO 22 system with Analog/Digital converters was used to interface the thermocouples, flow meters and a PSI-Tronix pressure transmitter to the PC. The LabVIEW program was used to monitor 15 process variables (10 thermocouple readings, 3 flow measurements, 1 pressure reading and time) and logged them to an EXCEL file. When running the program, all process and control parameters were displayed in the LabVIEW front panel in real time and all data were logged and plotted in EXCEL simultaneously. The data log rate and reactor temperature set point could be altered from the LabVIEW control panel at any time during a run. Plotted data from a typical copolymerization run showing some of the recorded information is shown in Figure 3.5 as an example.

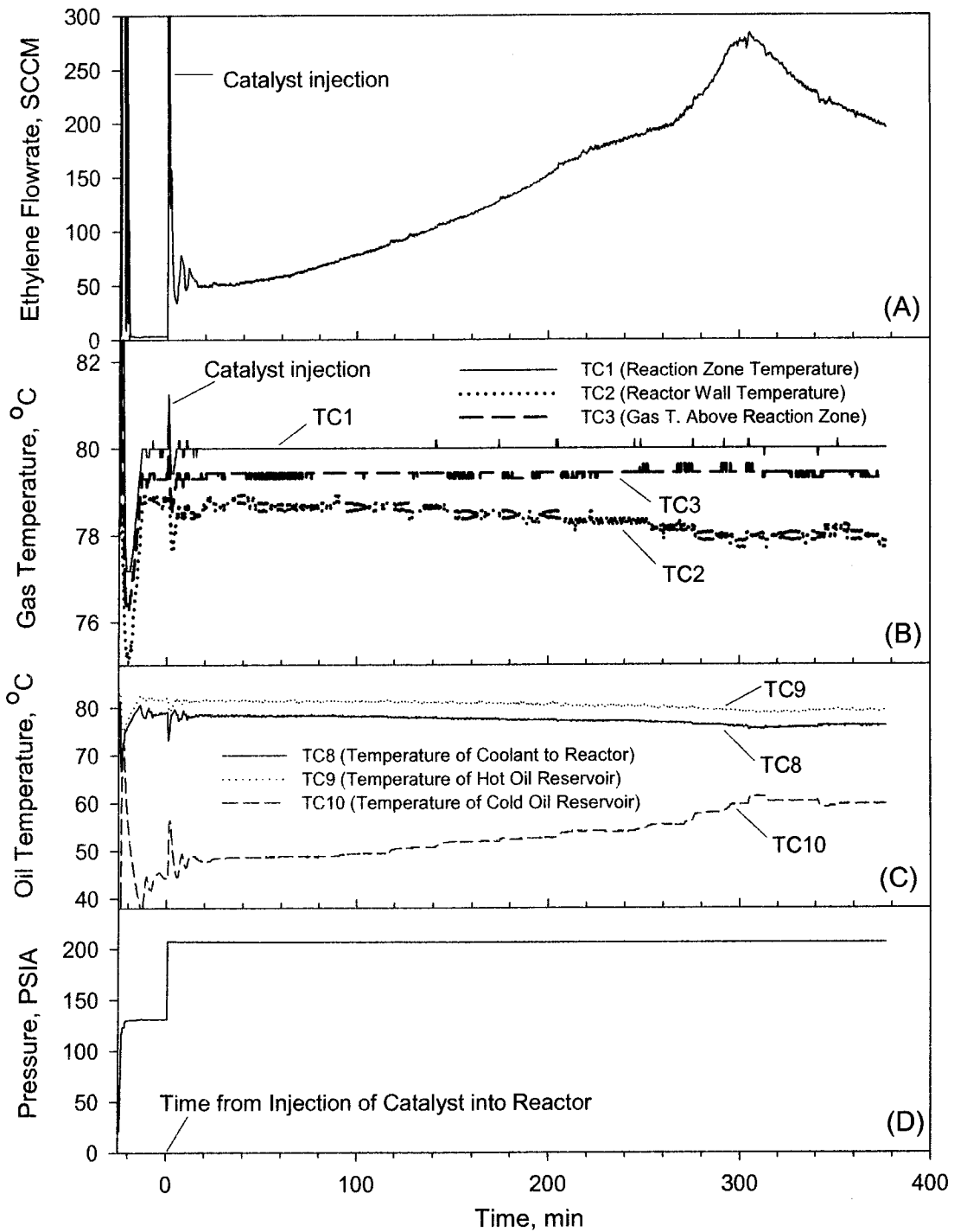


Figure 3.5: Data gathered during a typical polymerization run shown graphically giving (A) ethylene flowrate into reactor, (B) temperature at different locations in the reactor, (C) circulating coolant oil temperature at different locations, and (D) reactor gas pressure.

### 3.1.2 The Gas-Phase Analysis System

The composition of the gas phase in the reactor was determined by gas chromatography. A Hewlett Packard 5890 Series II gas chromatograph equipped with a 6-port gas sample valve, a flame ionization detector and a thermal conductivity detector was used for the analyses. The flame ionization detector was used to determine ethylene/1-hexene ratios and the thermal conductivity detector was used for the determination of hydrogen concentrations. A 3.2 mm (1/8 in) diameter and 0.9 m long column packed with 80/100 mesh (180-150  $\mu\text{m}$ ) HayeSep-Q porous polymer was used for the separation of ethylene and 1-hexene. The column was operated isothermally at 185°C with an argon carrier flow rate of 30  $\text{cm}^3$  (STP)/min. The retention times of ethylene and 1-hexene were 0.20 and 2.0 min, respectively. For hydrogen analysis the same column was also used at 35°C isothermal operation with an argon carrier flow rate of 30  $\text{cm}^3$  (STP)/min. The retention times of hydrogen and ethylene were 0.15 and 1.22 min, respectively.

Gas samples were withdrawn continuously from the reactor at a rate of 4 to 10  $\text{cm}^3$  (STP)/min; the flow rate was measured by a mass flow meter located downstream from the gas sampling valve. The flow rate of the gas-sample stream was kept low to avoid changes to the gas-phase composition due to gas withdrawal. The total amount of gas withdrawn from the reactor at a gas withdrawal rate of 5  $\text{cm}^3$  (STP)/min was less than 2% of the initial reactor contents for a 60 min run at a total pressure of 200 psia (1.4 MPa). However, low gas sampling rates can introduce significant delay times in sensing changes in composition if the volume between the reactor and the gas chromatograph is significant. The valve, and any connecting tubing from the reactor to this valve, in which

the pressure is dropped from the reactor pressure to the atmospheric pressure in the gas-sampling valve of the chromatograph can be a major source of delay time. For example, it takes over 2 min for a gas sample to reach the gas-sampling valve from the reactor at a sampling rate of 5 cm<sup>3</sup> (STP)/min if the pressure-drop valve and connecting tubing has a volume of 1 cm<sup>3</sup> and is filled with reactor gas at 1.4 MPa. A zero-volume pressure drop valve was installed inside the reactor below the top flange to eliminate this delay. This valve consisted of a modified Nupro SS-SS2 metering valve whose inlet half up to the valve seat had been cut away. With this arrangement, the pressure drop from reactor pressure to sampling pressure occurred inside the reactor without any time delay (zero dead volume on the high pressure side). Dropping the pressure inside the reactor, at reactor temperature, also decreased the chance of 1-hexene condensing in the sampling line. The pressure drop valve inside the reactor was connected to an external shut-off valve by a 200 mm long 3.2 mm (1/8 in) diameter stainless steel tube. An 860 mm long piece of Teflon tubing (0.5 mm inside diameter) connected the shut-off valve and the sampling valve in the gas chromatograph. This arrangement resulted in a sampling delay of less than 1 min for a 5 cm<sup>3</sup> (STP)/min gas-sampling flow rate. The use of stainless steel in the sampling line was minimized by the use of Teflon lines because prior experience has shown that olefin adsorption/ desorption on stainless steel can introduce time delays in the analysis. The stainless steel and Teflon lines between the reactor and the gas chromatograph were heated to 80°C to further ensure that condensation of 1-hexene did not occur and that adsorption on the stainless steel tubing was reduced.

### 3.2 Micro-Reactor for Observation of Polymer Growth

To observe the catalyst particle during polymerization a simple micro-reactor was built from a 3/4 inch Swagelok Union Tee. Two 1/8 in thick Pyrex discs each sandwiched between an O-ring and Teflon spacer act as windows to this reactor as shown in Figure 3.6 and were used to seal the two opposite ends of the Union Tee; a Swagelok Plug Valve was connected to the third end. This valve was connected to a port in the main reactor by stainless steel tubing and gases from the main reactor entered the micro-reactor through it. The whole assembly can be easily removed and loaded with catalyst inside the glove box. Heating tape was used to keep the mini-reactor at the desired temperature. A microscope video camera was used to record the growing particles during polymerization.

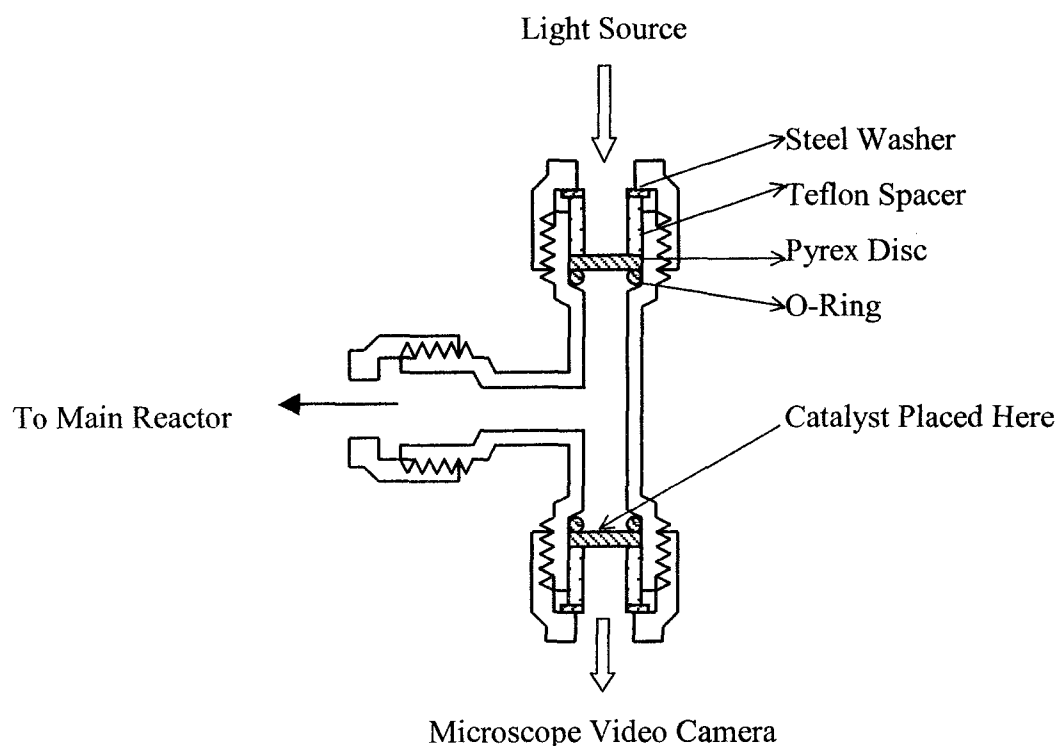


Figure 3.6 Schematic of Micro-Reactor

### 3.3 Catalyst Preparation

Catalyst Supports: For preparation of supported catalysts both in-house and commercial porous, spherical polymeric particles were used. The in-house supports were prepared in our laboratories by suspension polymerization as described by Li and Mazid (1992) and Zhou et al. (2003). Essentially, the porous particles were made from polymerization of 2-hydroxyethyl methacrylate (HEMA) and divinyl benzene (DVB) and contained both macropores and micropores. The commercial supports consisted of different size ranges of HayeSep-R and HayeSep-Q porous particles. These are polymers of divinyl benzene and *n*-vinyl-2-pyrrolidinone.

A method of indirect heterogenation (Kaminsky et al., 1999) together with activation of the metallocene before precipitation that has been found to least effect the homogeneous nature of metallocene/aluminoxane catalytic system (Arrowsmith et al., 2001) was chosen for preparing the supported catalysts. The preparation procedure is similar to that described by Zhou et al. (2003). A typical catalyst was prepared as follows. About 2 g of support was placed in a 250 mL three-necked round bottom flask and evacuated overnight at 65 to 75°C. The support was wetted with 5 mL of anhydrous toluene under nitrogen followed by the slow addition of 20 mL of 10 mass % methyl aluminoxane (MAO) in toluene. The slurry was shaken with a Thermolyne Maxi-Mix III shaker (Fisher Scientific) at room temperature from this addition to the end of the preparation. After two hours about 40 mg of bis-*n*-butyl cyclopentadienyl zirconocene dichloride, (*n*-BuCp)<sub>2</sub>ZrCl<sub>2</sub> which had been loaded in a Schlenk tube in the glove-box and sealed was dissolved in 5 mL of anhydrous toluene and the solution was slowly added to the slurry. The tube was further washed with 5 mL of anhydrous toluene and the

washing was added to the slurry. After two hours the toluene was removed by evaporation under vacuum at room temperature. The free flowing dry supported catalyst in the flask was then transferred under vacuum to the glove-box for storage. NOVA Chemicals donated the zirconocene while the toluene and MAO were bought from Aldrich Canada and used without further purification.

### 3.4 Polymerization Procedure

The supported catalysts produced were used for both homo-polymerization and co-polymerization experiments. To perform an experiment the reactor was prepared from the previous day. The reactor was first cleaned and loaded with a sodium chloride seed bed, usually 80 g of 0.4 mm NaCl crystals from Fisher Scientific. The reactor was then evacuated overnight at 90 – 100°C to remove moisture and oxygen. To reduce further the amount of adsorbed oxygen or moisture in the reactor a chemical scavenger was injected into the reactor prior to catalyst injection into it. Usually tri-isobutyl aluminum, TIBA, or tri-ethyl aluminum, TEA, and for a few runs MAO solution in toluene was used. Two types of runs were done: in one type, Type A the scavenger would be vented and reactor evacuated so that only trace amount of the scavenger remained in the reactor during polymerization, and in the other type, Type B the scavenger would remain in the reactor during polymerization. Depending on the type of run, the general procedure was as follows:

1. The heated evacuated reactor and connecting feed lines was filled with UHP nitrogen to 0.3 MPa (50 psia).

2. The catalyst injector, which had been loaded with catalyst in the glove-box was then connected to the reactor under flowing nitrogen. For Type A runs, the scavenger was injected into the reactor at this point and the reactor was stirred for 20 – 30 minutes; while for Type B runs it was injected later.
3. The reactor pressure was raised to 0.7 MPa (100 psia) with the nitrogen and then vented to atmospheric pressure. For Type A runs this was repeated. The reactor was then evacuated to less than 3 Pa while cooling it to the required reaction temperature.
4. Ethylene was then introduced into the reactor. For Type B runs the pressure was raised to 0.1 MPa (20 psia) and the scavenger was injected into the reactor with a 0.5 mL gas-tight (Hamilton) syringe. Ethylene pressure was raised to 0.7 MPa (100 psia). For Type B runs, scavenging was then done for 20 - 30 minutes. For co-polymerization with 1-hexene, desired amount of liquid 1-hexene was injected into the reactor at this point. The reactor pressure was raised to 1.0 MPa (150 psia) with ethylene.
5. The feed lines pressure was then raised to the desired polymerization pressure, usually 1.4 MPa (200 psia) (only the lines and not the reactor were pressurized in this step).
6. The catalyst in the holder was forced into the reactor under pressure and reactor pressure was raised to the desired polymerization pressure.
7. Ethylene was continuously fed to the reactor to maintain the total reactor pressure at the desired value. To maintain constant gas-phase composition 1-hexene can also be fed into the reactor continuously during co-polymerization using the

syringe pump. But for most runs the 1-hexene was only injected at the beginning of the run.

8. After a desired length of time the reactor was vented to atmospheric pressure and rapidly cooled to terminate polymerization. The reactor was repressurized to 0.7 MPa (100 psia) with nitrogen and then vented to atmospheric pressure, twice to ensure that only trace amount of 1-hexene or scavenger remains with the polymer product.
9. The product polymer was washed repeatedly with water to remove the salt. The product was finally dried overnight in an oven and weighed. The bulk density of the product was then measured according to the ASTM D 1895-96 procedure.

### 3.5 Characterization of Supports, Catalysts, and Products

#### 3.5.1 Surface Area Determination

Nitrogen sorption measurements at 77 K with an Omnisorp 360 sorptometer (Miami Lakes, FL) were used to determine the porous support surface areas using the Brunauer, Emmett and Teller (BET) method. The desorption branch of the nitrogen physisorption isotherm was used to obtain pore size distribution and pore volumes with the Barrett-Joyner-Halenda method as described by Gregg and Sing (1982). Before each analysis the samples were outgassed at 398 K for at least 4 hours in vacuum.

#### 3.5.2 Scanning Electron Microscopy

The morphologies of the porous supports, catalysts, and product polyethylene particles were examined with a Hitachi S-2700 scanning electron microscope (SEM). Representative samples were first selected and placed on specimen stubs. Some catalyst and polymer particles were cut with a scalpel so as to see the internal structures. The samples were coated with carbon under vacuum by high temperature evaporation then sputter coated with gold to improve conductivity. In most cases a Secondary Electron (SE) detector was used to image the particle morphologies and the images were stored in digital format. The SEM was operated at 10 keV and low beam current to reduce charging. The SEM is also equipped with a back scattered electron (BSE) detector and an energy dispersive X-ray (EDX) spectrometer. EDX spectroscopy was used to map the distribution of aluminum in some of the cut catalyst and polymer particles. The concentration of zirconium was below the detection level of the instrument.

### 3.5.3 Instrumental Neutron Activation Analysis

Instrumental neutron activation analysis (NAA) was used to determine quantitatively the aluminum and zirconium concentrations in samples of the catalysts. These analyses were done at the University of Alberta Slowpoke Reactor facility. The samples were first irradiated in the Slowpoke reactor to produce radioactive isotopes. The decay rates of these isotopes were used to calculate the amount of Al and Zr in the samples.

### 3.5.4 Molar Masses of Polymer Products

The molar masses and polydispersities of the product polyethylene resins were measured by gel permeation chromatography (GPC) or size exclusion chromatography (SEC) with an Alliance GPCV2000 equipped with three HT6E columns from Waters Corp. (Milford, MA). The detectors and columns were maintained at 145°C and high performance liquid chromatography (HPLC) grade 1,2,4-trichlorobenzene (TCB) from Fisher Scientific was pumped at 1.0 cm<sup>3</sup>/min. 0.25 g/L of the antioxidant 2,6-tert-butyl-4-methylphenol from Sigma-Aldrich had been added to the TCB. Polyethylene samples that had been dissolved in TCB at concentrations of 0.5 to 0.7 mg/mL were used for molar mass determination. Polystyrene standards (from TSK Standards), linear paraffins (C20, C40, and C60) and polyethylene reference materials 1482, 1483, and 1484 from NIST were used for calibration. Each analysis was repeated and the average values of two or more analyses are reported as linear PE equivalent molar masses.

### 3.5.5 Temperature Rising Elution Fractionation

Temperature rising elution fractionation, TREF, is a method capable of analyzing short chain branching distribution, SCBD, in a polymer and is especially useful for characterizing  $\alpha$ -olefin/ethylene copolymers. This is based on the facts that higher the degree of crystallinity the higher is the dissolution temperature of the polymer and the degree of crystallinity is strongly dependent on SCBD.

A custom built apparatus described previously by Lacombe (1995) and Zhang (1999) was used for TREF analyses of polymer samples. The polymer samples to be analyzed were prepared as follows:

- 1) Each sample weighing between 5 to 10 mg was placed in a glass vial and about 1.5 g of glass beads (80-100 mesh) and a Teflon-coated magnetic stirrer bar were added to it.
- 2) The vials were sealed after o-xylene has been added to form a solute concentration of 0.001 g-PE/mL solvent in each.
- 3) The vials were slowly heated to 125°C while being stirred continuously and maintained at this temperature for 2 h to ensure that the samples were dissolved.
- 4) The vials were transferred to a temperature-controlled bath where they were maintained at 125°C for further 2 h without stirring before being cooled at 1.5°C/h to -8°C. The slow cooling ensures that the polymer precipitates according to its crystallinity. The samples were then stored in a freezer at -19°C until the TREF analyses.

During analysis the crystallized sample was transferred carefully from the vial to the TREF column, a stainless steel tube with inside diameter of 9.5 mm and length of

63.5 mm and Swagelok fittings at both ends with an inlet filter having 10  $\mu\text{m}$  pore size and outlet filter having 5  $\mu\text{m}$  pore size. The column was attached to the TREF apparatus that was at 0°C. O-dichlorobenzene solvent was pumped through the column at a constant flow rate of 1.0 mL/min while the sample was heated at 1°C/min from 0°C to 125°C. The PE molecules eluted with the solvent at different temperature according to their crystallinity, the molecules with higher short chain branching having lower crystallinity eluting at lower temperature. An on-line IR detector tuned at 2859  $\text{cm}^{-1}$  was used to detect the polymer concentration coming out of the column.

## 4. Supports and Catalysts

Since the discovery of the metallocene-methylaluminoxane system for olefin catalysis by Sinn and Kaminsky, much work has been done on homogeneous metallocene catalyst systems. These very high activity catalyst systems produce polymers with high molecular weights having a narrow molecular weight distribution and homogeneous chemical composition (Ribeiro et al., 1997). However, in order for the metallocene catalyst systems to be used for large-scale industrial production of poly-olefins they need to be heterogenized for drop-in replacement in a slurry or gas-phase plants (Chien, 1999). Although inorganic supports, such as silica have been widely used to heterogenize metallocene catalysts (Hlatky, 2000), only few studies on organic support have been reported in literature. However, organic supports have a number of advantages including providing a more homogeneous environment to the metallocene catalysts and not leaving inorganic residue in the polymer (Meng et al., 1999); hence, organic supports should be explored.

In this work, in-house and commercial organic supports were used to make twenty-two batches of supported zirconocene catalysts. A method of indirect heterogenization (Kaminsky et al., 1999) together with activation of the metallocene before precipitation was used to fix the metallocene onto the support as described previously because the chemical nature of the metallocene is least changed by this method (Arrowsmith et al., 2001). The catalysts had high activities and produced free flowing polymer particles that replicated the support shapes and did not foul the reactor.

#### 4.1 Supports Used for Catalyst Preparation

The porous organic supports used for catalyst preparation can be divided into two groups: in-house and commercial. Four of the in-house supports that were polymers of 2-hydroxyethyl methacrylate (HEMA) and divinyl benzene (DVB) had particle size range between 53 to 400  $\mu\text{m}$ . Polymer particles of size 5  $\mu\text{m}$  made from polystyrene (PS) and DVB were also used as a support. These in-house supports were prepared by suspension polymerization as described by Li and Mazid (2003) and Zhou et al. (2003) in our laboratories. The commercial supports, HayeSep (HS) porous polymers, were polymers of DVB and *n*-vinyl-2-pyrrolidinone (NVP) (HS-R) and DVB alone (HS-Q) and had been obtained from Mandel Scientific Company LTD, Guelph, Ontario, Canada. These spherical supports ranged in particle sizes from 75 to 850  $\mu\text{m}$ . Details regarding the supports are given in Table 4-1.

Optical microscope and scanning electron microscope (SEM) imaging showed that both the commercial and in-house supports mainly consisted of uniform spherical particles of diameters within the specified size ranges. Typical SEM images of some supports are shown in Figure 4.1. The smaller supports had more uniform shapes and narrower size distribution than the larger support particles. Nitrogen sorption measurements at 77 K indicate that the supports had specific surface areas of the order of 600 to 800  $\text{m}^2/\text{g}$  and specific pore volumes of 1 to 2  $\text{cm}^3/\text{g}$ . The smaller supports usually tended to have larger specific areas and pore volumes (see Table 4.1). The supports contained both micro- and meso-pores with the most of the pore volume in the pore size range of 1-20 nm. The porous nature of the supports ensured that the aluminum and

zirconium were distributed throughout each catalyst particle. Further information regarding the supports is given in Appendix A, Table A3.

Table 4.1: Description of supports used for making catalysts

Support Designation	Source	Composition of Support*	Particle Diameter, $\mu\text{m}$	Surface Area, $\text{m}^2/\text{g}$	Pore Volume, $\text{cm}^3/\text{g}$
60HEMA-1	Inhouse	Poly(HEMA/DVB)	78-200	300**	0.73**
60HEMA-2	Inhouse	Poly(HEMA/DVB)	53-74	48	0.18
60HEMA-3	Inhouse	Poly(HEMA/DVB)	78-200	276	0.65
60HEMA-4	Inhouse	Poly(HEMA/DVB)	200-400	168	0.43
PS/DVB-1	Inhouse	Poly(Styrene/DVB)	~5	840	1.80
HS-Q-1	Commercial	Poly(DVB)	150-180	641	0.75
HS-R-1	Commercial	Poly(DVB/NVP)	600-850	584	1.01
HS-R-2	Commercial	Poly(DVB/NVP)	250-300	619	1.07
HS-R-3	Commercial	Poly(DVB/NVP)	180-250	656	1.05
HS-R-5	Commercial	Poly(DVB/NVP)	125-150	696	1.08
HS-R-6	Commercial	Poly(DVB/NVP)	75-90	715	1.12

\* HEMA: 2-hydroxyethylmethacrylate, 60 mass% initial monomer mix;  
DVB: divinyl benzene;  
NVP: *n*-vinyl-2-pyrrolidinone.

\*\* Estimated values as insufficient amount of support remained to perform BET analysis

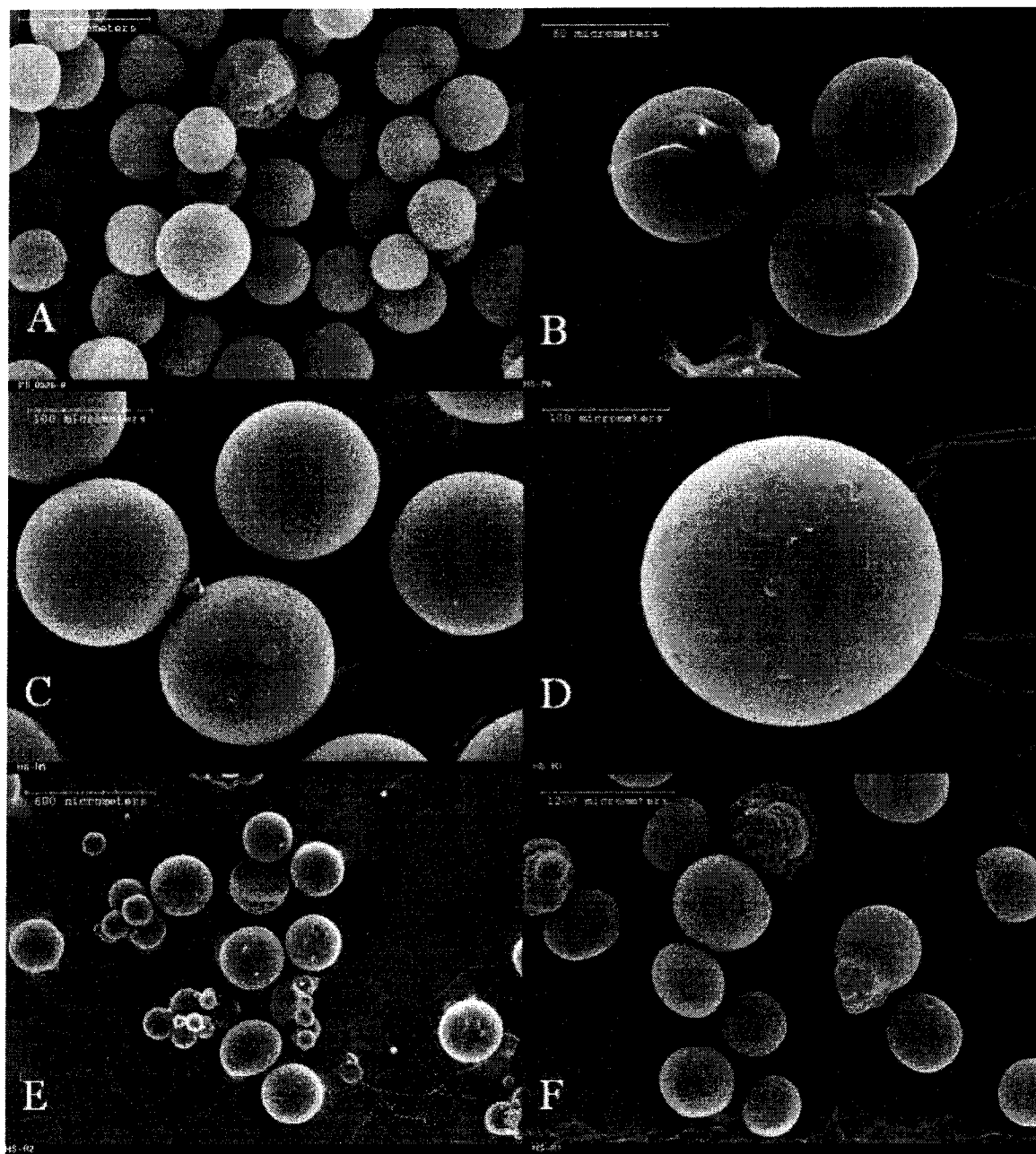


Figure 4.1: SEM images of supports of different sizes used for catalyst preparation – (A) 5  $\mu\text{m}$  PS/DVB-1; (B) 75-90  $\mu\text{m}$  HS-R6; (C) 125-150  $\mu\text{m}$  HS-R5; (D) 180-250  $\mu\text{m}$  HS-R3; (E) 250-300  $\mu\text{m}$  HS-R2; and (F) 600-850  $\mu\text{m}$  HS-R1

## 4.2 Prepared Supported Catalysts

Catalysts were prepared by first contacting the supports with MAO solution in toluene, followed by the addition of the bis(*n*-butylcyclopentadienyl)zirconium dichloride solution in toluene, and then drying the catalyst in vacuo as described previously. Table 4.2 below lists the catalyst batches made and their aluminum and zirconium concentrations determined by instrumental neutron activation analysis, INAA.

Table 4.2 Catalysts Batches and their composition

Catalyst	Support*	Composition**, Mass %		Al:Zr (Molar Ratio)
		Aluminum	Zirconium	
TM01	60HEMA-1	12.9	0.25	176
TM02	60HEMA-1	20.1	0.18	382
TM03	60HEMA-1	17.6	0.19	306
TM04	60HEMA-2	21.2	0.24	301
TM05	60HEMA-2	18.2	0.27	229
TM06	60HEMA-2	19.6	0.35	191
TM07	60HEMA-2	20.1	0.32	212
TM08	60HEMA-3	18.9	0.23	275
TM09	60HEMA-4	18.3	0.22	282
TM10	60HEMA-4	19.7	0.23	285
TM11	HS-R-5	13.8	0.28	168
TM12 <sup>1</sup>	HS-R-5	–	–	–
TM13	HS-Q-1	13.4	0.21	220
TM14	PS/DVB-1	16.6	0.12	452
TM15	HS-R-1	15.4	0.23	227
TM16	HS-R-3	15.1	0.23	218
TM17	HS-R-2	13.5	0.23	202
TM18A	HS-R-6	14.3	0.28	174
TM18B	HS-R-2	14.6	0.27	185
TM19A	HS-R-6	15.1	0.27	189
TM19B	HS-R-2	14.1	0.27	178
TM20 <sup>2</sup>	HS-R-6	15.3	0.25	207
TM21 <sup>3</sup>	HS-R-2	13.9	0.24	195
TM22	HS-R-2	14.3	0.24	203

\* See Table 4.1 for details of supports

\*\* From INAA results

<sup>1</sup> – Insufficient catalyst remained for INAA

<sup>2</sup> – Sieved support using acetone to collect size range: 250-300  $\mu\text{m}$

<sup>3</sup> – Sieved support using anhydrous hexane to collect size range: 300-350  $\mu\text{m}$

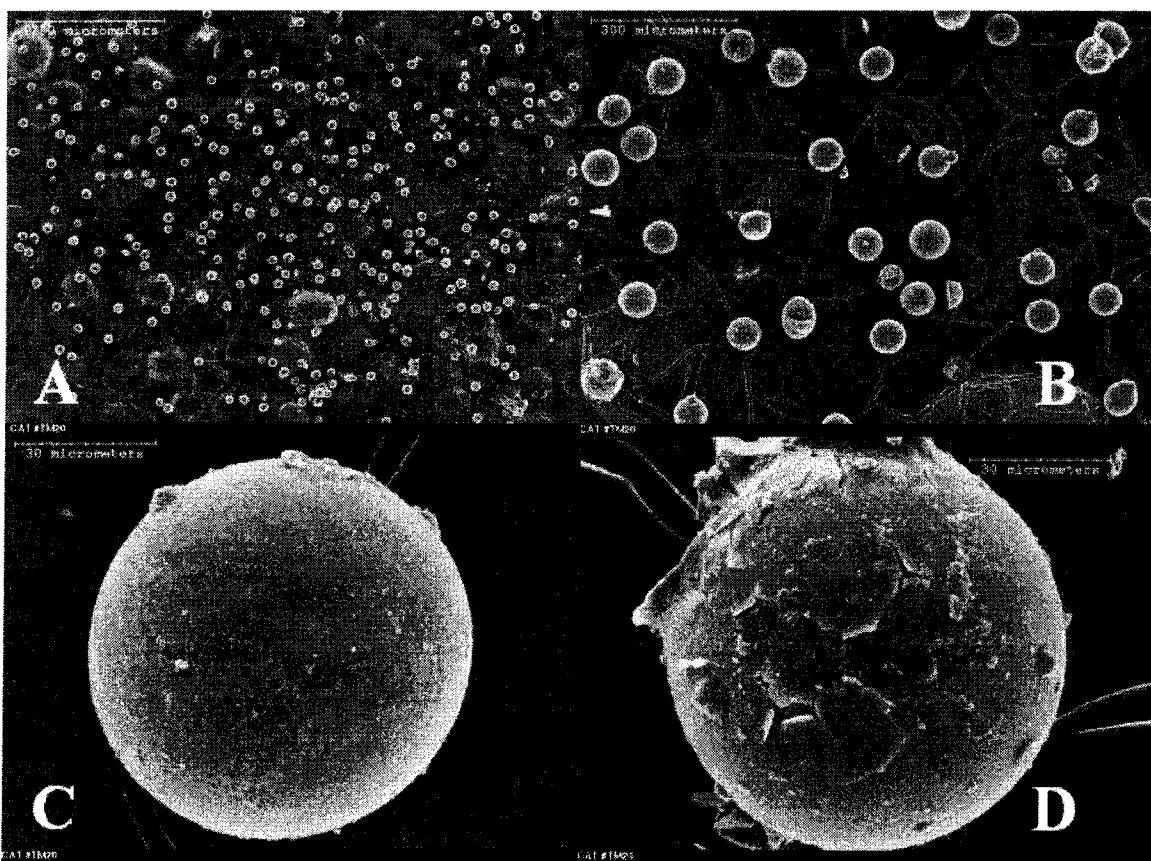


Figure 4.2: SEM images of catalyst TM20; (A) low magnification showing the uniform distribution of particle sizes; (B) higher magnification showing the catalyst particles having mainly uniform morphologies similar to support (HS-R6); (C) individual catalyst particle having relatively smooth surface; (D) individual particle having flaky surface.

Visual inspection and SEM imaging, as shown in Figure 4.2, show that although most catalyst particles had morphologies similar to the supports used some catalyst fragments and fines were also produced. These fines and fragments probably resulted from attrition of the catalyst particles during agitation in the production process and from excess MAO/zirconocene that had not been absorbed into the support particles. Moreover some catalyst particles had flaky outer crusts (see Figure 4.2 (D)) that had likely formed

on the surface when the toluene was being removed by evaporation from the catalyst suspension during production. Although the amount of fines and fragments are much less than the amount of spherical particles, the differences within a batch of catalyst are likely to influence the activity profiles of the catalyst and will be discussed later.

To see how well the MAO and zirconocene was distributed within the catalyst particles, some particles were cut or fragmented and prepared for SEM analysis, Figures 4.3(A) and 4.4 show such particles. Energy dispersive X-ray (EDX) spectroscopy was used to map the distribution of aluminum. Figure 4.3(B) shows that aluminum, hence MAO, is present across the cross-section of the catalyst particle. There were higher concentrations of aluminum towards the periphery of the particle than in the center. This concentration gradient likely arose when the toluene was being removed by evaporation and progressively higher concentration of MAO/zirconocene surrounded the particles. The increasingly more viscous fluid was less likely to penetrate well inside the particles. As the concentration of zirconium in the particle is near the detection limit of the EDX probe, the EDX linescan for zirconium shown in Figure 4.3 (C) was barely able to show the presence of zirconium throughout the cross-section of the particle. The EDX linescans are only good for qualitative representation of how well the MAO and zirconocene were distributed across the catalyst particles.

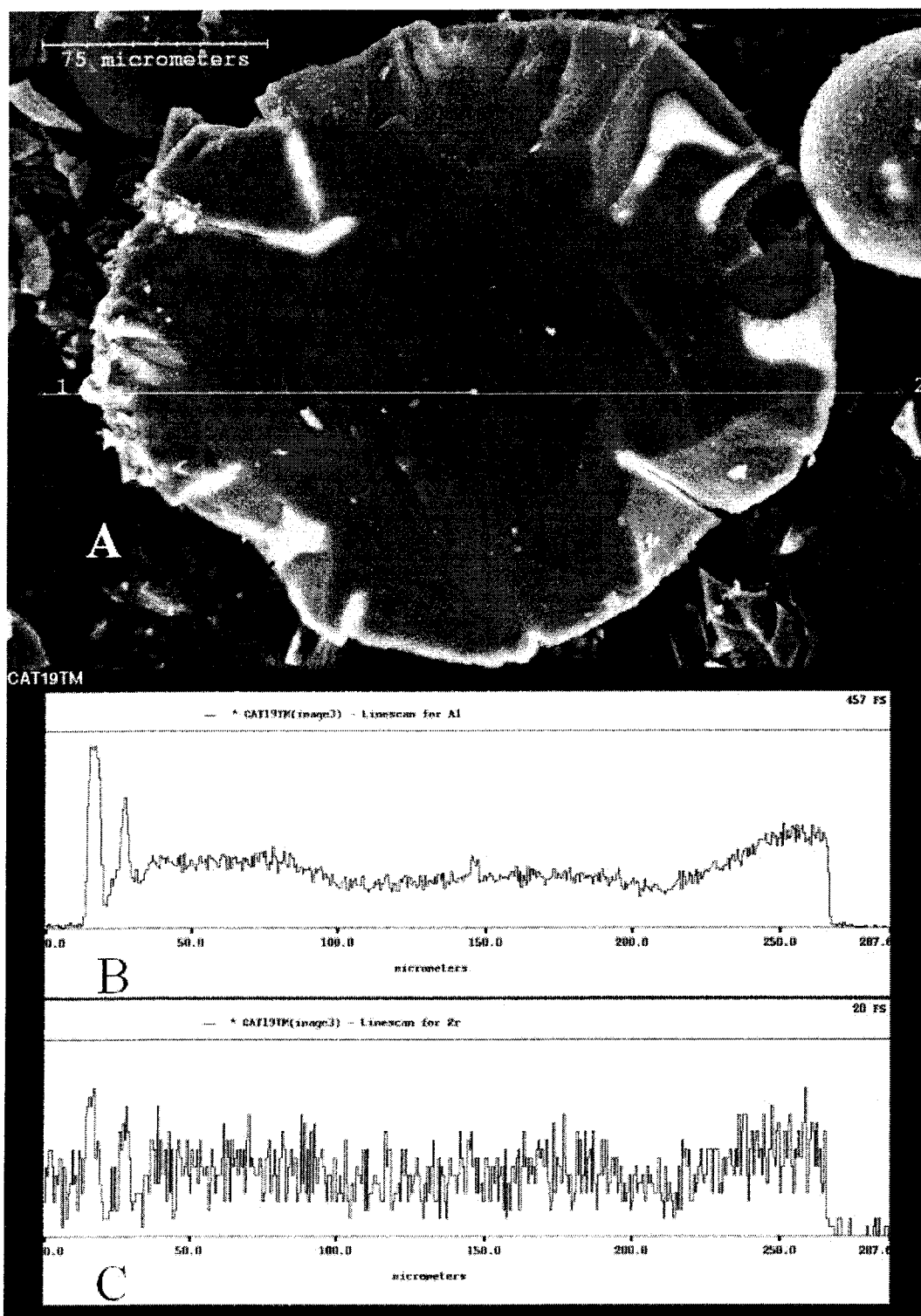


Figure 4.3: (A) Cut TM19B particle for determining distribution of metal showing line-scanning position; (B) EDX linescan for aluminum; (C) EDX linescan for zirconium

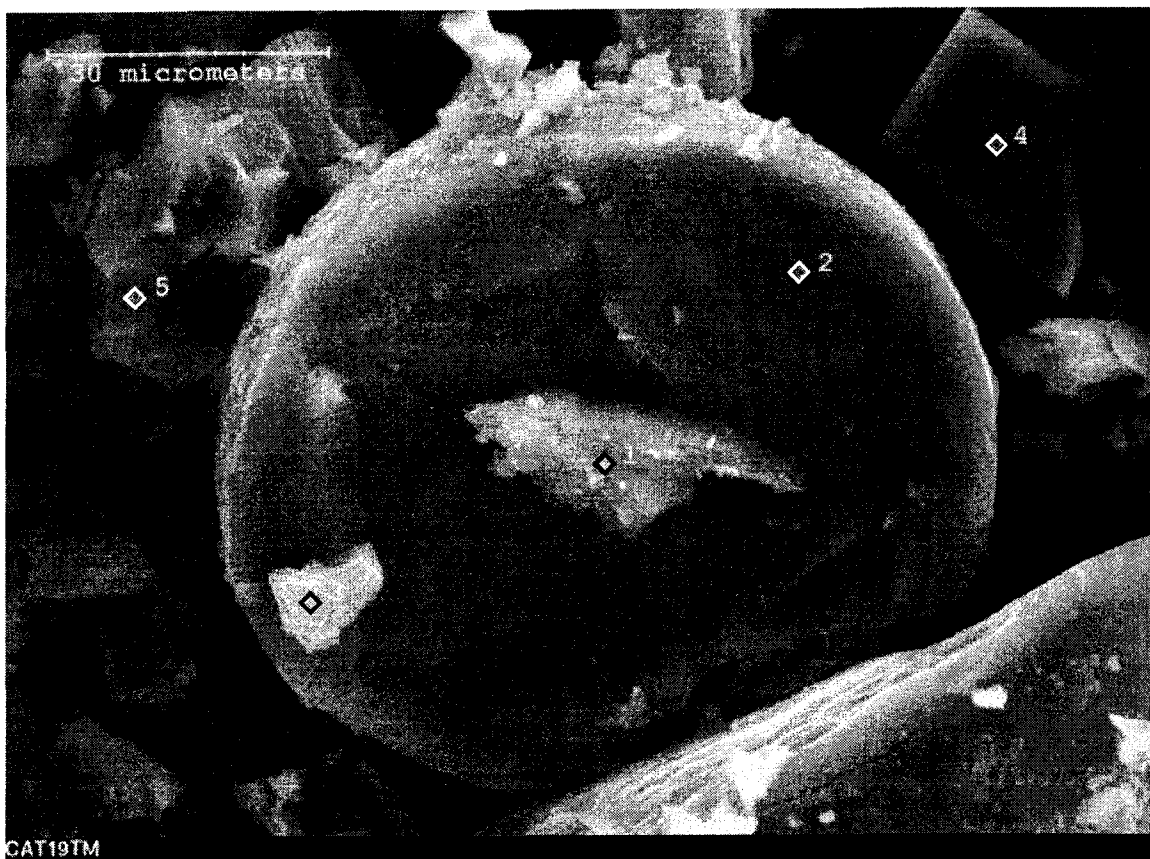


Figure 4.4 Fragmented TM19A particle for EDX probe analysis showing probe positions

Table 4.2: Elemental analysis of probe positions showing normalized mass percentage

Position Element	1 (Mass %)	2 (Mass %)	3 (Mass %)	4 (Mass %)	5 (Mass %)
O	23.3±3.0	7.3±2.0	33.7±1.5	19.1±3.6	15.1±3.4
Al	60.9±1.2	70.1±1.4	60.9±0.6	74.7±1.8	65.5±1.6
Si	6.4±0.8	12.2±1.1	1.9±0.2	not detected	5.4±1.4
S	5.5±0.5	5.6±0.7	0.55±0.1	not detected	9.0±0.9
Cl	2.1±0.4	3.3±0.5	0.58±0.1	1.6±0.4	2.8±0.6
Zr	1.9±1.0	1.5±0.9	2.4±0.3	4.6±1.0	2.2±2.0

Results of semi-quantitative analysis using EDX micro-probe of catalyst particle of TM19A shown in Figure 4.4 are given in Table 4.2. As EDX micro-probe results for

very low atomic number elements are unreliable, values for carbon have not been reported and the values shown have been normalized with respect to the other elements detected. Also, oxygen having low atomic number was likely underreported. Moreover, as the sample surfaces were not flat, the take-off angle for X-rays most likely varied from point to point and this would affect the results. However, it is apparent that aluminum and zirconium were distributed throughout the catalyst particles and fragments. The small amounts of sulfur and silicon detected were present in the support as these had been detected when EDX micro-probe analyses were done on the support particles alone. As the zirconocene used was a dichloride salt the presence of chlorine can be expected. From the data in Table 4.2 it can be concluded there was some variation in concentration of aluminum within the catalyst with the catalyst particle edge (Position 2 in Figure 4.4) having a greater concentration of aluminum than the catalyst centre (Position 1 in Figure 4.4). The catalyst flake under probe position 4 in Figure 4.4, showing larger concentration of aluminum and zirconium and no silicon or sulfur, most likely formed from excess MAO/zirconocene that had coagulated outside the support particles during the drying process.

Because EDX probe analyses results were semi-quantitative, instrumental neutron activation analyses (INAA) were done on catalyst samples to determine the composition of aluminum and zirconium in the catalysts. Moreover, from the initial amounts of MAO, bis(*n*-butyl cyclopentadienyl) zirconium dichloride, and support used to make a batch of catalyst and assuming no loss of reagents estimates of the aluminum and zirconium concentration in the catalyst were made. Figures 4.5 and 4.6 shows the both the calculated and measured concentration of aluminum and zirconium in the catalysts.

Because insufficient amount of catalyst remained, INAA could not be done for catalyst TM12. Further details about the catalysts, including details of preparation conditions, values of calculated and measured concentrations of aluminum and zirconium are given in Appendix A Tables A1 and A2.

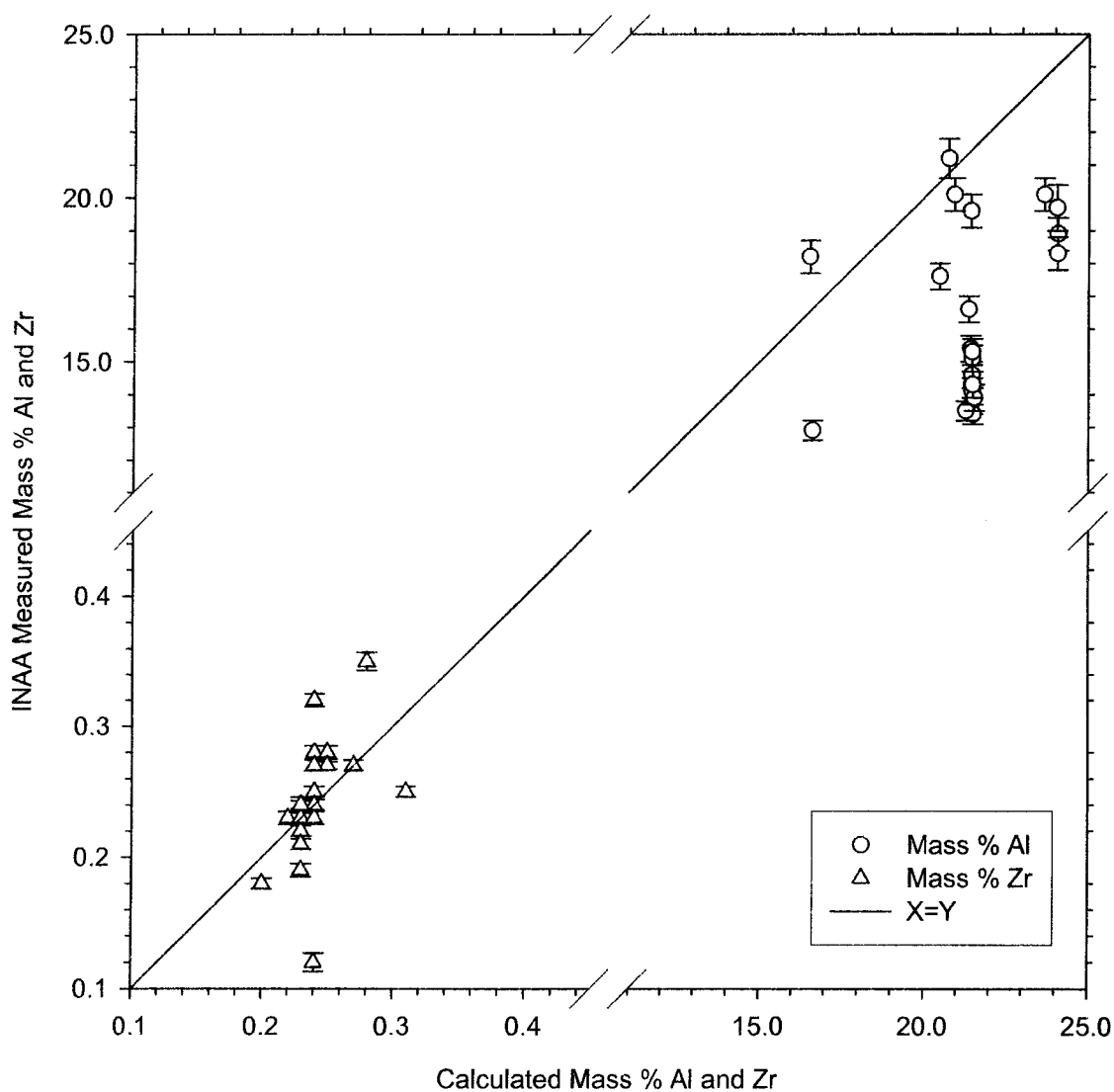


Figure 4.5: Plot of measured Al and Zr concentration versus estimated Al and Zr concentration in prepared catalysts.

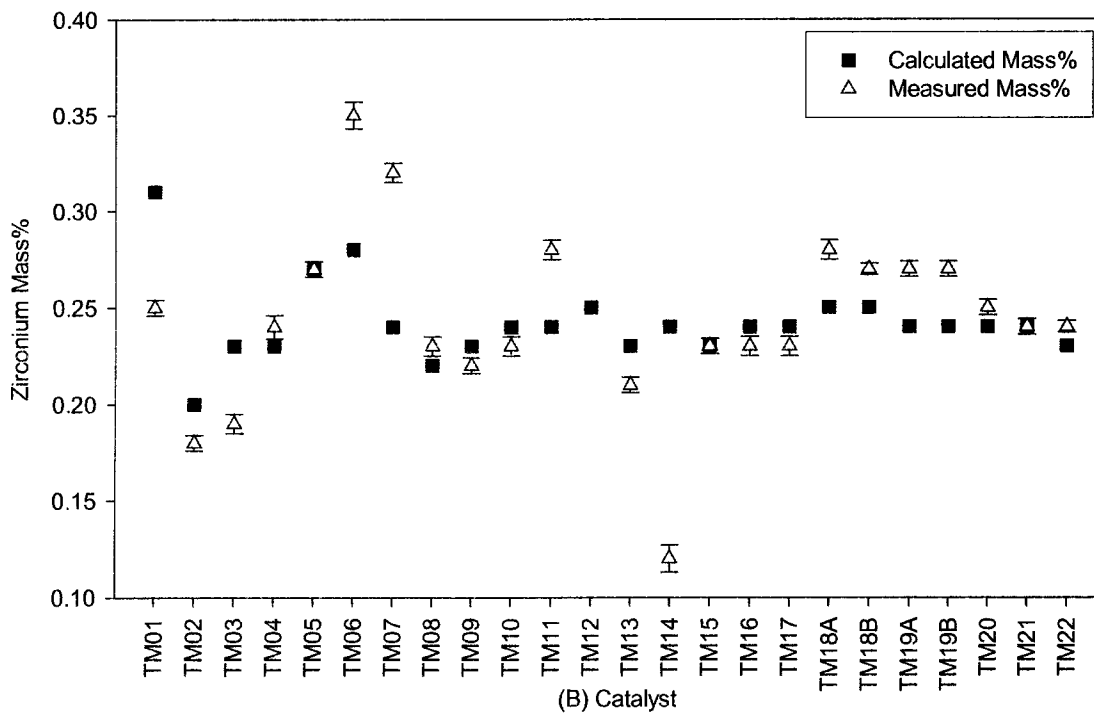
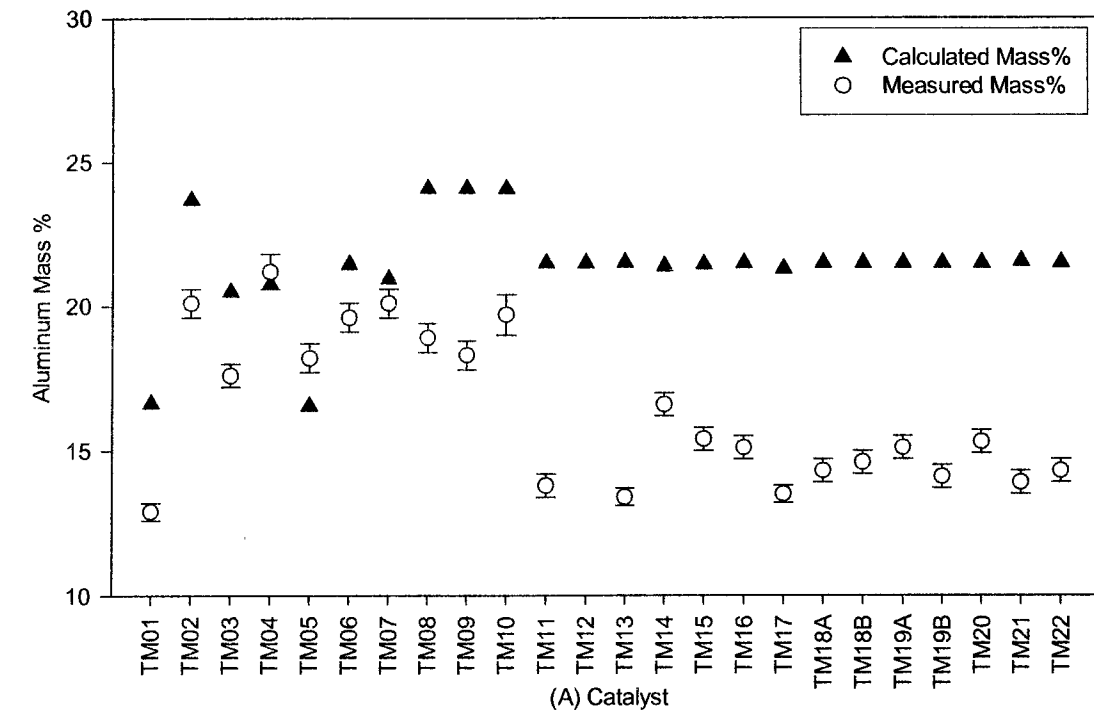


Figure 4.6: (A) Aluminum and (B) zirconium concentrations in catalysts, calculated from amounts of reagents used and measured using instrumental neutron activation analysis.

From Figures 4.5 and 4.6 (A) it can be seen that the INAA measured aluminum contents for most of the catalysts were less than the calculated values. This had probably resulted because usually only clear MAO solution from the top of the MAO bottle was used for preparing the catalyst and its aluminum concentration was most likely less than the value stated in the bottle as some MAO had gelled and precipitated out of the solution. Also as the MAO solution was very viscous some of it remained in the syringe used to transport the MAO solution from the glove-box to the flask after injection. To minimize this, after injection of MAO solution into the reaction flask, the MAO syringe was refilled with anhydrous toluene and this washing was then added to the flask.

If the calculated concentration of aluminum was greater than the INAA measured value because the assumption of aluminum concentration in the MAO solution was greater than the actual value, then the calculated zirconium concentration based on the same assumptions should be less than INAA measured values. It can be seen from Figures 4.5 and 4.6 (B) that in most cases the measured INAA concentration of zirconium was indeed larger than the calculated values. However, in some cases the calculated concentrations of zirconium were greater than the INAA measured values. The discrepancy was specially large for catalyst TM14, where only 10 mg of zirconocene was used to make the catalyst. (See Appendix A, Table A1 for details of amounts of reagents used to make the catalysts.) These differences probably arose due to inaccuracies in measuring small amounts of zirconocene inside the glove-box. Moreover, as each batch of catalyst was made some reagents dried on the walls of the reaction flask and were not incorporated into the catalyst; this would affect the final composition of the catalyst.

## 5. Exploratory Experiments<sup>1</sup>

### 5.1 Test Runs and Gas Phase Temperature Control

One of the objectives of this project was to design and construct a gas-phase polymerization reactor with improved temperature control and gas phase analysis capabilities. A second objective was to determine the effects of operation conditions such as temperature, pressure, amount of catalyst, co-catalyst type and concentration on the rate behaviour and product properties. Results of some of the experiments that were carried out to achieve these objectives are presented in this chapter.

The 2 L gas phase reactor described previously in Chapter 3 was used to carry out the gas phase homo and co-polymerization of ethylene. To simulate industrial conditions, it was decided to perform polymerization runs at about 80°C and 200 psia (1.38 MPa) total pressure. Initial test runs were carried out using existing proven supported metallocene catalysts, JM29 and JM38 produced in our laboratory by J.-M. Zhou (Zhou et al. 2003). These experiments were done to test the performance of the PID temperature controller in maintaining the gas phase temperature at a set value.

In Figure 5.1, activity profiles as measured by the flow rate of ethylene into the reactor, bulk gas temperature profiles, and gas pressure profiles from three test polymerization runs using catalyst JM29 are shown. Time was counted from the time of injection of the catalyst into the reactor. In run 01Test the oscillatory nature of the PID temperature controller, Figure 5.1(C), was evident. The gas pressure was controlled by an

---

<sup>1</sup> Some of the material in this chapter has been published; Mannan et al., *Canadian Journal of Chemical Engineering* ( **82**, 371-381 (2004)) and Hammawa et al., *Journal of Applied Polymer Science* (**92**, 3549-3560 (2004)).

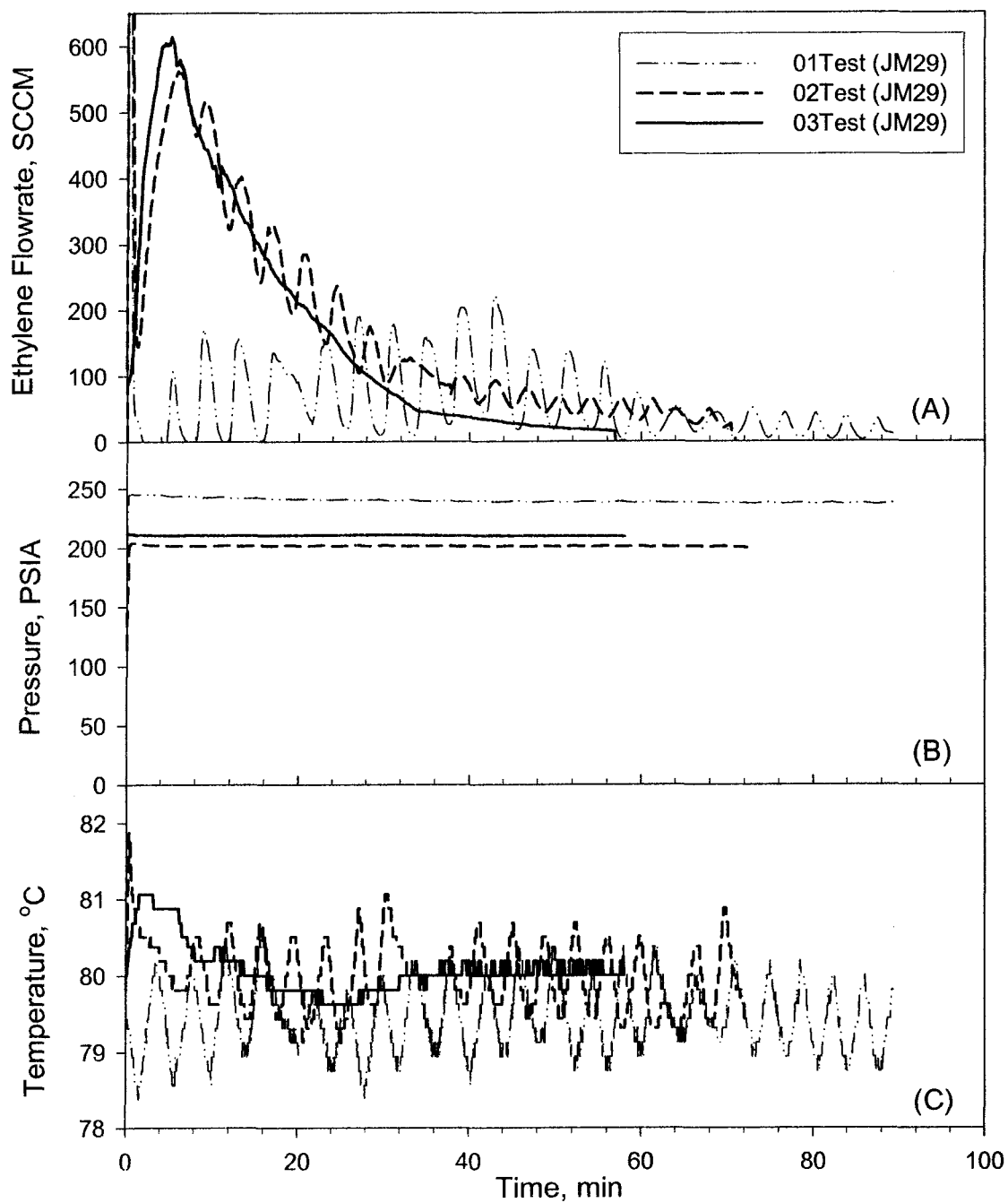


Figure 5.1: Effect of controller tuning on reaction profiles. Polymerization data from test runs using Catalyst JM29 showing (A) rate of ethylene flow into reactor, (B) reactor gas pressure, and (C) bulk gas temperature.

independent backflow pressure regulator and was not affected by these oscillations (see Figure 5.1(B)). Here, the activity oscillations (see Figure 5.1 (A)) were due to temperature oscillations. By changing the PID controller parameters these oscillations were reduced in run 02Test. Further tuning of the PID controller eliminated these temperature oscillations completely in run 03Test. Although the gas temperature rose by 1°C from the set value of 80°C immediately after the injection of the catalyst into the reactor, the gas temperature was maintained to within  $\pm 0.3^\circ\text{C}$  of the set temperature for rest of the run. The initial spike in temperature was due to sudden compression of the gas in the reactor during catalyst injection. The initial conditions for these test runs and two other runs using larger amount of catalyst and scavenger tri-isobutyl aluminum (TIBA) amounts are given in Table 5.1.

Table 5.1: Initial polymerization conditions of test runs

Run Number	01Test	02Test	03Test	10Test	12Test
Date Performed	11/20/00	11/27/00	13/12/00	01/17/01	01/22/01
Catalyst - Type	JM29	JM29	JM29	JM38	JM29
Amount, (mg)	151.1	80.8	80	109	109
Scavenger -- Type	TIBA	TIBA	TIBA	TIBA	TIBA
Amount, (mL)	0.15	0.15	0.15	0.30	0.30
Salt Bed, (g)	132	99.5	80	80	80
Initial Temperature, ( $^\circ\text{C}$ )	80	80	80	80	80
Total Pressure, (MPa)	1.65	1.41	1.41	1.41	1.41
Initial $\text{C}_6\text{H}_{12}$ , ( $\text{mol}/\text{m}^3$ )	0	13.0	10.6	9.3	8.0

The polymerization profiles for runs 10Test and 12Test using catalysts JM29 and JM38, respectively are shown in Figure 5.2. This figure shows that when the activity increased very quickly immediately after catalyst injection, Run 10Test, the temperature controller was unable to maintain the gas temperature at the desired set point and the gas temperature oscillated. However, for a more gradual increase in activity, Run 12Test, the temperature was maintained to within  $\pm 0.5^{\circ}\text{C}$  of the desired value up to a polymerization rate of about 0.03 mol/min. This limitation of the temperature controller system arose because of constraint in the rate of heat removal from coolant reservoir.

To test further the reactor system's ability to control gas phase temperature during polymerization a set of experiments was performed to compare its performance under various modes of operations and with that of an older 1 L polymerization reactor in our laboratory described previously by Lynch and Wanke (1991). During polymerization at 1.36 MPa total pressure and initial 1-hexene concentration of  $17.6 \text{ mol/m}^3$ , the older 1 L reactor was immersed in a constant temperature circulating oil bath. Under similar polymerization conditions, the new 2 L reactor was operated in three different modes as follows:

- 1) The PID temperature controller was switched on and temperature of the coolant oil varied as required to control to maintain the gas phase temperature.
- 2) The PID temperature controller was switched off and oil at constant temperature was pumped to the coolant circulation channels in the reactor walls.
- 3) Static mixers were inserted into coolant circulation channels in the reactor walls to improve heat transfer. The PID temperature controller was switched off and oil at constant temperature was pumped to the reactor coolant channels.

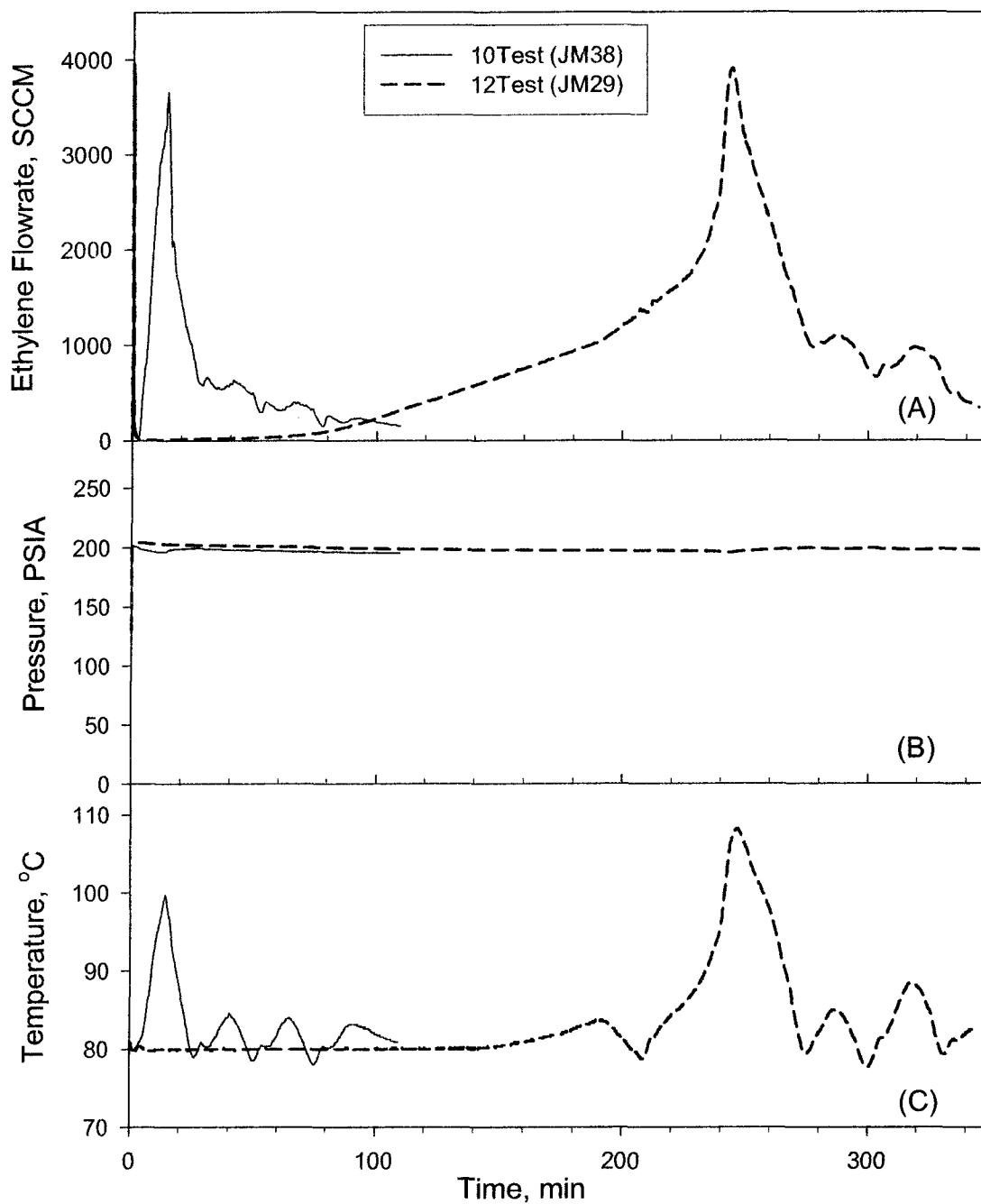


Figure 5.2: Effect of high activity on reaction profiles. Polymerization data from test runs using Catalysts JM38 and JM29 showing (A) rate of ethylene flow into reactor, (B) reactor gas pressure, and (C) gas temperature.

These polymerization experiments to compare gas phase temperature control under different modes of operation and with that of the 1 L reactor were done with another graduate student, Hassan Hammawa and the results have been published (see Mannan et al. (2004)). Further information about these experiments is given in Table 5.2 below. Catalyst HH15 used for these experiments was supported on in-house porous polymer particles of size range 60-300  $\mu\text{m}$  and had zirconium concentration of 0.187 mass % and aluminum concentration of 11.6 mass %. The activity and gas phase temperature profiles from these runs are shown in Figure 5.3.

Table 5.2: Experiments to compare gas phase temperature control during polymerization.

Run Number	HH88 <sup>1</sup>	HH89 <sup>2</sup>	HH90 <sup>3</sup>	HH92 <sup>4</sup>
Date Performed	09/12/01	09/13/01	09/14/01	09/21/01
Catalyst HH15 Amount, (mg)	42.5	42.6	42.7	42.8
Scavenger TIBA Amount, (mL)	0.17	0.08 <sup>5</sup>	0.08 <sup>5</sup>	0.08 <sup>5</sup>
Salt Bed, (g)	80	80	80	80
Initial Temperature, ( $^{\circ}\text{C}$ )	80	80	80	80
Maximum Temperature,	110.9	82.4	92.7	87.6
Time Averaged Temperature, ( $^{\circ}\text{C}$ )	90.8	80.0	86.0	84.6
Total Pressure, (MPa)	1.36	1.41	1.37	1.39
Initial $\text{C}_6\text{H}_{12}$ , ( $\text{mol}/\text{m}^3$ )	17.6	15.2	15.2	15.4
Total PE Yield, (g)	60.7	56.4	62.8	52.3

<sup>1</sup> Old 1L Reactor immersed in constant temperature circulating oil bath

<sup>2</sup> New 2L Reactor with PID temperature control switched on

<sup>3</sup> New 2L Reactor with oil at  $80^{\circ}\text{C}$  circulated in coolant channels

<sup>4</sup> New 2L Reactor with oil at  $80^{\circ}\text{C}$  circulated in coolant channels with static mixers inside

<sup>5</sup> TIBA removed after scavenging for 25 min by evacuating reactor to 10 Pa.

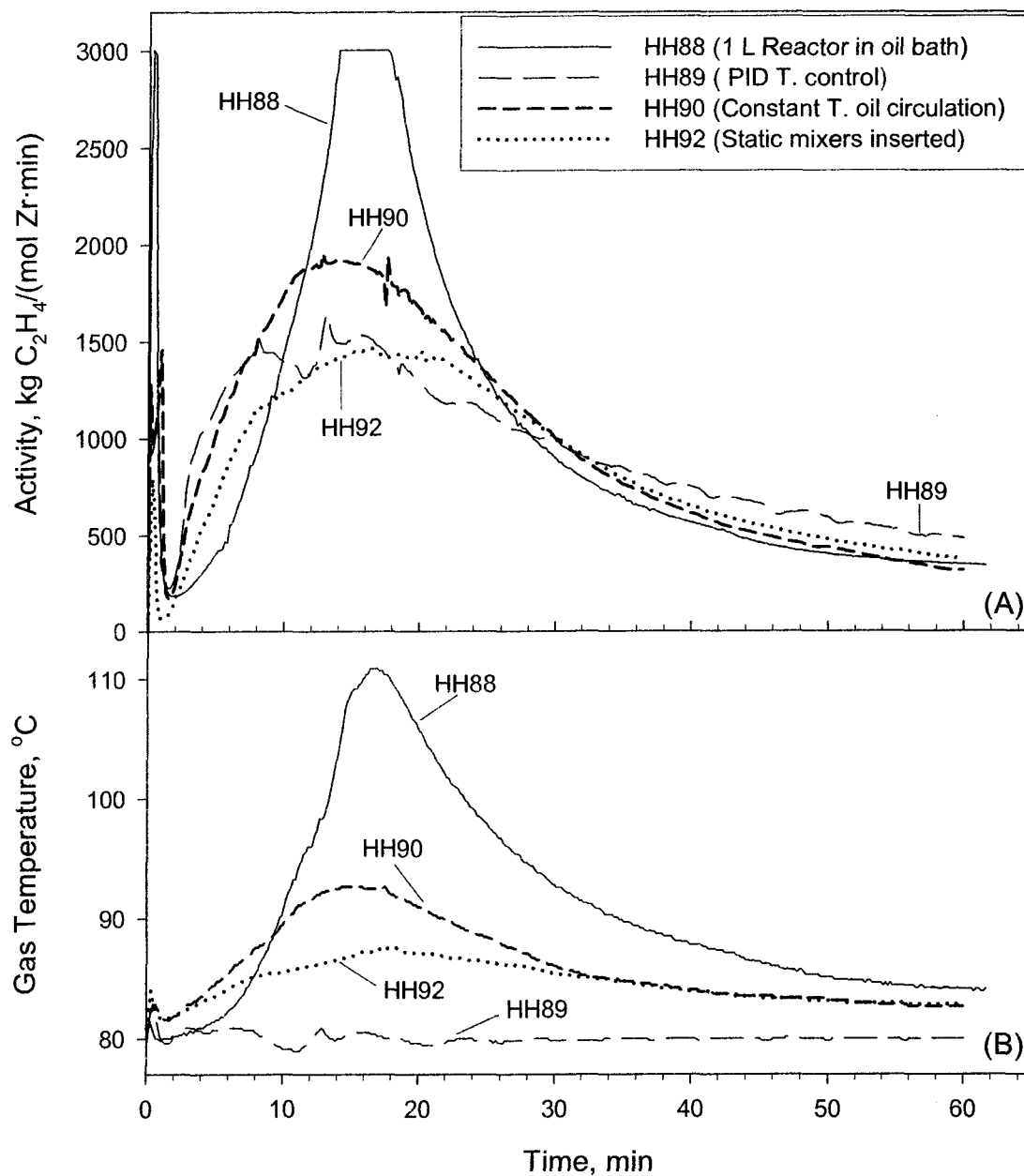


Figure 5.3: Comparison of gas phase temperature control during polymerization under various modes of operation showing (A) activity profiles, and (B) the corresponding temperature profiles.

The results in Table 5.2 shows that during ethylene 1-hexene copolymerization in the 1 L reactor the bulk gas phase temperature went up to 111°C from the initial temperature of 80°C. The average temperature during the run was 91°C. The temperature and activity plots for this run, HH88 (see Figure 5.3) showed this large increase in temperature resulted in the corresponding increase in activity. The flat part near the top of the activity curve was because the ethylene flowrate into the reactor exceeded the flowmeter maximum limit during this interval.

In comparison, the Run HH89 showed that under similar polymerization conditions the gas phase temperature in the 2 L reactor with the PID temperature controller switched on was kept remarkably near the initial temperature of 80°C. The average temperature during this run was 80°C, and the maximum temperature of 82°C that was reached immediately after catalyst injection due to adiabatic compression of the gases as the pressure in the reactor was raised. This was a remarkable improvement of bulk gas temperature control during polymerization.

Even with the PID temperature controller switched off, and oil at constant temperature (80°C) being pumped to the reactor coolant channels (see Run HH90) the gas phase temperature rise during polymerization was less than that of the 1L reactor. This was because of two reasons; namely, the better heat transfer to coolant oil flowing in channels in the reactor walls than that to oil circulating in an oil bath around the 1 L reactor, and due to the larger heat capacity of the 2 L reactor. The heat transfer to the coolant oil flowing in channels in the 2 L reactor walls was further improved by the insertion of static mixers into these channels (cf. Run HH90 and HH92, the only

difference in the operating conditions of these two runs was the use of static mixers for Run HH92).

From these early test runs a number of preliminary observations were drawn for this polymerization reactor system. These were as follows:

- 1) Gas phase ethylene polymerization could be carried out using this reactor system using supported metallocene catalyst.
- 2) The PID temperature controller was able to maintain gas phase temperature at desired level below total polymerization rates of about 0.04 mol C<sub>2</sub>H<sub>4</sub> /min (900 cm<sup>3</sup> (STP)/min).
- 3) Gas phase temperature affected polymerization activity profiles and vice versa.
- 4) Homopolymerization activity, Run 01Test, was much less than copolymerization activity for the catalyst used.
- 5) Amount of scavenger present initially affected the reaction profiles (Runs 03Test and 12Test).
- 6) Amount of catalyst injected into the reactor affected reaction profiles (Runs 03Test and 12Test).
- 7) Type of catalyst used affected reaction profiles (Runs 10Test and 12Test).

These observations shed light into which direction further experiments should be carried out to better understand the reactor system behaviour and gas phase ethylene polymerization.

## 5.2 Effect of Scavenger on Activity Profiles

Alkyl aluminums have been used by researchers as cocatalysts for supported metallocene catalysts (Fink et al (2000), Hlatky (2000), Pryzbyla et al (1999) and Ribeiro et al (1997)). Thus any unreacted alkyl aluminums remaining in the reactor after scavenging will influence the catalyst activity. Experiments were performed to determine the effect of amount of scavenger on activity profiles. The initial conditions of a set of runs to determine the effect of TIBA are given in Table 5.3 and the activity, gas phase temperature and pressure profiles are given in Figure 5.4. Further details regarding the catalysts and runs are given in Appendixes A and B respectively.

Table 5.3: Initial conditions of runs to determine effect of TIBA (tri-isobutyl aluminum) on polymerization using Catalyst TM01 (all Type B runs, see Chapter 3)

Run Number	001TM	002TM	004TM	005TM
Date Performed	02/01/01	02/05/01	02/09/01	02/13/01
Catalyst Amount, (mg)	100	100.7	100.8	100.7
Scavenger Amount, (mL)	0.30	0.50	0.20	0.40
Salt Bed, (g)	80	80	80	80
Initial Temperature, (°C)	80	80	80	80
Total Pressure, (MPa)	1.43	1.48	1.40	1.39
Initial C <sub>6</sub> H <sub>12</sub> , (mol/m <sup>3</sup> )	9.4	9.1	8.6	10.6
PE Yield, (g)	65.9	55.4	2.5	51.7

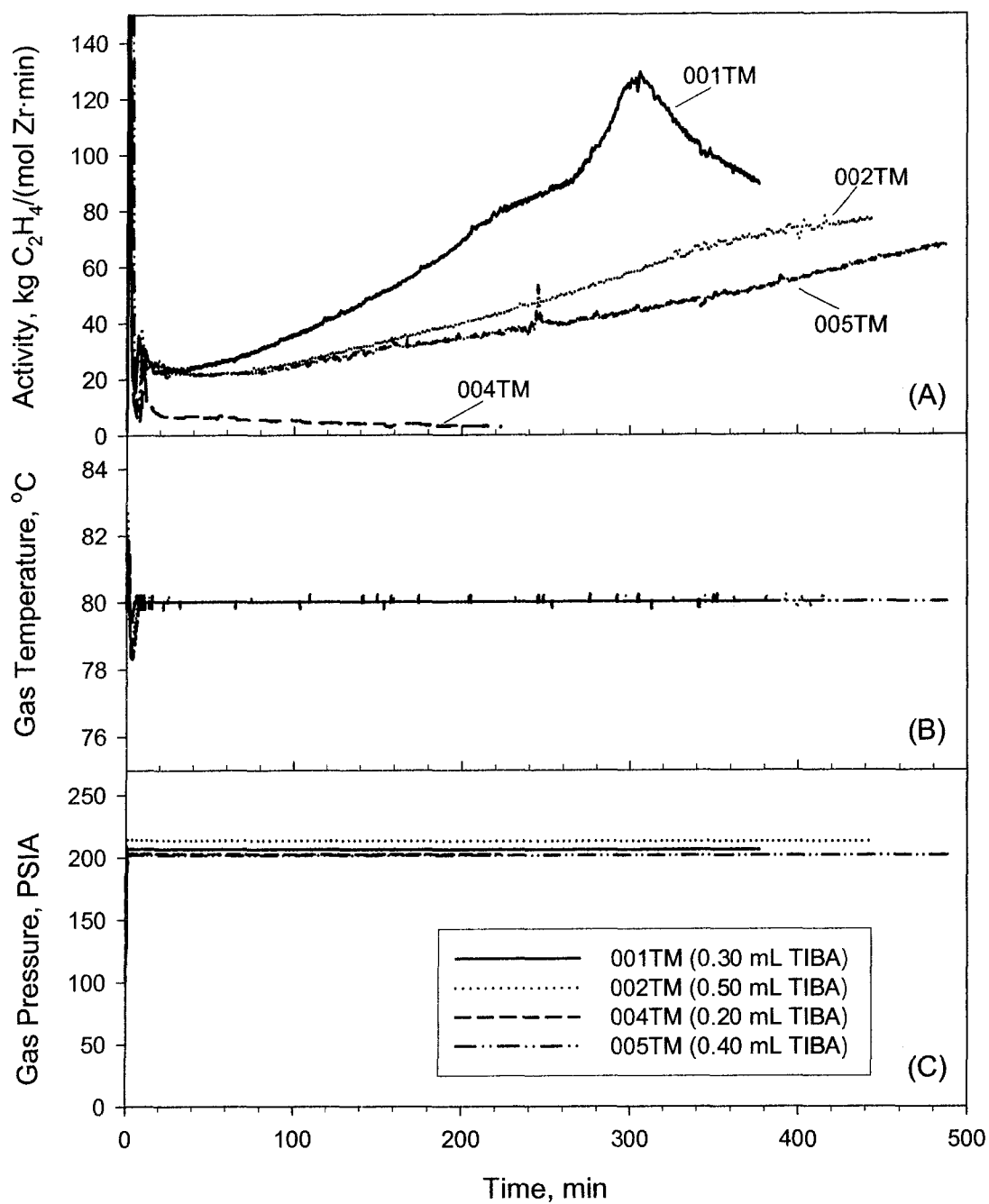


Figure 5.4: Effect of TIBA (tri-isobutyl aluminum) on polymerization profiles (A) activity measured from flow rate of ethylene into reactor, (B) gas phase temperature, and (C) gas pressure.

The polymerization runs using Catalyst TM01 and TIBA as scavenger show that there is an optimum amount of the scavenger to obtain maximum activity. For this set of runs, Run # 001TM with 0.30 mL of TIBA reached the maximum activity after 5 hours. But the activities for the runs using more TIBA increased more gradually and had not reached maximum activity even after 7 hours. The activity for run 004TM using 0.20 mL TIBA was very low and the catalyst had probably deactivated. To study the effect of other scavengers on polymerization a set of experiments using triethyl aluminum, TEA as scavenger were done. The initial conditions of these runs are given in Table 5.4 and the activity profiles of the runs are given in Figure 5.5.

Table 5.4: Experiments to determine effect of TEA (triethyl aluminum) on polymerization using Catalyst TM01 at 80°C (Type A runs, see Chapter 3).

Run Number	Date	Catalyst Amount, (mg)	Scavenger Amount, (mL)	Salt Bed, (g)	Total Pressure, (MPa)	Initial C <sub>6</sub> H <sub>12</sub> , (mol/m <sup>3</sup> )
006TM	02/16/01	80.0	0.20	80	1.41	10.0
007TM	02/20/01	86.0	0.10	80	1.39	9.4
008TM	02/21/01	87.7	0.15	80	1.41	9.2
010TM	02/23/01	88.0	0.05	80	1.42	9.8
012TM	02/28/01	102.0	0.15	80	1.43	9.0
013TM	03/01/01	105.0	0.15	0	1.42	10.0
016TM	03/08/01	102.0	0.15	80	1.40	10.2

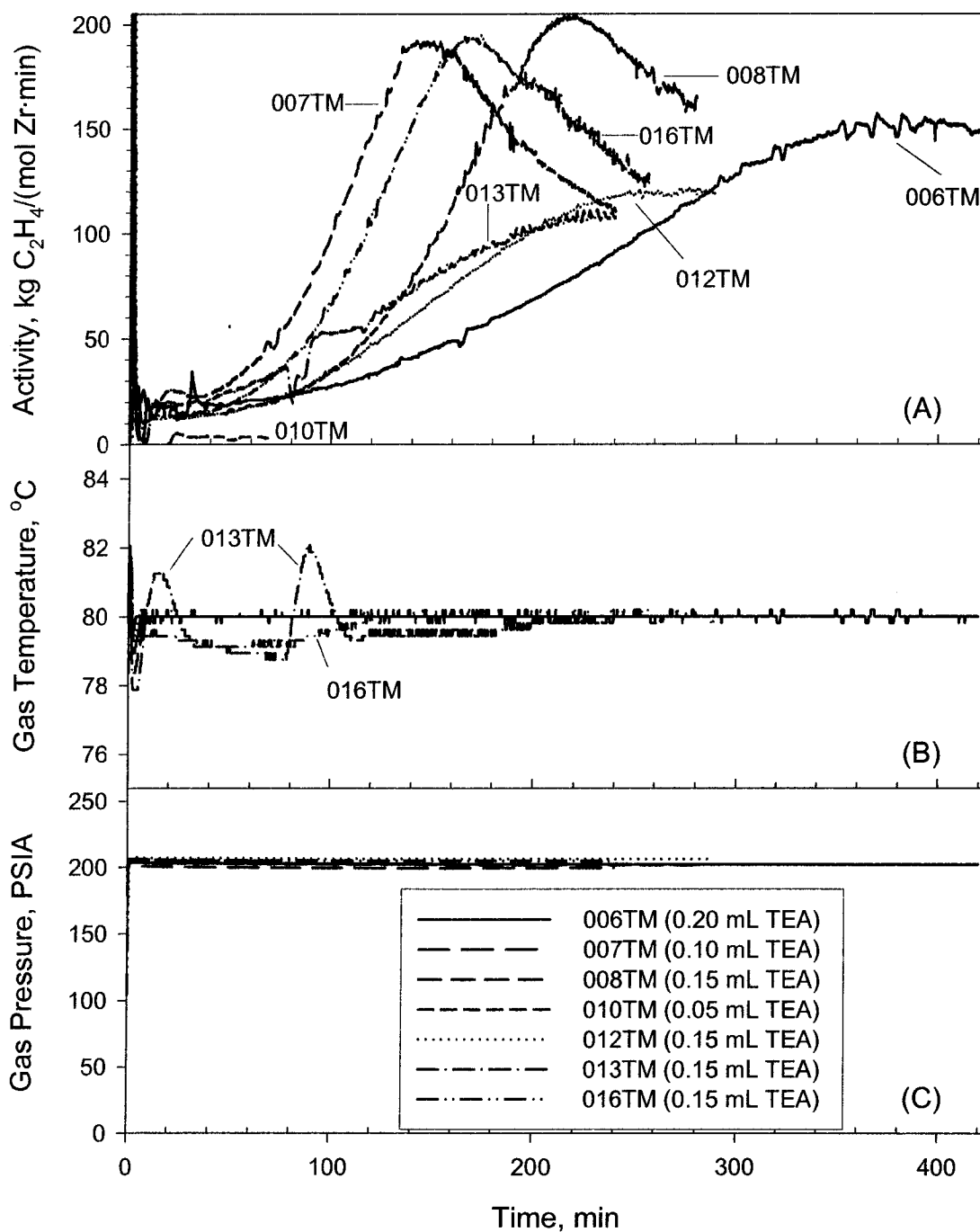


Figure 5.5: Effect of TEA (triethyl aluminum) on polymerization profiles (A) activity measured from flow rate of ethylene into reactor, (B) gas phase temperature, and (C) gas pressure

The effect of TEA was similar to that of TIBA during copolymerization of ethylene and 1-hexene. The activity was very low, Run 010TM using 0.05 mL TEA, when the amount of scavenger used was very small. For this set of runs the optimum amount of scavenger TEA to use was about 0.10 to 0.15 mL when the maximum activity was attained fastest. Use of 0.20 mL TEA broadened the activity profile and delayed the maximum activity in Run 006TM. In Run 013TM salt bed was not used. The gas phase temperature oscillations during this run clearly showed the essential part the salt bed plays in heat transfer from the gas phase and temperature control. However, although salt bed and the same amount of TEA were used for Runs 008TM, 012TM, and 016TM there were some differences in the activity profiles. These differences likely arose from the effect of the temperature controller and differences in the initial concentration of 1-hexene in the reactor.

Thus, to eliminate the effect of 1-hexene a set of homopolymerization runs were carried out with varying TIBA concentrations. The PID temperature controller was also switched off and oil at constant temperature was circulated in the coolant channels. These runs were part of work done with another graduate student, Hassan Hammawa, and results have been published in a paper on the effects of aluminum alkyls on ethylene polymerization (Hammawa et al., 2004). In Table 5.5 the polymerization conditions of these homopolymerization runs using catalyst TM02 and the product polymer properties are given. Initially the gas temperature was about 81°C for these runs and as polymerization proceeded the gas temperature rose. The average temperature during each run is also given in Table 5.5.

Table 5.5: Experiments to determine the effect of TIBA (tri-isobutyl aluminum) on homopolymerization using Catalyst TM02 (Type B runs, see Chapter 3).

Date	04/09/01	04/23/01	04/28/01	04/29/01	04/30/01	05/01/01
Catalyst, mg	105	107	103	104	103	103
TIBA, mL	0.30	0.10	0.20	0.05	trace*	0
Run Time, min	300	120	255	60	60	60
Temperature <sup>!</sup> , °C	82.0	84.9	82.8	86.2	87.7	86.1
Pressure, MPa	1.40	1.41	1.40	1.40	1.39	1.39
Mn, kg/mol	51.7	74.1	64.8	77.3	72.3	63.1
Mw, kg/mol	143	169	159	182	186	181
Polydispersity	2.77	2.29	2.46	2.35	2.57	2.87

! Time averaged gas phase temperature

\* 0.07 mL TIBA was injected into reactor; reactor was scavenged at 90°C and 0.7 MPa ethylene pressure before being vented to atmospheric pressure and evacuated to 6 Pa.

The activity and temperature profiles for these homopolymerization runs are shown in Figure 5.6(A) and 5.6(B) respectively. It is clear from the figure that the temperature profile is very similar to the activity profile for each run. Since ethylene polymerization is an exothermic reaction as the activity increased heat generation would increase and gas temperature would go up because the PID temperature controller was switched off and rate of heat removal would not change significantly. Moreover, as the temperature increased the activity would increase and further increase the gas

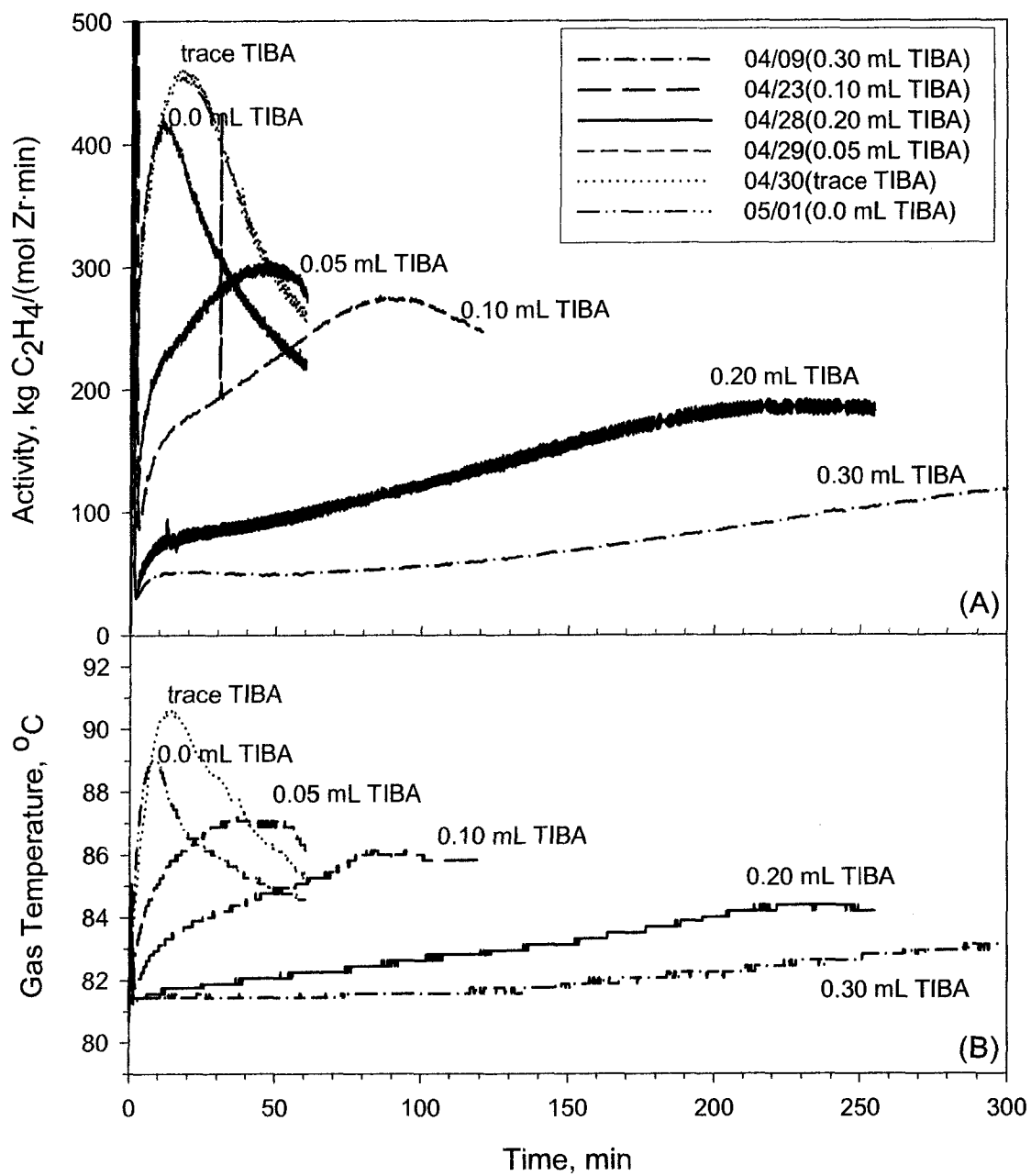


Figure 5.6: Effect of TIBA on gas phase homopolymerization using Catalyst TM02 showing (A) activity profiles, and (B) temperature profiles.

temperature. The catalyst/polymer particle temperature will be higher than the gas phase temperature because of low gas heat transfer coefficient. This will be especially significant for small catalyst particles, such as during start of polymerization, with low surface areas and with high activities as discussed by Floyd et al (1986) and McKenna et al. (1999). Large increases in catalyst particle temperature will deactivate the catalyst, Meier et al. (2001). This is likely what happened for the two runs with zero and trace amount of TIBA where there were rapid increases in activities with accompanying increases in temperatures followed by rapid decreases in activities. The similar activity profiles of these two runs and the higher maximum activity of the run with trace amount of TIBA suggest that there was some catalyst poison present initially in the reactor that the TIBA scavenged. However, from Figure 5.6 it is apparent that increasing TIBA concentration during polymerization decreased activity and delayed the time when maximum activity was reached. This also resulted in a more gradual increase in gas phase temperature.

In Table 5.5 the molar masses of the product PE resins and the time averaged gas phase temperatures are given. These results plotted in Figure 5.7, show that amount of TIBA present has significant effects on the molar mass of the PE product. In general the molar mass decrease with increase in TIBA concentration. This can be expected, as aluminum alkyls are known to act as chain transfer agents during ethylene polymerization. Polymerization temperature also influences the molar mass, Eskelinen and Seppala (1996) and Meier et al. (2001), with molar mass decreasing with increasing polymerization temperature. This could explain why the two runs with very high initial activities in Figure 5.6 had lower molar mass than that the trend from other runs with

higher initial amount of TIBA. As explained previously the catalyst/polymer particles for these two runs most likely had significantly higher temperature than the gas phase.

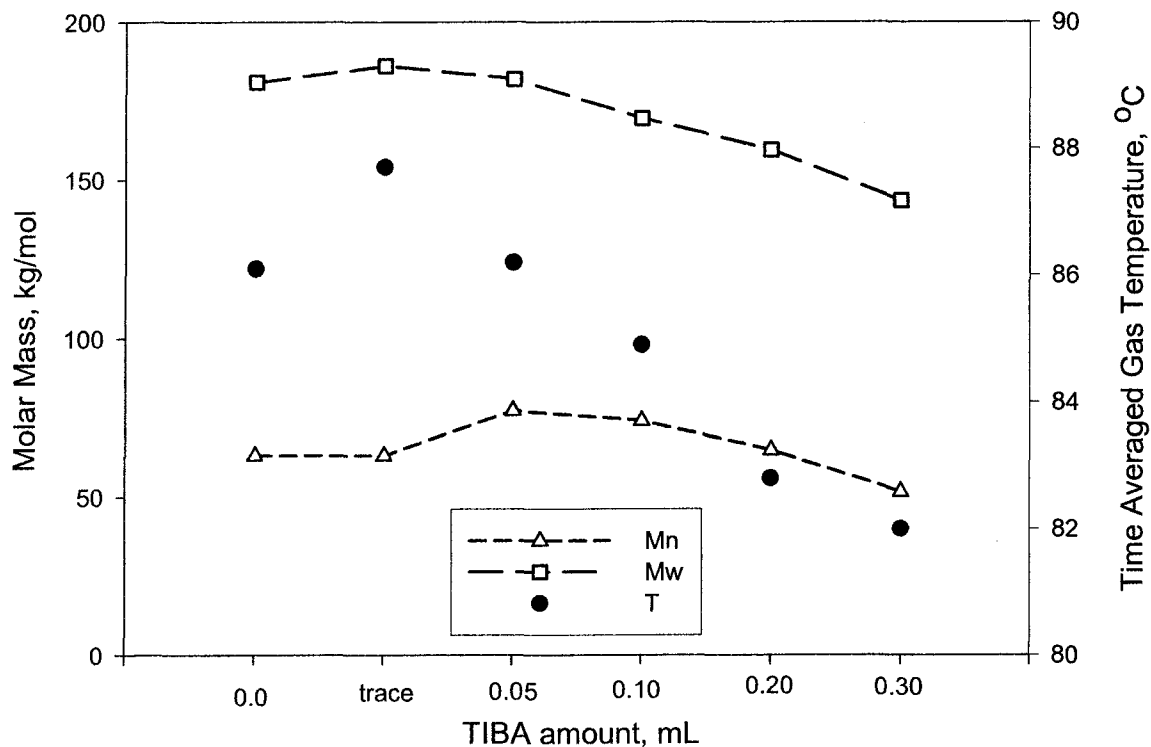


Figure 5.7: Effect of scavenger TIBA (tri-isobutyl aluminum) on PE molar masses, Mn and Mw, and time averaged gas phase temperature, T.

These polymerization runs suggest that aluminum alkyls like TIBA not only act as scavengers but also can be used to control the activity profiles, reactor temperature, and molar masses of the product polymer resins.

### 5.3 Effect of Temperature on Activity Profiles

The experiments described previously showed that polymerization temperature had significant effects on activity profiles and product polyethylene properties. Thus further systematic studies of the effect gas phase temperature were carried out. A set of ethylene/1-hexene copolymerization experiments was carried out within the temperature range 70°C to 90°C using Catalyst TM11. Catalyst TM11 was supported on HayeSep-R porous particles of size range 125 – 150 µm diameter and had zirconium concentration of 0.28 mass % and aluminum to zirconium molar ratio of 168:1. The initial conditions for this set of runs are given in Table 5.6. The activity profiles of these runs are plotted in Figure 5.8 (A) and in Figure 5.8 (B) the gas phase temperature profiles show that the temperature is well controlled by the PID temperature controller.

Table 5.6: Polymerization runs using Catalyst TM11 to study effect of gas phase temperature on activity profiles (Type A runs, see Chapter 3).

Run Number	Date Performed	Catalyst Amount, (mg)	Initial Temperature, (°C)	Total Pressure, (MPa)	Initial C <sub>6</sub> H <sub>12</sub> conc., (mol/m <sup>3</sup> )
101TM	12/19/01	75	80	1.41	10.70
102TM	12/20/01	76	75	1.38	10.60
103TM	12/21/01	75	85	1.40	10.99
104TM	01/04/02	75	90	1.40	11.94
105TM	01/07/02	76	70	1.38	10.60

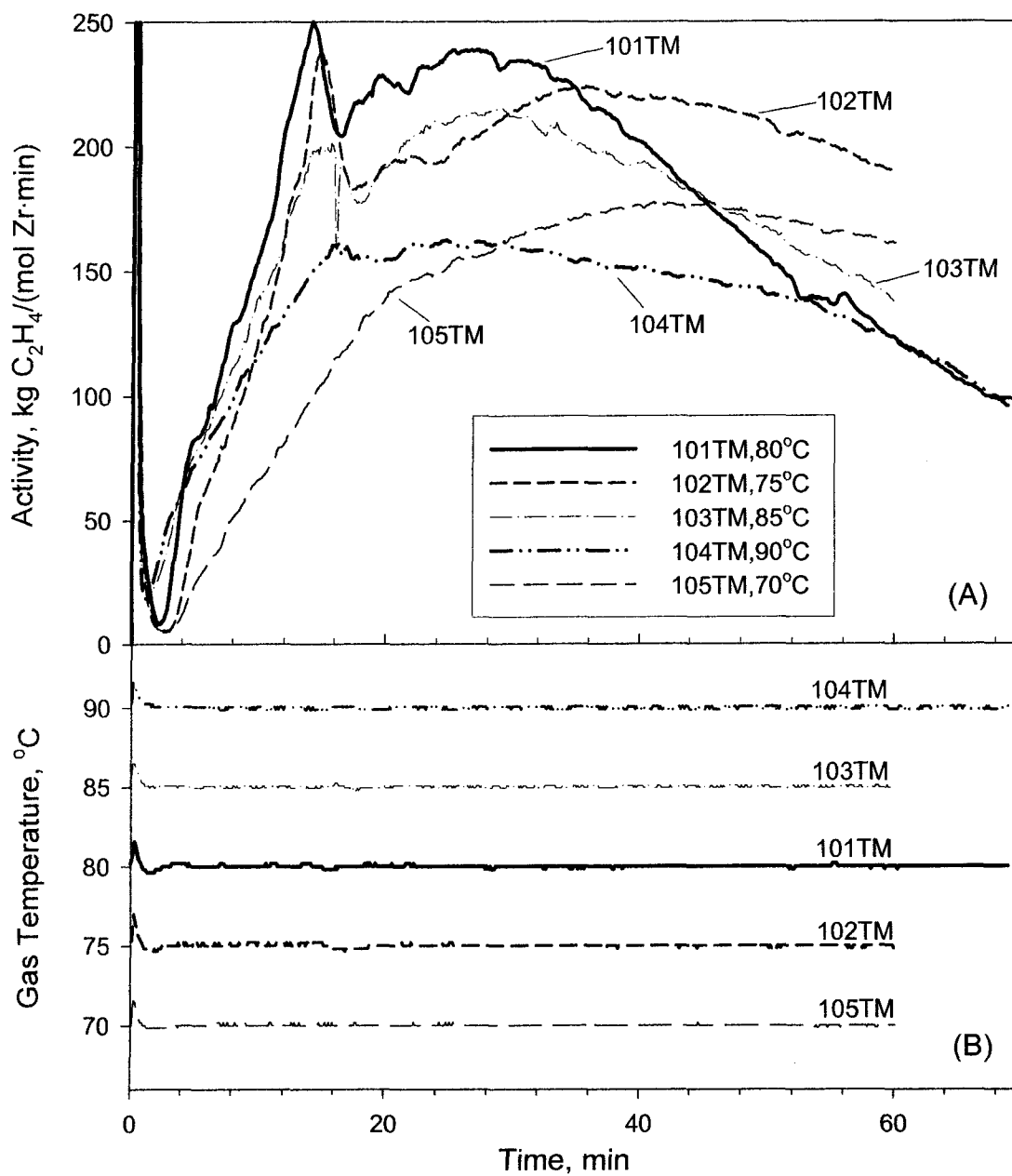


Figure 5.8: Effect of temperature on gas phase polymerization of ethylene and 1-hexene using Catalyst TM11 showing (A) activity profiles, and (B) temperature profiles.

From Figure 5.8 (A) a general trend in the effect of increasing the gas phase polymerization temperature from 70°C to 90°C can be seen. As temperature was increased, the rate increased more rapidly during the initial stages of polymerization. There was an “optimum” temperature at which the highest activity was reached; for this set of experiments this temperature was 80°C. For polymerization below 80°C the maximum activity was reached after a longer period but the activity decreased more slowly once maximum activity had been reached. For polymerization at higher temperature, although the maximum activity was reached a little earlier it was less than that at optimum temperature. After an hour of polymerization the activities of the runs carried out at 80°C and above were quite similar and decreasing at similar rates but the runs carried out at lower temperature had higher activities that were decreasing at slower rates.

As the polymerization temperature was increased, the catalyst activity also increased. Thus polymer built up inside the catalyst pores and fractured the catalyst particle faster and enhanced diffusion of monomer gases into the catalyst particle and further increased activity; this resulted in a shorter induction period. However, when the temperature increased too much, the co-catalyst MAO broke down, (Meier et al., 2001), and deactivated the catalyst. Moreover, the catalyst/polymer particle temperature is higher than the bulk gas phase temperature, especially during the early stages of polymerization when the particles are small and activity increases rapidly as discussed previously. Thus it is reasonable to expect that there will be temperature at which the activity will be maximum. At temperature below this “optimum” temperature, the rate of catalyst activation (fracturing) is dominant in determining the polymerization rate. At

temperature above the “optimum” temperature, the catalyst deactivation rate is the dominant factor in determining the polymerization rate.

To observe the effect of polymerization temperature on polymer particles, scanning electron microscope (SEM) images of the polymer particles produced during this set of experiments were taken. SEM images of external morphologies at low and high magnification of the polymer particles produced during polymerization at 70°C, 80°C, and 90°C are shown in Figure 5.9 (A), (B), and (C) respectively, and the inner structures of cut polymer particles from the same runs are shown in Figure 5.10 (A), (B), and (C) respectively.

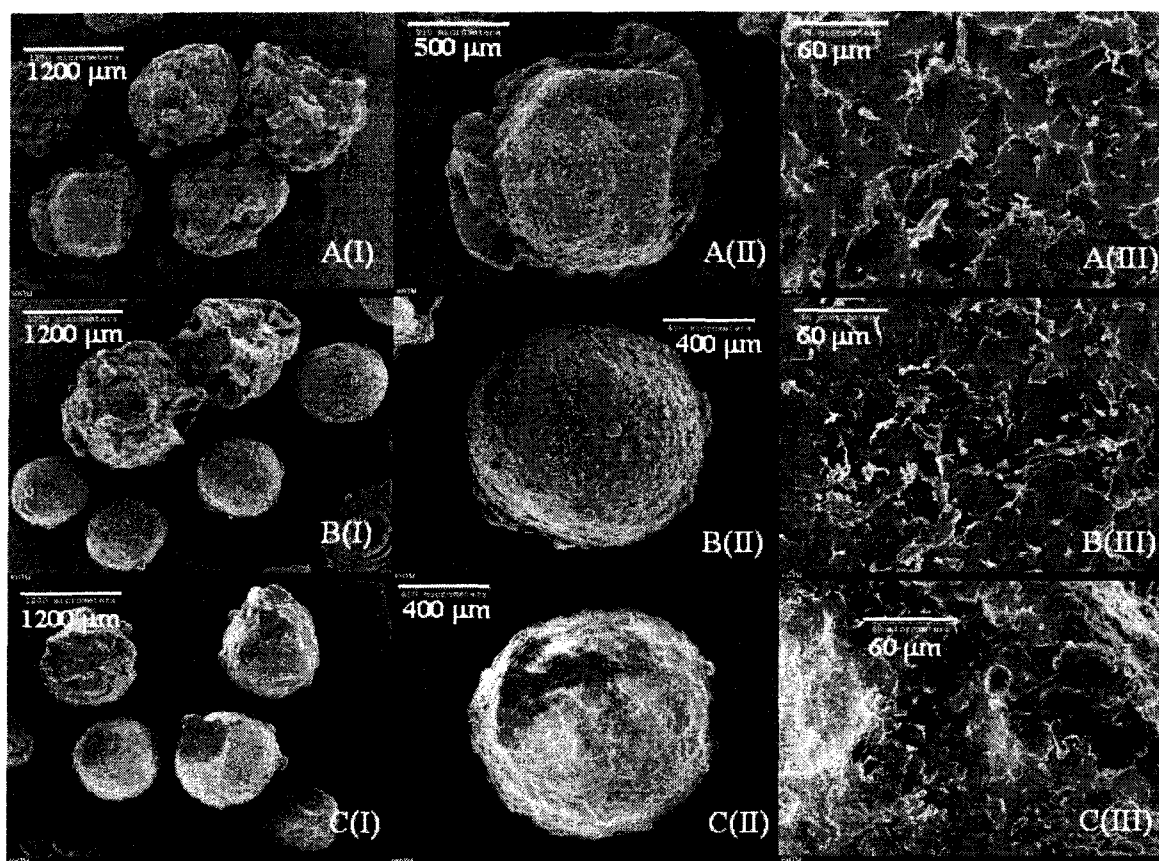


Figure 5.9: SEM images of polymer particles showing effect of gas phase polymerization temperature on outer morphologies at (A) 70°C (Run # 105TM), (B) 80°C (Run # 101TM), and (C) 90°C (Run # 104TM) using Catalyst TM11.

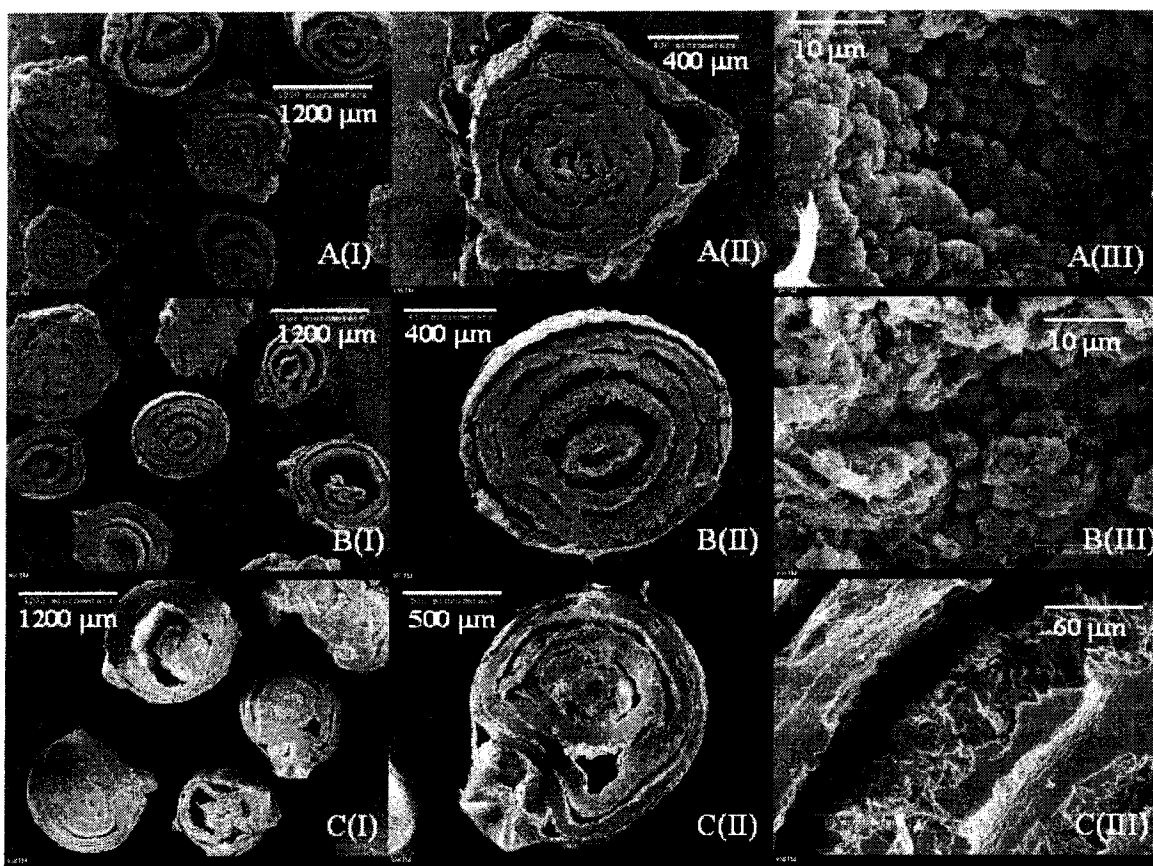


Figure 5.10: SEM images of polymer particles showing effect of gas phase polymerization temperature on inner morphologies at (A) 70°C (Run # 105TM), (B) 80°C (Run # 101TM), and (C) 90°C (Run # 104TM) using Catalyst TM11.

From Figure 5.9 it can be seen that as the polymerization temperature was increased from 70°C to 90°C, the polymer particles formed had less irregular external surfaces. This indicates that at the higher temperature there was some melting of the polymer particles. The internal morphologies of the polymer particles as seen from the SEM images of cut polymer particles in Figure 5.10 also show signs of polymer fusion at the higher polymerization temperature. Moreover, at the lower temperature the shells of polymer layers formed are more widely spaced than that formed at higher temperature.

The tightly packed layers of polymer formed at higher temperature are more likely to offer greater resistance to diffusion of monomer gases into the polymer particles. This will tend to reduce polymerization activity at higher temperature.

Another set of polymerization experiments using Catalyst TM17, which was supported on HayeSep-R porous particles of size range 250 – 300  $\mu\text{m}$  diameter and had zirconium concentration of 0.23 mass % and aluminum to zirconium molar ratio of 202:1 was carried out to investigate further the effect of gas phase temperature on polymerization. The initial conditions of the runs are given in Table 5.7 below. Although Catalyst TM17 was supported on bigger particles than Catalyst TM11, it had higher activity than Catalyst TM11 most likely due to its higher aluminum to zirconium ratio.

Table 5.7: Polymerization runs using Catalyst TM17 to study effect of gas phase temperature on activity profiles (Type B runs, see Chapter 3).

Run Number	Date Performed	Catalyst Amount, (mg)	Initial Temperature, ( $^{\circ}\text{C}$ )	Total Pressure, (MPa)	Initial $\text{C}_6\text{H}_{12}$ conc., ( $\text{mol}/\text{m}^3$ )
192TM	11/14/02	106	80	1.38	14.19
194TM	11/19/02	103	90	1.38	14.26
195TM	11/20/02	105	70	1.39	14.30
196TM	11/21/02	104	100	1.38	14.08
197TM	11/22/02	104	60	1.38	14.15

The activity profiles of the copolymerization runs carried out from 60°C to 100°C for this set of experiments are shown in Figure 5.11(A). The effect of increasing gas phase temperature on polymerization activity was similar to what was observed previously using Catalyst TM11. As polymerization temperature was increased from 60°C to 100°C, the induction time for activity to rapidly increase decreased. For this set of experiments also the “optimum” temperature was 80°C. The gas phase temperature profiles during these runs shown in Figure 5.11(B) again illustrate how well the PID temperature controller performed in controlling the gas phase temperature.

The external morphologies of the polymer particles produced by polymerization at 60°C, 80°C, 90°C, and 100°C are shown in Figure 5.12 (A), (B), (C), and (D) respectively. At 60°C and 80°C, the polymer particles produced had rough porous outer surface. However, the polymer particles formed at 90°C and 100°C had smoother surfaces with few visible pores. This seems to indicate that polymer tended to melt at these temperatures. The SEM images of cut polymer particles from this set of runs are shown in Figure 5.13. At 60°C, Figure 5.13 (A) the polymer shells formed were well spaced out and the unreacted catalyst core was clearly visible. At higher temperatures, Figure 5.13 (B), (C), and (D) larger number of polymer layers that were closer together was formed. Thus the polymer particles formed at higher temperature are likely to offer greater resistance to diffusion of monomer gases into the particles than those formed at lower temperature. These observations were consistent with that obtained from the previous set of experiments using Catalyst TM11. Similar results were obtained by Han-Adebekun et al. (1997) using  $\text{TiCl}_4/\text{MgCl}_2$  catalyst.

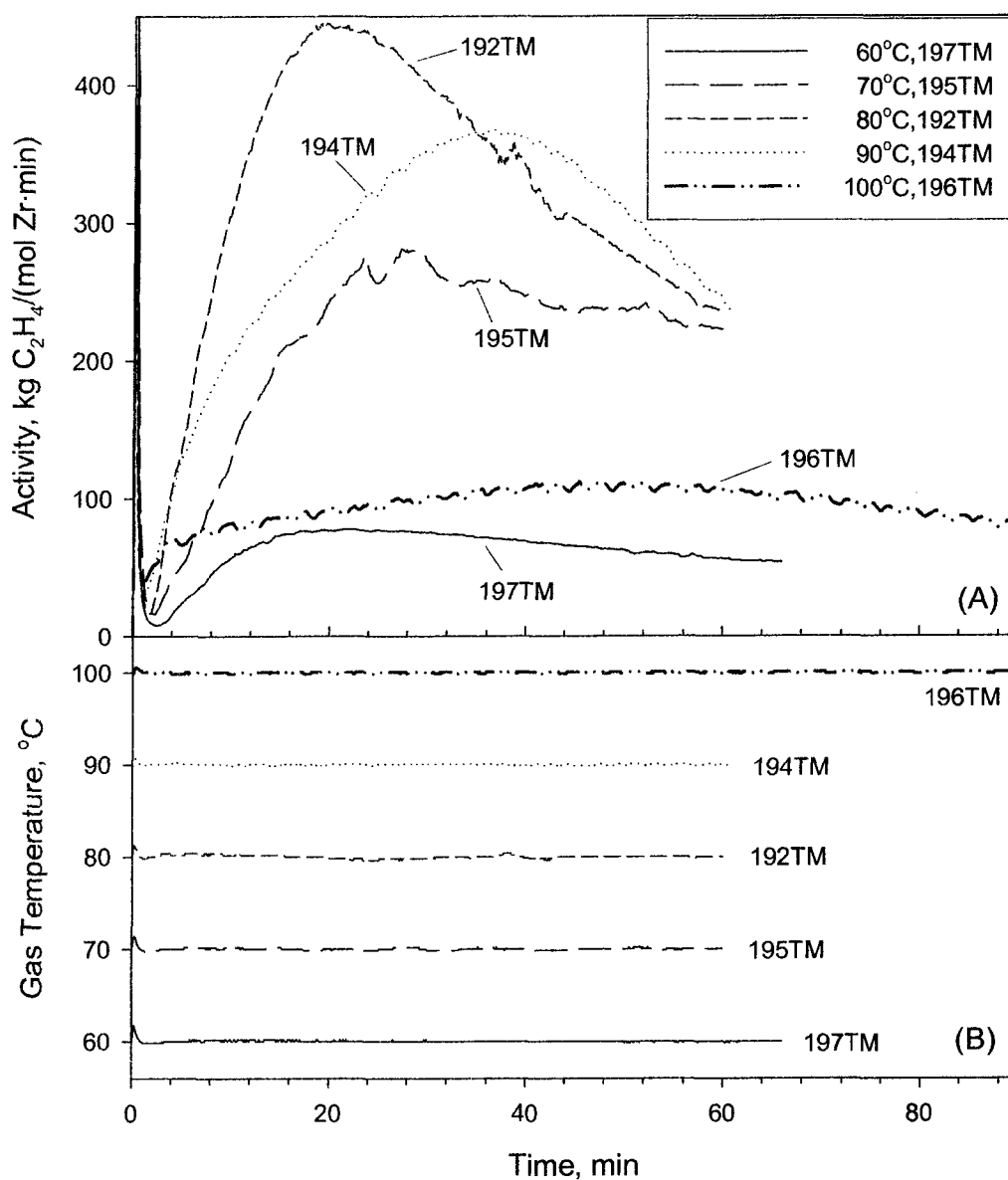


Figure 5.11: Effect of temperature on gas phase polymerization of ethylene and 1-hexene using Catalyst TM17 showing (A) activity profiles, and (B) temperature profiles.

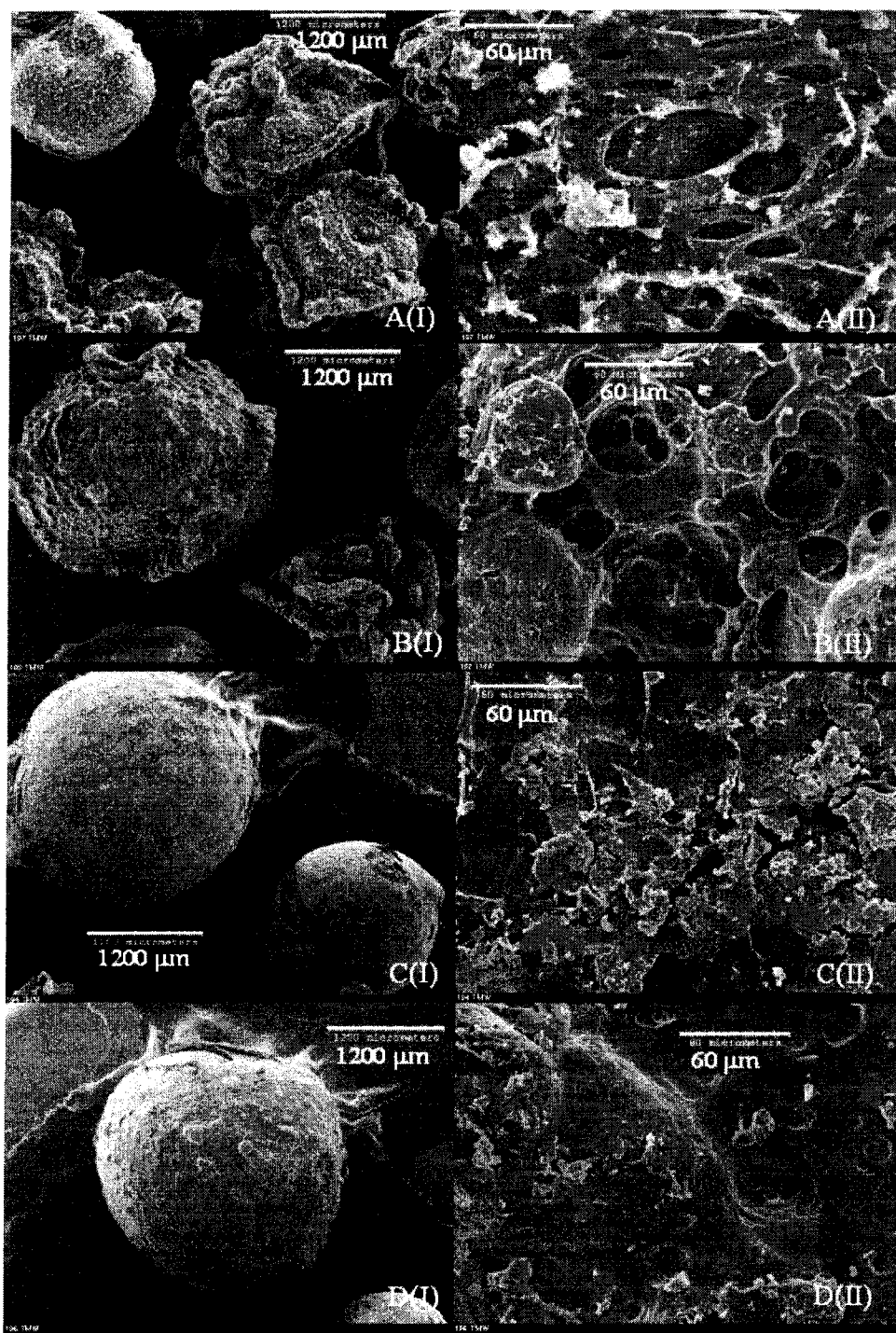


Figure 5.12: SEM images of polymer particles showing effect of gas phase polymerization temperature on outer morphologies at (A) 60°C (Run # 197TM), (B) 80°C (Run # 192TM), (C) 90°C (Run # 194TM), and (D) 100°C (Run # 196TM) using Catalyst TM17.

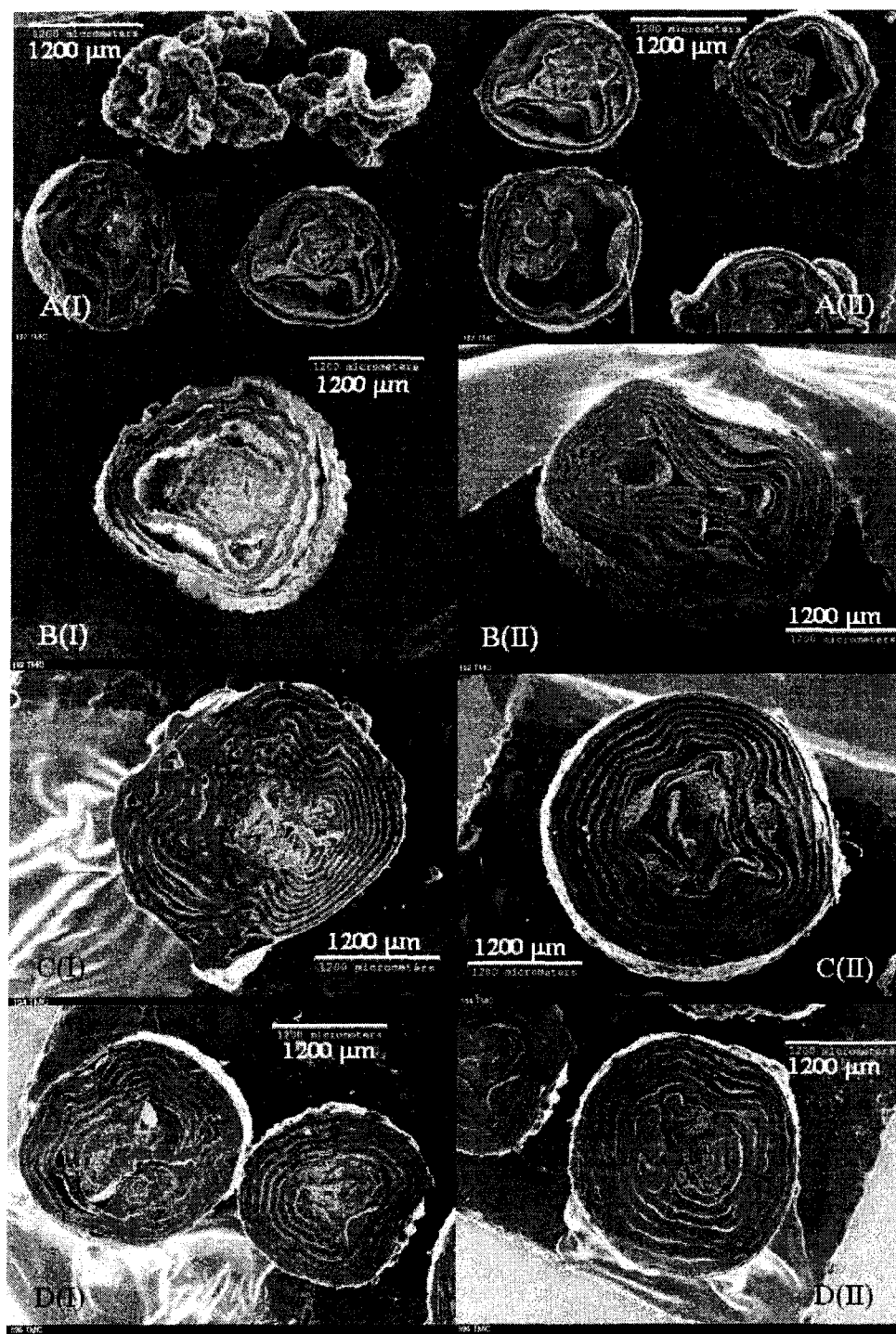


Figure 5.13: SEM images of polymer particles showing effect of gas phase polymerization temperature on inner morphologies at (A) 60°C (Run # 197TM), (B) 80°C (Run # 192TM), (C) 90°C (Run # 194TM), and (D) 100°C (Run # 196TM) using Catalyst TM17.

The polymerization temperature influences molar masses of polymer resins. The number averaged and weight averaged molar masses ( $M_n$  and  $M_w$ ) of the polymer resins produced in this set of experiments have been plotted in Figure 5.14. Although for homopolymers increasing polymerization temperature decreases the molar masses of the polymers monotonically, dos Santos et al. (1999) such trend was not apparent for copolymers produced in this set of experiments. The result was likely due to variation during the experiment in concentration of 1-hexene, which had been charged initially before the start of the run. The change in concentration of 1-hexene was most during the high activity runs at 70, 80 and 90°C. However, overall for runs from 60 to 100°C there was reduction in molar mass with increase in temperature.

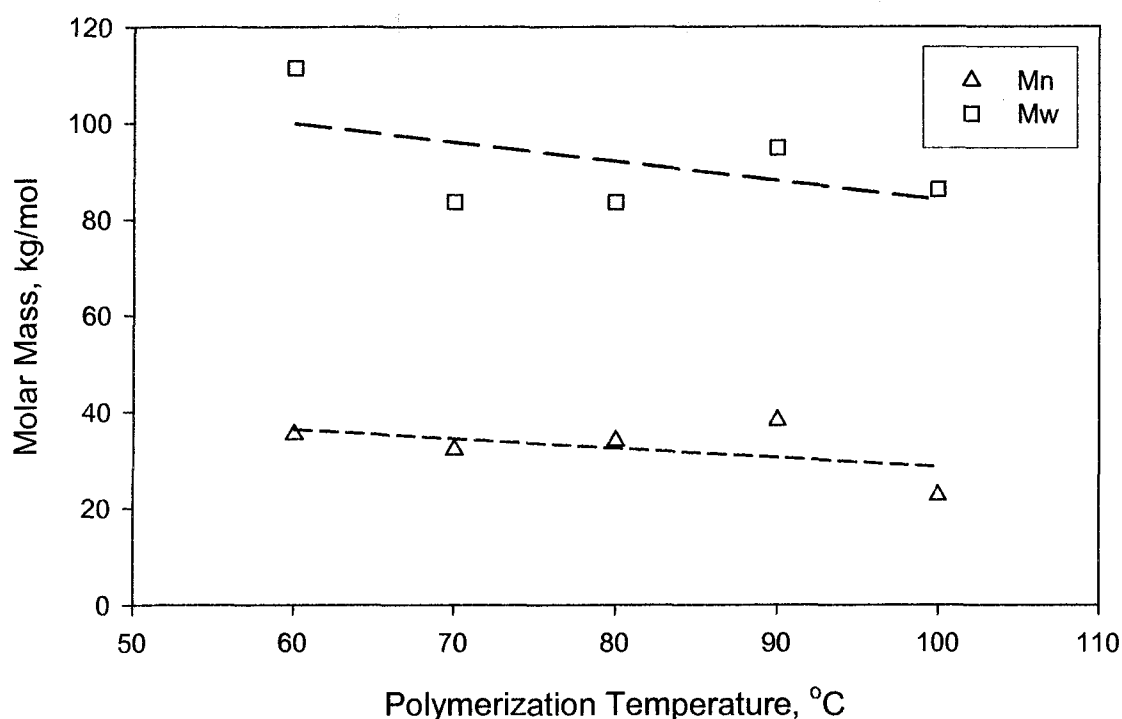


Figure 5.14: Effect of polymerization temperature on product polymer molar mass.

#### 5.4 Effect of Ethylene Pressure on Activity Profiles

A set of copolymerization experiments was done to determine the effect of changing monomer concentration by varying ethylene pressure. The initial 1-hexene concentration was about 11 mol/m<sup>3</sup> for all these runs. As 1-hexene was not injected during the run its concentration varied over the polymerization period. Catalyst TM10 supported on 400–200 µm in-house 2-hydroxyethylmethacrylate divinyl benzene (HEMA/DVB) porous polymer support particles was used for this set of experiments. The catalyst had zirconium concentration of 0.23 mass % and molar ratio of aluminum to zirconium of 285:1. The initial conditions of these runs are given in Table 5.8 below, and the activity profiles and bulk gas temperature profiles are shown in Figure 5.15 (A) and (B) respectively.

Table 5.8: Polymerization runs using Catalyst TM10 to study effect of ethylene pressure on activity profiles (Type A runs, see Chapter 3).

Run Number	Date Performed	Catalyst Amount, (mg)	Initial Temperature, (°C)	Total Pressure, (MPa)	Initial C <sub>6</sub> H <sub>12</sub> conc., (mol/m <sup>3</sup> )
74TM	10/15/01	115	80	0.70	10.81
75TM	10/16/01	115	80	2.06	10.88
76TM	10/17/01	115	80	1.05	10.88
77TM	10/18/01	115	80	1.74	10.84
78TM	10/19/01	115	80	1.39	11.34

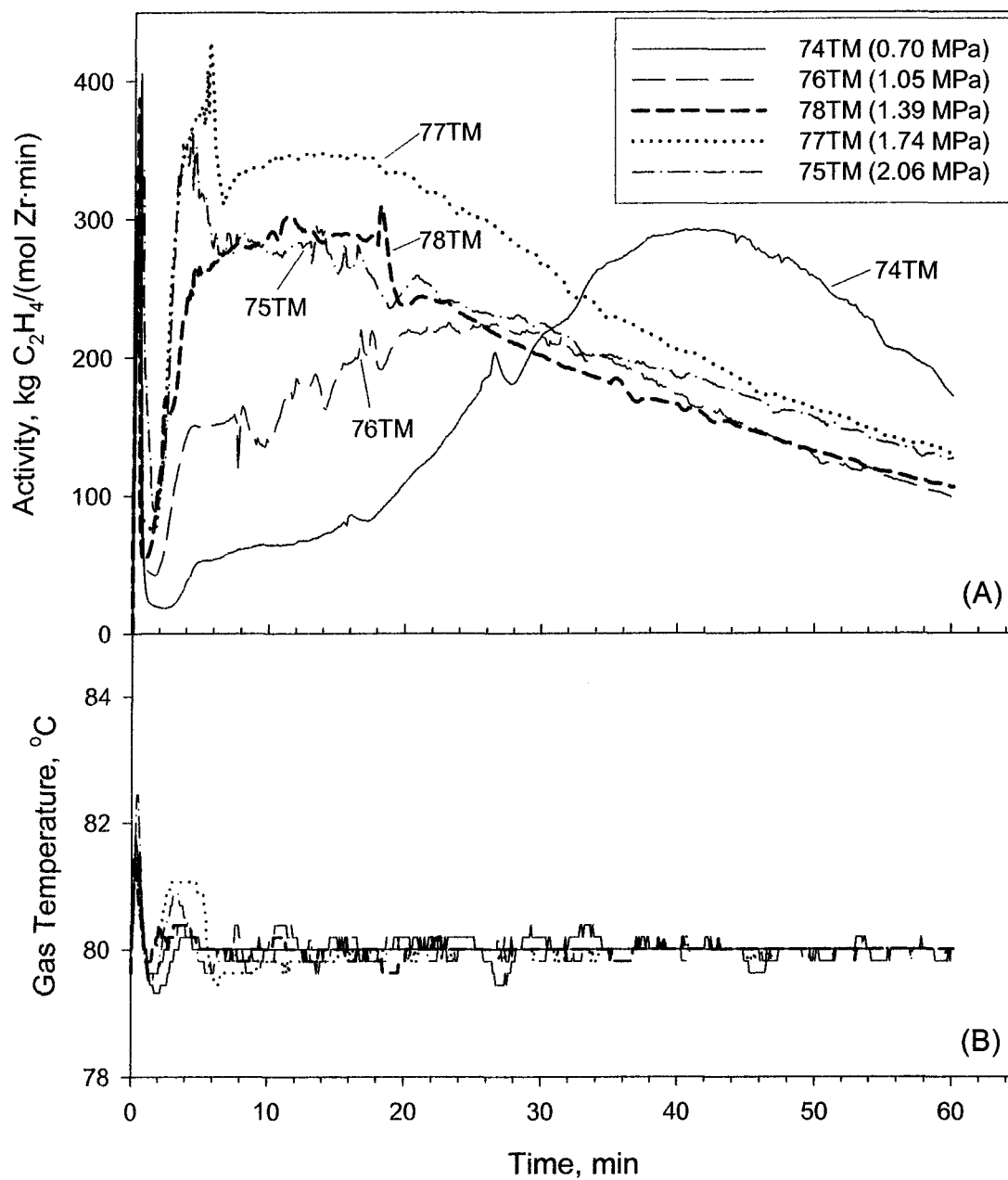


Figure 5.15: Effect of ethylene pressure on gas phase copolymerization using Catalyst TM10 showing (A) activity profiles, and (B) temperature profiles.

Figure 5.15 (A) shows that as ethylene concentration was increased the activity profiles changed from low initial activity, which increased slowly to a maximum before decreasing, to high initial activity that was reached very quickly and then decreased. Moreover, the higher the ethylene pressure the shorter was the time taken for activity to start increasing rapidly after the initial spike in activity profile due to filling of the reactor with ethylene. Although it can be expected that polymerization activity will increase with increase in monomer concentration, Meier et al. (2001) a number of other factors were also important for these profiles. As mentioned previously the 1-hexene concentration decreased during the course of the experiments and this decrease would be more rapid for the runs which had high initial activities. Rise in internal temperature of catalyst/polymer particles especially during high initial activities would also affect activity profiles. Also, for supported catalysts of this size range it is likely that support breakup will influence diffusion of monomer into the catalyst particles.

Morphologies of the polymer particles produced during this set of experiments were studied using scanning electron microscope. External morphologies of particles produced at various ethylene pressures are shown in Figure 5.16 and their internal morphologies are shown in Figure 5.17. The particles produced at higher pressures had rougher external surfaces than those produced at lower pressures. The typical internal annular polymer layers formed during copolymerization were more widely spaced in particles formed at higher pressures. These differences arose most likely due to the lower initial activity and the corresponding slower rate of polymer formation at lower ethylene pressure that would have resulted in more gradual fracturing of the catalyst support particle.

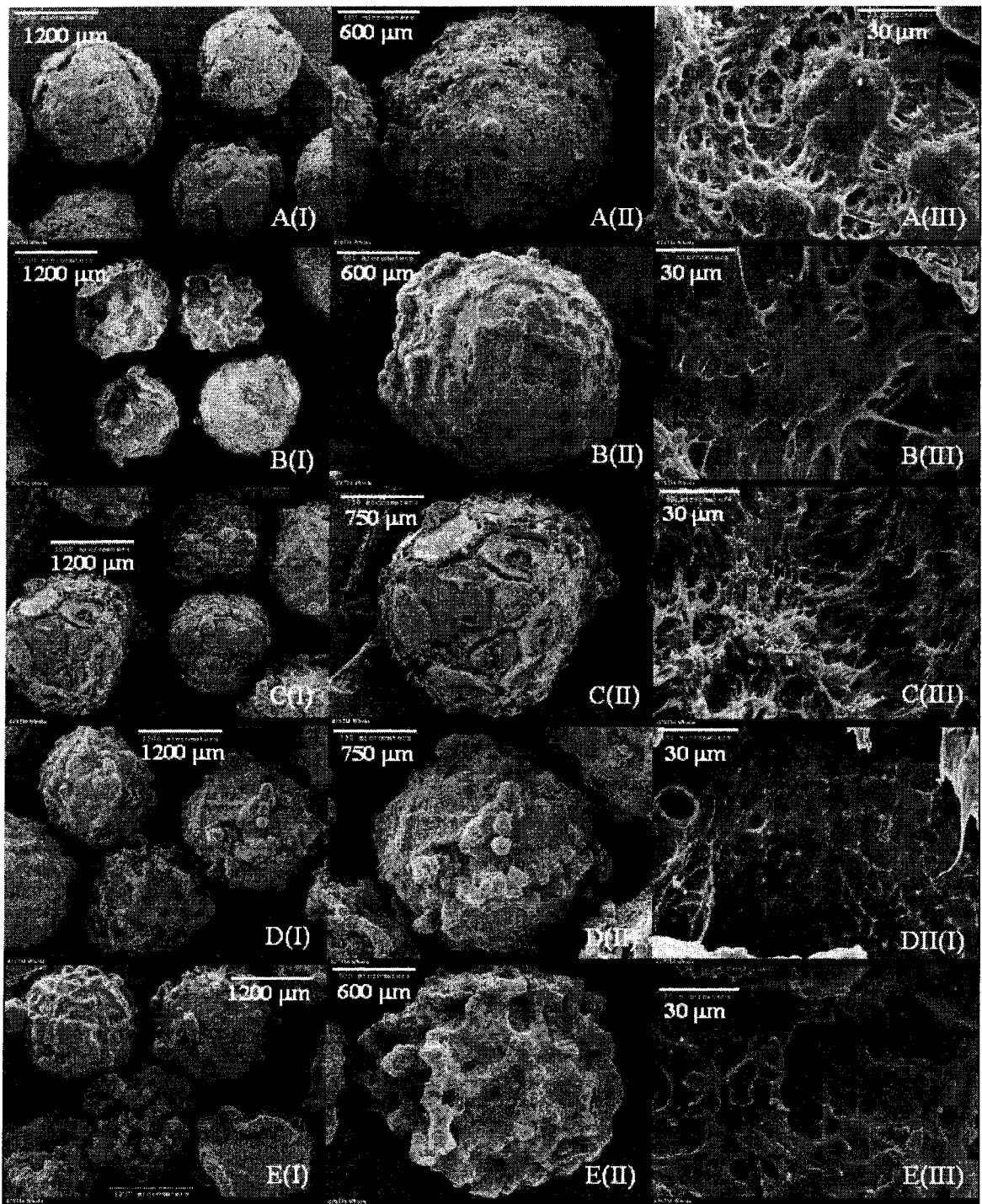


Figure 5.16: SEM images of polymer particles showing effect of gas phase pressure on outer morphologies at (A) 0.70 MPa (Run # 74TM), (B) 1.05 MPa (Run # 76TM), (C) 1.39 MPa (Run # 78TM), (D) 1.74 MPa (Run # 77TM), and (E) 2.06 MPa (Run # 75TM) produced by polymerization at 80°C using Catalyst TM10.

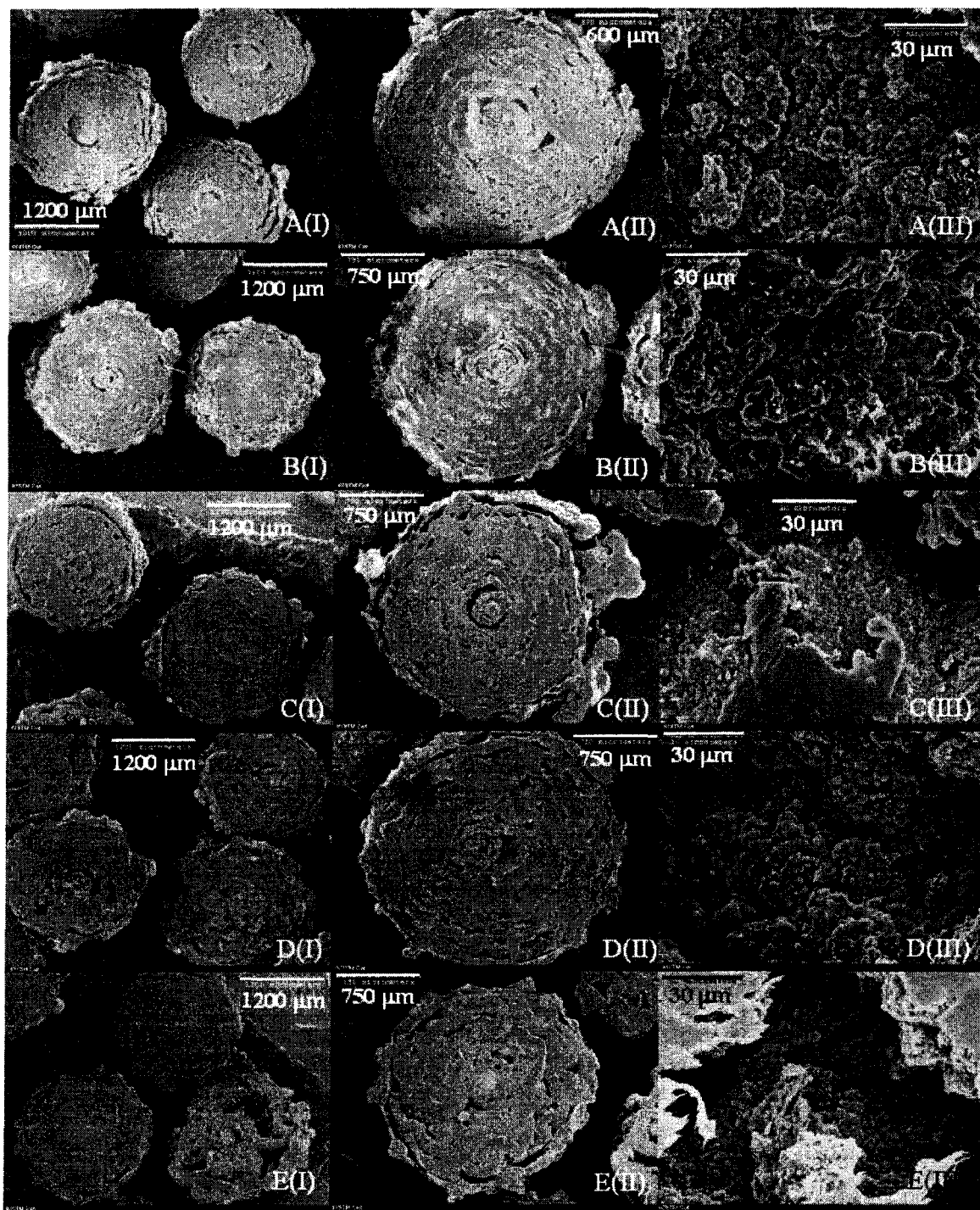


Figure 5.17: SEM images of polymer particles showing effect of gas phase pressure on inner morphologies at (A) 0.70 MPa (Run # 74TM), (B) 1.05 MPa (Run # 76TM), (C) 1.39 MPa (Run # 78TM), (D) 1.74 MPa (Run # 77TM), and (E) 2.06 MPa (Run # 75TM) produced by polymerization at 80°C using Catalyst TM10.

The effect of increasing ethylene pressure on molar masses of the product polymer particles is shown in Figure 5.18. GPC analyses of the polymer particles showed that in general as ethylene concentration was increased the molar masses increased. This result was reasonable, as approximately the same amount of 1-hexene was injected during each of these runs; hence, the ratio of 1-hexene to ethylene decreased with increase in ethylene concentration. 1-Hexene is known to act as a chain transfer agent during polymerization and ethylene/hexene copolymers have much lower molar masses than ethylene homopolymers formed using the same catalyst.

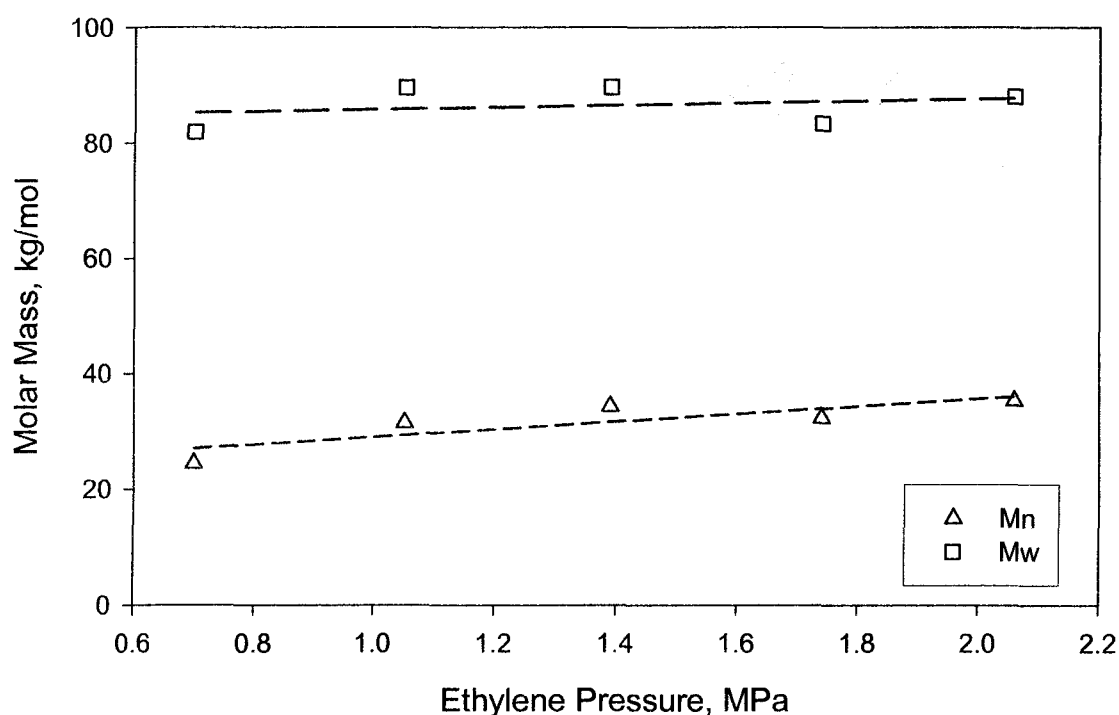


Figure 5.18: Effect of ethylene concentration on product polymer molar masses.

### 5.5 Effect of Nitrogen on Activity Profiles

The presence of an inert gas during polymerization can be used to moderate activity and improve gas phase temperature control. A set of experiments, listed in Table 5.9 below, were done to determine the effect of nitrogen on activity during copolymerization of ethylene and 1-hexene using catalyst TM10. Nitrogen partial pressure was varied from 0 to 1.4 MPa while ethylene partial pressure was about 0.7 MPa and initial concentration of 1-hexene was approximately 11 mol/m<sup>3</sup> for each run. The activity and temperature profiles of these polymerization runs are shown in Figure 5.19 (A) and (B) respectively. The activity profiles revealed that as partial pressure of nitrogen was increased, the induction period required before catalyst activity started to rise rapidly also increased. However, the activity profiles at later periods showed very similar trends and activities. For all three experiments the gas phase temperature was maintained very close to the set-point temperature of 80°C.

Table 5.9: Experiments using Catalyst TM10 to study effect of nitrogen pressure on activity profiles during ethylene polymerization at 80°C (Type A runs, see Chapter 3).

Run Number	Date Performed	Catalyst Amount, (mg)	N <sub>2</sub> Partial Pressure, (MPa)	Total Pressure, (MPa)	Initial C <sub>6</sub> H <sub>12</sub> conc., (mol/m <sup>3</sup> )
79TM	10/25/01	116	0	0.69	10.99
80TM	10/26/01	115	0.69	1.37	10.67
81TM	10/31/01	115	1.39	2.10	10.63

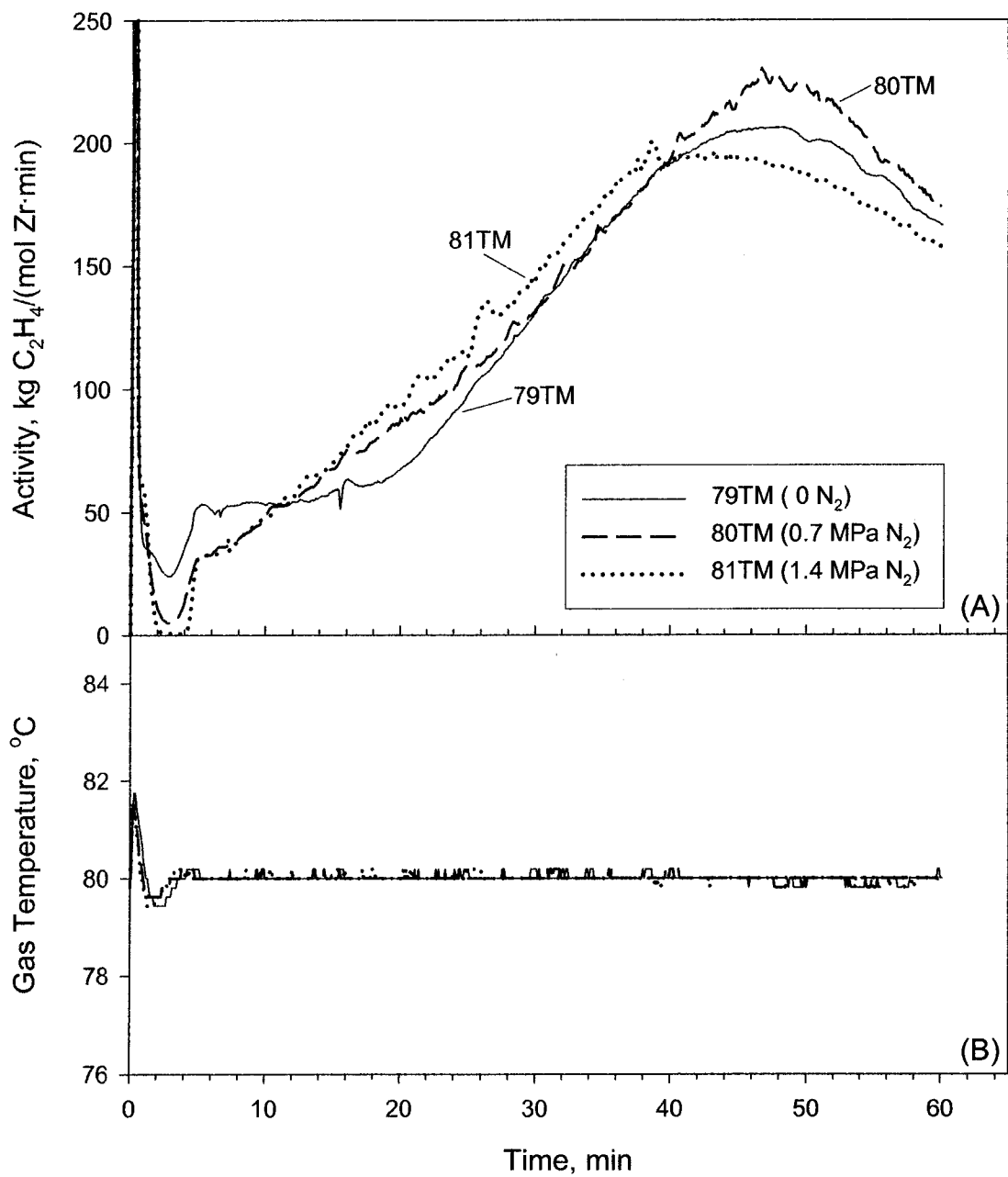


Figure 5.19: Effect of presence of nitrogen on gas phase copolymerization using Catalyst TM10 showing (A) activity profiles, and (B) temperature profiles.

The differences in the initial induction periods revealed that at higher partial pressures of nitrogen the catalyst activity is less, this could be due to diffusion limitation of monomer gas to the active sites on catalyst surface. Moreover, it is likely that in the absence of nitrogen the internal temperature of the polymerizing catalyst particles was higher than that of catalyst particles in presence of nitrogen due to lower gas heat transfer coefficients at lower pressures. This would further tend to increase activity in absence of nitrogen, but the similarities of the activity profiles after the first few minutes indicate that external monomer diffusion was no longer rate controlling. This implies that during the induction period, the polymer built up in the pores of the catalyst particle, resulting in catalyst particle fragmentation that greatly enhanced the diffusion of monomer gases to the active sites. Also as the catalyst/polymer particle increased in size heat transfer from the external surface increased and the difference between particle temperature and bulk gas temperature decreased.

The temperature profiles shown in Figure 5.19 (B) showed no significant effect of nitrogen in the gas phase temperature profiles. Closer inspection showed that the initial spike in the temperature profile due to sudden compression of gas upon catalyst injection was less for the runs with greater amount of nitrogen present in the reactor. This is to be expected because the relative increase in pressure is less if nitrogen is present resulting in lower adiabatic temperature rise.

## 5.6 Effect of Catalyst Amount on Activity Profiles

The amount of catalyst used is another parameter that influences the activity profile during polymerization. A set of experiments using Catalyst TM10 was performed to study this effect. For each of these runs, the initial concentration of 1-hexene was about  $11 \text{ mol/m}^3$  and total pressure was around 1.4 MPa. Tri-isobutyl aluminum, TIBA (0.1 mL) injected into the reactor as a scavenger was removed from the reactor by evacuation before start of each polymerization run. Some details about these experiments are given in Table 5.10 below. PID temperature controller was used to control the gas phase temperature during polymerization. The activity profiles and temperature profiles of the polymerization runs are shown in Figure 5.20. The total activity in  $\text{g-C}_2\text{H}_4/\text{min}$  consumed is shown in Figure 5.20 (A); the activity per mole of metallocene is shown in Figure 5.20 (B); and the gas phase temperature profile during polymerization is shown in Figure 5.20 (C).

Table 5.10: Experiments using Catalyst TM10 to study effect of amount of catalyst on activity profiles during ethylene polymerization at  $80^\circ\text{C}$  (Type A runs, see Chapter 3).

Run Number	Date Performed	Catalyst Amount, (mg)	Initial Temperature ( $^\circ\text{C}$ )	Total Pressure, (MPa)	Initial $\text{C}_6\text{H}_{12}$ conc., ( $\text{mol/m}^3$ )
78TM	10/19/01	115	80	1.41	11.34
82TM	11/01/01	83	80	1.40	10.95
83TM	11/02/01	42	80	1.39	11.48

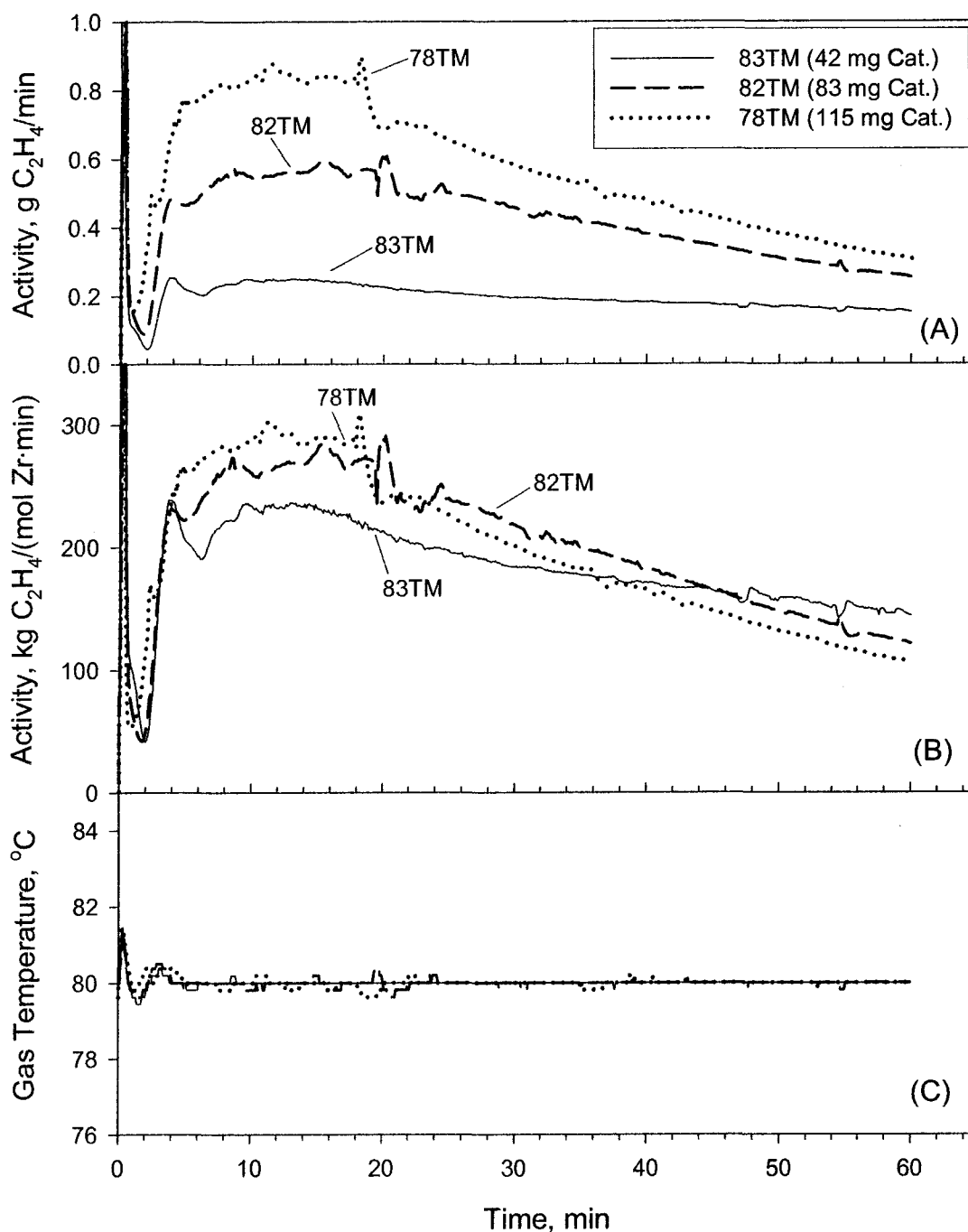


Figure 5.20: Effect of amount of catalyst used on gas phase copolymerization using Catalyst TM10 showing (A) activity profiles, (B) activity profiles per mole of zirconium, and (C) temperature profiles with PID temperature controller switched on.

From the activity profiles it can be seen that larger the catalyst amount used, the greater was the activity per mole of zirconium. This can be explained in terms of there being similar amounts of catalyst poison initially present in the reactor in each polymerization run and effect of this poison would be more pronounced in the run with the lesser amount of catalyst. Moreover, the rate of decline in activity was greater for the runs with more catalyst and higher activity. This could be the result of the catalyst poisoning being reversible, which would result in new active catalytic sites being generated during polymerization while old active sites were deactivating. This again would be more significant when less catalyst was used during polymerization. It is also likely that the catalyst particle temperature is higher than the gas phase temperature, especially when activity per mole of zirconium is a high. This would also contribute to more rapid catalyst deactivation at higher catalyst loading, as catalyst deactivation is greater at higher temperature.

A significant problem with increasing the amount of catalyst is the increase in total thermal energy generated during polymerization, that can lead to a rapid increase in the gas phase temperature. In this set of experiments the coolant system of the reactor with PID temperature controller was able to deal with the increased thermal load and the gas phase temperature was maintained near the set point temperature, 80°C throughout the polymerization runs. With the PID temperature controller switched off and oil at 80°C circulating in reactor coolant channels, a set of polymerization runs using Catalyst TM11 were carried out to study the effect of increasing catalyst loading into the reactor. This mode of operation simulated the temperature control in a laboratory reactor immersed in a circulating oil bath at constant temperature or a jacketed reactor with coolant flow at

constant temperature. In Table 5.11 some experimental details of these polymerization runs are given. The time averaged temperature from time of catalyst injection into the reactor to end of the run are given in Column 4 of Table 5.11.

The activity profiles and temperature profiles of the runs given in Table 5.11 are shown in Figure 5.21. It can be seen from Figure 5.21 (A) that greater the amount of catalyst used the larger the consumption of ethylene per minute and the greater the increase in corresponding gas phase temperature, see Figure 5.21 (C). The temperature profiles were very similar to the activity profiles. However, the activity profiles per mole of zirconium, see Figure 5.21 (B), show that although the activity per mole increased initially as amount of catalyst loading was increased from 50 mg to 100 mg, it decreased when 150 mg was used. This was due to increased catalyst deactivation at higher temperature that resulted from the higher overall activity (g C<sub>2</sub>H<sub>4</sub>/min) for larger amounts of catalyst. The initial increase in activity per mole of zirconium was most likely due to catalyst poisoning as explained previously.

Table 5.11: Experiments using Catalyst TM11 to study effect of amount of catalyst on activity profiles during ethylene polymerization (Type A runs, see Chapter 3).

Run Number	Date Performed	Catalyst Amount, (mg)	Time Averaged Temp., (°C)	Total Pressure, (MPa)	Initial C <sub>6</sub> H <sub>12</sub> conc., (mol/m <sup>3</sup> )
94TM	12/04/01	50	81.5	1.41	11.37
95TM	12/05/01	150	84.1	1.40	11.69
96TM	12/06/01	100	83.5	1.39	11.41
97TM	12/07/01	75.6	82.1	1.39	11.30

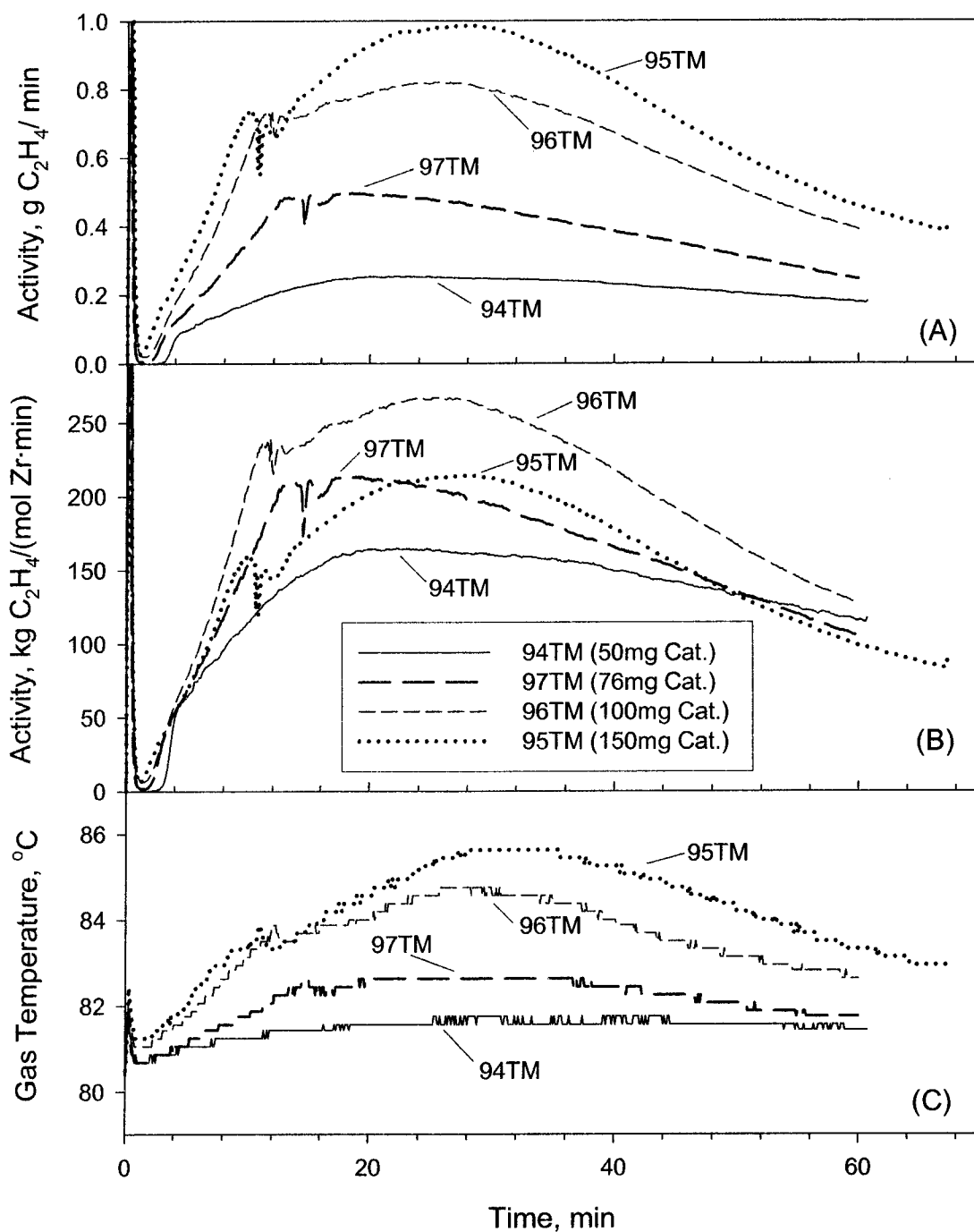


Figure 5.21: Effect of amount of catalyst used on gas phase copolymerization using Catalyst TM11 showing (A) activity profiles, (B) activity profiles per mole of zirconium, and (C) temperature profiles with coolant oil at  $80^\circ\text{C}$  circulating in reactor channels.

## 5.7 Summary of Observation from Exploratory Experiments

The exploratory polymerization runs revealed the effects of various parameters on the activity profiles and product polymer properties. These results helped in better understanding of the reactor system and can be used to predict trends in reactor behavior and product polymer properties. Some of the observations drawn from these experiments are as follows:

- 1) Alkyl aluminum scavengers used initially to remove catalyst poisons from the reactor have significant effects on subsequent polymerization activity and product properties. The effect depends on the type and amount of scavenger used. Small amounts of scavenger resulted in a rapid attainment of maximum activity. Larger amounts of scavenger broadened activity profiles and reduced molar masses of polymer products. Hence, alkyl aluminums can be used to moderate activity and thus control gas phase temperature. For quantification see Figure 5.6.
- 2) The gas phase polymerization temperature has profound effect on the activity profiles and product polymer properties. Although increase in polymerization temperature initially increased activity, at temperatures above 85°C overall polymerization activities were reduced probably due to deactivation of the co-catalyst. Moreover at higher temperatures, partial polymer fusion resulted in changes in internal and external morphologies of product polymer particles. Increase in polymerization temperature in general resulted in decrease in molar masses of polymer product. Activity rates were maximum about 80 - 90°C for all catalysts and decreased thereafter.

- 3) Monomer concentration as measured by ethylene pressure affected polymerization activity profiles with increases in pressure reducing the time taken to reach maximum activity. However at ethylene pressures greater than 1.4 MPa these differences were not prominent. The ethylene pressure did not significantly affect the inner and outer morphologies of the product polymer particles. Keeping initial co-monomer, 1-hexene, concentration constant increases in ethylene pressure increased the molar masses of the product polymer.
- 4) The presence of an inert gas like nitrogen can be used to improve gas phase heat transfer. Although increase in partial pressure of nitrogen increased the induction period required before catalyst activity started to increase rapidly, overall activity profiles were not much affected by the presence of nitrogen. For the polymerization runs studied no significant effect of nitrogen on gas phase temperature was observed.
- 5) The amount of catalyst loaded into the reactor and its activity determine the thermal energy to be dissipated by the coolant system of the reactor to maintain the gas phase temperature. However, the presence of catalyst poison, which has greater proportional effect on smaller amount of catalyst, requires use of larger amounts of catalysts to minimize the effect of the poison. Thus experiments showed that there was an optimum amount of catalyst, typically about 100 mg for most of the supported catalysts used, to get maximum activity per mole of metallocene. The amount of catalyst used significantly influenced the activity profiles by affecting the gas phase temperature in runs where the PID temperature controller was switched off.

## 6. Imaging of Growing Polymer Particles

Although the novel gas phase reactor described previously was suited to study the overall kinetics of polymerization catalysts, activities of individual particles cannot be observed. Video imaging of the catalyst particles during polymerization can yield catalyst-specific information such as shape replication, distribution of activity, and activation (Pater et al., 2003). In order to get insight into how individual catalyst particles behaved during polymerization, a micro-reactor with Pyrex windows was made as described in Chapter 3. A microscopic lens (Navitar Inc., Rochester, NY) attached to video camera (Pulnix America, Inc.) was used to image the growing particles in the micro-reactor. However, in situ video imaging only observed the outer morphologies of the growing particles and could not provide information about the development of their inner structures.

With the aim of obtaining information about the development of internal and external structures of the growing polymer particles, a series of experiments was performed under similar conditions where polymerization was stopped after different intervals of time. Scanning electron microscopy analyses of whole and cut particles from these runs revealed how the external and internal structures of the polymer particles developed during both homo- and co-polymerizations. Similar work has been reported by Fink et al. (2000) for silica supported metallocene catalyst for propylene polymerization.

## 6.1 Micro-Reactor Operation Procedure

About 2 mg of the catalyst was first placed on a monofilament nylon sieve on the bottom Pyrex window of the unassembled micro-reactor inside the glove-box. The reactor was carefully reassembled with the inlet valve closed and taken out of the glove-box. The sieve hindered the movement of catalyst particles during transport and polymerization and was also used as a reference for particle size. Under flowing nitrogen the inlet valve of the micro-reactor was then connected to the main reactor that had previously been pressurized to 0.14 MPa (20 psia) with ultra high purity nitrogen. The main reactor was then evacuated to less than 5 Pa. After pressurizing with ethylene to 0.11 MPa, TIBAL scavenger was added to the main reactor followed by the addition of the desired amount of 1-hexene and further pressurizing with ethylene to the desired pressure of 1.4 MPa. Scavenging was done for thirty minutes while the gases were heated to the polymerization temperature.

A videocassette recorder, which was connected to the microscope video camera, was switched on and polymerization was started by turning on the inlet valve of the micro-reactor. An electric heating tape wound around the micro-reactor was used to keep it at the desired polymerization temperature. As the optical video-microscope had a shallow depth of field, during polymerization the images of the growing catalyst/polymer particles tended to blur and the microscope sometimes required to be manually refocused. Polymerization was stopped by venting the main reactor to atmospheric pressure, followed by purging it with nitrogen. Still images from such polymerization runs as shown in Figure 6.1 and 6.2 were obtained from the videotape.

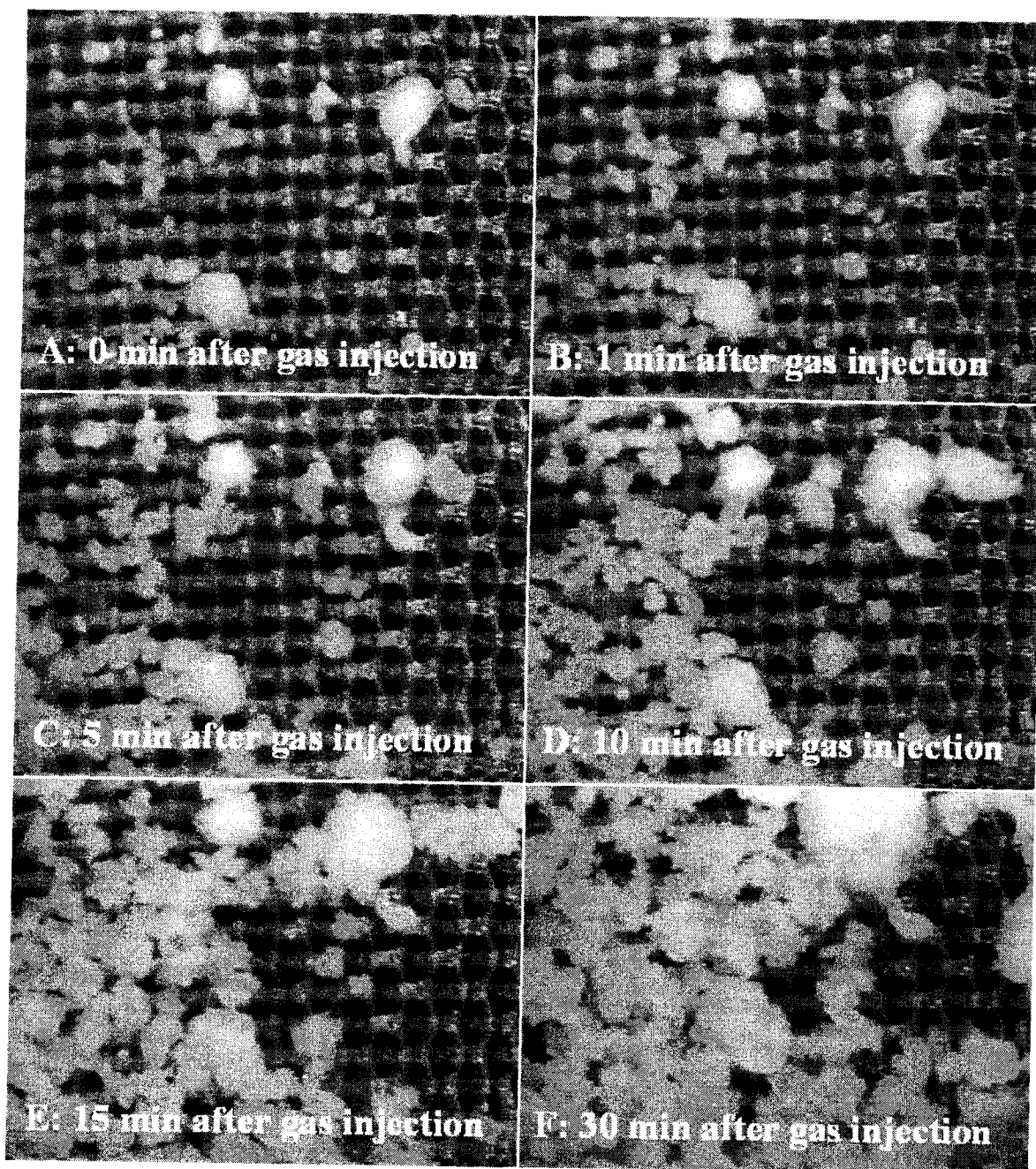


Figure 6.1: Growth of Catalyst TM15 (600–850  $\mu\text{m}$  support size range) particles and fragments on 250  $\mu\text{m}$  sieve during polymerization from (A) immediately after gas entry into micro-reactor to (F) 30 minutes later.

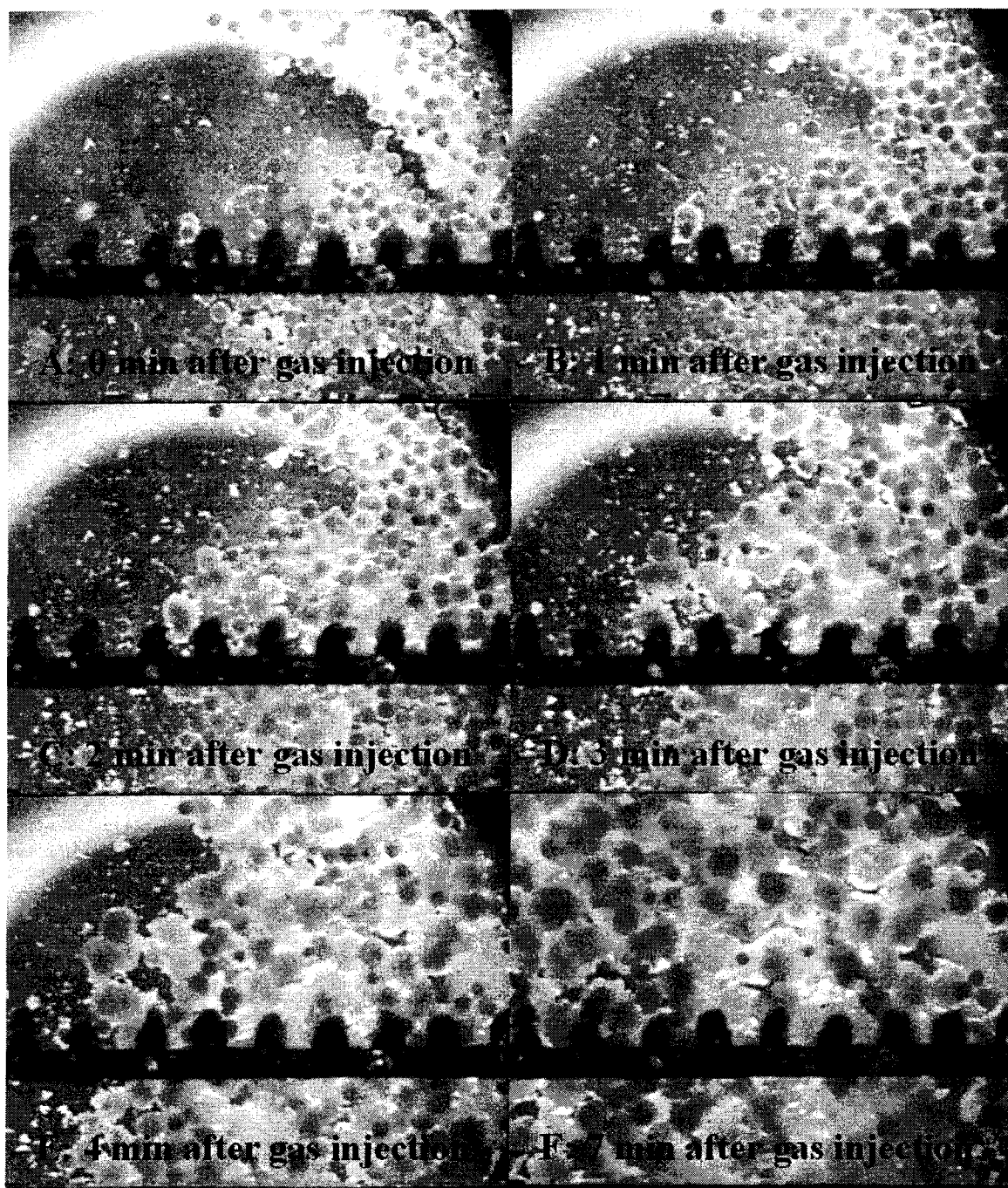


Figure 6.2: Growth of Catalyst TM22 (300-350  $\mu\text{m}$  support size range) particles and fragments during polymerization from (A) immediately after gas entry into micro-reactor to (F) 7 minutes later. Black scale markings are approximately 1 mm apart.

## 6.2 In Situ Video Imaging of Growing Particle

The video-photography of the growing catalyst particles was used for qualitative analysis purpose only. Figure 6.1 shows a time series of images obtained from a typical co-polymerization run in the micro-reactor using Catalyst TM15. This catalyst was made from HS-R1 support containing particles of size range 600-850  $\mu\text{m}$ . The situation immediately after the monomer gas mixture containing ethylene and 1-hexene with trace TIBAL was let into the micro-reactor from the main reactor is shown in Figure 6.1 (A). Three whole catalyst particles and number of smaller catalyst fragments are visible in the picture. After 1 minute, Figure 6.1(B) only a few of the catalyst fragments showed any growth. After 5 minutes, Figure 6.1(C) most of the catalyst fragments were growing but the larger whole catalyst particles did not have any visible growth. However, after 10 minutes, Figure 6.1 (D) all the particles had increased in size. Polymerization with the accompanying growth of particle continued even after 30 minutes, Figure 6.1 (E). As the images became very crowded with the particles after 30 minutes further photos are not shown. However, polymerization continued even after 60 minutes before being stopped by venting the monomer gases.

In Figure 6.2 a series of images from ethylene/1-hexene copolymerization using Catalyst TM22 is shown. The catalyst was made from sieved HS-R2 support particles of size range 300–350  $\mu\text{m}$  and had lesser variation in particle sizes than that of catalyst TM15. A large number of catalyst particles were visible immediately after the injection of ethylene/1-hexene into the microreactor in Figure 6.2 (A). Most of the particles had started to grow within a minute, Figure 6.2 (B) and were significantly larger after 2 minutes of polymerization, Figure 6.2 (C). Although the particle growth rate initially

increased during the third and fourth minutes of polymerization, Figures 6.2(D) and 6.2 (E) respectively the rate became less afterwards. After 7 minutes of polymerization, Figure 6.2 (F) the image became too crowded with polymer particles to follow the growth of individual particles and more images are not shown. Even after 7 minutes few particles appeared to be inactive and showed no growth. The graduated scale visible in the pictures marked approximately 1 mm apart was used as a reference for qualitative guide to observing particle growth.

Listed below are a number of deductions that were drawn from visual examination of these and other similar images:

- 1) There was short time interval –“induction period”- before there was any visible growth of the catalyst fragments or particles after they came in contact with the monomer gas mixture. Some catalyst particles/fragments remained inactive throughout the run.
- 2) The smaller catalyst fragments or particles in general had a shorter induction period than the larger catalyst particles. There were however variations in induction time within each type of size ranges of catalyst particles and fragments.
- 3) As polymerization proceeded the growing catalyst fragments and particles tended to replicate their original shapes. The growth rate of particles increased initially before decreasing and finally becoming negligible.

These observations were consistent with the overall activity profiles for copolymerization of ethylene and 1-hexene in the main reactor using the same or similar catalysts where the activity increased rapidly after a short period of low or no activity before diminishing again.

The differences in start of activity of catalyst particles have also been observed by other researchers, such as Zöllner and Reichert (2002) for gas phase butadiene polymerization, and Fink et al. (2000) and Steinmetz et al. (1997) for propylene polymerization. The induction period has been attributed to the time taken for the catalyst support particles to breakup due to hydraulic forces caused by polymer buildup in the pores of the support (Fink et al. (2000)). The smaller catalyst fragments having less resistance to monomer diffusion into their pores because of larger surface area to volume ratio than the bigger catalyst particles will tend to breakup faster. Moreover, it is likely that the smaller catalyst fragments that were present when drying the catalyst slurry during catalyst production have higher overall concentration of zirconocene and MAO than the unfragmented catalyst particles because of lower resistance to permeation of the increasingly concentrated MAO/zirconocene solution into the support particles/fragments. Thus, these smaller catalyst fragments will have greater activities.

It was observed that the activity of the catalyst in the micro-reactor was less than the activity of the same catalyst under similar conditions in the main reactor. This is to be expected for a number of reasons. In the stirred bed reactor the catalyst particles are constantly moving through the gas-phase while in the micro-reactor the particles are lying still on the Pyrex window. This will tend to limit diffusion of monomer gases to the catalyst particles. As the polymerization proceeded in the micro-reactor the growing particles came into physical contact with each other and thus further limiting the diffusion of monomer gases to the particles. Also the temperature of the catalyst particles lying on the unheated Pyrex window is likely to be lower than the bulk gas temperature.

### 6.3 Ex Situ SEM Imaging of Growing Polymer Particles

Although the in situ video imaging was good for qualitative analysis of the growing polymer particles the images were of low resolution and internal morphologies of the particles could not be discerned. Scanning electron microscopy (SEM) is suitable for taking high-resolution images of polymer particles. However, as the samples usually need to be prepared for this method, the analysis is possible only after the polymerization is over. Therefore, to observe ex situ growth of particles using electron microscopy it was necessary to run a series of experiments performed under similar conditions but terminated at different times with the assumption that the runs were reproducible. Environmental transmission electron microscopy had been used to observe in situ growth of Ziegler-Natta catalyst using special cells (Oleshko et al. (2002)) but the conditions of polymerization were far different from that under actual industrial practice and only external particle features could be observed.

Four sets of time series polymerization runs were done for ex-situ SEM analysis of particle growth. For study of particle growth during copolymerization of ethylene and 1-hexene, Catalyst TM20 made from HS-R-6 support particles (size range: 75–90  $\mu\text{m}$ ) and Catalyst TM22 made from sieved HS-R-2 support particles (size range: 300–350  $\mu\text{m}$ ) were used. As it was difficult to cut and prepare very small polymer particles for SEM analysis and, using same catalyst homopolymerization produced much smaller polymer particles than copolymerization due to much lower activity for homopolymerization, only the larger Catalyst TM22 was used for homopolymerization particle growth study. Details of the polymerization run conditions and product properties are given in Table 6.1 and more information can be found in Appendixes A and B.

Table 6.1: Polymerization runs used for ex-situ SEM study of growing polymer particles (Type B runs, see Chapter 3).

Run Number	Date Performed	Catalyst		Scavenger TIBAL, (mL)	Initial Temp., (°C)	Total Initial Pressure, (MPa)	Initial C <sub>6</sub> H <sub>12</sub> conc., (mol/m <sup>3</sup> )	Length of run, (min)	Molar Mass		Pd
		Type	Amount, (mg)						Mn (kg/mol)	Mw (kg/mol)	
239TM	03/24/03	TM20	100.3	0.15	80	1.40	14.7	60	33.9	90.1	2.66
240TM	03/25/03	TM20	100.7	0.15	80	1.39	14.8	2	8.1	88.7	10.95
241TM	03/26/03	TM20	100.3	0.15	80	1.40	14.7	4	10.7	114.3	10.68
242TM	03/27/03	TM20	102.2	0.15	80	1.40	14.7	15	17.7	112.8	6.37
243TM	03/28/03	TM20	102.5	0.15	80	1.39	14.7	10	15.4	120.0	7.79
248TM	04/28/03	TM22	101.0	0.15	80	1.38	14.8	60	32.0	82.8	2.59
249TM	04/29/03	TM22	100.0	0.15	80	1.40	14.6	2	7.3	72.5	9.93
250TM	05/01/03	TM22	101.5	0.15	80	1.39	14.7	10	13.2	103.6	7.85
251TM	05/02/03	TM22	101.3	0.15	80	1.41	14.5	4	10.0	76.2	7.62
252TM	05/09/03	TM22	104.0	0.15	80	1.39	14.6	15	33.5	126.7	3.78
253TM	05/13/03	TM22	103.0	0.15	70	1.41	14.8	60	33.4	87.5	2.62
254TM	05/14/03	TM22	99.0	0.15	70	1.39	14.8	2	7.0	49.5	7.07
255TM	05/21/03	TM22	101.5	0.15	70	1.38	14.6	15	31.3	144.0	4.60
256TM	05/22/03	TM22	101.5	0.15	70	1.38	14.7	10	23.3	133.6	5.73
257TM	05/23/03	TM22	102.5	0.15	70	1.39	14.6	4	9.9	57.7	5.83
258TM	05/28/03	TM22	101.9	0.15	80	1.38	0	30	77.2	239.2	3.10
259TM	06/20/03	TM22	101.6	0.15	80	1.39	0	2	96.2	242.9	2.52
260TM	07/18/03	TM22	100.5	0.15	80	1.42	0	10	91.6	263.2	2.87

### 6.3.1 Growth of Polymer Particles during Copolymerization

SEM analyses of polymer particles from a series of copolymerization runs of various lengths of times using Catalyst TM20 are shown in Figure 6.3. Images taken at low magnification (Series (I)) showing many particles and images of single particles (Series (II)) taken at higher magnification are shown. In Figure 6.3(A) the catalyst particles are shown for comparison. Figure 6.3(B) shows that after 2 minutes of polymerization, Run # 240TM, the polymer particles are more than twice the size of the original catalyst particles. Further growth of the particles after 4 minutes (Run # 241TM), 10 minutes (Run # 243TM), 15 minutes (Run # 242TM), and 60 minutes (Run # 239TM), are shown in Figures 6.3(C), 6.3(D), 6.3(E), and 6.3(F) respectively. These runs were carried out at total pressures of about 1.40 MPa and initial 1-hexene concentrations of about  $14.7 \text{ mol/m}^3$  corresponding to  $4.0 \text{ cm}^3$  of injected 1-hexene.

The activity and bulk gas temperature profiles of these runs are shown in Figure 6.4. The initial spike in the consumption rate of ethylene was due to filling of the reactor with ethylene when the catalyst was injected into the reactor and reactor pressure increased from 1.0 MPa to 1.4 MPa. There was a corresponding spike in the gas temperature profile because of the increase in temperature of the gas in the reactor due to sudden increase in pressure. The 2, 4, 10, and 15 minutes runs were remarkably consistent but the 1 hour run deviated from the others after 5 minutes. During the 1 hour run the activity of the catalyst was so high that the reactor temperature controller was unable to maintain the reactor at the set value of  $80^\circ\text{C}$  and bulk gas temperature went up to about  $98^\circ\text{C}$ . Manual intervention was required to bring the temperature down.

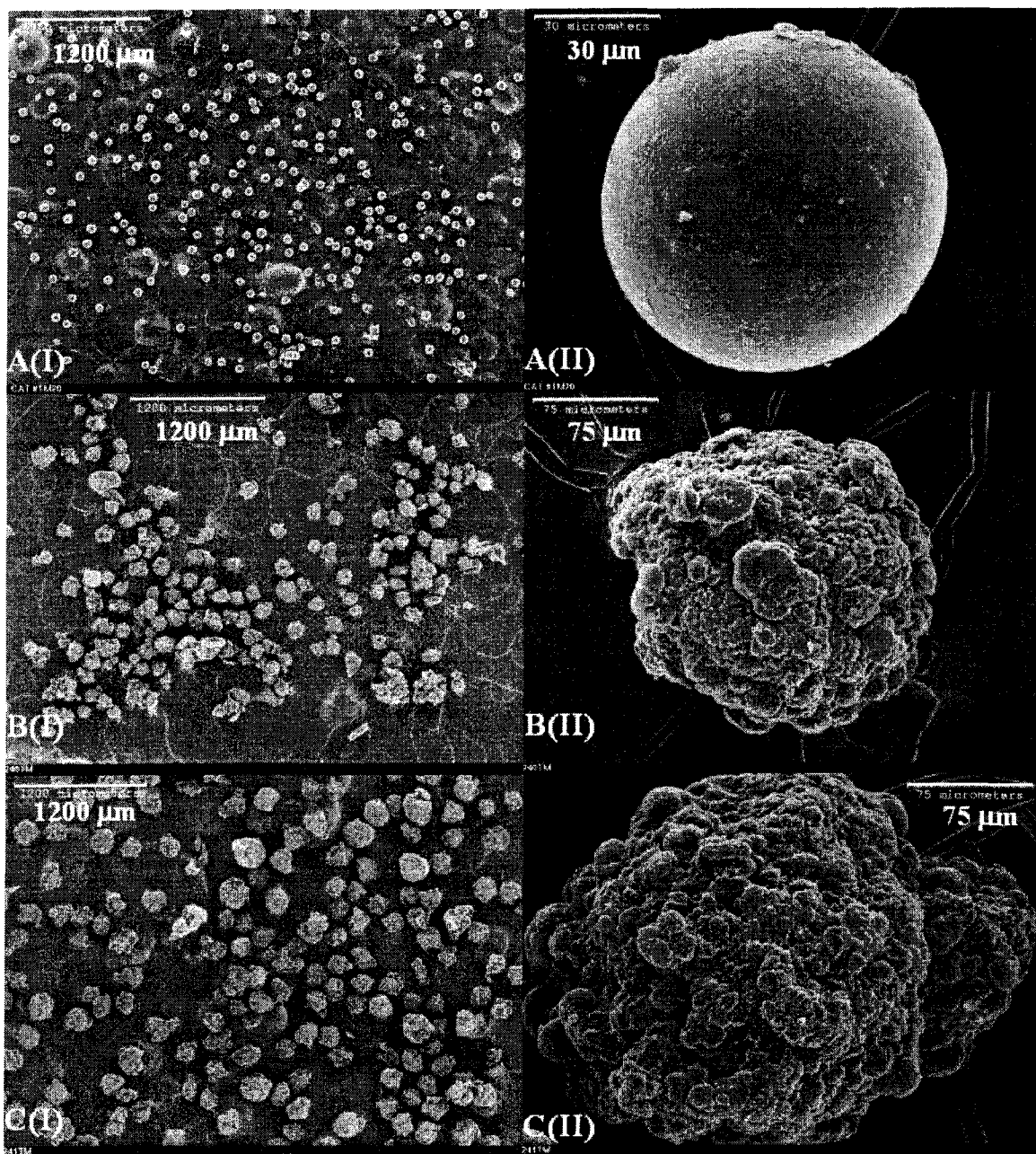


Figure 6.3: SEM of copolymerization of Catalyst TM20 at low (I) and high (II) magnifications for runs of different lengths – (A) catalyst particles; (B) 2 min polymerization; (C) 4 min polymerization; (continued in next page).

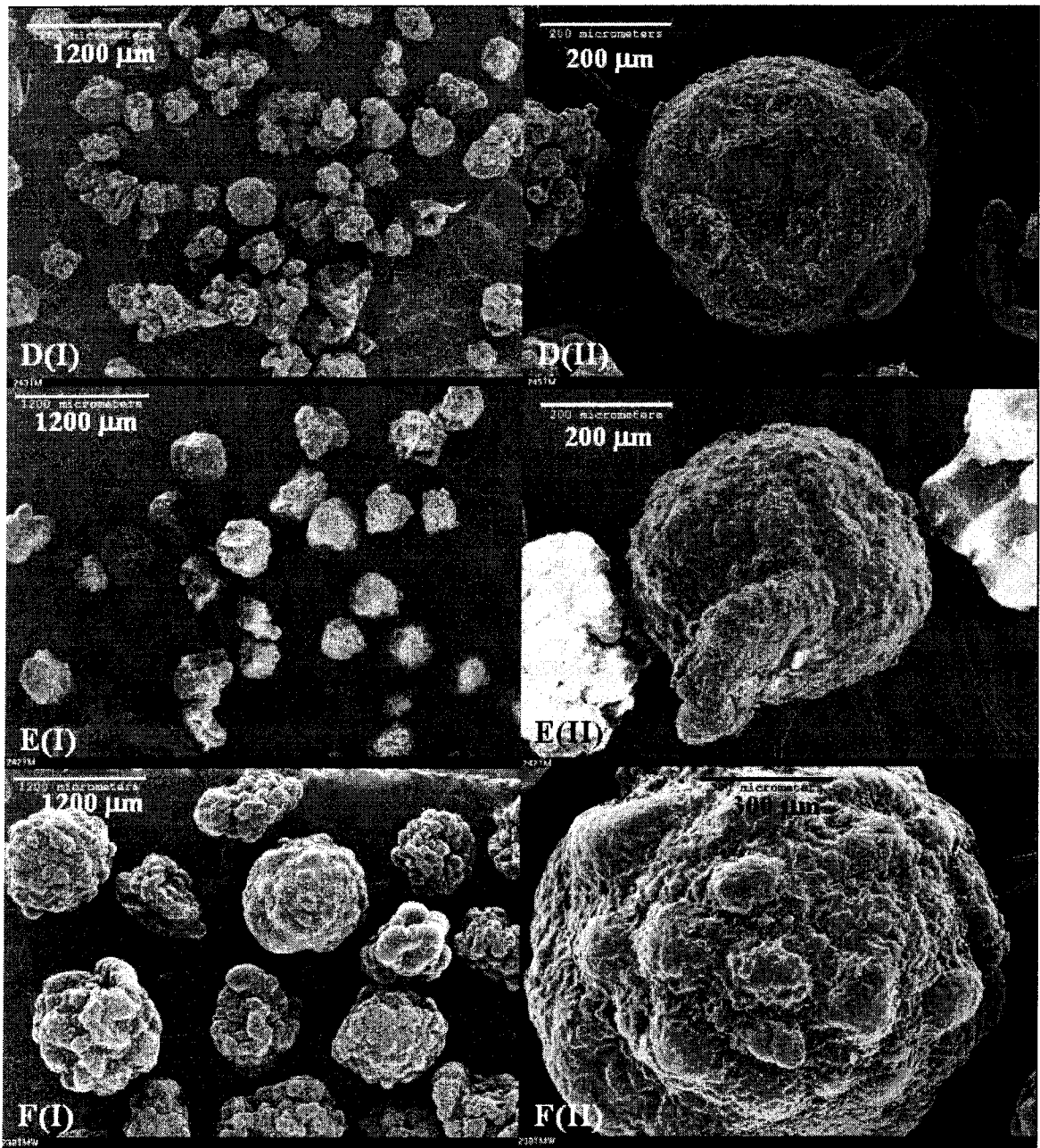


Figure 6.3: (continued from last page) SEM of copolymerization of Catalyst TM20 at low (I) and high (II) magnifications for runs of different lengths – (D) 10 min polymerization; (E) 15 min polymerization; (F) 60 min polymerization.

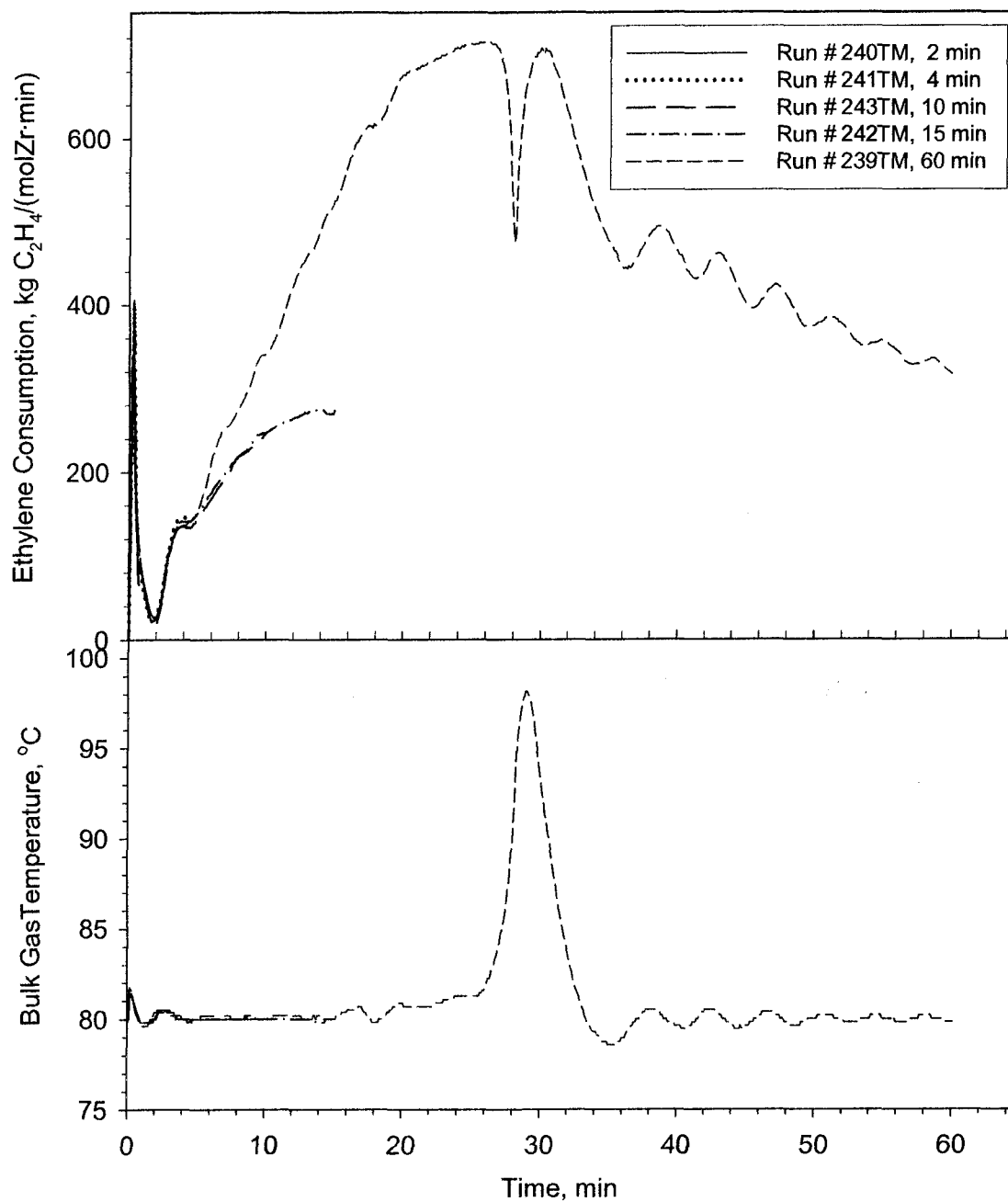


Figure 6.4: Activity and bulk gas temperature profiles of copolymerization of ethylene and 1-hexene at 80°C for runs of various lengths using Catalyst TM20

This corresponds to the dip in the activity profile and spike in temperature profile of the run at about 29 minutes into the run. Non-reproducibility of runs is a major problem for gas phase polymerization experiments in laboratory reactors and can result from various factors, such as thermal runaway – as in this case, differences in activities within the same catalyst batch as observed previously, variation of concentration of impurities in the reactor, and impurities introduced into the reactor with the feed. However, as all the runs are essentially similar for the first 5 minutes and follow similar trends the ex situ SEM images can be meaningfully compared to see how particles developed during polymerization.

It is clear from these images in Figure 6.3 that there was continuous growth of the particles during polymerization. Within the first 2 minutes of polymerization the particles had more than doubled in diameter compared to that of the initial catalyst particles, by 15 minutes the particles were 5 times the initial diameter and after 1 hour they were 15 times the diameter of initial catalyst particles. Moreover, once the polymer had formed the external appearance of the particles did not change significantly, that is the particles replicated their shapes while increasing in size only. To see how the particles developed internally some particles were cut and prepared for SEM analyses. While the small catalyst particles were frozen in liquid nitrogen and fragmented to reveal internal structures the polymer particles were cut with a sharp scalpel to reveal their internal morphology. As the particles were initially very small, less than 0.4 mm in diameter for the first few minutes, only particles formed after 10 minutes could be cut manually. Images of cut polymer particles revealing internal development with polymerization are shown in Figure 6.5.

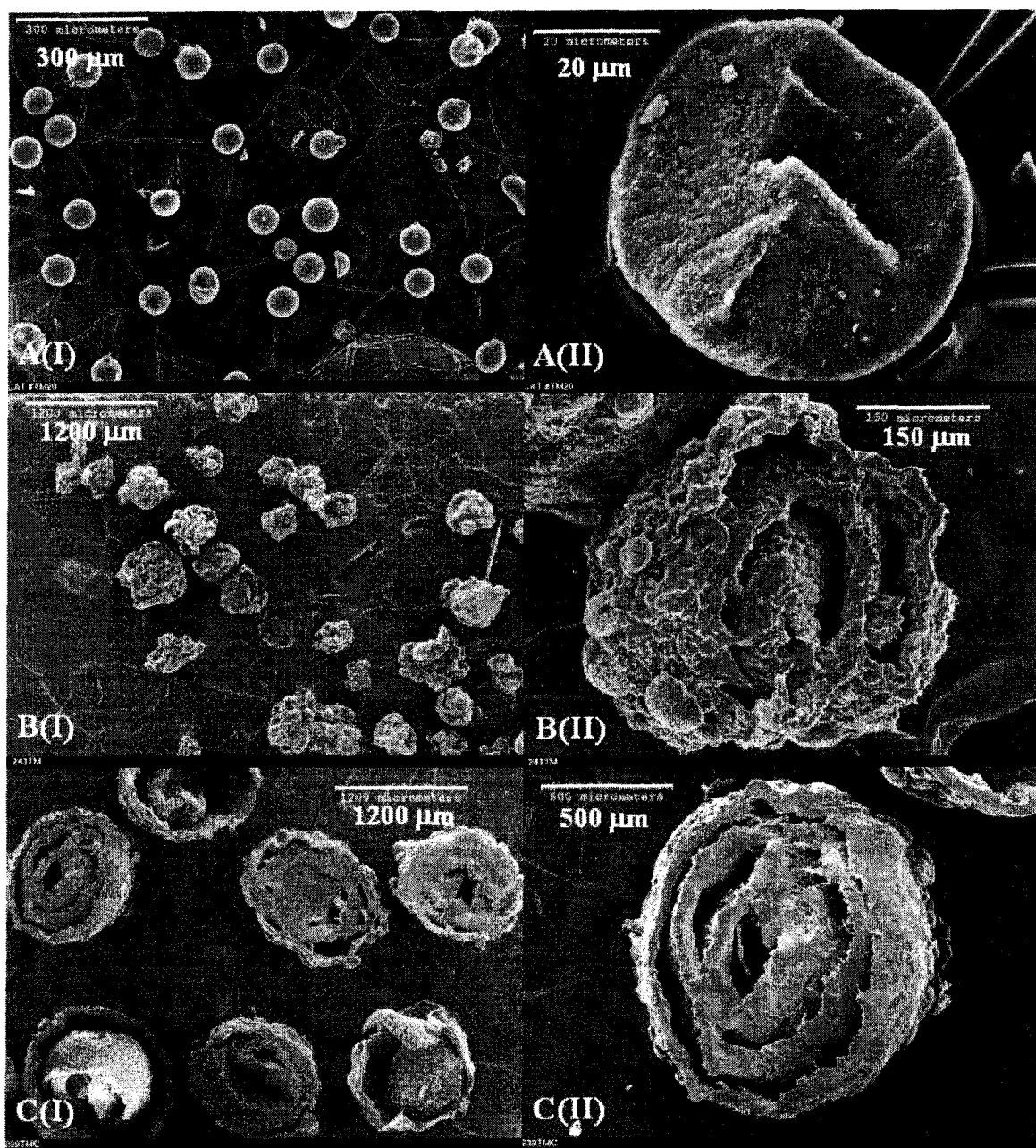


Figure 6.5: SEM of development of internal structure of particles during copolymerization with (A) Catalyst TM20 at 80°C after (B) 10 minutes, and (C) 60 minutes taken at low (I) and high (II) magnification.

It is apparent from Figure 6.5(B) that after 10 minutes of copolymerization with Catalyst TM20 of ethylene and 1-hexene at 80°C concentric layers of polymer had formed. Further polymerization increased thickness and diameter of the layers (Figure 6.5(C)) and no unreacted catalyst core was visible at the center of the particles. These layers had not been present in the initial catalyst particle structure, Figure 6.5(A) but resulted from the polymerization. This suggests that the catalyst particles did not breakup completely immediately after polymerization started but annular layers of the catalyst broke away from the core in sequence and formed these distinctive shells. This conclusion was further supported by the trend in polydispersity of the developing polymer particles as shown in Figure 6.6. As polymerization time was increased the product polydispersity decreased from about 11 initially to 2.7 for the hour long run, suggesting that the active catalytic sites became more homogeneous as polymerization proceeded. As the fresh catalyst particles were exposed to the monomer gases, the active sites on the surface of the catalyst particles would be exposed to greater concentration of monomer gases than those sites inside the particles and ethylene was likely to diffuse into the catalyst particles faster than 1-hexene. This would result in formation of polymers with greater incorporation of 1-hexene on the surface than those formed inside the catalyst particle, explaining the large values of polydispersities observed initially. As polymerization progressed the catalyst particles fragmented in layers and active sites inside the particles became more easily accessible for both monomers. This homogenizing of the surface and inner active sites due to catalyst particle breakup would result in decrease in polydispersity of polymer product.

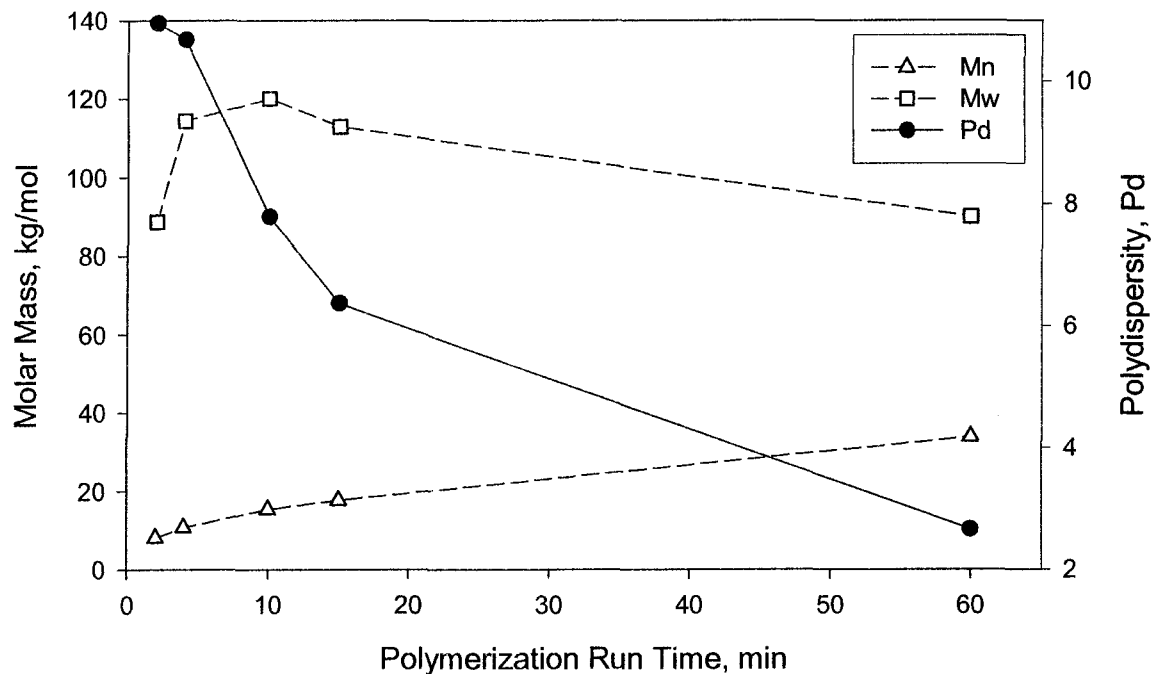


Figure 6.6: Development of molar masses and polydispersities with time during ethylene/1-hexene copolymerization at 80°C using Catalyst TM20.

Figure 6.6 also shows that Mn increased monotonously with increase in polymerization time while Mw initially increased and then decreased. The increase in molar masses was likely due to two reasons: 1) breakup of catalyst particles resulting in increase in local concentration of monomer gases at the active sites inside the particles, and 2) decrease in 1-hexene concentration with time. As the polymer built up around the active sites, the effective local concentration of monomer gases at the active sites would decrease and result in decrease in molar mass of the product polymer. If the effect of decrease in concentration of 1-hexene on Mn was greater than the effect of decrease in monomer concentration at local active site due to polymer buildup, the monotonous increase in Mn with polymerization time can be expected. If this effect on Mw was less

significant then the observed initial increase in  $M_w$  followed by the decrease can be expected. The changes in the slopes of the plots of molar masses in Figure 6.6 suggested that the catalyst particles had broken up completely after 10 minutes of polymerization.

To study further the development of inner morphology of the polymer particles, sets of time series experiments were performed with Catalyst TM22 that had been supported on sieved HS-R2 support particles of size range 300-350  $\mu\text{m}$ . Due to the larger particle size compared to catalyst TM20, this catalyst and its product were better suited for cutting and preparing for SEM analyses and hence studying the early stages of internal development. Two sets of copolymerization experiments, one at 80°C and the other at 70°C, were performed.

The activity and bulk gas temperature profiles of the copolymerization runs carried out at 80°C are shown in Figure 6.7. It can be seen that the bulk gas temperature was maintained remarkably well at the set point temperature, 80°C for the runs. Although the activity profiles were essentially similar for the first 4 minutes, they differ afterwards. In looking at the chronology of experiments in Table 6.1 a trend is apparent; Run # 248TM was run after a period of 6 days during which the reactor was idle, followed by Runs # 249TM, 250TM, 251TM, and 252TM while the initial activities of the runs are as follows: Run # 252TM > Run # 250TM > Run # 248TM. This suggests that a contaminant was initially present in the reactor and it reduced the catalyst activity; as more experiments were performed the concentration of contaminants went down and initial activity increased.

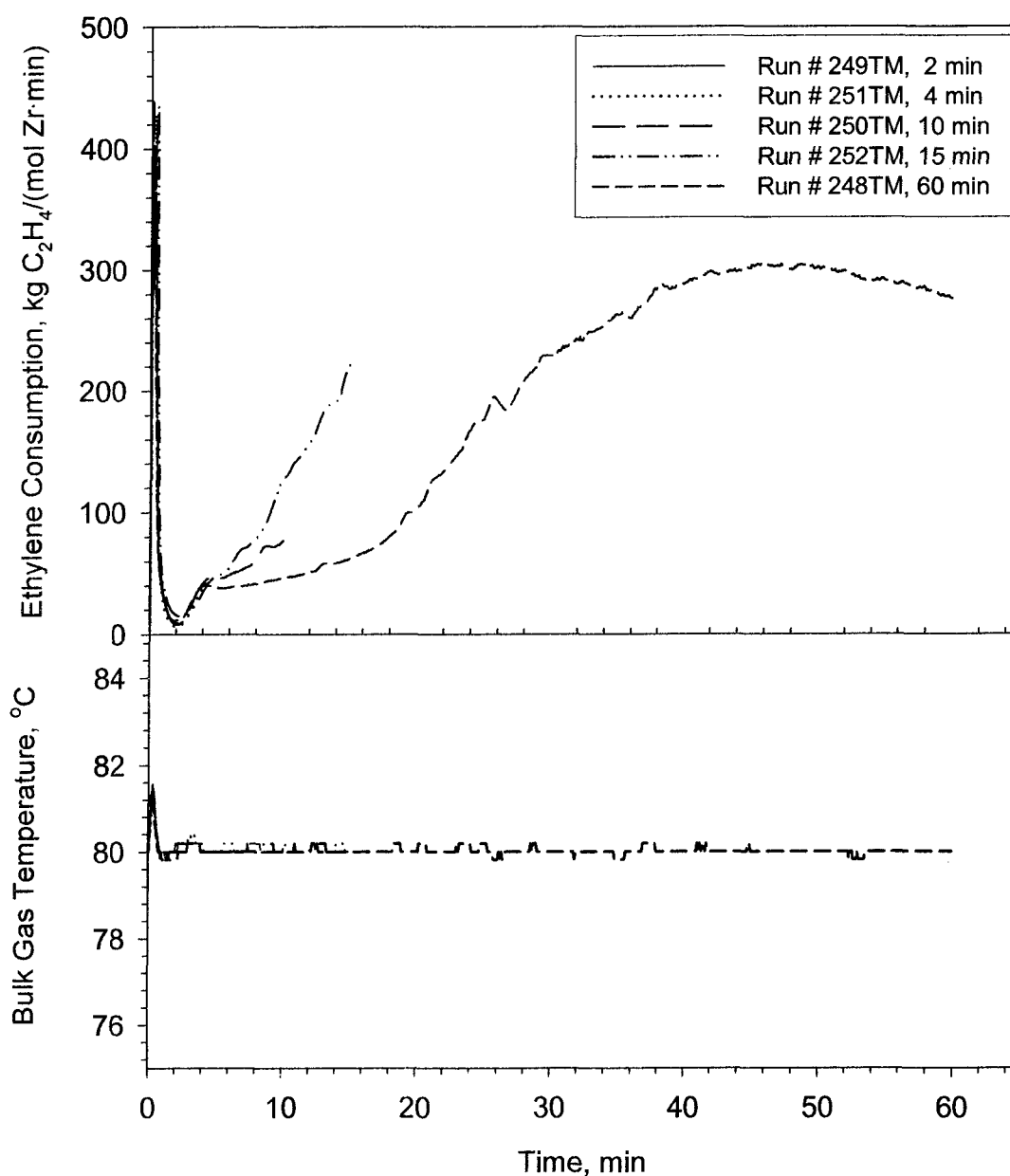


Figure 6.7: Activity and bulk gas temperature profiles of copolymerization of ethylene and 1-hexene with Catalyst TM22 at 80°C

A similar pattern can also be observed for the activity profiles of the set of copolymerization experiments carried out at 70°C as shown in Figure 6.8. Run # 253TM was performed after a new cylinder of ethylene had been connected to the reactor

followed by Run # 254TM the next day. After a period of 6 days during which the reactor was idle, Runs # 255TM, 256TM, and 257TM were carried out in consecutive days. The initial activities were of the sequence Run # 253TM < Run # 255TM < Run # 256TM.

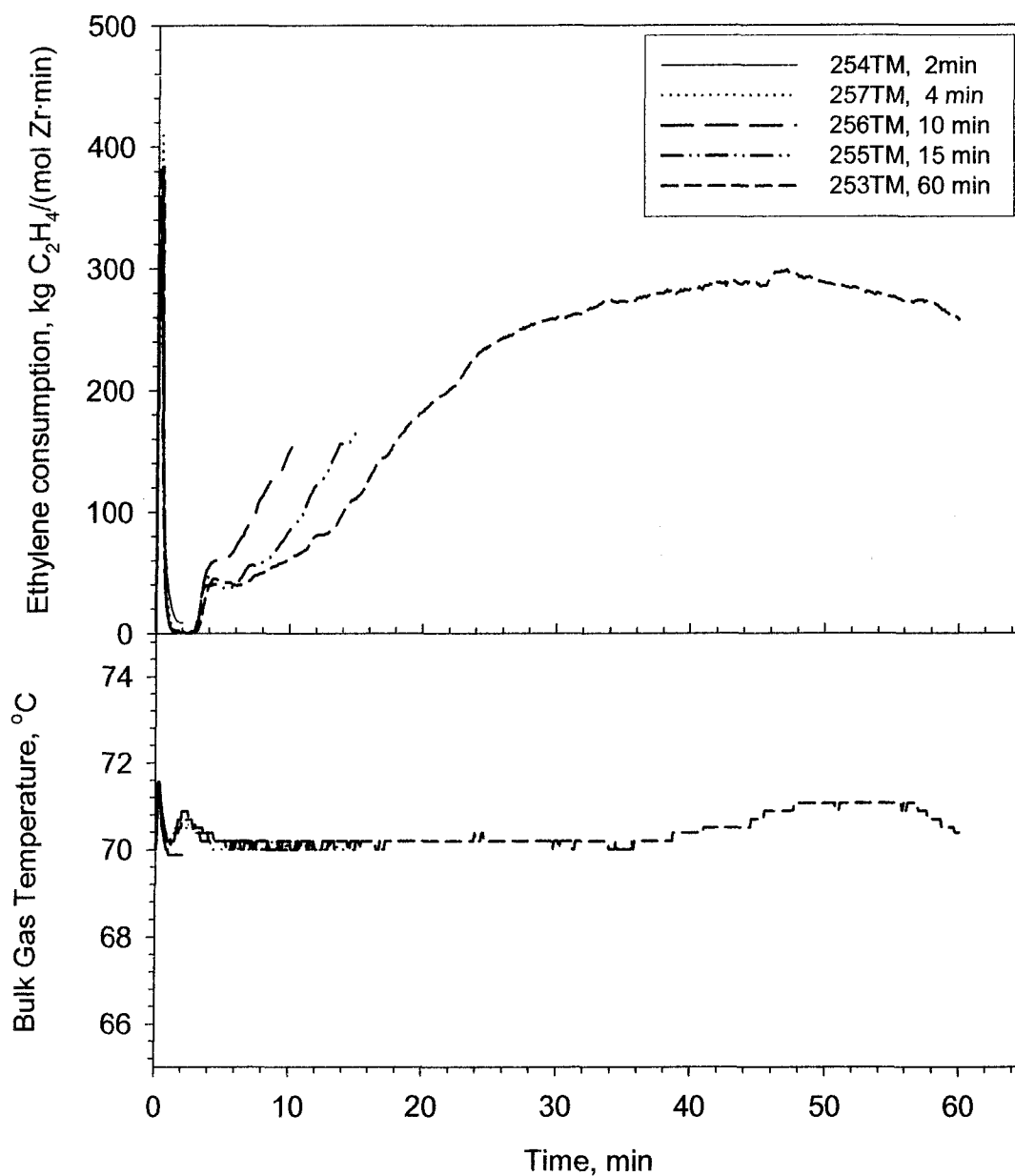


Figure 6.8: Activity and bulk gas temperature profiles of copolymerization of ethylene and 1-hexene with Catalyst TM22 at 70°C.

This apparent increase in initial activity was most likely related to a decrease in contaminant concentration in the reactor. For this set of runs as well the reactor temperature controller was able to maintain the bulk gas temperature at the set point temperature, 70°C very consistently with a deviation of only 1°C for the longer run.

Comparing the activity profiles of the experiments carried out at 70°C and 80°C the difference in initial activities is apparent. For the 80°C runs after the initial spike in ethylene consumption due to reactor pressurizing, the consumption did not come down to zero but took off again after falling to a low value (10 –20 kg C<sub>2</sub>H<sub>4</sub>/(mol Zr·min)) while for the 70°C runs the ethylene consumption came down to zero and stayed at this value for about 2 minutes before increasing rapidly again. This suggests that at the lower temperature, it took longer for the catalyst particles to break apart and become more porous to gaseous diffusion and for activity to take off because of lower intrinsic activity at the lower temperature.

The differences in initial activities of the catalyst at the two temperatures were also supported by SEM images of cut polymer particles after 2 minutes of copolymerization at 80°C and 70°C as shown in Figures 6.9(A) and 6.10(A), respectively. The polymer layer formed around the catalyst particles at 80°C were further away from the catalyst cores than that formed around catalyst particles at 70°C after 2 minutes thus forming a more porous structure. However, after 4 minutes multiple layers of polymer had formed at both temperatures and the structures were more porous, Figures 6.9(B) and 6.10(B). At longer copolymerization times the polymer particles formed had more concentric polymer rings of greater thickness, Figures 6.9 and 6.10 as had been observed

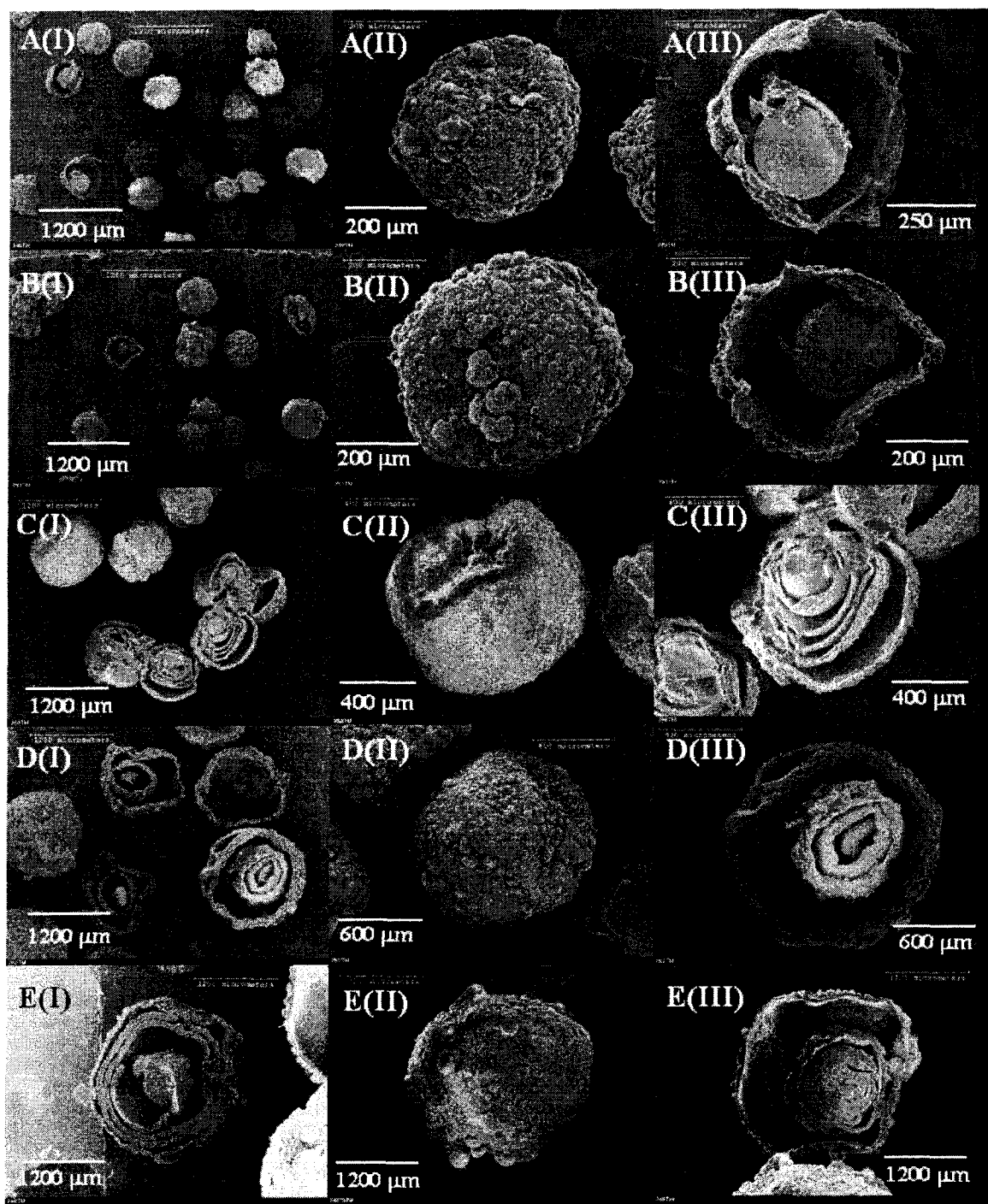


Figure 6.9: SEM of polymer particles produced by copolymerization at 80°C with Catalyst TM22 for (A) 2 minutes, (B) 4 minutes, (C) 10 minutes, (D) 15 minutes, and (E) 60 minutes at low (I) and high magnification showing whole (II) and cut (III) particles.

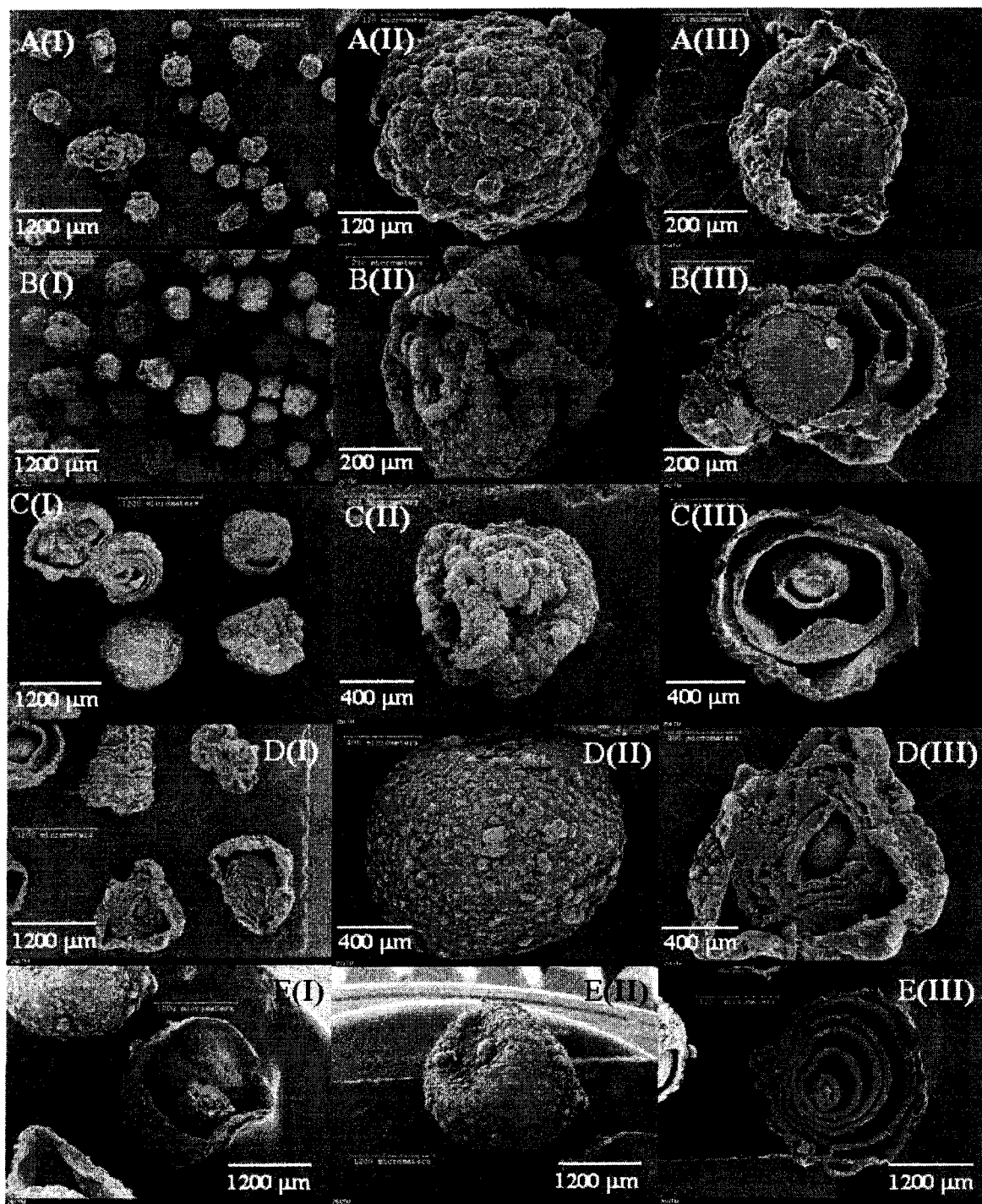


Figure 6.10: SEM of polymer particles produced by copolymerization at 70°C with Catalyst TM22 for (A) 2 minutes, (B) 4 minutes, (C) 10 minutes, (D) 15 minutes, and (E) 60 minutes at low (I) and high magnification showing whole (II) and cut (III) particles.

previously, Figure 6.5 using the smaller catalyst TM20. Moreover, the unreacted catalyst core that was clearly visible during the early periods was not apparent after 60 minutes of copolymerization.

Closer examination of the surface of catalyst in Figures 6.11 and 6.12 revealed clearly how the concentric polymer layers arose. After 2 minutes of polymerization at both 80°C and 70°C, Figures 6.11(A) and 6.12(A) respectively it could be seen that a layer of polymer had formed at the catalyst outer surface and then broke off to expose fresh catalyst surface. As polymerization continued the catalyst particle fragmented in layers; the outermost exposed surface polymerized and fragmented first, and then moved away from the core and exposed fresh catalyst surface underneath. As the separated polymer layer containing active catalyst was more loosely bound and porous than the nascent polymer layer formed at the catalyst surface and exposed to higher concentration of monomers, it grew at a faster rate than the polymer at the catalyst surface. This process led to the formation of multiple layers of polymers with spaces in between.

Plots of molar masses and polydispersities with polymerization at 80°C and 70°C are shown in Figures 6.13 and 6.14. These plots were similar to those observed previously in Figure 6.6 for copolymerization with the smaller sized Catalyst TM20. The decrease in polydispersity with time was indicative of the fragmentation process allowing easier access to all active sites both inside and on the surface of the catalyst particles. Interestingly,  $M_w$  of polymer formed in the first few minutes at 70°C was less than that formed at 80°C at similar times, but as polymerization progressed the  $M_w$  of the polymer formed at lower temperature became more than that formed at the higher temperature. Also polydispersities of polymers formed at 70°C was initially less than that formed at 80°C but became about the same as polymerization progressed. This was probably due to the lower intrinsic polymerization activity at 70°C as compared to that at 80°C that would have provided more time for the monomer gases, especially 1-hexene to diffuse into the catalyst particles before polymerizing thus reducing differences between the local concentrations of monomer gases at the active sites on the surface and inside the catalyst particles before complete fragmentation of the catalyst particles.

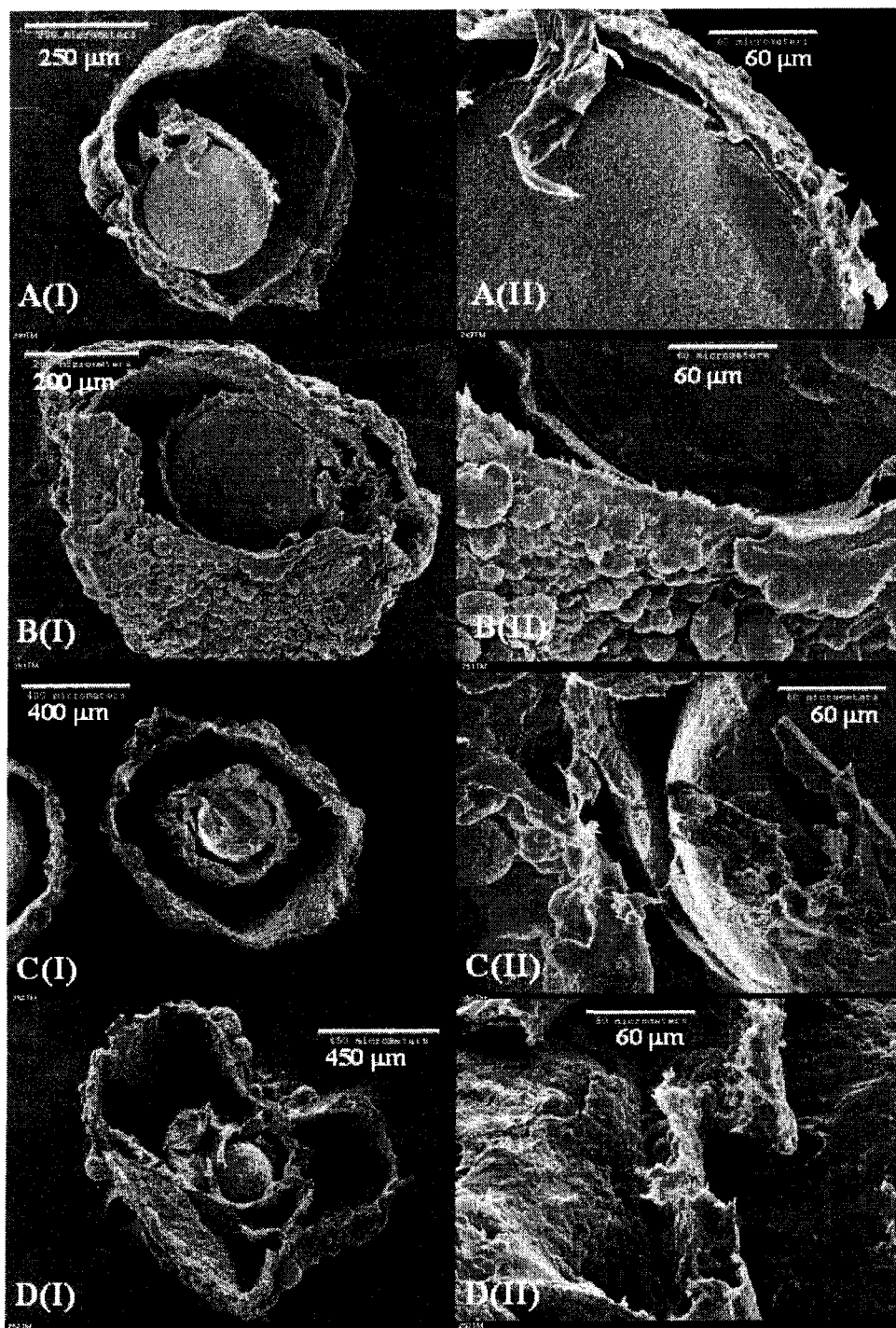


Figure 6.11: SEM showing formation of shells by catalyst/polymer breaking away from surface of catalyst core after (A) 2 min, (B) 4 minutes, (C) 10 minutes, and (D) 15 minutes of copolymerization at 80°C with Catalyst TM22.

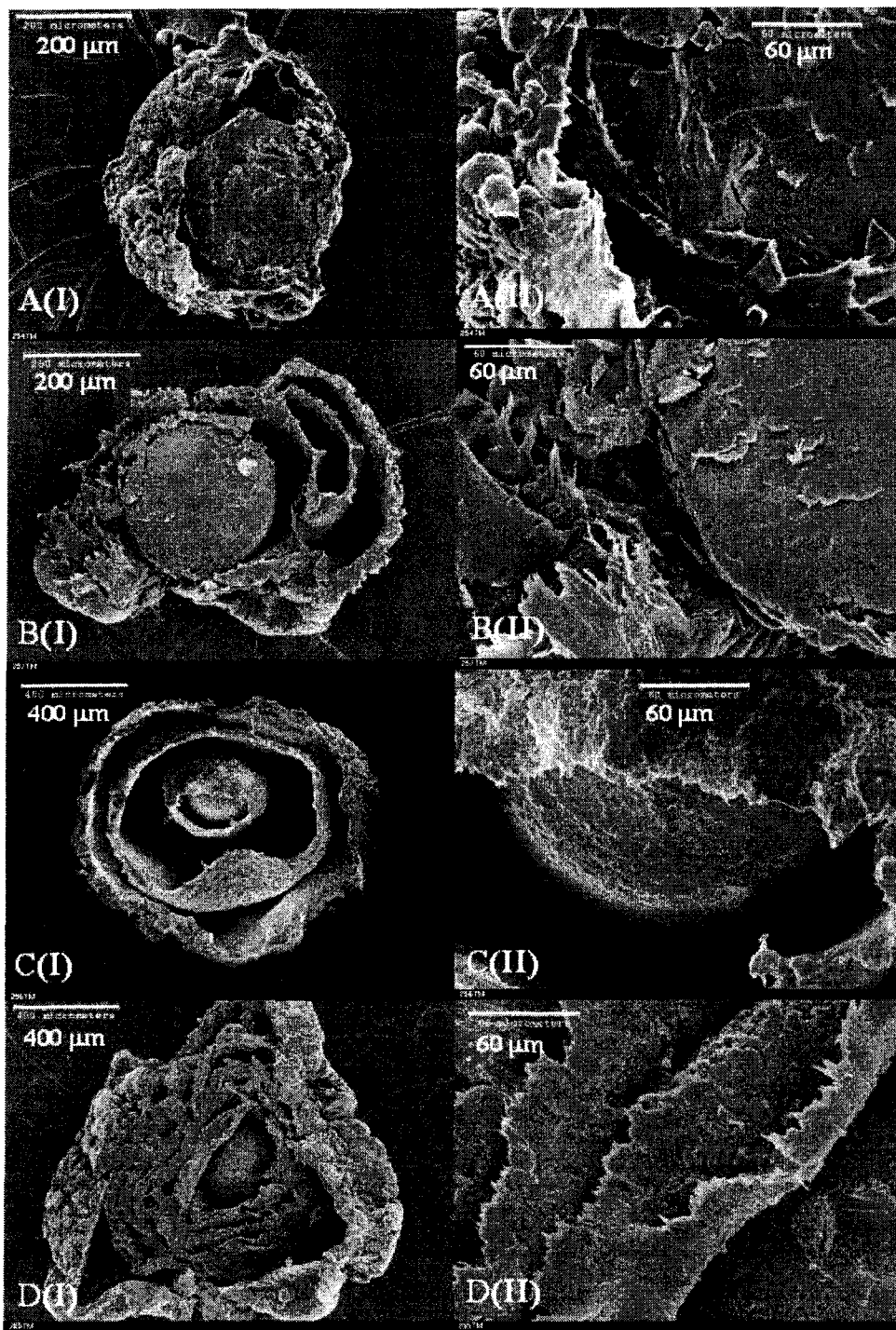


Figure 6.12: SEM showing formation of shells by catalyst/polymer breaking away from surface of catalyst core after (A) 2 min, (B) 4 minutes, (C) 10 minutes, and (D) 15 minutes of copolymerization at 70°C with Catalyst TM22.

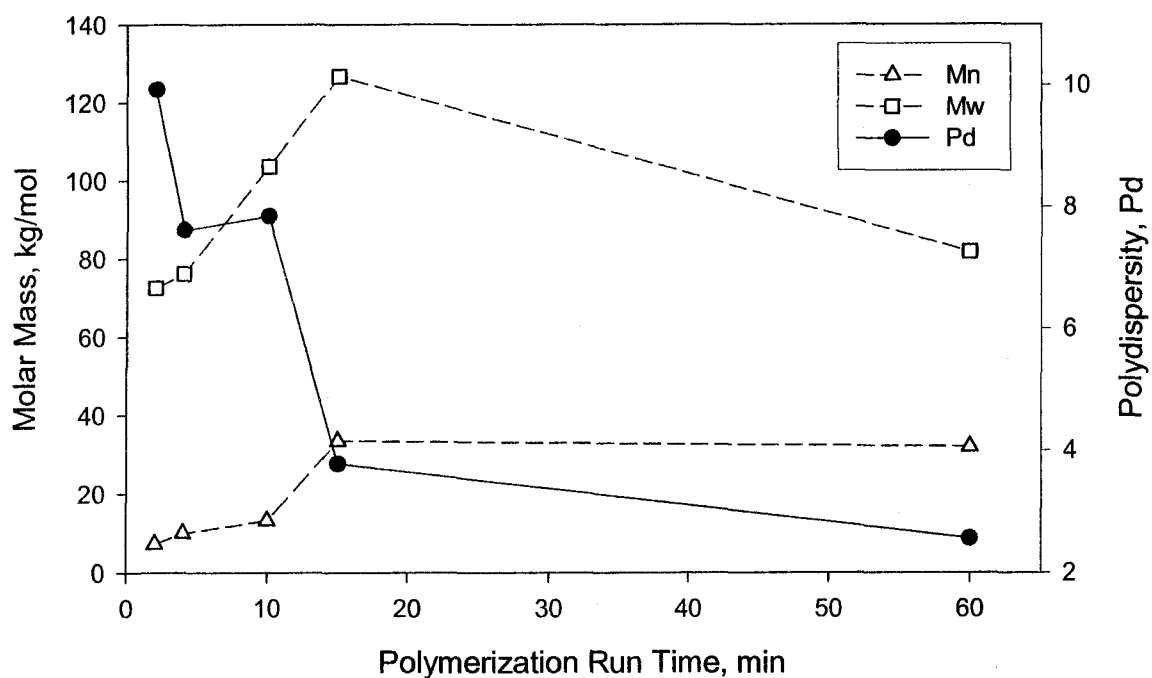


Figure 6.13: Development of molar masses and polydispersities with time during ethylene/1-hexene copolymerization at 80°C using Catalyst TM22.

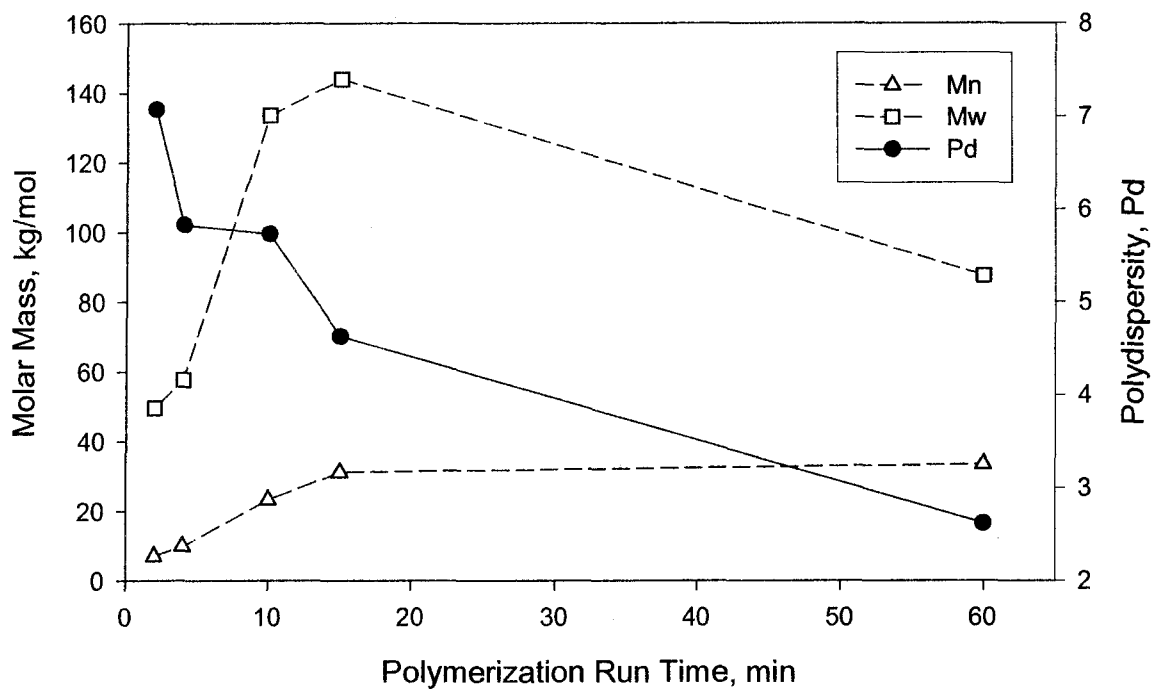


Figure 6.14: Development of molar masses and polydispersities with time during ethylene/1-hexene copolymerization at 70°C using Catalyst TM22.

### 6.3.2 Growth of Polymer Particles during Homopolymerization

As it had been observed that the homopolymerization activities of most of the catalysts made were much less than the copolymerization activities, for SEM analyses of polymer particle growth during homopolymerization a set of experiments was performed using the larger Catalyst TM22. The activity and bulk gas temperature profiles of three homopolymerization runs are shown in Figure 6.15. The initial spike in ethylene consumption was due to pressurizing the reactor during catalyst injection as reported earlier. Although for the first two minutes when the reactor was being filled with ethylene the activity profiles were similar, the 10 minutes run, 260TM seems to have higher activity than the 30 minutes run, 258TM. However, both the runs have very low activities and similar patterns. In both cases after equilibration of reactor pressure there was an initial very short period of rapid increase in activity followed by a much more gradual change in activity period as compared to copolymerization where there was a longer period of sustained increase in activity. At such low polymerization activities the temperature controller was able to maintain the bulk gas temperature at the set point, 80°C throughout the runs.

SEM of whole and cut Catalyst TM22 particles and polymer particles produced by homopolymerization for 2, 10, and 30 minutes are shown in Figure 6.16. Although the external appearance of the homopolymer particles was similar to the copolymer particles shown in Figures 6.3, 6.8 and 6.9 produced by catalysts TM20 and TM22 the internal structures of the homopolymer particles were remarkably different. Within 2 minutes, Figure 6.13(B) a layer of polymer had formed around the catalyst particle. As

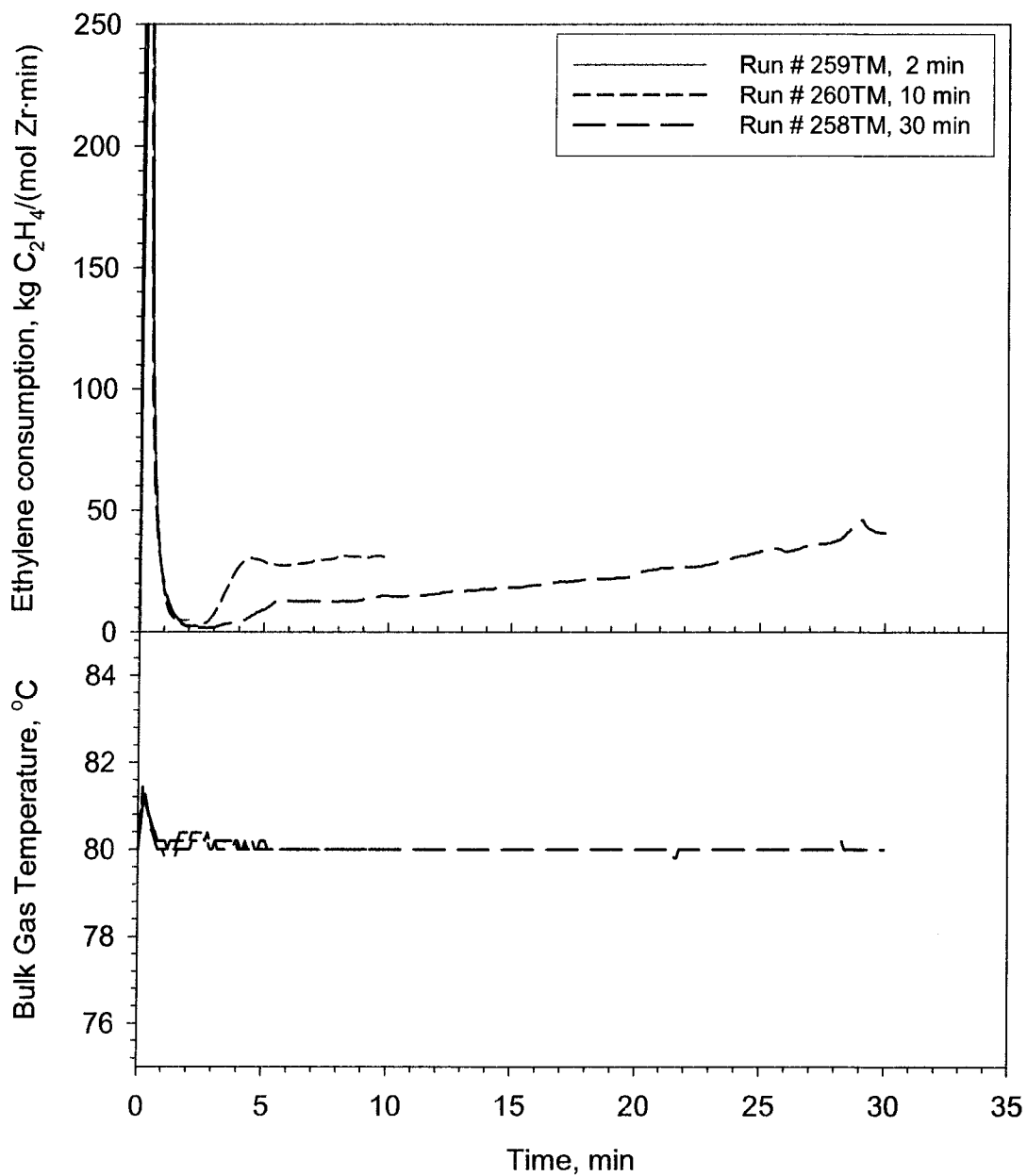


Figure 6.15: Activity and bulk gas temperature profiles of homopolymerization of ethylene using Catalyst TM22 at 80°C

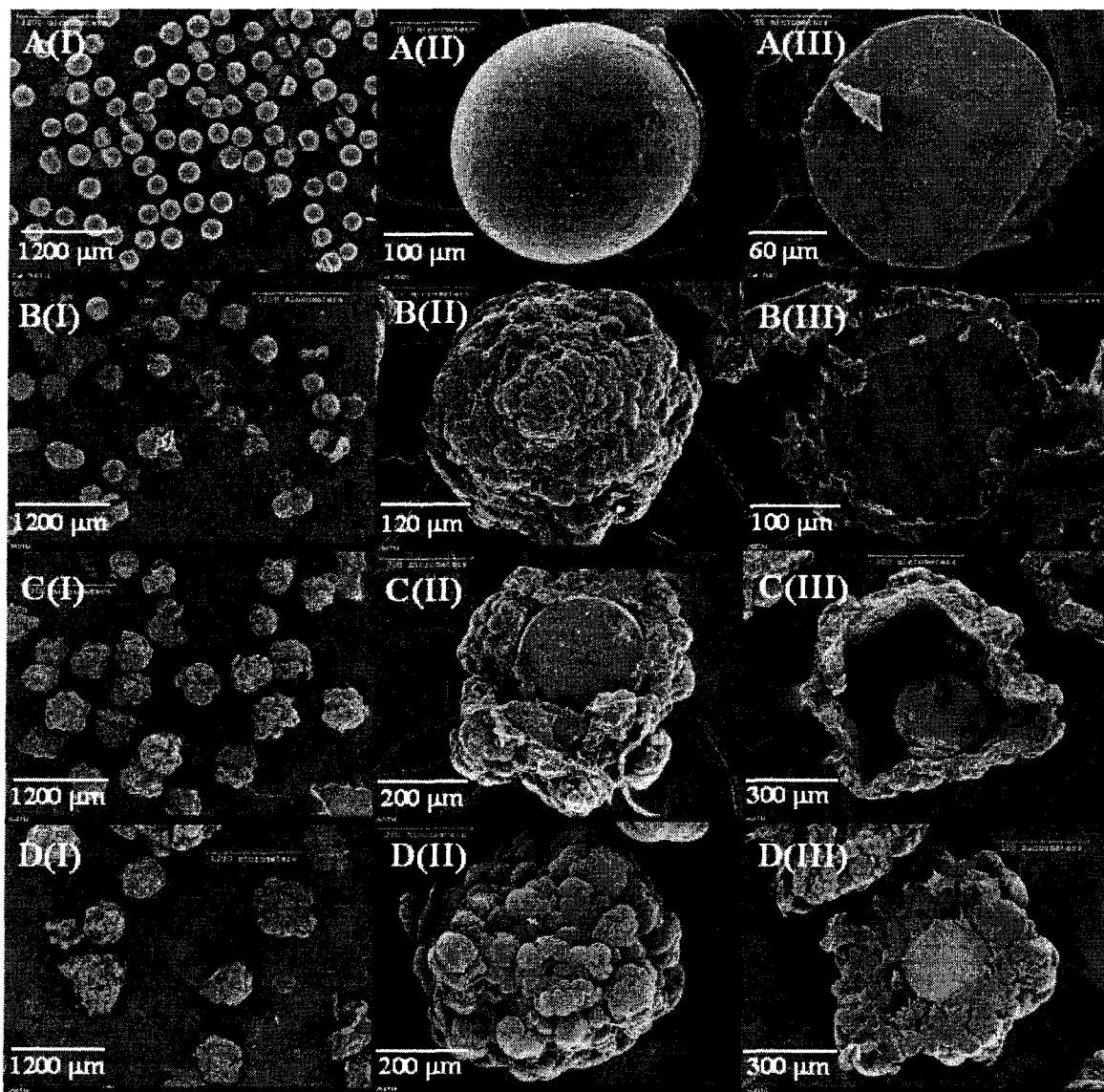


Figure 6.16: Homopolymerization with (A) Catalyst TM22 showing result of polymerization for (B) 2 minutes, (C) 10 minutes, and (D) 30 minutes at low, (I), and high, (II) and (III), magnifications for whole and cut particles.

polymerization proceeded the polymer layer grew in thickness, but the catalyst particle did not fragment and multiple layers of polymer shells did not form as had been observed for copolymerization. Closer inspection of the cut homopolymer particles as shown in Figure 6.17 can help explain this difference. The dense layer of HDPE formed within 2 minutes of homopolymerization was not as permeable to monomer diffusion as the LLDPE formed by copolymerization around the catalyst particle because of HDPE's higher crystallinity. This would limit diffusion of monomer to the active catalyst surface and the activity would be lower as was observed. The maximum activity for homopolymerization was about an order of magnitude less than that for copolymerization using Catalyst TM22 at 80°C. Moreover, at these low polymerization rates the polymer buildup within the catalyst particle pores was not sufficient to fracture the surface and expose the active sites beneath. Thus, the homopolymer grew outwards from the catalyst surface only. In contrast, during copolymerization the catalyst surface fragmented and came off in layers, exposing new catalytic sites as well as enhancing diffusion of monomer gases into the catalyst core. Whether the catalyst particle fragmented during polymerization would also depend on the friability of the catalyst support particles as well as their porosity. The catalysts examined here were supported on commercial porous polymer supports that were not very friable. The 1-hexene present during copolymerization could also affect the friability of the catalyst support and enhance its fragmentation. Thus the activity of the catalyst and the internal morphology of the polymer particles would be affected by the friability of the catalyst support under the polymerization condition.

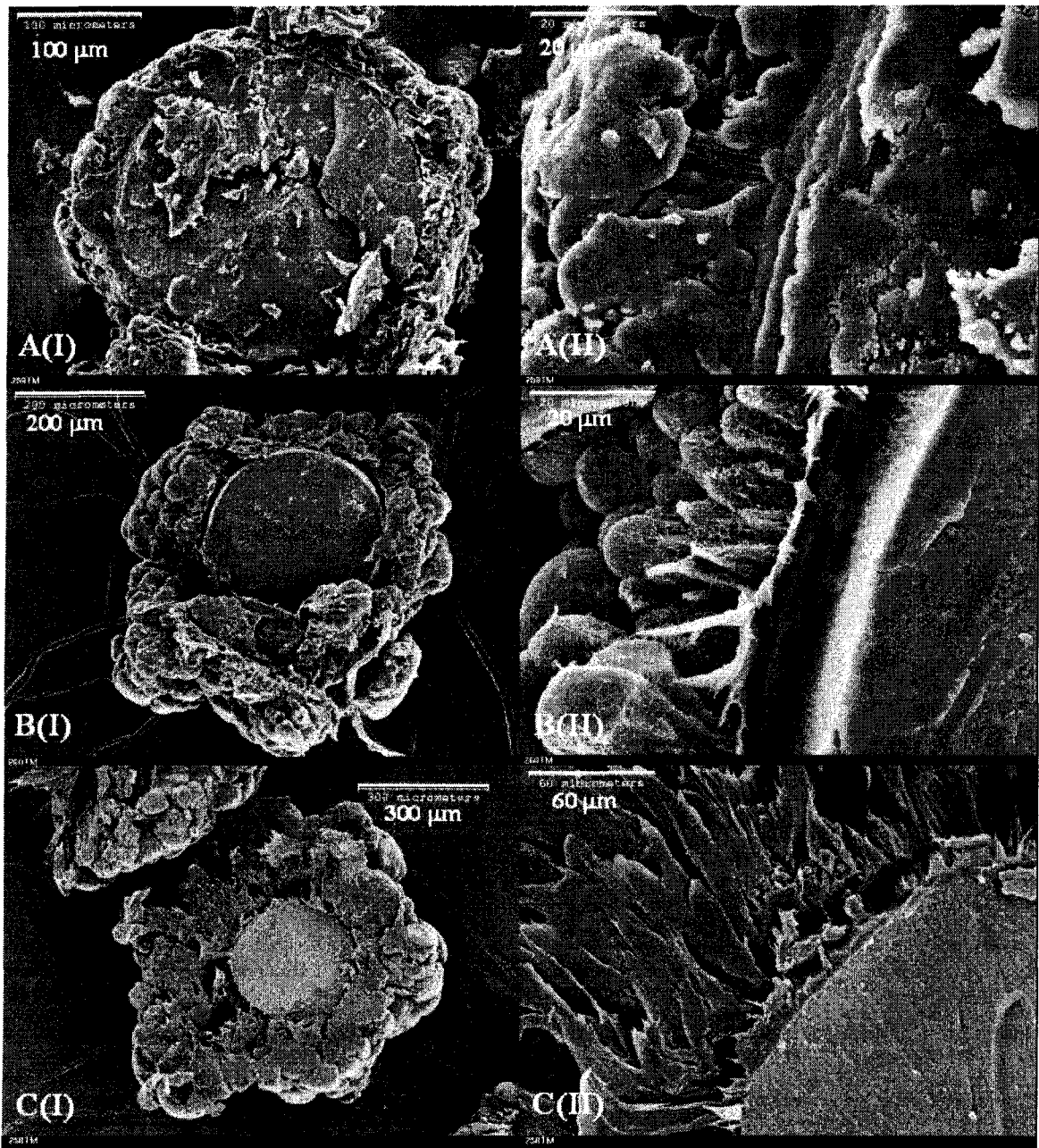


Figure 6.17: SEM of homopolymer particles showing radial growth of polymer outwards from catalyst core after (A) 2 minutes, (B) 10 minutes, and (C) 30 minutes of polymerization.

Plots molar masses and polydispersity of homopolymer particles with polymerization time are shown in Figure 6.18. The results were distinctly different from that observed for ethylene/1-hexene copolymers in Figures 6.6, 6.13 and 6.14. The molar masses decreased and polydispersity increased a little as polymerization time increased. The results were consistent with the observation that the catalyst particle did not fragment during homopolymerization and the polymer built up around the catalyst core. This would have resulted in reduction of monomer concentration at the catalyst surface as polymerization proceeded with the corresponding decrease in molar masses of the polymer formed.

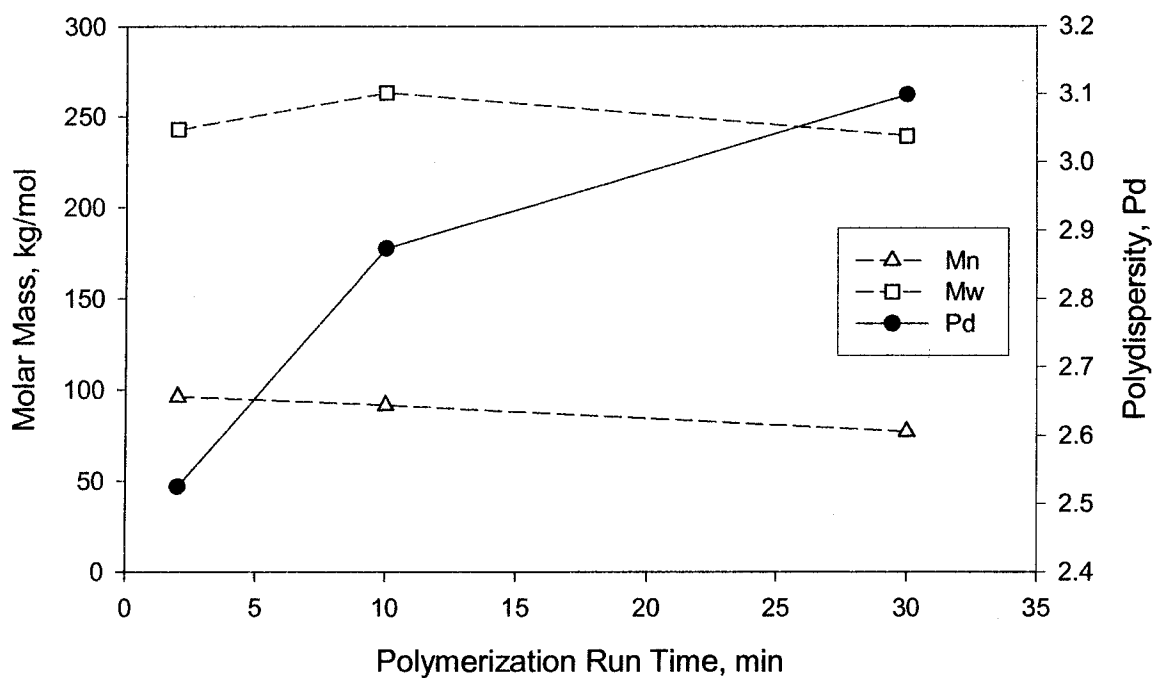


Figure 6.18: Development of molar masses and polydispersities with time during ethylene homopolymerization at 80°C using Catalyst TM22.

#### 6.4 Summary of Observations from Imaging of Growing Particles

The micro-reactor in conjunction with the microscope video camera was very useful for in situ imaging of growing catalyst/polymer particles. A number of observations could be made from the in-situ imaging experiments as follows:

- 1) Within a batch of catalyst of nominal size range, there was significant variation of sizes due to presence of catalyst fragments and fines.
- 2) There was a short induction period during which there was no apparent growth of catalyst particles.
- 3) The induction period varied from particle to particle being smaller for catalyst fragments and small particles.
- 4) During polymerization the original shape of the catalyst particle or fragment tended to be replicated.

Scanning electron microscopy was very useful for taking high resolution images of whole and cut polymer particles showing their external and internal morphologies, and provided insight into the morphology development. Some of the important observations from the SEM of growing polymer particles were as follows:

- 1) There was marked differences between the growth of homopolymer particles and copolymer particles for the type of supported catalyst used.
- 2) During homopolymerization the polymer grew radially outwards from the unfragmented catalyst core and the polymerization activity was very low.
- 3) During copolymerization successive annular layers of polymer formed around and broke off from the catalyst core; these polymer layers moved outwards and grew thicker and the core slowly disappeared.

- 4) The annular polymer layer morphology was observed for both small and large catalyst particles during copolymerization at different temperatures.
- 5) The polymer particles tended to replicate the shape of the original catalyst particles.

Moreover, it was observed that there could be significant differences in activity profiles for runs carried out under similar conditions using the same catalyst. These irreproducibilities of the runs might be the consequences of the differences in induction periods of individual particles within the same catalyst, thermal runaway, and/or presence of impurities in the reactor or feed.

The molar masses and polydispersities of copolymer particles formed at various polymerization times also provided evidence for fracture of catalyst particles in stages during ethylene/1-hexene copolymerization. The following were observed for copolymer particles formed during polymerization where 1-hexene was only injected before the start of the run:

- 1) The polydispersity decreased significantly with increase in polymerization time.
- 2)  $M_w$  initially increased, reached a maximum value, and then decreased.
- 3)  $M_n$  increased monotonously with polymerization time.

However, for ethylene homopolymerization study of the molar masses indicated that the catalyst particles did not breakup during polymerization. The following were observed:

- 1) The polydispersity increased a little with increase in polymerization time.
- 2) The molar masses decreased with polymerization time.

## 7. Effect of Comonomer on Ethylene Polymerization

### 7.1 Effect of 1-Hexene on Ethylene Polymerization

It is well known that comonomer 1-hexene has a profound effect on the polymerization activity of heterogeneous metallocene catalysts and properties of the product polymer (see Chien and Nozaki (1993), Koivumaki and Seppala (1993), and Quijada et al. (1997)). Although for most of the prepared supported metallocene catalysts that were studied during the course of this research work, the copolymerization activity was usually very high as compared to homopolymerization activity; a few catalysts had both high homo- and co-polymerization activities. Moreover, catalyst activities varied with time, and little changes in the reactor conditions had significant influence on activity. These resulted in difficulties in reproducibilities; nevertheless, definite trends in behaviour were very noticeable.

A set of experiments were performed using Catalyst TM08, supported on in-house porous polymer particles of size range 78-200  $\mu\text{m}$ , to study the effect of varying initial concentration of 1-hexene. Some details about the initial runs are given in Table 7.1 and the corresponding activity and temperature profiles are shown in Figures 7.1 (A) and (B) respectively. The low homopolymerization activity in Run 61TM was likely due to some contamination as repeated later runs showed higher homopolymerization activity. In comparison, copolymerization activity was relatively high throughout.

Table 7.1: Experiments to study effect of initial concentration of 1-hexene on polymerization using Catalyst TM08 (Type A runs, see Chapter 3).

Run No.	Date	Catalyst Amount, (mg)	Avg. Temp., (°C)	Max. Temp., (°C)	Total Pressure, (MPa)	Initial C <sub>6</sub> H <sub>12</sub> conc., (mol/m <sup>3</sup> )	Total PE Yield, (g)
61TM	07/24/01	109	80.0	81.4	1.39	0.0	9.7
62TM	07/25/01	101	80.0	81.8	1.38	11.2	33.9
63TM	07/26/01	100	80.2	84.4	1.38	21.9	47.8

The ethylene homopolymerization and ethylene 1-hexene copolymerization activity profiles were distinctly different. It can be seen from Table 7.1 and Figure 7.1(A) that as the initial concentration of 1-hexene was increased from 0 to 21.9 mol/m<sup>3</sup> the polymerization activity increased and PE yield increased. During homopolymerization the maximum activity was reached very quickly, in less than 8 minutes after catalyst injection and the activity decreased gradually thereafter. However, during copolymerization the maximum activity was reached later depending on the initial concentration of 1-hexene, with the maximum activity being reached earlier at the lower 1-hexene concentration. There were oscillations in the gas phase temperature due to the nature of the feedback PID temperature controller; these oscillations were more prominent for the very high activity Run 63TM. This resulted because thermal energy removal from the coolant oil was insufficient to maintain it at the required temperature. Modifications to increase thermal energy removal rate were done to the coolant reservoir to overcome this before further experiments were carried out.

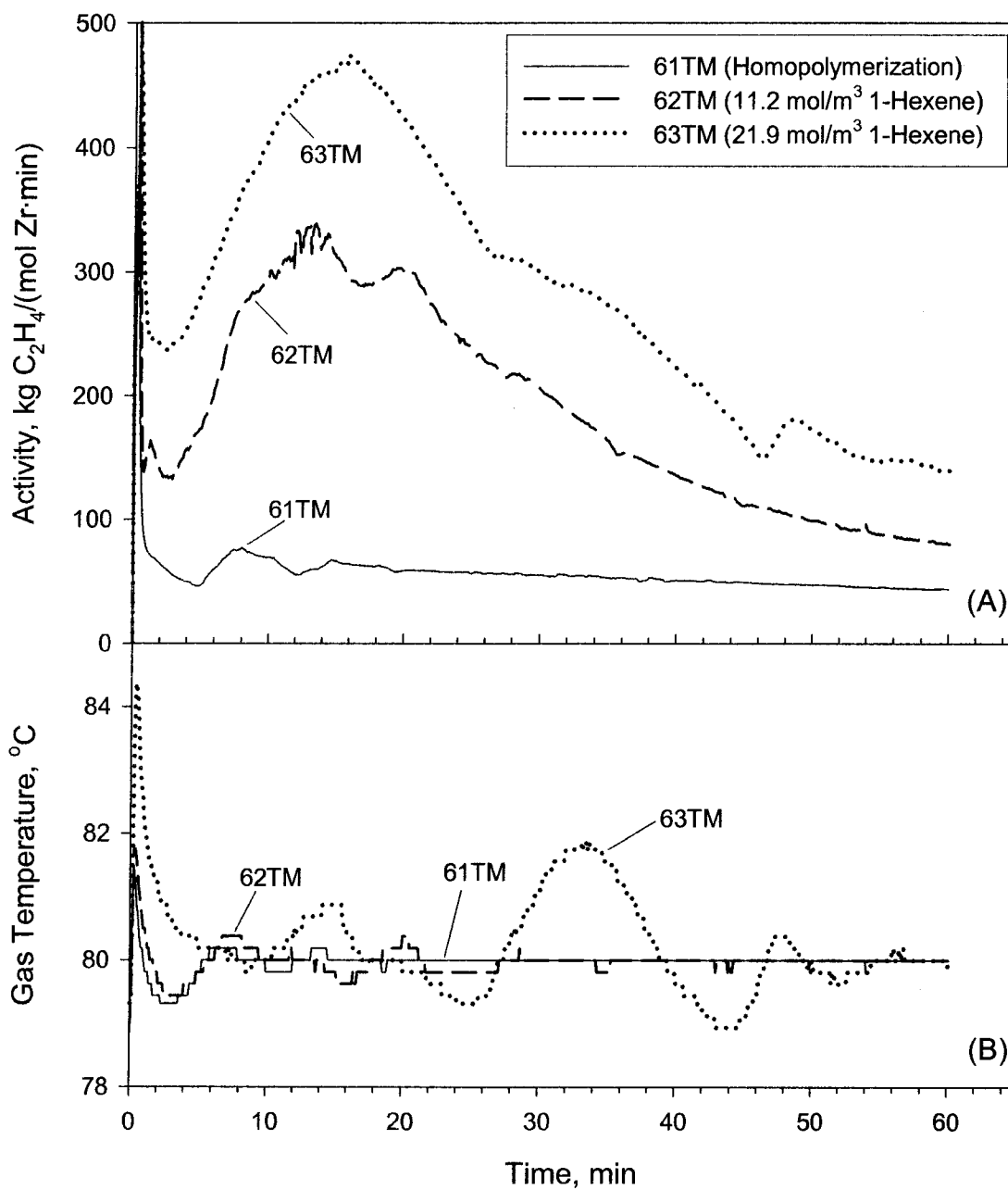


Figure 7.1: Effect of varying initial concentration of 1-hexene on polymerization using Catalyst TM08 showing (A) the activity profiles, and (B) the corresponding gas phase temperature profiles

Details about the later experiments using Catalyst TM08 to study effect of initial concentration of 1-hexene on activity are given in Table 7.2. The activity and the temperature profiles of these runs are shown in Figure 7.2. After the coolant reservoir modification, oscillatory deviations of the gas phase temperature from the set point temperature (80°C) were less than that for the runs described previously. To further improve thermal energy removal rate, static mixers were inserted into the coolant channels in the reactor walls after Run 66TM. Apart from the initial gas phase temperature hikes due to adiabatic gas compression in the reactor, the gas phase temperatures were much better controlled in Runs 67TM and 68TM.

Table 7.2: Experiments to study effect of initial concentration of 1-hexene on polymerization using Catalyst TM08 after coolant reservoir modification (Type A runs, see Chapter 3).

Run No.	Date	Catalyst Amount, (mg)	Avg. Temp., (°C)	Max. Temp., (°C)	Total Pressure, (MPa)	Initial C <sub>6</sub> H <sub>12</sub> conc., (mol/m <sup>3</sup> )	Total PE Yield, (g)
64TM	09/07/01	100	80.0	82.4	1.39	22.4	38.2
65TM	09/11/01	100	80.0	82.4	1.41	12.1	21.0
66TM	09/12/01	100	80.0	83.1	1.38	0.0	30.2
67TM <sup>1</sup>	09/24/01	102	80.0	82.4	1.37	0.0	22.5
68TM <sup>1</sup>	09/25/01	102	80.0	84.4	1.38	12.6	43.9

<sup>1</sup> After insertion of static mixers into coolant channels in reactor walls

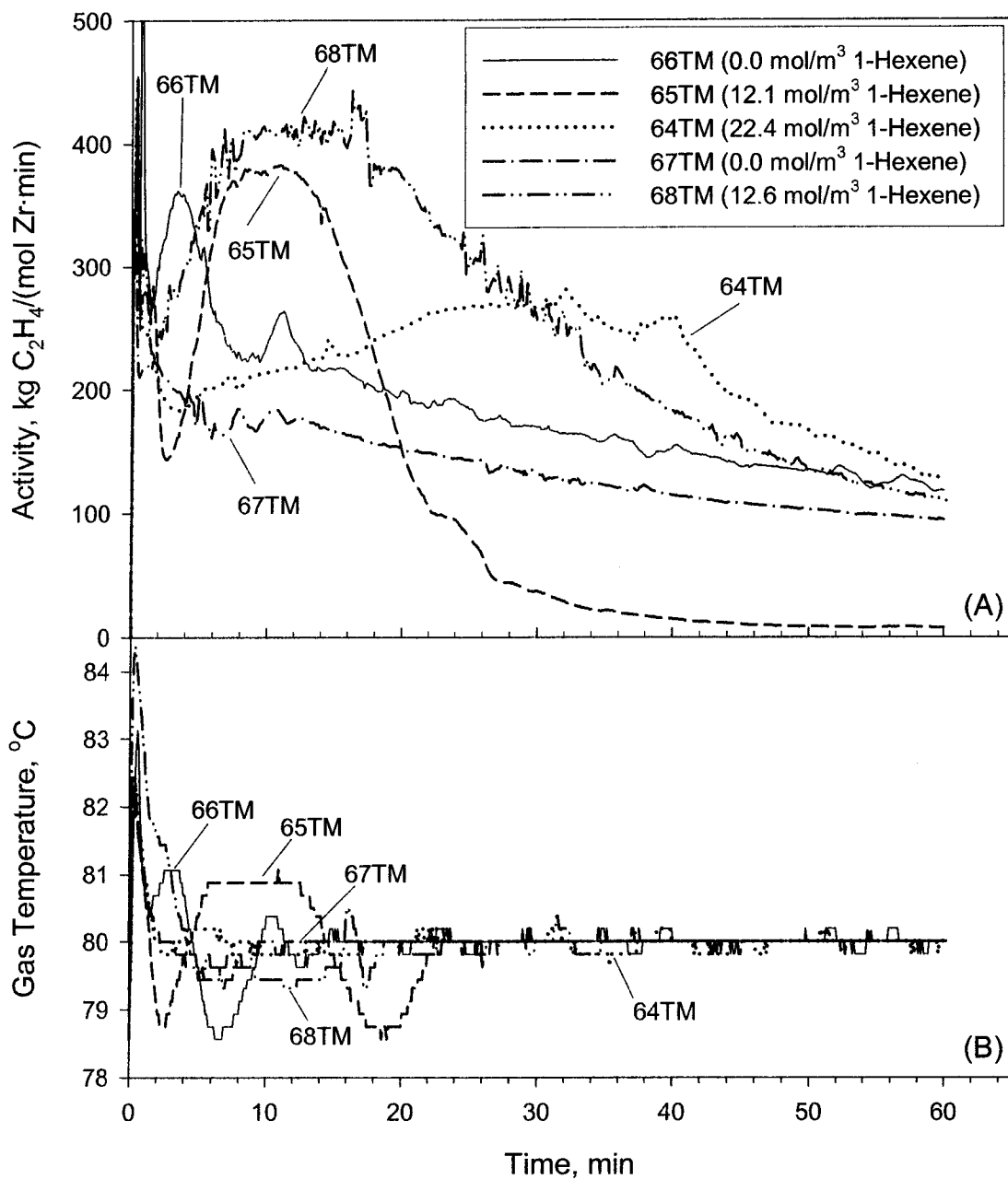


Figure 7.2: Effect of varying initial concentration of 1-hexene on polymerization using Catalyst TM08 showing (A) the activity profiles, and (B) the corresponding gas phase temperature profiles after coolant reservoir modification.

Although the polymerization activity profiles of the runs carried out after the cold oil reservoir modifications (see Figure 7.2(A)) look different from those described previously (see Figure 7.1(A)) there are some similarities. During homopolymerization, the maximum activity was reached very quickly, in less than 5 minutes after catalyst injection and the activity decreased thereafter. While during copolymerization, the maximum activity was reached later depending on the initial concentration of 1-hexene with the maxima being reached earlier at the lower 1-hexene concentration. The high initial activities of Runs 66TM and 65TM resulted in oscillations of the bulk gas temperature as seen in Figure 7.1(B), but the deviation were less than 1°C from the controlled temperature of 80°C. Although the initial concentration of 1-hexene in Run 68TM was only slightly higher than that in Run 65TM, Run 68TM had more than double the yield of polyethylene compared to Run 65TM after an hour of polymerization. This was because the catalyst in Run 65TM deactivated more rapidly than in Run 68TM probably due to the larger oscillations in the gas temperature.

To study the effect of initial concentration of 1-hexene in absence of gas-phase temperature oscillations a set of copolymerization runs were carried out with the PID gas phase temperature controller switched off and coolant oil at 80°C being circulated to the reactor. These experiments were carried using Catalyst 11TM supported on commercial HayeSep-R porous polymer support of size range 125 – 150 µm. Polymerization conditions and other information about these runs are given in Table 7.3, and the activity and gas phase temperature profiles are shown in Figure 7.3.

Table 7.3: Experiments to study effect of initial concentration of 1-hexene on polymerization using Catalyst TM11 with circulation of coolant oil at 80°C to reactor (Type A runs, see Chapter 3).

Run No.	Date	Catalyst Amount, (mg)	Avg. Temp., (°C)	Max. Temp., (°C)	Total Pressure, (MPa)	Initial C <sub>6</sub> H <sub>12</sub> conc., (mol/m <sup>3</sup> )	Total PE Yield, (g)
90TM	11/23/01	147	84.9	87.4	1.38	10.9	50.0
91TM	11/28/01	100	80.5	81.6	1.39	0.0	3.2
96TM	12/06/01	100	83.5	84.8	1.38	11.4	39.1
98TM <sup>†</sup>	12/12/01	100	81.9	82.9	1.39	11.9	3.3
99TM	12/13/01	100	83.1	84.2	1.38	21.1	31.6
100TM	12/14/01	101	82.9	83.9	1.39	4.0	27.3

<sup>†</sup> Polymerization carried out for 10 minute only and rest for 60 minutes.

The experiments using Catalyst TM11 showed that ethylene/1-hexene copolymerization activity was much higher than that of ethylene homopolymerization. In Run 98TM having similar polymerization conditions as Run 96, polymerization was carried out for only 10 minutes. The similarities of the activity profiles of these two polymerization runs showed good reproducibility in reactor behaviour. The gas phase temperature profiles of the runs had similar profiles to the activity profiles and, as the polymerization activity increased, the gas phase temperature increased. During copolymerization the activity initially increased rapidly, followed by slower increase in activity until maximum activity was reached and then activity decreased. There was an

optimum initial concentration of 1-hexene,  $11.4 \text{ mol/m}^3$ , that resulted in attainment of maximum activity in shortest time.

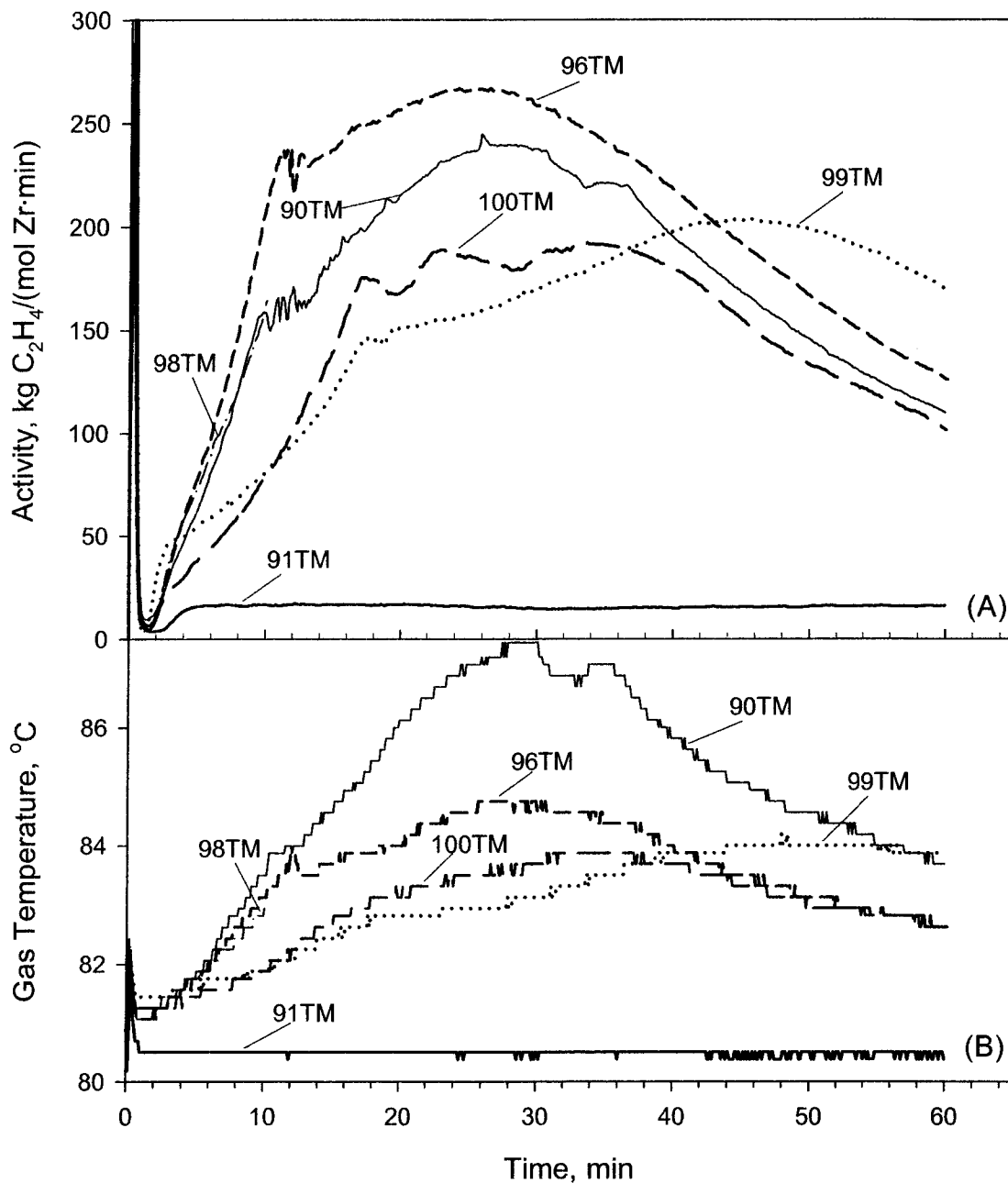


Figure 7.3: Effect of varying initial concentration of 1-hexene on polymerization using Catalyst TM11 showing (A) the activity profiles, and (B) the corresponding gas phase temperature profiles with circulation of coolant oil at  $80^\circ\text{C}$  to reactor.

In Run 90TM similar initial concentration of 1-hexene ( $\sim 11 \text{ mol/m}^3$ ) but larger amount of catalyst were used as compared to Run 96TM. Although initially both had similar activities per mole of zirconium, the activity profiles deviated after 9 minutes with Run 90TM having lower activity per mole of zirconium. The higher gas phase temperature of Run 90TM as compared to Run 96TM as can be seen from their gas temperature profiles (see Figure 7.3 (B)) probably deactivated the catalyst faster than in Run 96TM and resulted in this difference. The higher temperature resulted from the greater thermal energy released by the larger amount of catalyst used in Run 90TM as compared to Run 96TM.

Gel permeation chromatography, GPC, characterization of the product polymer from this set of experiments showed that the comonomer 1-hexene had considerable effect on molar masses of the polymer. The number average,  $M_n$ , and weight average,  $M_w$ , molar masses of polymer resins from some of these runs and the corresponding average gas phase temperature during polymerization are given in Table 7.4 and plotted in Figure 7.4. The results showed that even the presence of a small amount of 1-hexene reduced the molar masses of the product PE significantly as compared to the homopolymer. Moreover, as the initial concentration of 1-hexene was increased, the molar masses decreased or essentially remained constant and polydispersity,  $P_d$ , increased. This result seems reasonable as the comonomer 1-hexene is known to act as a chain transfer agent during polymerization and decrease molar mass of the polymer. The small discrepancy in this trend in  $M_w$  with initial concentration of 1-hexene in Run 90TM was due to the higher average temperature of the run as molar masses of PE decreases with increase in polymerization temperature.

Table 7.4: Effect of initial concentration of 1-hexene on polymer product molar masses (Type A runs, see Chapter 3).

Run Number	Average Temp., (°C)	Initial C <sub>6</sub> H <sub>12</sub> conc., (mol/m <sup>3</sup> )	Mn, (kg/mol)	Mw, (kg/mol)	Pd
90TM	84.9	10.9	32.2	92.6	2.88
91TM	80.5	0.0	57.1	209.7	3.67
99TM	83.1	21.1	24.2	93.6	3.87
100TM	82.9	4.0	37.6	102.9	2.74

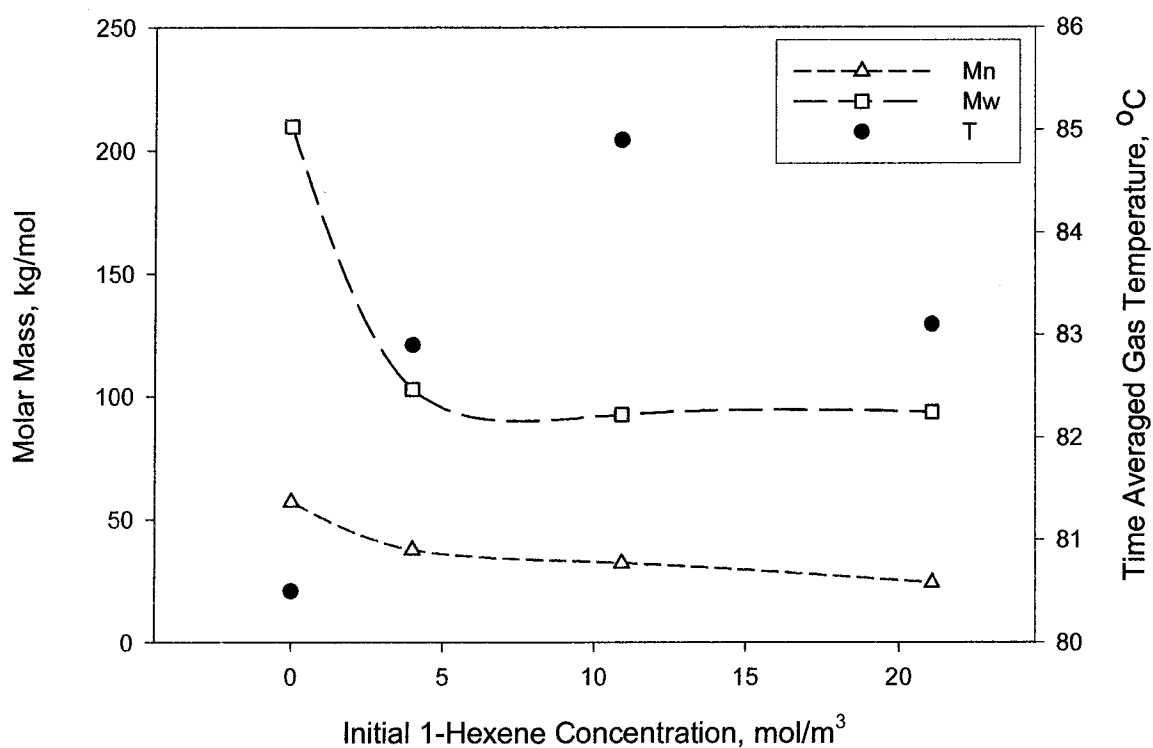


Figure 7.4: Effect of varying initial concentration of 1-hexene on PE molar masses, Mn and Mw, and time averaged gas phase temperature, T.

The observation of ex-situ growth of homopolymer and copolymer particles using scanning electron microscope, SEM, has been described previously in Chapter 6. SEM images of homopolymer and copolymer particles from runs using Catalyst TM11 showed distinct differences as shown in Figure 7.5. The copolymer particles from Run 90 showed the presence of annular shells of polymer layers (see Figure 7.5(B)) as described previously in Chapter 6. However, cut particles of homopolymers from Run 91TM did not have these shell-like polymer layers as shown in Figure 7.5(D).

At high magnifications the surfaces of whole and cut copolymer particles showed a porous and open structure that would enhance the diffusion of monomer gases into the core of the particles (see Figures 7.5 A(III) and B(III)). Such a porous structure would facilitate high polymerization activities and this has been observed for copolymerization of ethylene and 1-hexene using Catalyst TM11. However, the SEM images of homopolymer particles (see Figures 7.5 C and D) from Run 91TM showed a dense and packed morphology that would increase resistance to diffusion of monomer gases into the core of the particles. This type of dense structure was most likely responsible for the very low homopolymerization activity observed during Run 91TM. Moreover, the “cold-drawn” structures visible at high magnification of homopolymer particles (see Figures 7.5 C(III) and D(III)) but not in copolymer particles suggest that during homopolymerization the catalyst/polymer particle temperature was less than that during copolymerization. The higher average and maximum bulk gas temperatures during copolymerization Run TM90 as compared to homopolymerization Run TM91 were indications of higher polymer particle temperature during copolymerization. Moreover, the temperatures of

catalyst/polymer particles were likely higher than the gas phase temperature especially during high polymerization activity.

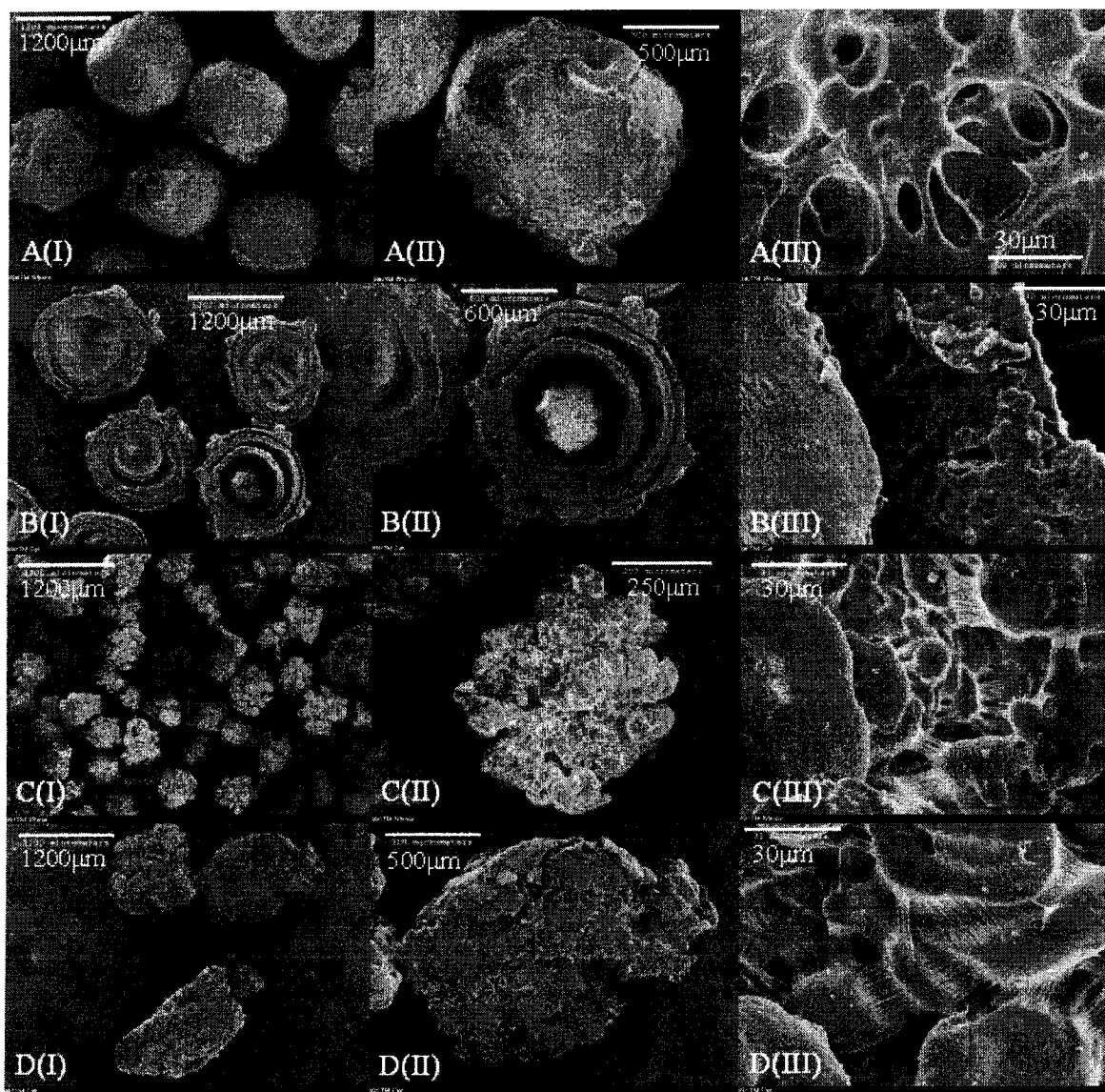


Figure 7.5: SEM images of copolymer particles from Run 90TM showing (A) whole and (B) cut particles; and homopolymer particles from Run 91TM showing (C) whole and (D) cut particles at increasing magnification.

In the previous set of polymerization runs to study the effect of initial concentration of 1-hexene on polymerization activity, the gas phase temperature was allowed to vary. However, as the temperature affects both the activity profiles and molar masses of the product polymer further studies on the effect of initial concentration of 1-hexene on polymerization at constant temperature were done. Catalyst TM17, based on commercial porous polymer support HayeSep R of size range 250 - 300  $\mu\text{m}$  and having a composition of 13.5 mass% aluminum and 0.23 mass% zirconium, was used for these experiments. Both the initial concentration of 1-hexene and ethylene, denoted by the total pressure, were varied during this set of experiments whose details are given in Table 7.5. The activity and the normalized activity per MPa profiles of these runs are shown in Figures 7.6(A) and 7.6(B); and the gas phase temperature profiles are shown in Figure 7.6(C).

Table 7.5: Experiments to study effect of initial concentration of 1-hexene and ethylene pressure on polymerization at 80°C using Catalyst TM17 (Type B runs, see Chapter 3).

Run No.	Date	Catalyst Amount, (mg)	Total Pressure, (MPa)	Initial C <sub>6</sub> H <sub>12</sub> conc., (mol/m <sup>3</sup> )	PE Yield, (g/h)	Mn (kg/mol)	Mw (kg/mol)	Pd
188TM	11/06/02	105.2	1.41	0.0	4.8	57.8	224.0	3.88
198TM	11/26/02	102.2	1.41	14.0	37.3	33.5	86.3	2.58
200TM	12/02/02	100.4	2.76	28.1	43.6	31.1	83.2	2.68
201TM	12/03/02	100.2	2.76	21.2	53.2	36.1	85.2	2.36
202TM	12/04/02	104.0	2.07	21.4	31.1	25.2	89.9	3.57

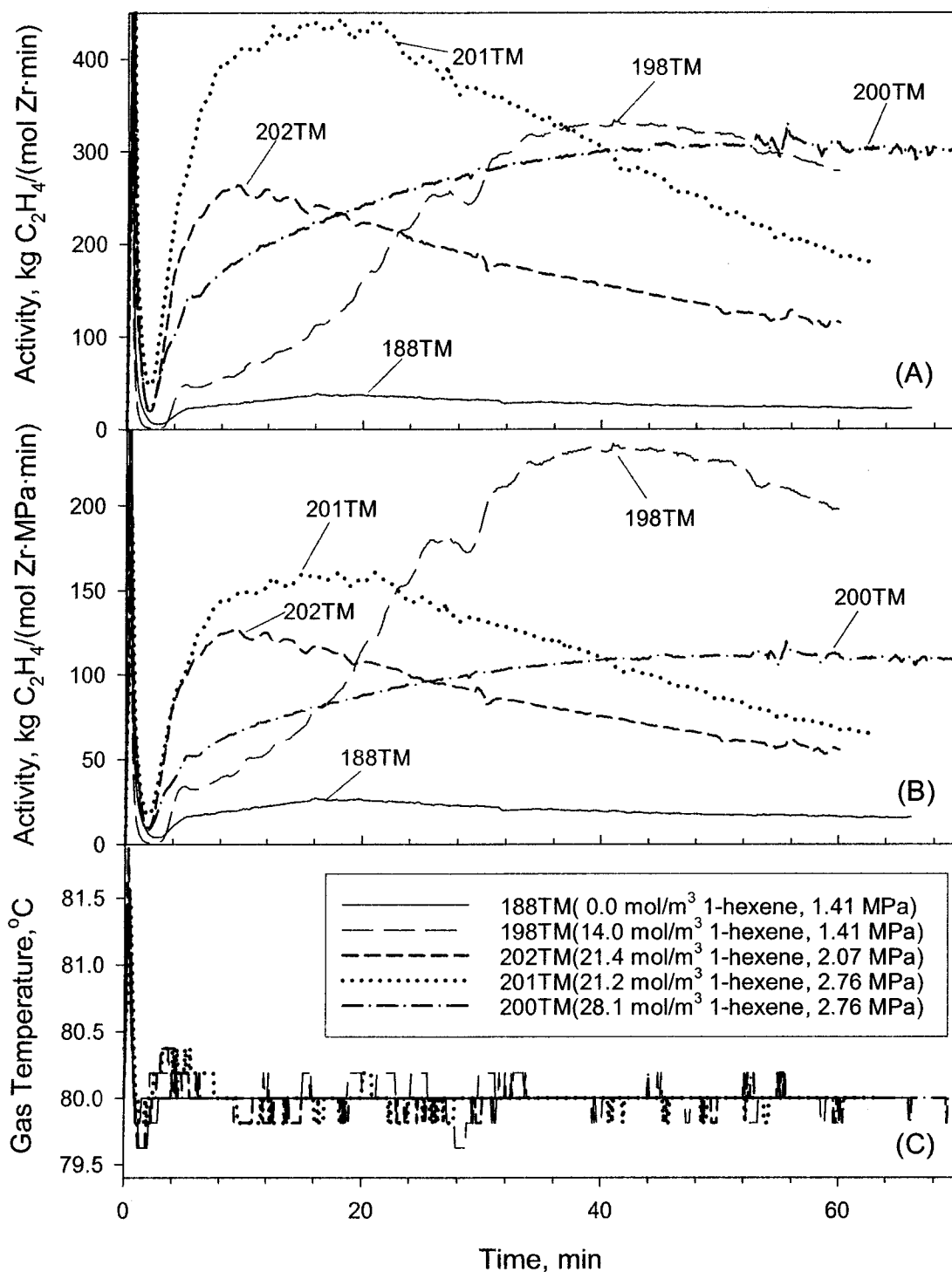


Figure 7.6: Effect of varying initial concentration of 1-hexene and ethylene pressure on polymerization using Catalyst TM17 showing (A) activity profiles, (B) activity profiles normalized with respect to total pressure, and (C) gas phase temperature profiles.

The polymerizations runs showed that the activity of ethylene/1-hexene copolymerization was much higher than that of ethylene homopolymerization. There was an optimum initial concentration of 1-hexene ( $\sim 21 \text{ mol/m}^3$ ) that resulted in quickest attainment of maximum activity. At higher 1-hexene concentration the activity profile was broader and the maximum activity was reached later. Increasing the total pressure while keeping the concentration of 1-hexene constant increased the activity. For all these runs, apart from the initial spike in gas phase temperature due to adiabatic compression, the gas phase temperature was with  $\pm 0.5^\circ\text{C}$  of the set polymerization temperature of  $80^\circ\text{C}$ .

The molar masses of the polyethylene products from this set of runs are given in Table 7.5 and have been plotted in Figure 7.7. The copolymer products had much lower molar masses than that of the homopolymer product. Moreover, at a fixed ethylene pressure increase in initial concentration of 1-hexene resulted in decrease in molar masses of product PE and increase in polydispersity. At fixed concentration of 1-hexene, increase in ethylene pressure resulted in a decrease in the polydispersity of the product PE. This was most likely due to that fact that higher ethylene concentration corresponding to the higher ethylene pressure would incorporate more ethylene than 1-hexene in the polymer (see Quijada et al.(1997)).

The observed increase in polymerization activity in the presence of the comonomer 1-hexene can be attributed to a number of factors. The supported heterogeneous catalyst particle was encapsulated in a polymer layer on exposure to the monomer gas as has been observed previously in Chapter 6. The diffusion of monomer

gas through this polymer layer was facilitated by the decrease in molar mass and crystallinity of this layer due to presence of the comonomer and this enhanced polymerization activity. Moreover, the breakup of the catalyst particle in layers (see Chapter 6) resulting from high activity at the surface revealing new catalyst surfaces also contributed to the further increase in activity. As the 1-hexene concentration was increased, there was greater competition between 1-hexene and ethylene for  $\pi$ -complexation with the metallocene (see Chien and Nozaki (1993)) resulting in decrease in activity as measured by the flow of ethylene into the reactor. This manifested in there being an optimum 1-hexene concentration at a given ethylene pressure to obtain maximum activity as measured by ethylene flow into the reactor.

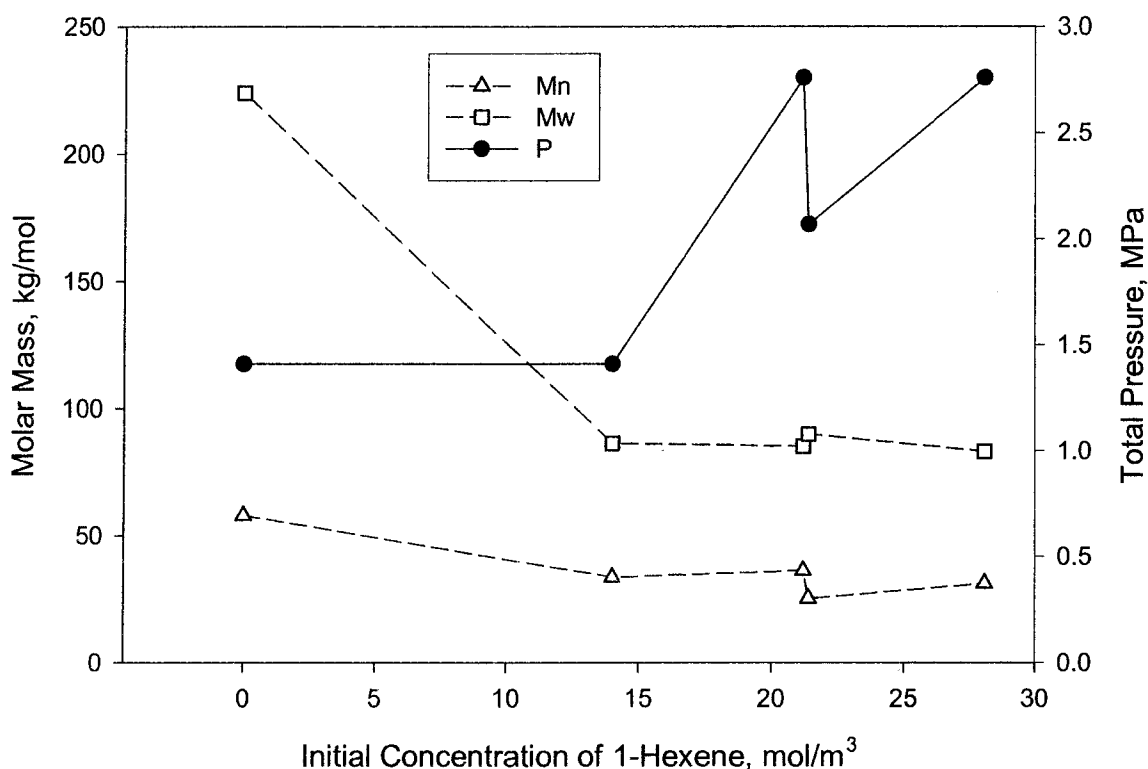


Figure 7.7: Effect of varying initial concentration of 1-hexene and ethylene pressure on PE molar masses, Mn and Mw during polymerization at 80°C using Catalyst TM17.

## 7.2 Control of Concentration of 1-Hexene during Polymerization

In the copolymerization runs described so far in this chapter the 1-hexene was injected into the reactor initially before catalyst injection. During the polymerization run only ethylene flowed into the reactor and the concentration of 1-hexene in the reactor decreased as it was consumed. To control the concentration of 1-hexene during polymerization, the gas in the reactor was continually analyzed and 1-hexene was pumped into the reactor as required. As discussed previously in Chapter 3 a Hewlett Packard 5890 Series II gas chromatograph equipped with a 6-port gas sample valve, a flame ionization detector and a thermal conductivity detector was used for analysis of the gas phase.

Initially a 1/16-inch stainless steel tube with one end tapered to form a tiny orifice was used to sample gas from inside the reactor to the gas chromatogram. A Swagelok on-off valve was used to intermittently sample gas from the reactor to the gas chromatogram through this tube. Experiments to study the variation in concentration of 1-hexene and to control this concentration were done using this setup. Details of two such experiments using Catalyst TM13 based on HayeSep-Q porous polymer support of size range 150-180 $\mu\text{m}$  are given in Table 7.6. The activity profiles, temperature profiles and the concentration of 1-hexene during the duration of the runs are shown in Figure 7.8.

It can be seen from Figure 7.8 that for the Run 130TM where 1-hexene was injected only once initially before the start of polymerization, the concentration of 1-hexene varied from about 14 mol/m<sup>3</sup> initially to about 4 mol/m<sup>3</sup> at the end of the run. In Run 132TM where 1-hexene was continuously pumped into the reactor at a flowrate that was manually controlled, the concentration of 1-hexene did not change much during the

duration of the run having an average value of 10.0 mol/m<sup>3</sup> and standard deviation of 0.85 mol/m<sup>3</sup>. This showed that concentration of 1-hexene could be manually controlled using data from the gas chromatogram during ethylene 1-hexene copolymerization.

However, it is apparent from the activity profiles in Figure 7.8 that the gas sampling technique used during these experiments caused significant distortions to the activity profiles as seen by the spikes in the activity plots each time gas was withdrawn for analysis. Moreover such spikes in ethylene flow into the reactor were likely to reduce the concentration of 1-hexene in the reactor at a faster rate than that due to consumption of 1-hexene by polymerization alone. Thus a new method for continuously sampling the headspace gas in the reactor without significantly affecting the concentration of 1-hexene in the reactor was developed using a modified Nupro SS-SS2 metering valve as described previously in Chapter 3. Further analyses of headspace gas during polymerization experiments were done using the new method.

Table 7.6: Experiments to determine change and control the concentration of 1-hexene during polymerization at 80°C using Catalyst TM13 (Type A runs, see Chapter 3).

Run No.	Date	Catalyst Amount, (mg)	Total Pressure, (MPa)	Initial C <sub>6</sub> H <sub>12</sub> conc., (mol/m <sup>3</sup> )	Total PE Yield, (g)	Mn (kg/mol)	Mw (kg/mol)	Pd
130TM	04/24/02	75	1.40	13.6	20.3	21.3	64.5	3.03
132TM	05/01/02	76	1.42	10.7	21.4	22.6	88.3	3.91

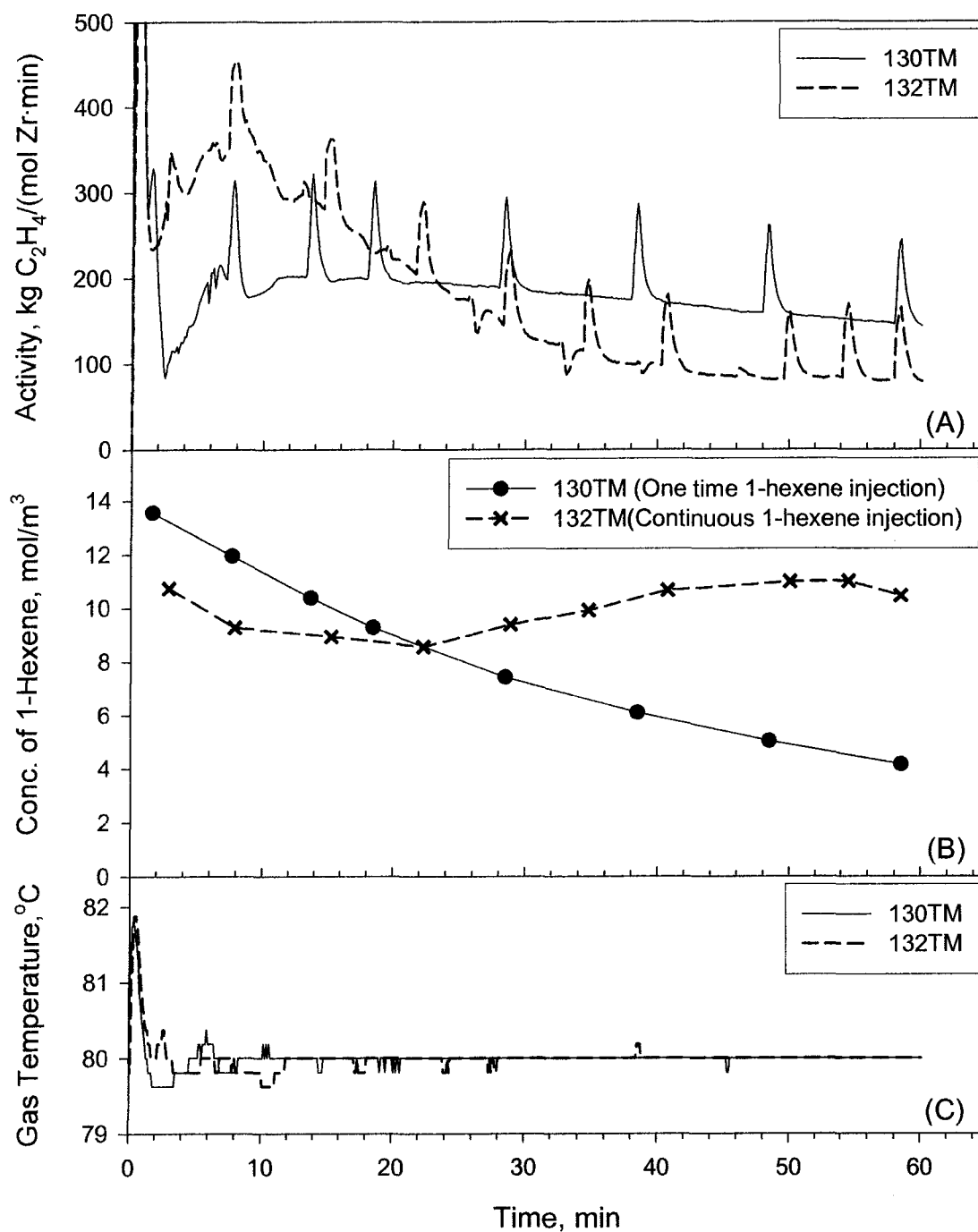


Figure 7.8: Experiments to study variation of concentration of 1-hexene during polymerization using Catalyst TM13 at 80°C showing (A) activity profiles, (B) gas phase concentration of 1-hexene, and (C) gas phase temperature profiles.

A set of polymerization runs were carried out to find the effect of continuously feeding 1-hexene into the reactor during polymerization using Catalyst TM17 at 80°C. Some details of these runs are given in Table 7.7 below. Both polymerization Runs 192TM and 193TM carried out at about 1.4 MPa total pressure had initial 1-hexene concentration of about 14 mol/m<sup>3</sup> but during Run TM193 1-hexene was continuously injected into the reactor to maintain concentration of 1-hexene near this level while in Run TM192 concentration of 1-hexene was allowed to decrease. The activity and temperature profiles and the concentration of 1-hexene in the reactors for these two runs are shown in Figure 7.9. Polymerization Runs TM205 and TM206 had initial 1-hexene concentration of about 21 mol/m<sup>3</sup> and were carried out at about 2.1 MPa total pressure. The activity and temperature profiles of these two runs are shown in Figure 7.10. In Figure 7.10(B) concentration of 1-hexene that was continuously injected into the reactor during Run TM206 is shown.

Table 7.7: Experiments to study effect of controlling the concentration of 1-hexene during polymerization at 80°C using Catalyst TM17 (Type B runs, see Chapter 3).

Run No.	Date	Catalyst Amount, (mg)	Total Pressure, (MPa)	Initial C <sub>6</sub> H <sub>12</sub> conc., (mol/m <sup>3</sup> )	Total PE Yield, (g)	Mn (kg/mol)	Mw (kg/mol)	Pd
192TM	11/14/02	106	1.38	14.2	56.6	33.9	83.5	2.46
193TM*	11/15/02	106	1.41	14.3	42.5	32.9	92.8	2.82
205TM	12/12/02	101	2.09	21.2	44.7	35.5	87.1	2.45
206TM*	12/17/02	104	2.07	21.2	63.0	33.2	89.1	2.68

\*1-hexene continuously fed to reactor to maintain its concentration.

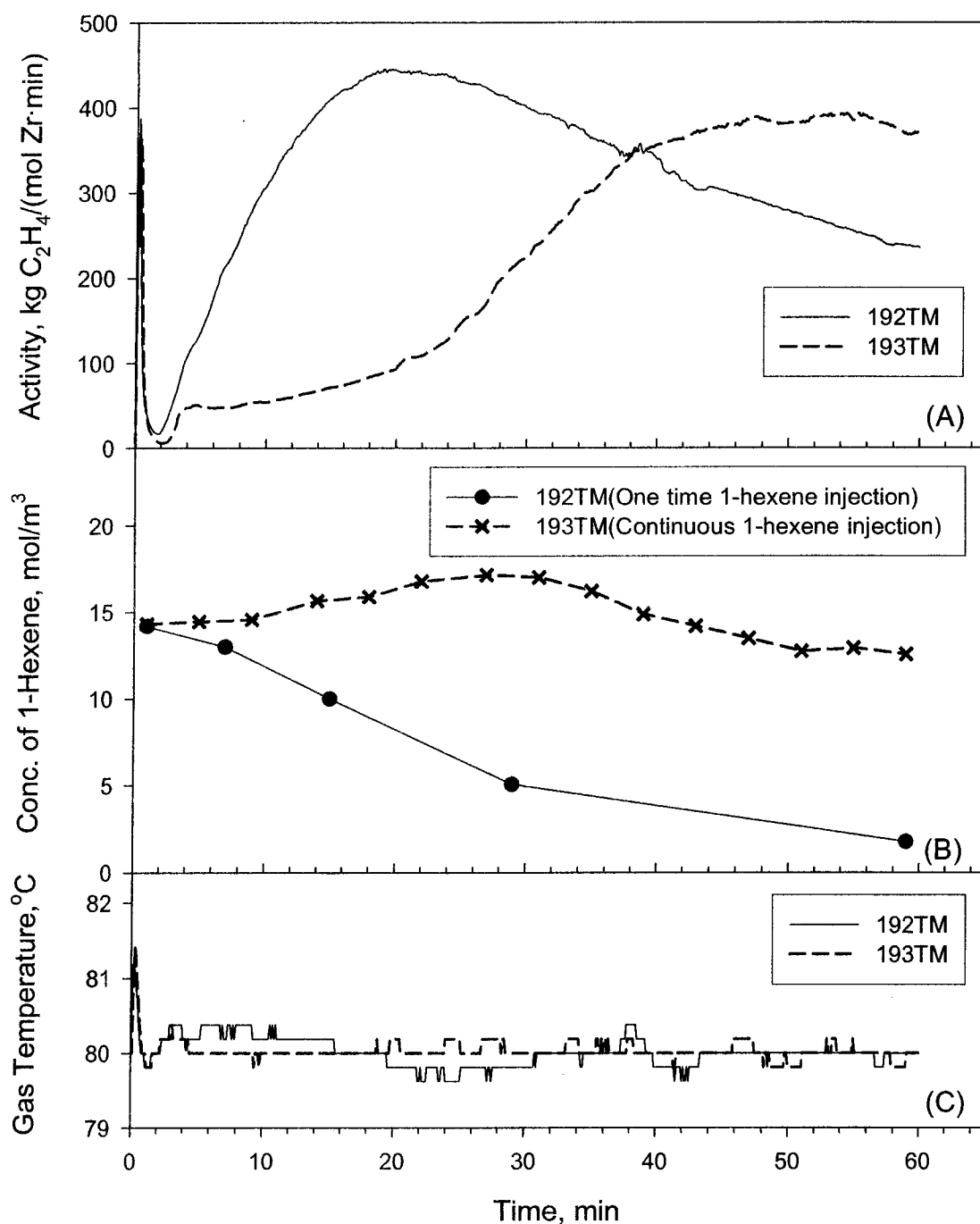


Figure 7.9: Effect of continuous injection of 1-hexene during polymerization at 1.4 MPa using Catalyst TM17 at 80°C showing (A) activity profiles, (B) concentration of 1-hexene, and (C) temperature profiles.

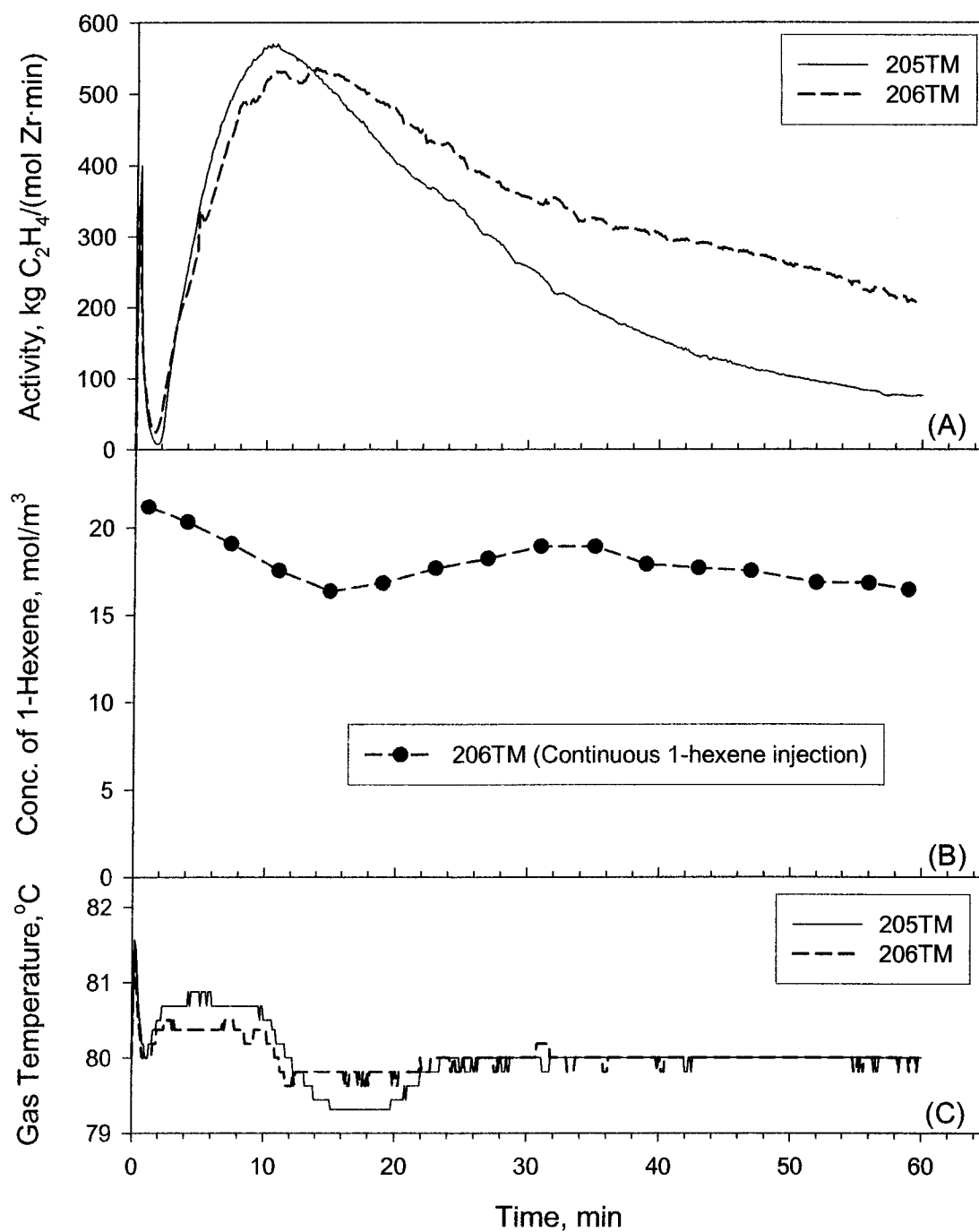


Figure 7.10: Effect of continuous injection of 1-hexene during polymerization at 2.1 MPa using Catalyst TM17 at 80°C showing (A) activity profiles, (B) concentration of 1-hexene, and (C) temperature profiles.

In Figure 7.9 it can be seen that the activity profiles of the two runs, TM192 and TM193 deviated considerably after about 4 minutes of polymerization. In Run TM192 the maximum activity was reached after about 20 minutes while in Run TM193 it was reached after about 55 minutes of polymerization. As the flowrate of the continuous feed of 1-hexene was manually controlled during Run TM193 the concentration of 1-hexene increased from the initial level before going down. This higher concentration of 1-hexene was most likely greater than the “optimum” concentration of 1-hexene at this ethylene pressure and resulted in delay in attainment of maximum activity. However, after maximum activity had been attained the rate of decrease in activity was less than that in Run TM192. By the time maximum activity was attained in Run TM192 the concentration of 1-hexene in the reactor had decreased significantly from about 14 mol/m<sup>3</sup> to less than 9 mol/m<sup>3</sup>. This likely contributed to the more rapid decline in activity as compared to Run TM193.

Runs TM205 and TM206 as seen in Figure 7.10(A) had similar activity profiles for the first 10 minutes until maximum activity were reached, thereafter the rate of decrease in activity of Run TM206 where 1-hexene was continuously pumped into the reactor was less than that of Run TM205. It can be expected that significant decrease in concentration of 1-hexene in Run TM205 was the reason for the more rapid decrease in activity than in Run TM206.

Apart from the initial spikes in temperature for all four runs the gas phase temperature was within  $\pm 0.5^{\circ}\text{C}$  of the set point temperature of  $80^{\circ}\text{C}$  during the runs. The weight averaged molar mass,  $M_w$  increased as a result of continuous injection of 1-hexene during the runs as did the polydispersity,  $P_d$ .

### 7.3 Effect of *n*-Heptane during Polymerization

The polymerization runs carried out during the course of this work showed that the presence of comonomer 1-hexene dramatically increased the activity for most of the prepared supported catalysts as compared to ethylene homopolymerization. Apart from chemically interacting with the catalyst active sites and being incorporated into the polymer 1-hexene might physically affect the environment of the catalyst and influence the activity. In order to see whether such physical effects were present some amounts of an inert hydrocarbon, *n*-heptane were added to two homopolymerization runs to find the effect on polymerization activity. Details about these experiments are given in Table 7.8 and the activity and temperature profiles are shown in Figure 7.11. Secondary Y-axis was used to show the activity during copolymerization as it was much higher than the homopolymerization activities.

Table 7.8: Experiments to study effect of addition of *n*-heptane during homopolymerization at 80°C using Catalyst TM15 (150TM and 151TM Type A runs, 152TM and 153TM Type B runs, see Chapter 3).

Run No.	Date	Catalyst Amount, (mg)	Total Pressure, (MPa)	Initial C <sub>6</sub> H <sub>12</sub> conc., (mol/m <sup>3</sup> )	PE Yield, (g/h)	Mn (kg/mol)	Mw (kg/mol)	Pd
150TM	06/27/02	116	1.41	12.5	47.8	33.2	86.3	2.60
151TM	07/02/02	104	1.37	0.0	1.1	36.3	131.3	3.62
152TM <sup>1</sup>	07/03/02	101	1.40	0.0	4.0	41.8	143.4	3.43
153TM <sup>2</sup>	07/04/02	104	1.40	0.0	3.4	52.7	146.2	2.77

<sup>1</sup> *n*-Heptane added to reactor = 3.4 mL

<sup>2</sup> *n*-Heptane added to reactor = 5.3 mL

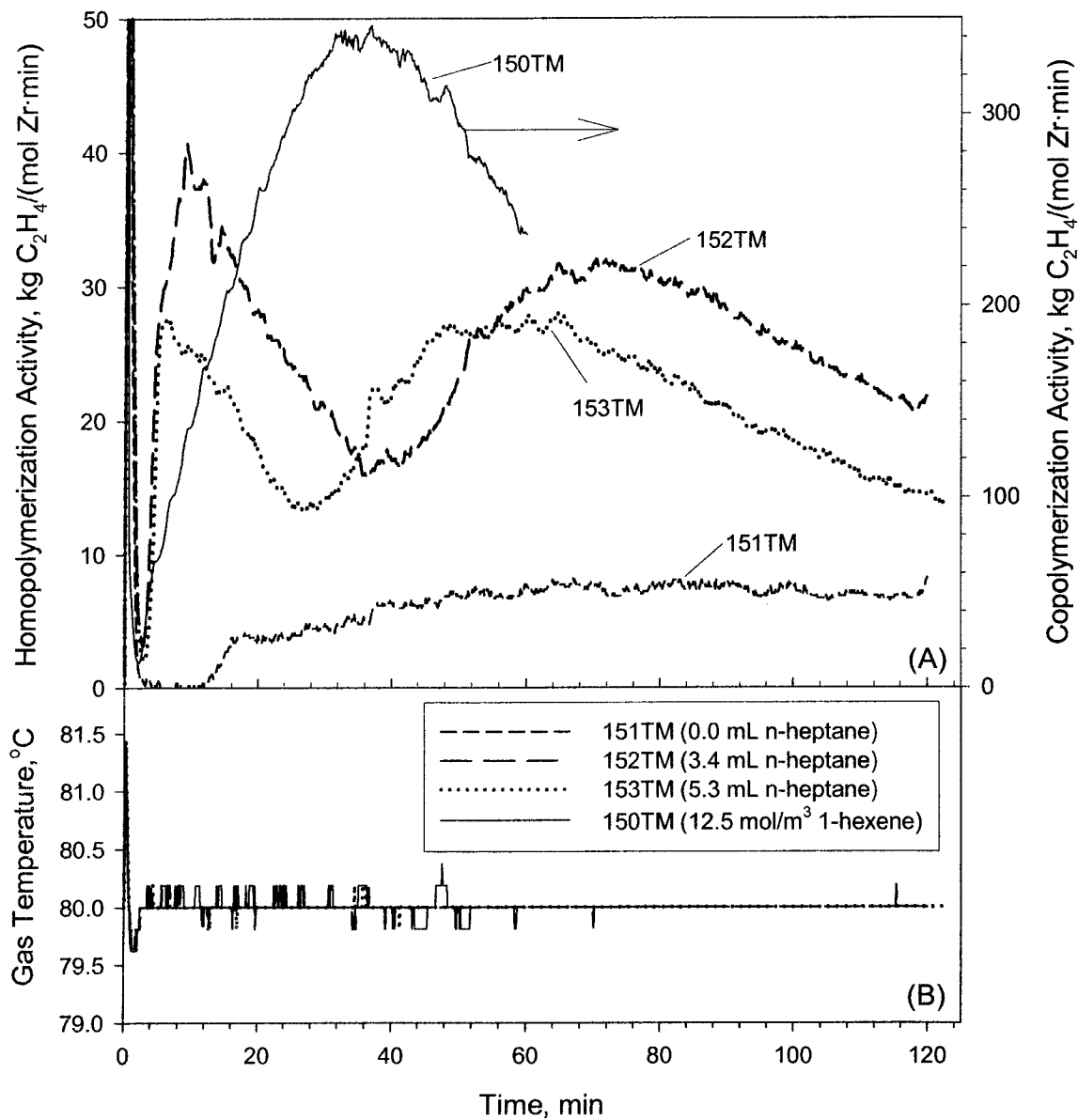


Figure 7.11: Effect of addition of *n*-heptane during homopolymerization at 1.4 MPa and 80°C using Catalyst TM15 showing (A) activity profiles, and (B) temperature profiles and compared to activity during copolymerization with 1-hexene (secondary Y-axis).

At 80°C polymerization temperature the saturated vapour pressure of *n*-heptane was 57 kPa and the heptane injected was in the vapour phase inside the reactor. The homopolymerization runs in presence of *n*-heptane vapour showed higher activities than that without *n*-heptane and the product molar masses increased and polydispersity decreased. This showed that the presence of the heavier hydrocarbon vapour as compared to ethylene influenced the behaviour of the supported metallocene catalyst during gas phase polymerization. However, copolymerization with 1-hexene showed much higher activity than that of homopolymerization with or without *n*-heptane. This suggests that chemical interaction with catalytic sites and incorporation of 1-hexene into the polymer were far more important in increasing the activity as compared to that during homopolymerization. Polymer product from solution polymerization of ethylene using homogeneous metallocene has polydispersity of about 2 (see Soares and Hameielec (1995)). The decrease in polydispersity of homopolymers made in presence of *n*-heptane from 3.6 to 2.8 thus suggested that the active catalytic sites on the supported catalysts became more uniform and accessible as a consequence of the presence of *n*-heptane. Even lower polydispersity, 2.6 of the copolymer of 1-hexene and ethylene indicated that 1-hexene further increased the accessibility of the monomer gases to the active catalytic sites.

#### 7.4 Temperature Rising Elution Fractionation (TREF) Analysis

Analytical temperature rising elution fractionation, TREF analysis was carried out with some polymer products to characterize them. TREF results indicate the degree of crystallinity and can be used to determine short-chain branching distribution in the polymer (see Soares and Hamielec (1995); Wild et al. (1982)). Empirical correlation can be used to relate elution temperatures to the methyl group concentration,  $[-CH_3]$  (see Kumkaew et al. 2003). Average short chain branching,  $C_N$  defined as  $-CH_3$  groups per 1000 carbon atoms is given by:

$$C_N = \frac{\int_{T_0}^{T_f} (IR)_{Signal} [CH_3]_T dT}{\int_{T_0}^{T_f} (IR)_{Signal} dT} \quad (7.1)$$

where,

$$[CH_3]_T = \frac{[CH_3]_{Groups}}{1000 \text{ Carbon Atoms}} = 76.37 - 1.20T + 4.4 \times 10^3 T^2 \quad (7.2)$$

$(IR)_{Signal}$  is the IR absorbance intensity and T is the elution temperature in °C.

The “broadness” of the short chain branching distribution is given by the ratio  $C_W/C_N$  where,

$$C_W = \frac{\int_{T_0}^{T_f} (IR)_{Signal} [CH_3]_T^2 dT}{\int_{T_0}^{T_f} (IR)_{Signal} [CH_3]_T dT} \quad (7.3)$$

To compare the effect of initial concentrations of 1-hexene on crystallinity of polymer product TREF analyses were carried out on products from a set of experiments described previously, details of which are given in Tables 7.3 and 7.4. Details about these

runs are summarized in Table 7.9. The short chain branching frequency and the broadness of its distribution for these runs are also shown in Table 7.9.

Table 7.9: TM11 catalyzed polymerization runs having various initial concentration of 1-hexene used for TREF analyses (Type A runs, see Chapter 3).

Run Number	91TM	98TM <sup>1</sup>	99TM	100TM
Avg. Temp., (°C)	80.5	81.9	83.1	82.9
Total Pressure, (MPa)	1.39	1.39	1.38	1.39
Initial C <sub>6</sub> H <sub>12</sub> , (mol/m <sup>3</sup> )	0.0	11.9	21.1	4.0
Total PE Yield, (g)	3.2	3.3	31.6	27.3
Mn, (kg/mol)	57.1	18.5	24.2	37.6
Mw, (kg/mol)	209.7	133.3	93.6	102.9
Polydispersity, Pd	3.67	7.21	3.87	2.74
C <sub>N</sub>	0.6	8.3	9.2	3.7
C <sub>W</sub> /C <sub>N</sub>	2.4	1.4	1.4	2.1

<sup>1</sup> Polymerization carried out for 10 minutes only, other runs were 60 minutes.

The TREF profiles showing IR absorbance intensity normalized with respect to mass of polymer sample and shifted to zero baseline versus elution temperatures are shown in Figure 7.12. The results showed that the maximum of the elution peak for the supported metallocene catalyst catalyzed ethylene homopolymer was near 100°C while those for the ethylene/1-hexene copolymers were at lower temperatures depending on the initial concentration of 1-hexene. The result agrees with literature (see Soares and Hamielec (1995)) that showed that the highly crystalline high density polyethylene, HDPE from homopolymerization of ethylene eluted about 100°C and less crystalline

linear low density polyethylene, LLDPE from co-polymerization of ethylene and 1-hexene eluted at lower temperatures. The experiments further indicate that greater the initial concentration of 1-hexene the greater was the short chain branching,  $C_N$  because of higher incorporation of 1-hexene into the polymer macromolecules that resulted in lower crystallinity and lower elution temperatures. Moreover, the broadening of the elution profiles at higher initial concentration of 1-hexene shows that the polymer had wider range of crystallinity corresponding to a wider range of incorporation of 1-hexene into the polymer macromolecules. This probably resulted because the concentration of 1-hexene was not controlled and decreased during the duration of the polymerization run.

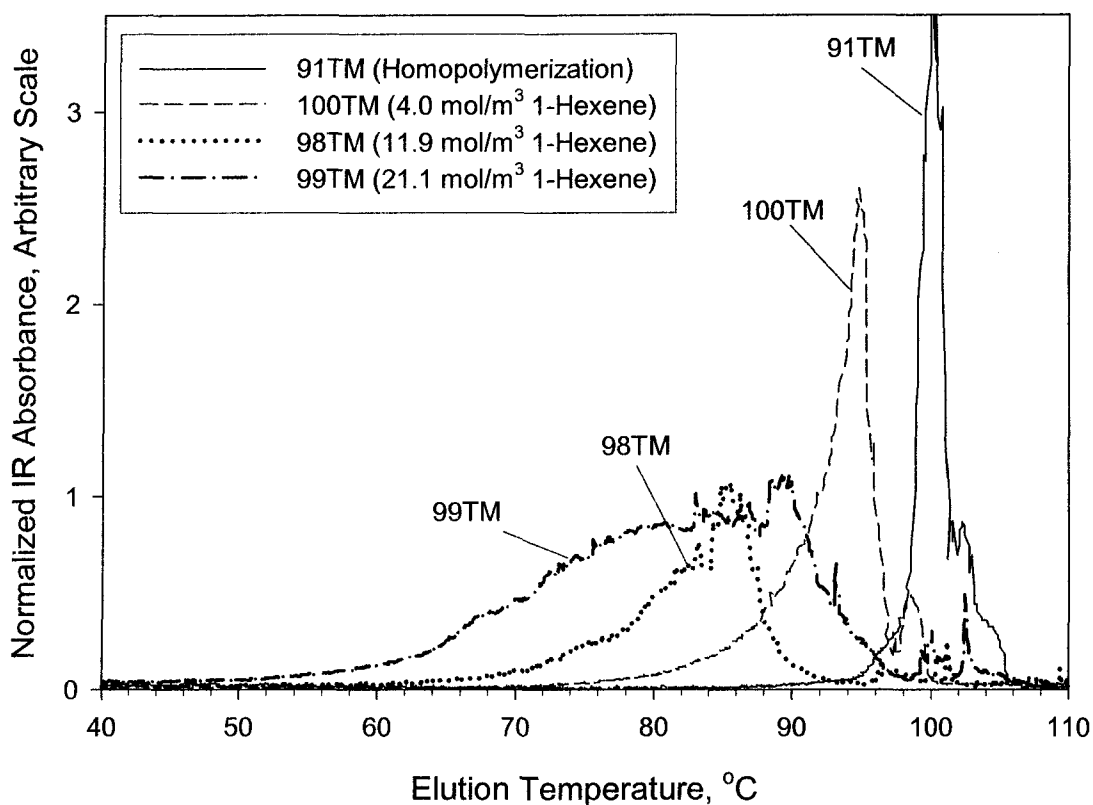


Figure 7.12: TREF profiles of homopolymer and copolymers formed from different initial concentration of 1-hexene.

To further study the effect of polymerization time on crystallinity, TREF analyses were done on a set of copolymers made with Catalyst TM12 under similar reactor conditions but with different run durations. Catalyst TM12 was supported on HayeSep-R porous particles of size range 125-150  $\mu\text{m}$  and had an estimated zirconium concentration of 0.25 mass%. Details of these runs carried out at 80°C, total pressure of about 1.4MPa, and initial concentration of 1-hexene of about 11 mol/m<sup>3</sup> are given in Table 7.10. The activity, temperature and pressure profiles of the polymerization runs used for studying effect of polymerization time are shown in Figure 7.13.

Table 7.10: Polymerization runs carried out using Catalyst TM12 at 80°C analyzed to determine effect of polymerization time on TREF profiles of product (Type A runs, see Chapter 3).

Run Number	118TM	119TM	120TM	121TM	123TM
Date	03/25/02	03/26/02	03/27/02	03/28/02	04/03/02
Run Duration, (min)	60	30	5	15	9
Total Pressure, (MPa)	1.41	1.40	1.41	1.39	1.41
Initial C <sub>6</sub> H <sub>12</sub> , (mol/m <sup>3</sup> )	10.7	11.2	10.8	10.7	10.6
Total PE Yield, (g)	12.4	3.8	0.3	1.0	0.5
Mn, (kg/mol)	34.1	37.8	9.8	25.9	19.4
Mw, (kg/mol)	103.2	124.8	94.6	124.8	119.7
Polydispersity, Pd	3.03	3.29	9.65	4.82	6.17
C <sub>N</sub>	7.8	9.2	7.4	9.5	9.1
C <sub>W</sub> /C <sub>N</sub>	1.3	1.3	1.5	1.5	1.3

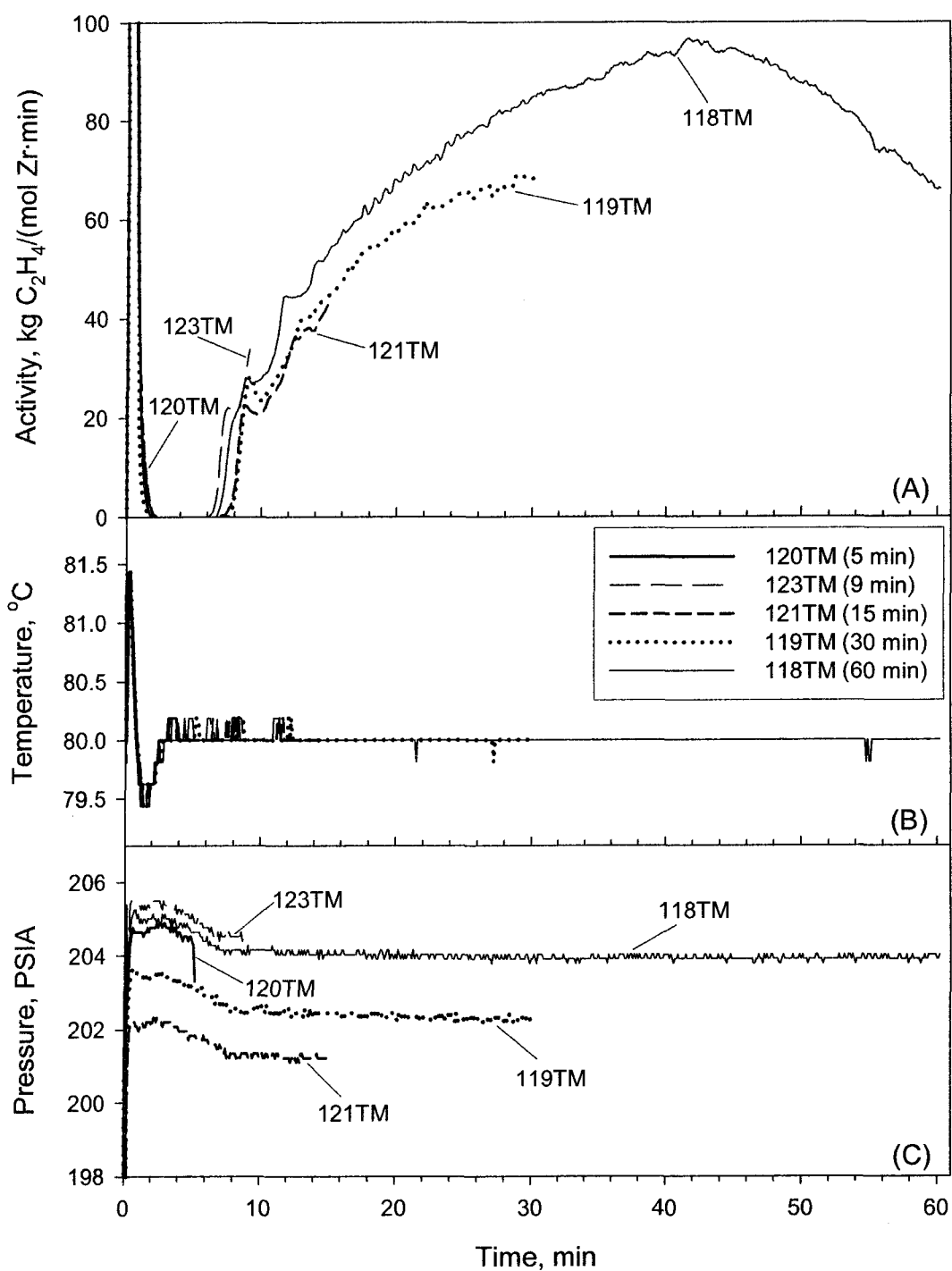


Figure 7.13: Catalyst TM12 catalyzed polymerization runs of various durations showing (A) activity profiles, (B) temperature profiles, and (C) pressure profiles.

The activity profiles showed excellent reproducibility of polymerization behaviour. From the pressure profiles it can be deduced that the little differences in activities most likely arose due to slight differences in the total pressures at which the polymerization runs were carried out; the runs carried out at higher pressures had greater activities. Apart from the initial spikes the gas phase temperatures were maintained at the set polymerization temperature of 80°C throughout the runs.

The molar masses of the produced polymers from this set of experiments are given in Table 7.10 and have been plotted in Figure 7.14. The results showed that initially the molar masses increased with increase in polymerization time and reached a maximum and then started to decrease with increase in polymerization time. The polydispersity decreased monotonously with increase in polymerization time. The initial increase in molar masses with increase in polymerization time was most probably due to decrease in concentration of 1-hexene as polymerization proceeded as 1-hexene is known to act as a chain transfer agent. The decrease in polydispersity indicated that the number of types of active sites decreased with increase in polymerization time. This probably arose due to the way this type of supported catalyst fragmented in layers during polymerization as described previously in Chapter 6. Initially the catalyst particles were compact and monomer had easier access to active catalytic sites near the surface than those further inside. Ethylene was likely able to diffuse into the catalyst particle faster than 1-hexene. As the catalyst fractured in layers it became easier for both monomers to diffuse to active catalytic sites inside the catalyst particles. Thus steric hindrance distinguished the active sites within the supported catalysts initially and this reduced as the catalyst fragmented. There are a number of reasons why the molar masses would decrease after 30 minutes of

polymerization. As the polymer built up around the active sites the effective concentration of monomers at those sites would decrease. Convection effects could build up the concentration of the less reactive comonomer inside the catalyst especially during high activity (see Kittilsen et al. 2001). The temperature of the growing catalyst/polymer particle could be higher than the bulk gas phase temperature especially during high activity. The observed decrease in molar mass could be for any of these reasons or a combination of them.

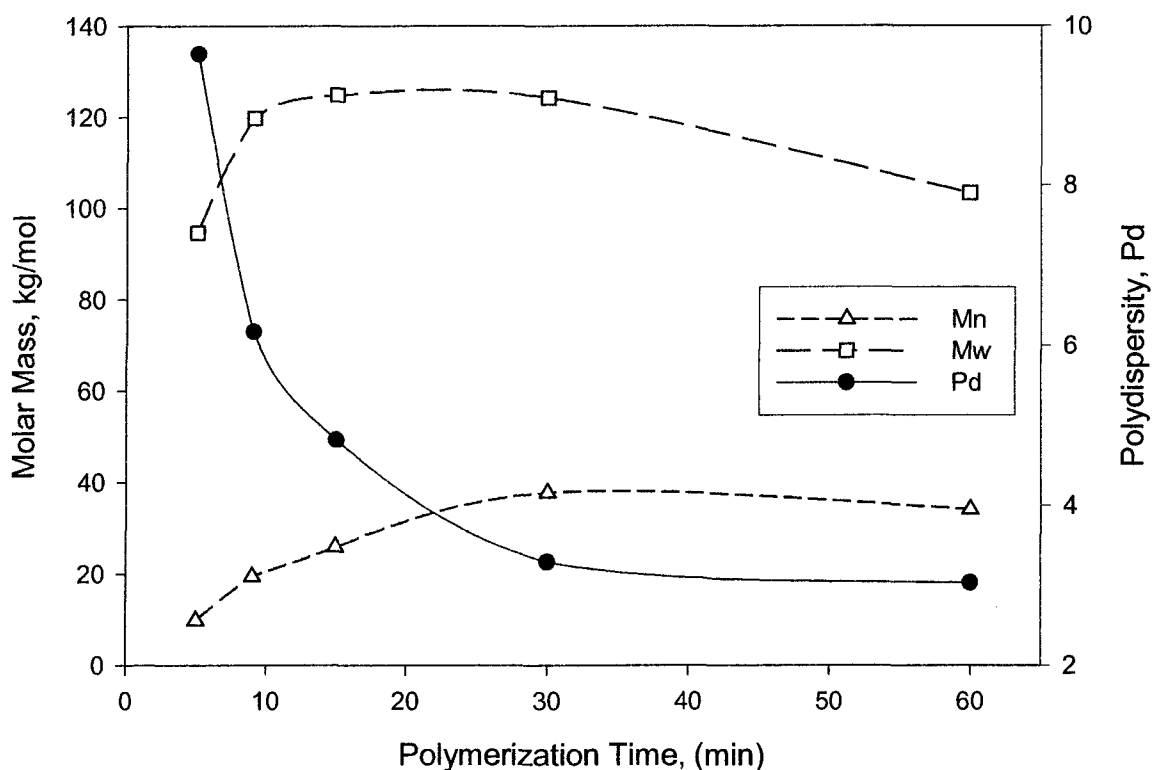


Figure 7.14: Effect of polymerization time on molar masses and polydispersity of copolymers catalyzed by Catalyst TM12 at 80°C.

To determine the effects of polymerization time on 1-hexene incorporation in the copolymer, TREF analyses were carried out with polymer samples from this set of runs. IR absorbance normalized with respect to sample mass and shifted to zero base versus elution temperature plots of these TREF analyses are shown in Figure 7.15. The 5 minute polymerization run, TM120 had two major peaks; one near 86°C and the other near 98°C. The runs from 9 to 30 minutes, 123TM, 121 TM, and 119TM had major peaks near 82°C while after 60 minutes of polymerization Run 118TM had an elution peak near 88°C. The number of short chain branching per 1000 carbon atoms,  $C_N$  value increased from 7.4 after 5 minutes of polymerization to a maximum of 9.5 after 15 minutes of polymerization and decreased to 7.8 after 60 minutes of polymerization.

The GPC and TREF results suggest that initially ethylene diffused into the catalyst particles faster than 1-hexene and polymer formed near the surface of the catalyst had greater 1-hexene incorporation than that formed inside. This is supported by the two elution peaks observed in TREF analysis of polymer from Run TM12. As polymerization proceeded the catalyst fragmented in layers and more 1-hexene was able to diffuse in and be incorporated into the polymer leading to an increase in  $C_N$ . However, as the bulk concentration of 1-hexene decreased with time less 1-hexene was copolymerized with ethylene. Therefore  $C_N$  initially increased and then decreased.

Catalyst TM15 was supported of HaysSep-R porous particle of size range 600-850 $\mu$ m and produced relatively large polymer particles of 3-9 mm diameters after an hour of copolymerization. These large polymer particles were peeled in layers to determine any variation in molar masses and short chain branching with radial distance. Particles from Run TM166 whose profiles are shown in Figure 7.16 were used for this purpose.

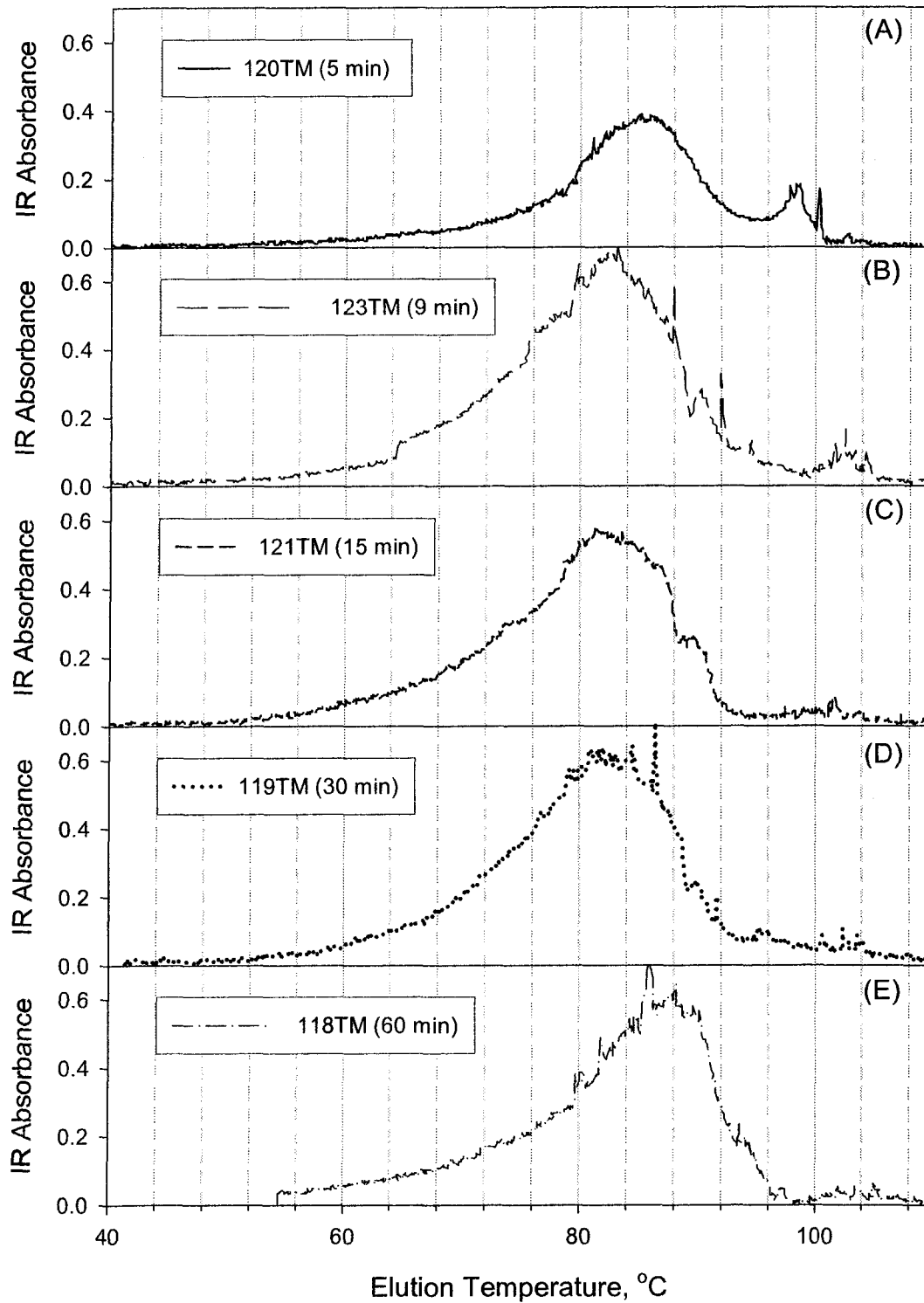


Figure 7.15: Effect of polymerization time on TREF profiles of copolymers showing elution curves for run of (A) 5, (B) 9, (C) 15, (D) 30, and (E) 60 minutes duration.

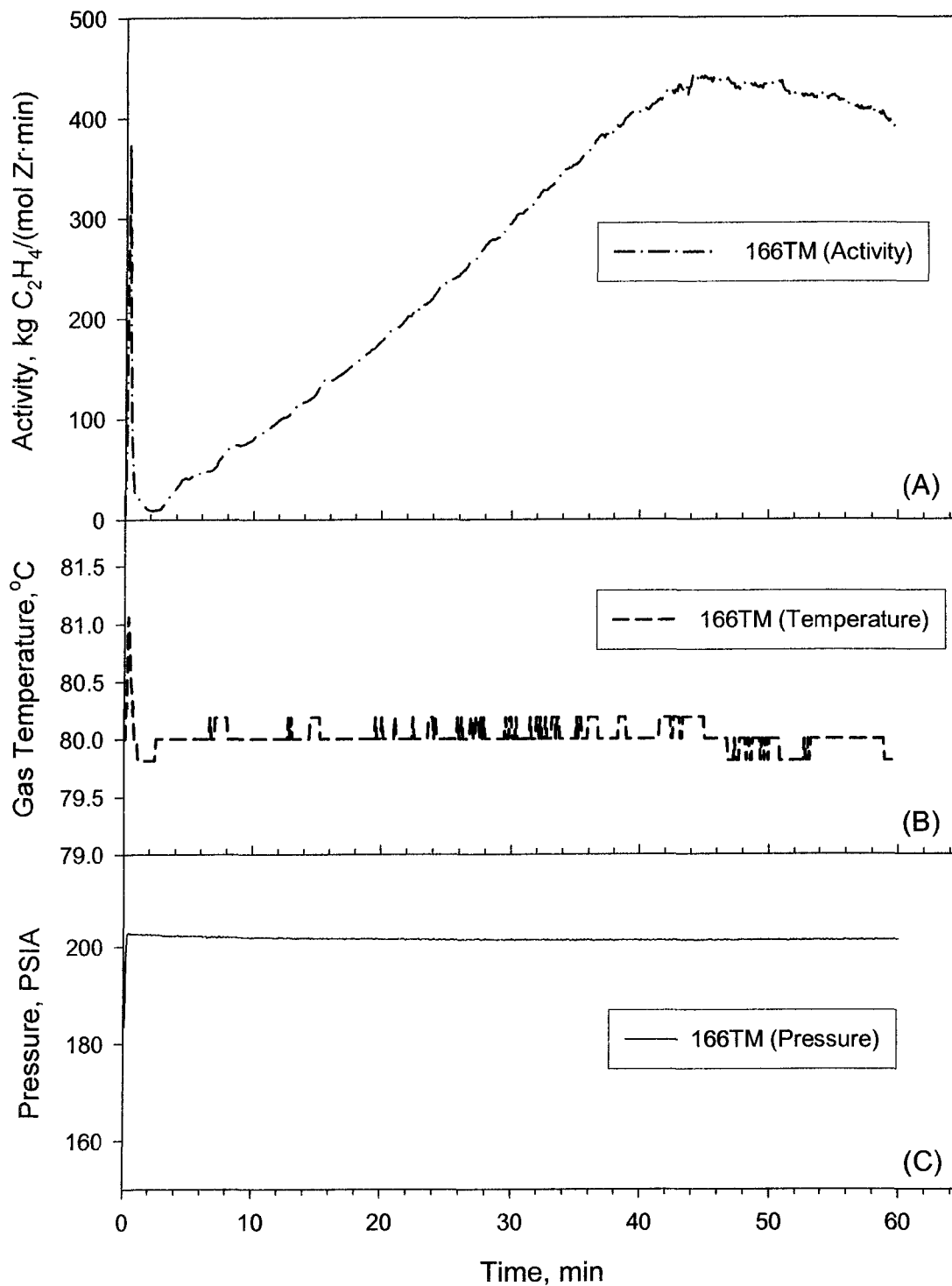


Figure 7.16: Run TM166 using Catalyst TM15 showing (A) activity, (B) gas phase temperature, and (C) pressure profiles.

In Run 166TM, polymerization was carried out for an hour using 100 mg of catalyst TM15 and the total yield was 45.7 g. The initial concentration of 1-hexene was  $14.8 \text{ mol/m}^3$  and total pressure was 1.40 MPa. Cross-sectional SEM image of a cut polymer particle from this run is shown in Figure 7.17. As the whole particle could not be seen in a single SEM image even at the lowest magnification ( $\times 25$ ) as it was too large, four SEM images were superimposed to produce Figure 7.17. Layers of polymers that were densely packed near the center and further apart near the outer surface can be seen from Figure 7.17. By carefully removing layers of polymer from outside of such polymer particles successive inner layers of polymers were exposed. Molar masses of polymer at different radial positions for small and large particles are shown in Figure 7.18.

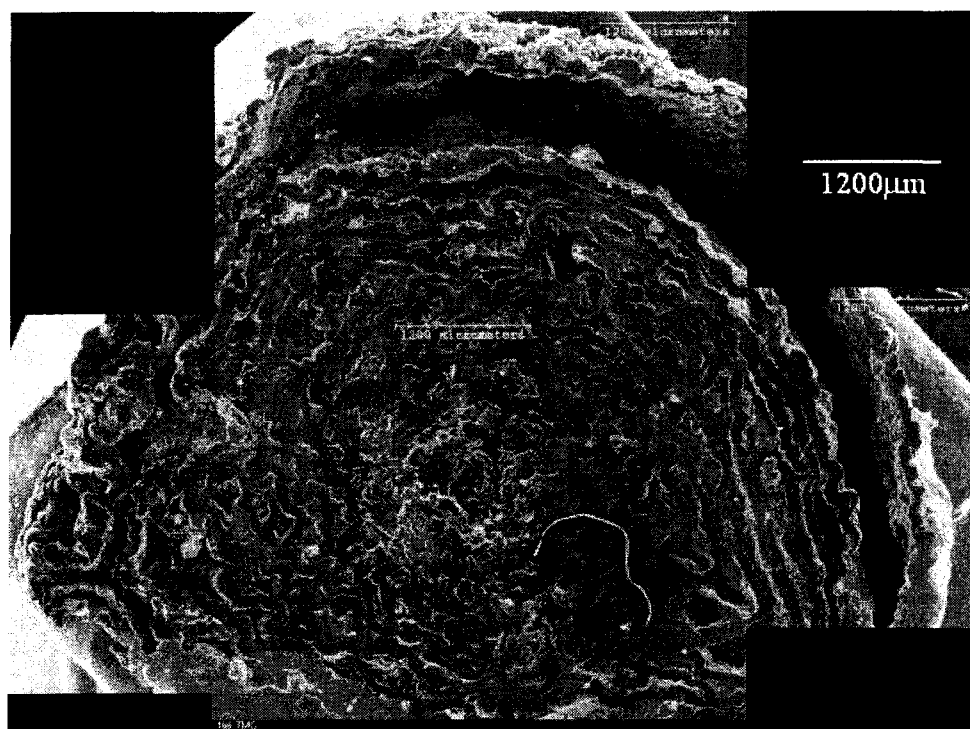


Figure 7.17: Image of a typical cut polymer particle from Run TM166 formed by superimposition of 4 SEM images.

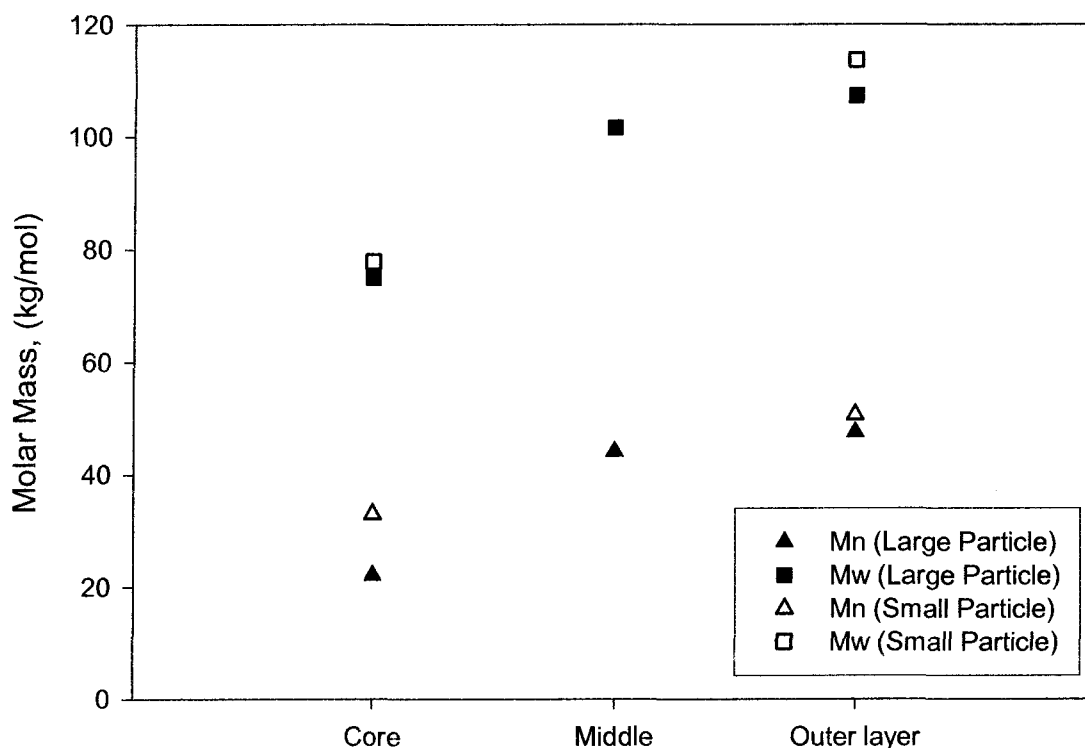


Figure 7.18: Variation of molar masses with radial distance in polymer particles (Large Particle  $\approx$  8 mm, and Small Particle  $\approx$  4 mm in diameter).

The GPC results showed that the molar masses increased with outward radial distance from the center of the polymer particle while the polydispersity decreased. Change in molar masses was more prominent from core to outer regions of large particles than that for small particles. TREF analyses carried with large polymer particles showed variation of short chain branching with radial position. The results are shown in Figure 7.19. The short chain branching, hence the 1-hexene incorporation was greatest in the polymer layer at the outer most surface of the polymer particle; it decreased further radially inwards and then increased at the core of the polymer particle.

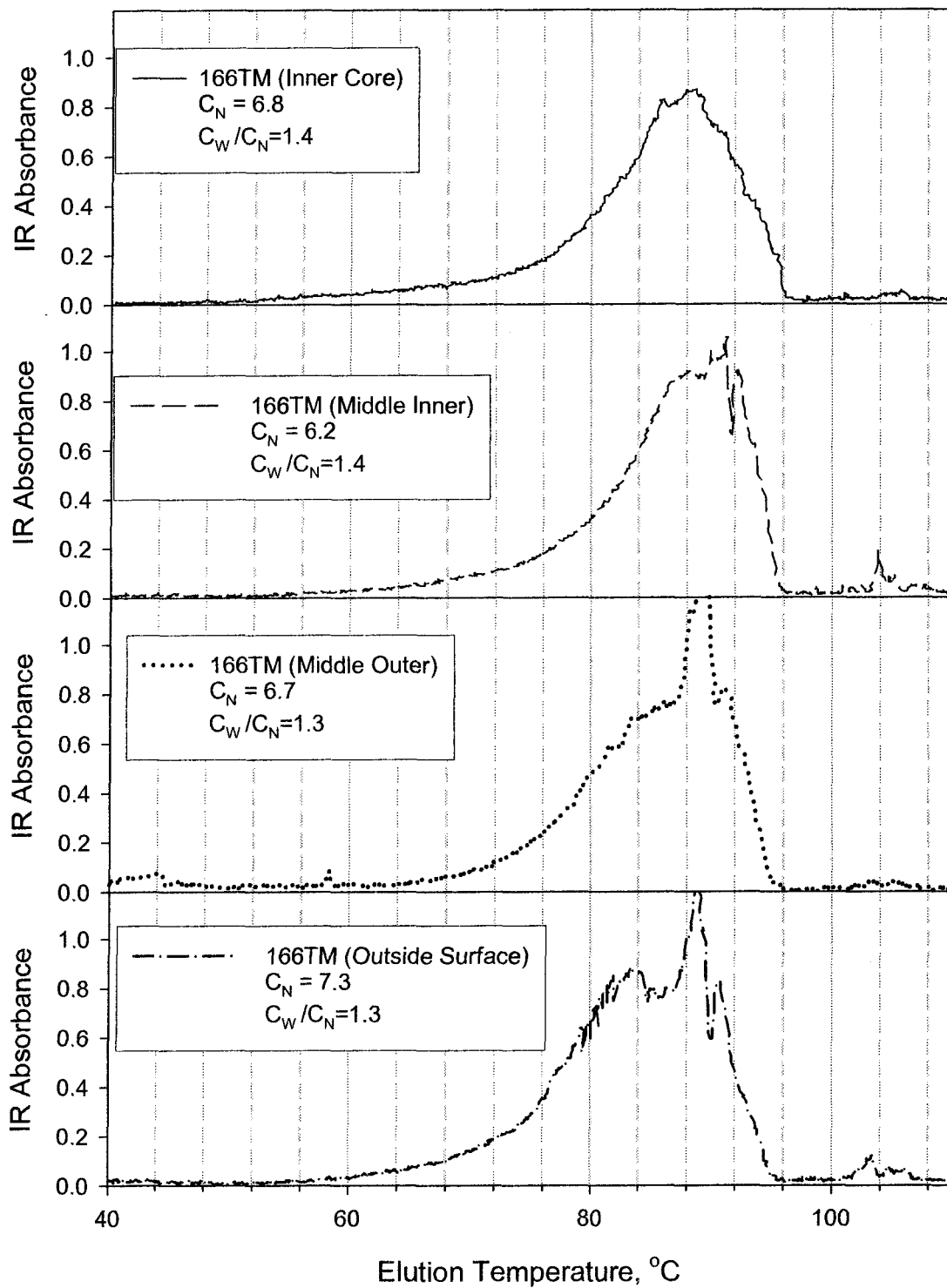


Figure 7.19: Variation of short chain branching with radial distance in a polymer particle.

The variation in molar masses and short chain branching with radial distance might be because of the following reasons. The catalytic sites at the outermost surface were closest to the bulk gas would have the highest concentration of monomer gases and had temperature close to the bulk gas temperature. Moreover, as the concentration of 1-hexene in the bulk gas was constantly decreasing its concentration at the outermost surface of the growing catalyst/polymer particle was highest at any time during polymerization. It was likely that there were temperature gradients in such large particles with highest temperature at the core and ethylene concentration gradients across the particles with reducing concentration of the monomer towards the core. This would explain the radial decrease in molar masses towards the center of the polymer particles. However, convection effects would likely build up concentration of the less active monomer, 1-hexene near the core of the particle as compared to that near the middle of the particles while the more porous outermost regions would have greater concentration of 1-hexene by diffusion from the bulk gas. This was most likely the reason for initial decrease in short chain branching with decrease in radial distance and the subsequent increase in short chain branching at the core of the polymer particle.

## 7.5 Summary of Effects of Comonomer 1-Hexene

The results from numerous experiments described in this chapter showed that the comonomer 1-hexene had profound effects on both the polymerization activity and polymer product properties. Some of the results obtained were as follows:

- 1) Copolymerization activity of ethylene and 1-hexene was in general much higher than that for homopolymerization for all of the supported metallocene catalysts except for Catalyst TM14 supported on 5  $\mu\text{m}$  particles.
- 2) There were optimum initial concentrations of 1-hexene, in the range of 11 – 21  $\text{mol/m}^3$ , that resulted in attainment of highest catalytic activity in shortest time for various catalysts and operating conditions.
- 3) There were large decreases in molar masses,  $M_w$  and  $M_n$ , of polymers in presence of even small concentrations of 1-hexene, the greater the initial concentration of 1-hexene the lower the molar masses. With Catalyst TM11,  $M_w$  decreased from 210  $\text{kg/mol}$  for homopolymer to 103 to 93  $\text{kg/mol}$  for copolymers formed with initial concentrations of 1-hexene between 4 to 21  $\text{mol/m}^3$ .
- 4) The polydispersity,  $P_d$  of copolymer was generally smaller than that of the homopolymer ( $P_d = 3.7$ ) produced by the supported Catalyst TM11. However, the polydispersity of copolymers ranging from 2.7 to 3.9 increased with increase in initial concentration of 1-hexene from 4 to 21  $\text{mol/m}^3$ .
- 5) Continuous injection of 1-hexene during polymerization to control the concentration of 1-hexene usually resulted in less rapid decline in activity after maximum activity was reached. Both  $M_w$  and  $P_d$  increased with the continuous injection of 1-hexene.

- 6) Presence of non-reacting hydrocarbon like heptane instead of a comonomer, like 1-hexene, resulted in up to 87% increase in average homopolymerization yield per hour. The product homopolymer from these runs had higher molar masses (about 10% greater  $M_w$ ) and lower Pd.
- 7) Temperature rising elution fractionation (TREF) analyses showed that the short chain branching (SCB) increased with increase in initial concentration of 1-hexene from  $C_N = 0.6$  for homopolymer to  $C_N = 9.2$  for copolymers formed with initial concentration of 1-hexene = 21 mol/m<sup>3</sup>.
- 8) SCB and molar masses of copolymers varied with polymerization time, initially increasing and then decreasing with decrease in bulk concentration of 1-hexene. Pd decreased monotonously.
- 9) There were variations of molar masses and SCB with radial position in large polymer particles. The molar masses increased with increase in distance away from the core while the SCB initially decreased and then increased to a maximum at the outer particle surface.

## 8. Effect of Catalyst Size on Polymerization Activity

### 8.1 Activity Profiles of Catalysts Supported on 5 $\mu$ m Porous Particles

Polymerization experiments carried out with the prepared supported catalysts had shown that generally the ethylene/1-hexene copolymerization had much higher activity than ethylene homopolymerization. It had been found that the catalyst particles fragmented in layers during high activity copolymerization and resulted in formation of concentric layers of polymer (see Chapters 6 and 7) while during homopolymerization the catalyst particles essentially did not break apart and a dense layer of polymer formed around the catalyst particle resulting in low activity. These results suggested that for very small catalyst particles with high surface areas the differences between activities of homopolymerization and copolymerization would be reduced.

Catalyst batch TM14 was made from in-house prepared support particles of about 5  $\mu$ m size, having surface area of about 840 m<sup>2</sup>/g. The zirconium concentration was 0.12 mass% and the molar ratio of Al:Zr was 452. This catalyst showed very high activities for both ethylene homopolymerization and ethylene/1-hexene copolymerization. Details of a set of polymerization runs using Catalyst TM14 are given in Table 8.1. During Run TM148, 1-hexene was continuously injected to control its concentration. The activity, temperature, pressure and concentration of 1-hexene profiles for the runs are shown in Figure 8.1. As Catalyst TM14 was very active only 30-40 mg of catalyst was used during each run, compared to about 100 mg normally used with other catalysts. Also as the catalyst particles were about 10 to 100 times smaller than that of other catalysts and were

prone to static charging, weighing this catalyst accurately inside the glove-box was not possible. This resulted in difficulties in getting reproducible results under similar conditions for example in Runs 143TM and 146TM; however, the activity profiles were similar apart from the differences in magnitude. There were also some oscillations in the gas phase temperature especially for the very high activity runs, 143TM and 148TM, due to limitation of the temperature controller system, but the temperature oscillations were less than  $\pm 3^{\circ}\text{C}$  of the set point temperature of  $80^{\circ}\text{C}$  even at the highest activities.

Table 8.1: Polymerization conditions and product properties of runs using very high activity Catalyst TM14 supported on  $5\mu\text{m}$  porous particles (Type A runs, see Chapter 3).

Run Number	143TM	146TM	147TM	148TM
Date	06/13/02	06/19/02	06/20/02	06/25/02
Catalyst Amount, (mg)	30	31	41	41
Avg. Temperature, ( $^{\circ}\text{C}$ )	80.1	80.0	80.0	80.1
Max. Temperature, ( $^{\circ}\text{C}$ )	82.9	82.1	81.9	82.4
Total Pressure, (MPa)	1.38	1.40	1.39	1.40
Initial $\text{C}_6\text{H}_{12}$ , ( $\text{mol}/\text{m}^3$ )	0.0	0.0	10.9	10.9
Run Duration, (min)	60	62	60	86
Total PE Yield, (g)	74.7	22.5	27.8	60.6
Mn, (kg/mol)	59.3	59.7	36.6	39.3
Mw, (kg/mol)	140.8	155.8	93.7	97.8
Polydispersity, Pd	2.37	2.61	2.56	2.49

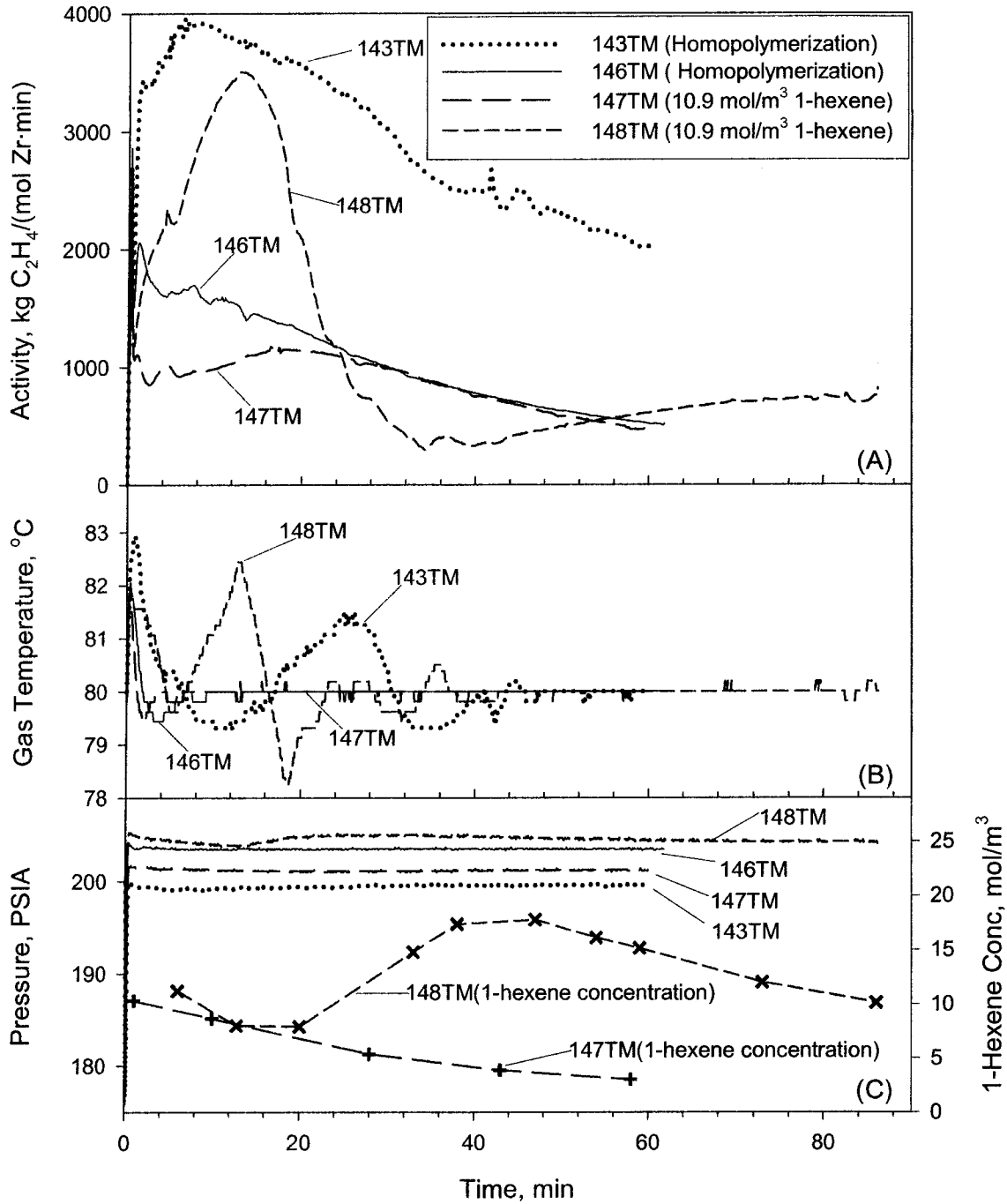


Figure 8.1: Polymerization runs using Catalyst TM14 showing (A) activity profiles, (B) gas phase temperature profiles, and (C) pressure profiles and concentration of 1-hexene.

The polymerization runs using Catalyst TM14 had very high activities for both homo- and co-polymerizations. However, during ethylene/1-hexene copolymerization the maximum activity was reached later than that during ethylene homopolymerization. This result had been observed in polymerization runs using other supported catalysts. The data given in Table 8.1 showed that the molar masses of ethylene/1-hexene copolymers were considerably less than that of the ethylene homopolymers. This was because 1-hexene enhances chain-transfer reactions during polymerization; and similar results had been obtained when using other supported catalysts. However, the polydispersity,  $P_d$  of the homopolymers were similar to that of the co-polymers and close to that cited for solution polymerization with metallocene catalyst, that is about 2.0 (Munoz-Escalona et al. (1999)). This result was different from that observed previously (see Chapter 7) with other prepared supported catalysts that had very low homopolymerization activity; the polydispersity of homopolymers were higher than that of co-polymers and usually greater than 3.0. This suggests that steric hindrance was not significant in distinguishing the active catalytic sites in supported Catalyst TM14. In other words, all the active sites on the surface of and within catalyst particles were easily accessible to monomer gases during both homo- and co-polymerization. This would explain the very high activity per mole of zirconium observed during polymerization with Catalyst TM14.

In Figure 8.2 SEM images of polymer particles from Runs 146TM and 147TM are shown. The external morphologies of the homopolymer and copolymer particles were similar and had similar size distributions and contrasted with that observed with supported catalysts that had low homopolymerization activity and moderate copolymerization activity. The images suggested that the growth of homopolymer

particles and copolymer particles were similar during polymerization with Catalyst TM14.

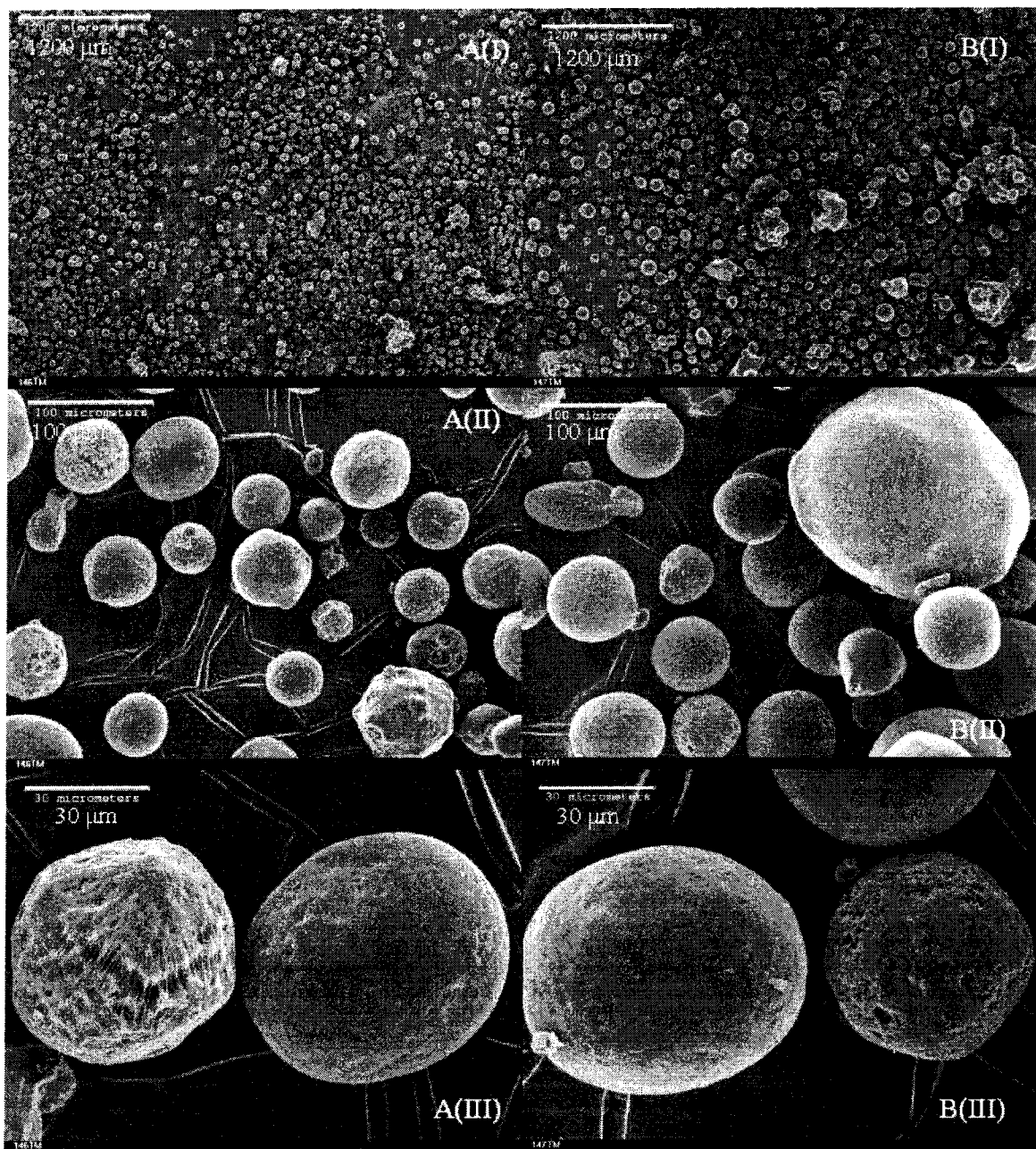


Figure 8.2: SEM images of polymer particles from (A) ethylene homopolymerization run 146TM and (B) ethylene/1-hexene copolymerization run 147TM using Catalyst TM14 taken at low (I) to high (III) magnifications.

## 8.2 Effect of Catalyst Particle Size on Polymerization Activity

To compare effect of support size on activity, Catalyst 19TM was prepared from HayeSep-R porous particles of two size ranges: 75-90  $\mu\text{m}$  and 250-300  $\mu\text{m}$ . After preparation, the catalyst particles were separated by sieving inside the glove-box into Catalysts TM19A containing the smaller particles and TM19B containing the larger particles. This was necessary to ensure that exactly same preparation conditions were present for both TM19A and TM19B as it had been found that the activity of prepared supported catalysts could vary from batch to batch depending on small differences in preparation conditions. An SEM image of Catalyst TM19 showing particles of the different size ranges is given in Figure 8.3. Instrumental Neutron Activation Analysis

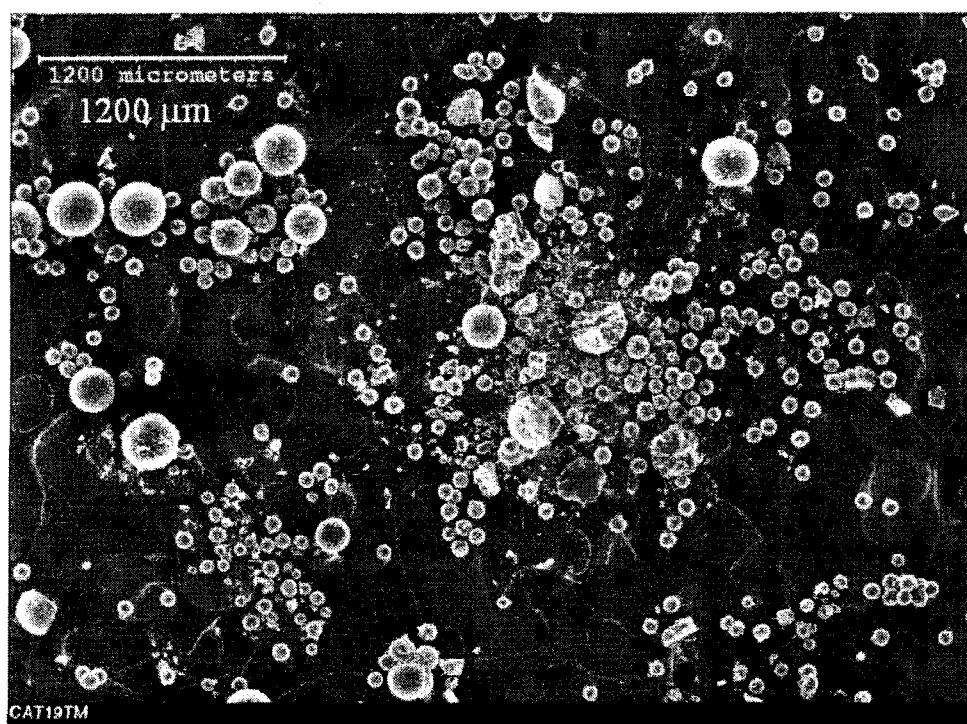


Figure 8.3: SEM image of Catalyst TM19 showing sizes of small (TM19A) and large (TM19B) particles.

measurements showed that both Catalysts TM19A and TM19B had same zirconium concentration (0.27 mass%) but the smaller sized Catalyst TM19A had little larger aluminum concentration (15.1 mass%) than the larger sized Catalyst TM19B (14.1 mass%). This was likely due to greater resistance to diffusion into larger particles of the MAO solution during the drying phase of catalyst preparation (see Chapter 4).

Polymerization runs to compare the effects of support size on activity were done using Catalysts TM19A and TM19B. A set of runs carried out at 80°C using these catalysts is detailed in Table 8.2. The activity, temperature and pressure profiles of these run are shown in Figure 8.4. Run 211TM using Catalyst TM19A with the smaller particles had much higher copolymerization activity than Run 212TM using Catalyst TM19B with the larger particles. Run 213TM with mixed Catalysts TM19A and TM19B had activity in between the other two. The homopolymerization run 221TM, using Catalyst TM19A, had much lower activity than that of ethylene/1-hexene copolymerization using either catalyst TM19A or TM19B.

During polymerization, the gas phase temperature was kept within  $\pm 0.5^\circ\text{C}$  of the desired polymerization temperature of 80°C for all the runs except for the initial spikes in gas phase temperature due to essentially adiabatic compression during reactor filling. Although there were some differences in the total pressure in the reactor for the polymerization runs, they were not likely to significantly affect the overall activity profiles. Table 8.2 shows that the ethylene/1-hexene copolymers produced with either Catalyst TM19A or TM19B had similar molar masses and polydispersities less than 3. However, the homopolymer from Run 221TM had much higher weight averaged molar

mass and polydispersity greater than 6. Similar results had been observed with other catalyst based on HayeSep-R porous polymer support.

To study further the effect of catalyst size on activity a series of experiments were performed using Catalyst TM19A and TM19B at different polymerization temperatures. Details of these polymerization runs are given in Table 8.3. The activity, temperature and pressure profiles of the runs are shown in Figure 8.5. The increase in polymerization temperature from 70°C to 80°C increased the activity significantly for both Catalysts TM19A and TM19B. However, the increase in polymerization temperature to 90°C did

Table 8.2: Polymerization conditions and product properties of runs to determine the effects of catalyst particle size on polymerization (Type B runs, see Chapter 3).

Run Number	211TM	212 TM	213 TM	221 TM
Date	01/08/03	01/09/03	01/10/03	01/28/03
Catalyst Type	TM19A	TM19B	TM-19A+19B	TM19A
Support Size, $\mu\text{m}$	75-90	250-300	75-300	75-90
Catalyst Amount, (mg)	100.5	100.7	51.2 + 50.6	102.1
Avg. Temperature, ( $^{\circ}\text{C}$ )	80.0	80.0	80.0	80.0
Total Pressure, (MPa)	1.38	1.40	1.41	1.40
Initial $\text{C}_6\text{H}_{12}$ , ( $\text{mol}/\text{m}^3$ )	14.3	14.1	14.1	0.0
Total PE Yield, (g)	50.1	23.5	48.9	2.6
Mn, (kg/mol)	32.5	31.0	37.3	30.1
Mw, (kg/mol)	88.1	90.7	89.8	191.8
Polydispersity, Pd	2.71	2.93	2.41	6.37

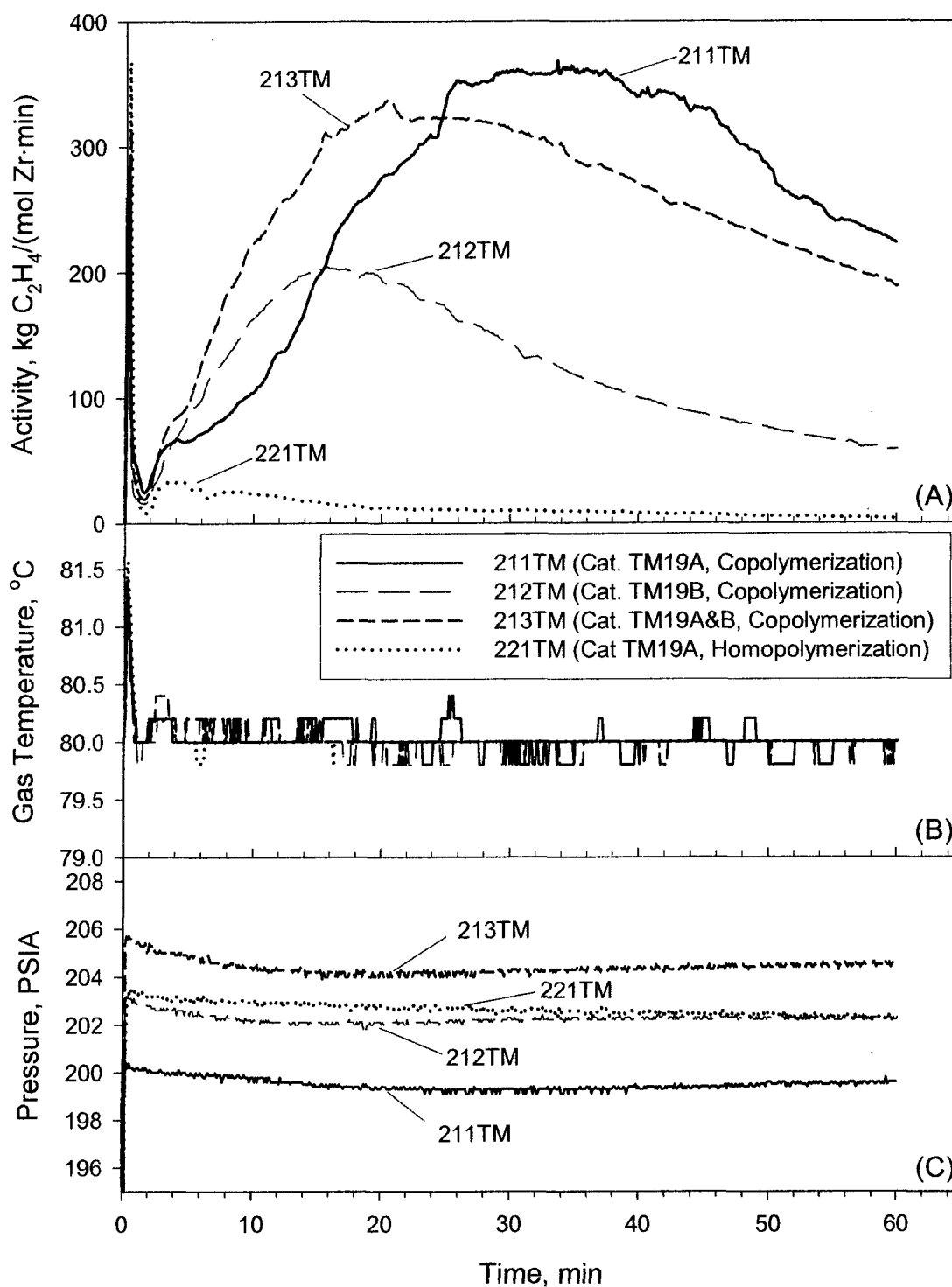


Figure 8.4: Effect of catalyst particle size on polymerization runs showing (A) activity profiles, (B) gas phase temperature profiles, and (C) pressure profiles.

Table 8.3: Polymerization conditions and product properties of runs to determine the effects of catalyst particle size and gas phase temperature on polymerization (Type B runs, see Chapter 3).

Run Number	216TM	218TM	219TM	220TM	225TM
Date	01/17/03	01/22/03	01/23/03	01/24/03	02/03/03
Catalyst Type	TM19B	TM19B	TM19A	TM19B	TM19A
Catalyst Amount, (mg)	100.2	102.3	102.4	100.6	100.4
Avg. Temperature, (°C)	80.0	70.0	70.0	90.0	80.0
Total Pressure, (MPa)	1.40	1.39	1.38	1.38	1.40
Initial C <sub>6</sub> H <sub>12</sub> , (mol/m <sup>3</sup> )	14.0	14.0	14.0	14.2	14.5
Total PE Yield, (g)	23.8	12.9	40.5	25.2	72.7
Mn, (kg/mol)	35.0	28.9	27.1	30.9	34.9
Mw, (kg/mol)	90.2	104.9	82.6	87.3	82.3
Polydispersity, Pd	2.58	3.63	3.05	2.83	2.36

not increase the activity significantly from that at 80°C for Catalyst TM19B. Also at any polymerization temperature the activity of the smaller size catalyst, TM19A was much higher than that of the larger size catalyst, TM19B. In fact, the yield after an hour of polymerization at 70°C using Catalyst TM19A was higher than that produced by Catalyst TM19B at 80 or 90°C. This showed that catalyst particle size had greater influence in determining its activity than polymerization temperature for these types of supported catalysts. Moreover, the polydispersity increased as the polymerization temperature was

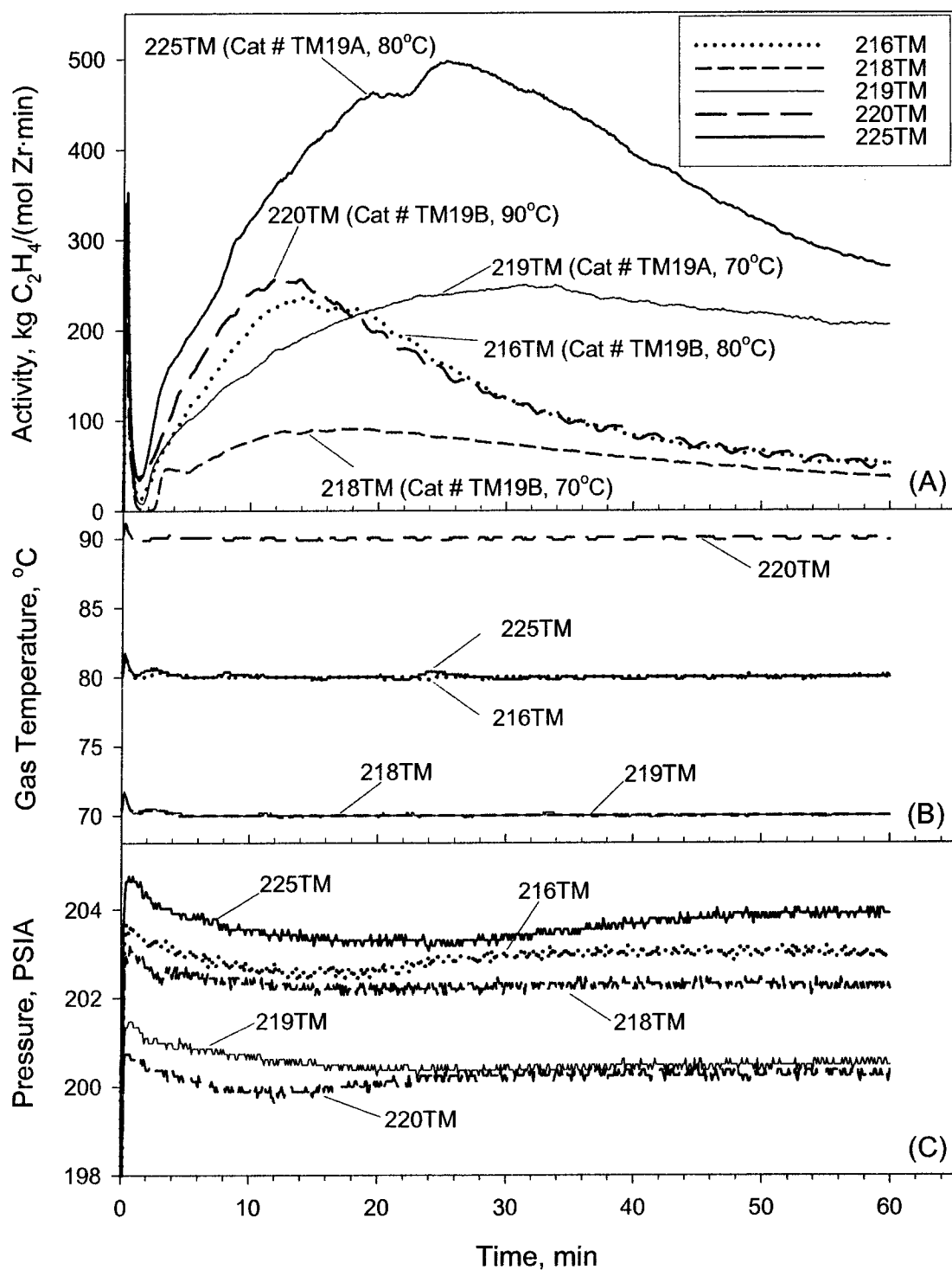


Figure 8.5: Effect of temperature on polymerization runs with different size catalysts showing (A) activity, (B) gas phase temperature, and (C) pressure profiles.

reduced from 80°C to 70°C with the corresponding reduction in activities for both catalysts, and at given temperature the more active Catalyst TM19A produced polymer with smaller polydispersity than that produced by Catalyst TM19B. This suggested that diffusion limitation into catalyst particles during polymerization differentiated active sites thus affecting product polydispersity, and controlled the polymerization activity of these types of supported catalysts. Furthermore, SEM images of polymer particles produced by ethylene/1-hexene copolymerization at 70°C (Run#217TM) and 80°C (Run#214TM), using Catalyst TM19A showed typical ring formation as shown in Figure 8.6. The SEM analyses showed that although most of the particles were formed from catalyst particles of size range 75-90  $\mu\text{m}$  there were some larger particles formed from catalyst particles of size range 250-300  $\mu\text{m}$ . In the polymer particles formed at 80°C, the layers of polymers were further apart and had more spaces between these layers than those formed at 70°C. Also the bigger polymer particles also had more layers than the smaller polymer particles formed indicating that there was greater resistance to diffusion of monomer gases into the core of the catalysts in bigger particles than in smaller particles. As SEM-EDX (Energy dispersive X-ray) spectroscopy had shown that the active metallocene catalyst was distributed throughout the porous support particles (see Chapter 4) the greater resistance to diffusion of monomer gases into the core of the catalysts in bigger particles than in smaller particles would explain the lower activity per mole zirconium observed for the larger Catalyst TM19B as compared to the smaller Catalyst TM19A under similar polymerization conditions.

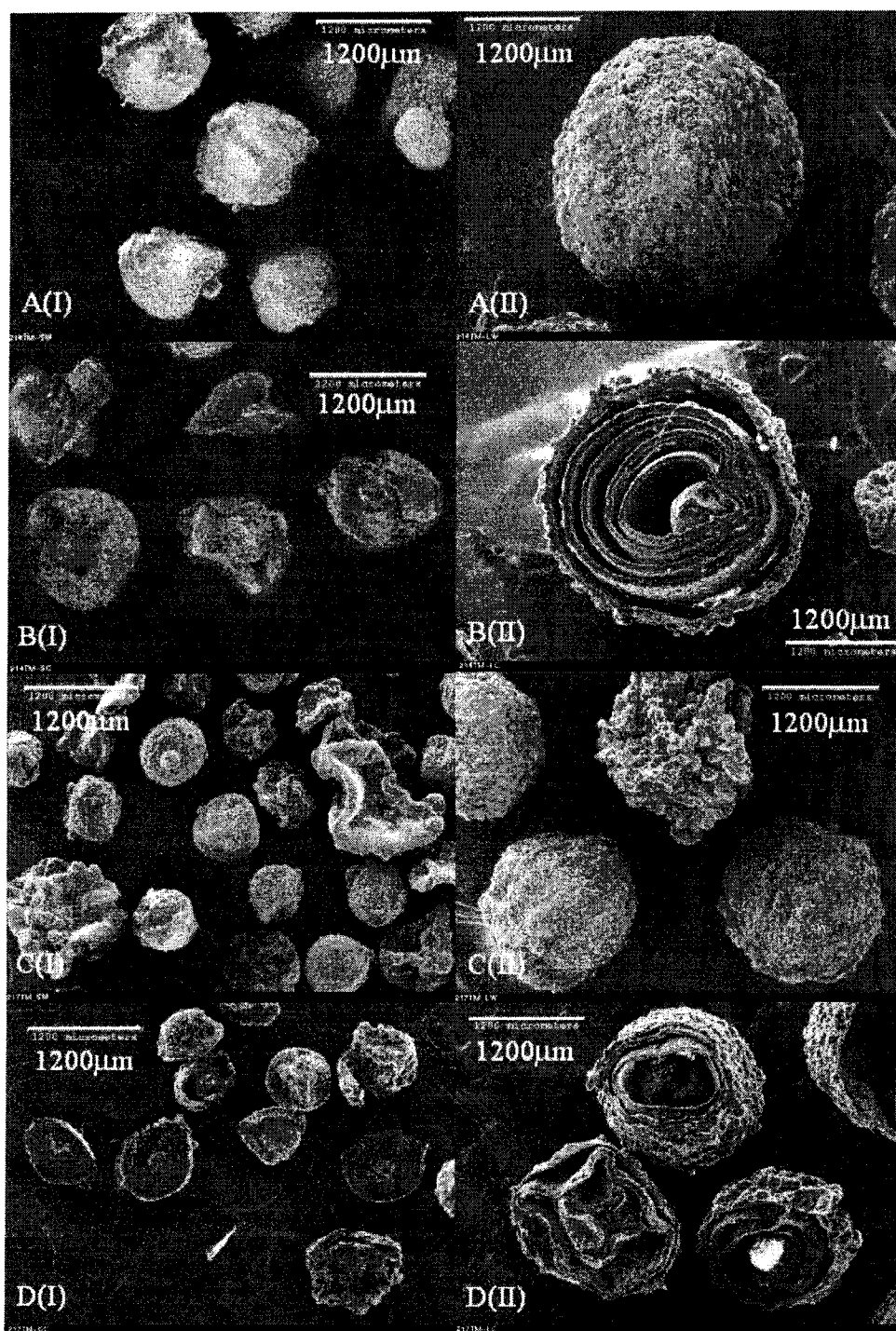


Figure 8.6: SEM images of Catalyst TM19 polymerized (I) small and (II) large particles, produced at 80°C, Run 214TM (A, B) and 70°C, Run 217TM (C, D) showing whole (A, C) and cut (B, D) particles.

### 8.3 Summary of Effects of Catalyst Size on Polymerization Activity

Polymerization experiments had shown that catalyst particle size had significant effect on activities of supported catalysts. The following was observed from runs using catalyst that was supported on very small support particles of the order of 5  $\mu\text{m}$  size:

- 1) The activity per mole of zirconium was very high for both ethylene homopolymerization and ethylene/1-hexene copolymerization, in the order of 189,000 and 78,000 kg-PE/(mol-Zr ·h) respectively.
- 2) Although the homopolymer product ( $M_w \approx 150$  kg/mol) had larger molar masses than the copolymer product ( $M_w \approx 95$  kg/mol), polydispersity (Pd) of both were similar (2.4 –2.6).
- 3) SEM examination showed that both homopolymer and copolymer particles had similar external morphologies and sizes.

Further polymerization experiments using catalysts that were prepared together but had different size ranges of support particles also highlighted the importance of particle size on activities. Some of the results obtained were as follows:

- 1) Although concentration of zirconium was the same in both large and small particles, aluminum concentration was slightly greater in the smaller catalyst particles.
- 2) The smaller catalyst particles (size range 75 – 90  $\mu\text{m}$ ) had higher activity per mole of zirconium than the larger particles (size range 250 – 300  $\mu\text{m}$ ) under similar polymerization conditions.
- 3) Reduction of polymerization temperature from 80°C to 70°C reduced the activities of both large and small catalysts.

- 4) Polydispersity of the polymer produced by the larger catalyst was greater than the corresponding polydispersity of the polymer produced by the smaller catalyst.
- 5) Larger copolymer particles in general had more layers of polymer than the smaller ones.

## 9. Conclusions and Recommendations for Future Work

### 9.1 Summary and Conclusions

The objectives of this research project were to build a novel laboratory-scale gas-phase polymerization reactor system with improved temperature control, prepare active supported metallocene catalysts, and to study the effects of various parameters on gas-phase polymerization activities and product polymer properties.

A laboratory-scale gas-phase polymerization reactor system was successfully designed, fabricated and commissioned. The system consisted of a 2L stainless steel reactor, gas purification trains, comonomer and catalyst injection devices, PID temperature control and data acquisition systems, and an on-line gas chromatograph for gas analysis. To ensure good mixing of gases within the reactor both anchor type impellers and axial flow turbines were used. The reactor was cooled by the flow of a coolant through cylindrical channels drilled in the reactor walls. The desired coolant temperature was attained rapidly by mixing proportioned amounts of hot and cold oil streams from a single partitioned heating bath. Static mixers were inserted inside the channels to further improve heat transfer. Control of the bulk gas temperature in the reactor to  $\pm 0.2^\circ\text{C}$  during polymerization at rates up to  $0.04 \text{ mol C}_2\text{H}_4 / \text{min}$  ( $900 \text{ cm}^3$  (STP)/min) has been achieved with this novel design. Such temperature control was not possible with jacketed reactors or with reactors immersed in a cooling baths.

A unique headspace-gas sampling valve with zero volume in the high-pressure reactor side was designed and connected to the gas chromatograph. This minimized lag time of gas sample in reaching the gas chromatogram and condensation of comonomer in

the sample line, thus ensuring that gas analyzed was representative of the actual gas composition in the reactor. Using this gas analysis system the concentration of the comonomer was successfully monitored and controlled during polymerization.

A micro-reactor with Pyrex windows made from a Swagelok Union Tee was used to observe catalyst/polymer growth during polymerization. A microscope video camera was used to record the particle growth. Data acquired by using this reactor, together with SEM analysis of whole and cut polymer particles provided details of catalyst/polymer particle growth during polymerization.

Both in-house and commercial organic polymeric porous particles were used to support bis(*n*-butylcyclopentadienyl)zirconium dichloride and methyl aluminoxane to make twenty two batches of supported metallocene catalysts. In these batches of catalysts mass per cent of aluminum and zirconium varied from 12.9 to 21.2% and 0.12 to 0.35%, respectively and Al:Zr ratio varied from 168 to 482. These catalysts were active for both ethylene homopolymerization and ethylene/1-hexene copolymerization but in general the copolymerization activity was much higher than that for homopolymerization.

Exploratory gas phase polymerization runs revealed effects of various parameters on the activities. Alkyl aluminum scavengers were found to broaden the activity profile and delay attainment of maximum activity and reduced molar masses of the polymer product. These could thus be used to moderate the activity and control the gas phase temperature. The activity increased with increases in temperature until maximum activity was reached at a temperature range of 80 – 90°C. The activity decreased at higher temperatures probably caused by catalyst deactivation due to MAO breakdown and easier dissociation of the olefin-metallocene  $\pi$ -complex formed during polymerization and due

to physical causes like reduction of porosity due to polymer fusion. The polymer molar masses decreased with increases in polymerization temperature.

Increases in ethylene pressure from 0.7 to 2.1 MPa with initial concentration of 1-hexene about  $11 \text{ mol/m}^3$  resulted in decrease in time of attainment of maximum activity. The increase in activity with ethylene pressure was linear in the pressure range of 1.39 to 1.74 MPa but the rate of increase was less at higher pressure probably caused by catalyst deactivation due to local overheating of catalyst particles resulting from very high rate of polymerization. At lower pressures the activity profiles were different resulting from very slow breakup of catalyst particles. In general the molar masses increased slightly with increases in ethylene pressure. Although presence of various amounts of an inert gas like nitrogen during polymerization did not have significant effect on the overall observed activity profiles there was initial increase in induction time with increases in nitrogen pressure. This suggested that once the catalyst particles fragmented bulk diffusion of monomer was not rate limiting.

Poisoning effects were pronounced when small amounts of catalysts were charged into the reactor while significant increases in gas-phase temperature occurred when large amounts of catalysts were charged into the reactor. The optimum amount of catalyst to be used during polymerization depended on its activity.

Observation of individual catalyst particles using the micro-reactor showed that although there were significant variations of induction periods and activities among particles from the same batch of catalyst, shapes of the particles were replicated during polymerization. The induction period was less for smaller catalyst particles and catalyst

fragments. These results helped to explain various types of overall activity profiles observed when using the gas phase reactor with the same or different catalysts.

SEM analyses of whole and cut homo- and co-polymer particles showed significant differences. During the very low activity ethylene homopolymerization, catalyst particles did not breakup and polymer grew radially outwards from catalyst particle surface; but during the higher activity ethylene/1-hexene copolymerization, catalyst particles fragmented in layers and successive annular layers of polymer formed and grew outwards. The molar masses of the copolymer products tended to increase with increases in polymerization time while the polydispersities decreased; however, the reverse trends were observed for the homopolymers. This indicated that during copolymerization catalyst particle fragmentation increased accessibility of monomer to all active sites while during homopolymerization the growing polymer layers around the catalyst cores reduced accessibility of the monomer.

In general the supported catalysts had much higher ethylene/1-hexene copolymerization activity than ethylene homopolymerization activity except for Catalyst TM14. There was an optimum initial concentration of 1-hexene that resulted in attainment of highest catalytic activity in shortest time under a given set of polymerization conditions.

Presence of small amounts of comonomer 1-hexene during polymerization caused significant reduction of molar masses ( $M_w$  and  $M_n$ ) of the polymer. Although molar masses decreased monotonously the polydispersity ( $P_d$ ) increased with increases in initial concentration of 1-hexene. However, continuous injection of 1-hexene to maintain constant 1-hexene concentration resulted in less rapid decline in activity after the

maximum activity was reached, and both  $M_w$  and  $P_d$  of the product polymer were higher compared to the case where 1-hexene was only added at the beginning. Moreover, presence of small amounts of *n*-heptane increased homopolymerization activity and molar masses of product but decreased polydispersity. Thus, the molar masses of the polymer not only depended on the ratio of concentration of monomer to comonomer but also on the catalyst activity.

TREF analyses showed that short chain branching (SCB), signifying incorporation of the comonomer, increased with increases in initial concentration of 1-hexene. However, SCB and molar masses of copolymers varied with polymerization time, initially increasing and then decreasing with decreases in bulk concentration of 1-hexene. The polydispersity decreased monotonically. Moreover, for large polymer particles there were radial variations of SCB and molar mass. The molar masses increased with increase in distance away from the core while the SCB initially decreased and then increased to a maximum at the outer particle surface. These were likely due to monomer concentration gradients and buildup of the less active comonomer by convection effects inside the polymer particles.

The activities of the supported catalysts also depended on the support sizes. The smaller catalysts had higher activity than the larger ones while the polydispersity of the product polymer was less than that produced by the larger catalyst. The much smaller Catalyst TM14 supported on very small (5  $\mu\text{m}$ ) PS porous particles had very high homo- and co-polymerization activities and the polydispersity was similar for both homo- and co-polymers. From these results, it can be deduced that by manipulating support sizes to

limit monomer diffusion to active sites inside catalyst particles polymerization activities and polymer properties can be controlled.

## 9.2 Recommendations for Future Work

Although the novel gas-phase polymerization reactor system showed excellent temperature control during polymerization the coolant system limited the maximum allowable polymerization rate. By improving the rate of thermal energy removal from the cold oil reservoir, the maximum polymerization rate could be easily increased. This would allow larger amounts of catalysts to be used during polymerization runs and could lead to better reproducibility of runs.

The online gas chromatography used to analyze the headspace gas is inherently slow compared to say an FTIR analyzer. An online FTIR analyzer connected via a feedback controller to 1-hexene injection pump could be used to automatically control the concentration of 1-hexene during polymerization. This would offer much better and more efficient control over concentration of 1-hexene than that produced manually.

The micro-reactor used to view polymerizing catalyst particles could be used for further experiments at various polymerization conditions. Moreover, image analysis software could be used to estimate particle sizes and hence the approximate polymerizations activities of individual particles during polymerization. This would lead to better understanding of how activities of individual particle relate to overall observed activities.

The method used to prepare the dry free-flowing supported catalysts likely resulted in smaller particles having greater concentration of MAO than larger particles

produced in the same batch. Modification to this method such as removing excess toluene from the suspension containing the supported catalyst particles during catalyst preparation by sieving and gently washing the supported catalysts with heptane and then drying under vacuum might be tried to find how the MAO distribution and the polymerization activity depended on catalyst particle size.

The 5 $\mu$ m PS support was prepared in-house while most of the other supports were commercial porous polymers used as column packing for chromatography. It would be better to prepare in-house PS supports of different sizes of similar porosity and surface area and use them for making catalysts for the purpose of comparing the effects of catalyst sizes on polymerization.

On the empirical side, more experiments should be carried out to determine how the presence of various amounts of nitrogen affected polymerization of very high activity catalysts under different polymerization conditions. Further, TREF and GPC analyses of polymer at different radial positions of polymer particles made by polymerization under constant concentration of 1-hexene should be made to determine whether convection effects indeed build up the concentration of 1-hexene inside the polymer particle.

The substantial amount of data on the effects of various parameters on polymerization activity profiles and polymer properties generated during the course of this work could be used to verify existing polymerization kinetic models given in the literature. Moreover, new improved models that give better insights into the polymerization kinetics could be developed that accounts for the observed catalyst fragmentation and polymer growth mechanisms.

## References

- Alt, H. G., The heterogenization of homogeneous metallocene catalysts for olefin polymerization, *Journal of Chemical Society, Dalton Transactions*, **11**, 1703-1709 (1999).
- Alt, H. G., From the Lab Bench to the Plant: How to Commercialize a Metallocene Catalyst?, *Macromolecular Symposia*, **173**, 65-75 (2001).
- Arrowsmith, D., W. Kaminsky, A. Laban, and U. Weingarten, Comparison of the Polymerization of Propene by Homogeneous and Heterogeneous Metallocene/MAO-Catalysts under Different Polymerization Conditions, *Macromolecular Chemistry and Physics*, **202**, 2161-2167 (2001).
- Barrett, A. G. M. and Y. R. de Miguel, A well-defined metallocene catalyst supported on polystyrene beads, *Chemical Communications*, 2079-2080 (1998).
- Barron, A. R., Alkylaluminumoxanes: Synthesis, structure and reactivity. In *Metallocene-based polyolefins. Preparations, properties and technology*, Vol 1. John Scheirs and W. Kaminsky Eds., John Wiley & Sons, Ltd. Chichester, pp 33-67 (2000).
- Britovsek, G. J. P., V. C. Gibson, and D. F. Wass, The search for new-generation polymerization catalysts: Life beyond metallocenes, *Angewandte Chemie International Edition*, **38**, 428-447 (1999).
- Chakravarti, S. and W. H. Ray, Kinetic study of olefin polymerization with a supported metallocene catalyst. II. Ethylene/1-hexene copolymerization in gas phase, *Journal of Applied Polymer Science*, **80**, 1096-1119 (2001).
- Chen, E. Y. X. and T. J. Marks, Cocatalysts for Metal-Catalyzed Olefin Polymerization: Activators, Activation Processes, and Structure-Activity Relationships, *Chemical Reviews*, **100**, 1391-1434 (2000).

Chien, J. C. W., Supported metallocene polymerization catalysis, *Topics in Catalysis*, **77**, 23-36 (1999).

Chien, J. C. W. and T. Nozaki, Ethylene-Hexene Copolymerization by Heterogeneous and Homogeneous Ziegler-Natta Catalysts and the “Comonomer” Effect, *Journal of Polymer Science: Part A: Polymer Chemistry*, **31**, 227-237 (1993).

Chien, J. C. W. and A. Razavi, Metallocene-Methylaluminoxane Catalyst for Olefin Polymerization. II. Bis- $\eta^5$ -(Neomenthyl Cyclopentadienyl)zirconium Dichloride, *Journal of Polymer Science: Part A: Polymer Chemistry*, **26**, 2369-2380 (1988).

Chien, J. C. W. and B. P. Wang, Metallocene-Methylaluminoxane Catalysts for Olefin Polymerization. I. Trimethylaluminum as Coactivator, *Journal of Polymer Science: Part A: Polymer Chemistry*, **26**, 3089-3102 (1988).

Chung, J. S. and J. C. Hsu, A kinetic analysis on the gas phase polymerization of ethylene over polymer supported  $(\text{CH}_3)_2\text{Si}[\text{Ind}]_2\text{ZrCl}_2$  catalyst, *Polymer*, **43**, 1307-1311 (2002).

Dos Santos, J. H. Z., M. B. Da Rosa, C. Krug, F. C. Stedile, M. C. Haag, J. Dupont and M. De C. Forte, Effects of Ethylene Polymerization Conditions on the Activity of  $\text{SiO}_2$ -Supported Zirconocene and on Polymer Properties, *Journal of Polymer Science: Part A: Polymer Chemistry*, **37**, 1987-1996 (1999).

Dos Santos, J. H. Z., T. Uozumi, T. Teranishi, T. Sano and K. Soga, Ethylene (co)polymerization with supported-metallocenes prepared by the sol-gel method, *Polymer*, **42**, 4517-4525 (2001).

Enderle, H. F., Polyethylene High Density, “Encyclopedia of Materials: Science and Technology”, Elsevier, 7172-7180 (2001)

Eskelinen, M., and J. V. Seppälä, Effect of polymerization temperature on the polymerization of ethylene with dicyclopentadienylzirconiumdichloride/methylaluminoxane catalyst, *European Polymer Journal*, **32**, 331-335 (1996).

Fink, G., B. Steinmetz, J. Zechlin, C. Przybyla, and B. Tesche, Propene Polymerization with Silica-Supported Metallocene/MAO Catalysts, *Chemical Reviews*, **100**, 1377-1390, 2000.

Floyd, S., K. Y. Choi, T. W. Taylor, and W. H. Ray, Polymerization of Olefins Through Heterogeneous Catalysis IV. Modeling of Heat and Mass Transfer Resistance in the Polymer Particle Boundary Layer, *Journal of Applied Polymer Science*, **31**, 2231-2265 (1986).

Floyd, S., K. Y. Choi, T. W. Taylor, and W. H. Ray, Polymerization of Olefins through Heterogeneous Catalysis. III. Polymer Particle Modeling with an Analysis of Intraparticle Heat and Mass Transfer Effects, *Journal of Applied Polymer Science*, **32**, 2935-2960 (1986).

Galland, G. B., M. Seferin, R. S. Mueler and J. H. Z. dos Santos, Linear low-density polyethylene synthesis promoted by homogeneous and supported catalysts, *Polymer International*, **48**, 660-664 (1999).

Gregg, S. J., and K. S. W. Sing, "Adsorption, Surface Area and Porosity", Academic Press, Toronto, 2<sup>nd</sup> Edition, pp 138-1142 (1982).

Hamielec, A. E. and J. B. P. Soares, Polymerization Reaction Engineering – Metallocene Catalysts, *Progress in Polymer Science*, **21**, 651-706 (1996).

Hammawa, H., Influence of supports on gas-phase olefin polymerization over polymer-supported  $(n\text{-BuCp})_2\text{ZrCl}_2/\text{MAO}$  catalysts, *Ph.D. Thesis, University of Alberta, Edmonton, Canada*, p 12 (2004).

Hammawa, H., T. M. Mannan, D. T. Lynch, and S. E. Wanke, Effects of Aluminum Alkyls on Ethylene/1-Hexene Polymerization with Supported Metallocene/MAO Catalysts in the Gas Phase, *Journal of Applied Polymer Science*, **92**, 3549-3560 (2004).

Han, T. K., Y. S. Ko, J. W. Park and S. I. Woo, Determination of the number of active sites for olefin polymerization catalyzed over metallocene/MAO using the CO inhibition method, *Macromolecules*, **29**, 7305-7309 (1996).

Han-Adebekun, C. G., J. A. Debling, and W. H. Ray, Polymerization of olefins through heterogeneous catalysis. XVI. Design and control of a laboratory stirred bed copolymerization reactor, *Journal of Applied Polymer Science*, **64**, 373-382, (1997a).

Han-Adebekun, G. C., M. Hamba, and W. H. Ray, Kinetic Study of Gas Phase Olefin Polymerization with a  $\text{TiCl}_4/\text{MgCl}_2$  Catalyst I. Effect of Polymerization Conditions, *Journal of Polymer Science: Part A: Polymer Chemistry*, **35**, 2063-2074 (1997).

Hlatky, G. G., Metallocene Catalysts for Olefin Polymerization – Annual Review for 1996, *Coordination Chemistry Reviews*, **181**, 234-296 (1999).

Hlatky, G. G., Heterogeneous Single-Site Catalysts for Olefin Polymerization, *Chemical Reviews*, **100**, 1347-1376 (2000).

Hong, S. C., H. T. Ban, N. Kishi, J. Jin, T. Uozumi and K. Soga, Ethylene polymerization with a poly(styrene-co-divinylbenzene) beads supported *rac*- $\text{Ph}_2\text{Si}(\text{Ind})_2\text{ZrCl}_2$  catalyst, *Macromolecular Chemistry and Physics*, **199**, 1393-1397 (1998a).

Hong, S. C., T. Teranishi, and K. Soga, Investigation on the polymer particle growth in ethylene polymerization with PS beads supported *rac*- $\text{Ph}_2\text{Si}(\text{Ind})_2\text{ZrCl}_2$  catalyst, *Polymer*, **39**, 7153-7157 (1998).

Huang, J. and G. L. Rempel, Ziegler-Natta Catalysts for Olefin Polymerization: Mechanistic Insights from Metallocene Systems, *Progress in Polymer Science*, **20**, 459-526 (1995).

Jejelowo, M. O., D. T. Lynch, and S. E. Wanke, Comparison of ethylene polymerization in gas-phase and slurry reactors, *Macromolecules*, **24**, 1755-1761 (1991).

Kaminsky, W., New Polymers by Metallocene Catalysis, *Macromolecular Chemistry and Physics*, **197**, 3907-3945 (1996).

Kaminsky, W., Highly active metallocene catalysts for olefin polymerization, *Journal of Chemical Society, Dalton Transactions*, **9**, 1413-1418 (1998).

Kaminsky, W., Olefin Polymerization Catalyzed by Metallocenes, *Advances in Catalysis*, **46**, 89-159 (2001).

Kaminsky, W., The Discovery of Metallocene Catalysts and Their Present State of the Art, *Journal of Polymer Science: Part A: Polymer Chemistry*, **42**, 3911-3921 (2004).

Kaminsky, W., D. Arrowsmith, and C. Strubel, Polymerization of Styrene with Supported Half-Sandwich Complexes, *Journal of Polymer Science: Part A: Polymer Chemistry*, **37**, 2959-2968 (1999).

Kaminsky, W. and R. Steiger, Polymerization of Olefins with Homogeneous Zirconocene/Alumoxane Catalysts, *Polyhedron*, **7**, 2375-2381 (1988).

Kaminsky, W. and H. Winkelbach, Influence of supported metallocene catalysts on polymer tacticity, *Topics in Catalysis*, **7**, 61-67 (1999).

Kissin, Y. V., Olefin Polymers, Introduction, "Kirk-Othmer Encyclopedia of Chemical Technology", 4<sup>th</sup> Ed., Vol. 17, pp. 702-707 (2000).

Kittilsen, P., H. Svendsen, and T. F. McKenna, Modeling of transfer phenomena on heterogeneous Ziegler catalysts. IV. Convection effects in gas phase processes, *Chemical Engineering Science*, **56**, 3997-4005 (2001).

Knoke, S., D. Ferrari, B. Tesche, and G. Fink, Microkinetic Videomicroscopic Analysis of Olefin Polymerization with a Supported Metallocene Catalyst, *Angewandte Chemie International Edition*, **42**, 5090-5093 (2003).

Koch, M., A. Falcou, N. Nenov, M. Klapper, and K. Müllen, Reversibly crosslinked networks of nanoparticles in metallocene-catalyzed olefin polymerization, *Macromolecular Rapid Communications*, **22**, 1455-1462 (2001).

Koch, M., M. Stork, M. Klapper, and K. Müllen, Immobilization of metallocenes through noncovalent bonding via MAO to a reversibly cross-linked polystyrene, *Macromolecules*, **33**, 7713-7717 (2000).

Koivumäki, J. and J. V. Seppälä, Observations on the rate enhancement effect with  $MgCl_2/TiCl_4$  and  $Cp_2ZrCl_2$  catalyst system upon 1-hexene addition, *Macromolecules*, **26**, 5535-5538 (1993).

Korber, F., K. Hauschild, and G. Fink, Reaction calorimetric approach to the kinetic investigation of the propylene bulk phase polymerization, *Macromolecular Chemistry and Physics*, **202**, 3329-3333 (2001).

Kumkaew, P., S. E. Wanke, P. Prasertdam, C. Danumah, and S. Kaliaguine, Gas-phase ethylene polymerization using zirconocene supported on mesoporous molecular sieves, *Journal of Applied Polymer Science*, **87**, 1161-1177 (2003).

Lacombe, Y., TREF and SEC Characterization of Ethylene/1-Butene Copolymers Produced at Various 1-Butene and Hydrogen Pressures, *M.Sc. Thesis, University of Alberta, Edmonton, Canada*, pp 55-69 (1995).

Laguna, M. F., M. L. Cerrada, R. Benavente, and E. Pérez, Effect of the comonomer content on the permeation behavior in polyolefin films synthesized with metallocene catalysts, *Journal of Membrane Science*, **212**, 167-176 (2003).

Li, N. -H. and M. A. Majid, U.S. Pat. 5,168,104 (1992).

Liu, S., F. Meng, G. Yu, and B. Huang, Preparation of polymer-supported zirconocene catalysts and olefin polymerization, *Journal of Applied Polymer Science*, **71**, 2253-2258 (1999).

Liu, W., Gas-Phase Ethylene/1-Hexene Copolymerization over  $MgCl_2$ -supported Ziegler-Natta Catalysts, *Ph.D. Thesis, University of Alberta, Edmonton, Canada*, pp 59-61 (2002).

Lynch, D. T. and S. E. Wanke, Reactor Design and Operation for Gas-Phase Ethylene Polymerization Using Ziegler-Natta Catalysts, *The Canadian Journal of Chemical Engineering*, **69**, 332-339 (1991).

Mannan, T. M., H. Hammawa, D. T. Lynch, and S. E. Wanke, A Laboratory Reactor for Gas-Phase Olefin Polymerization, *The Canadian Journal of Chemical Engineering*, **82**, 371-381 (2004).

McKenna, T. F., R. Spitz, and D. Cokljat, Heat Transfer from Catalysts with Computational Fluid Dynamics, *AIChE Journal*, **45**, 2392-22410 (1999).

Meier, G. B., G. Weickert, W. P. M. Van Swaaij, Gas-Phase Polymerization of Propylene: Reaction Kinetics and Molecular Weight Distribution, *Journal of Polymer Science: Part A: Polymer Chemistry*, **39**, 500-513 (2001).

Meng, E., G. Yu, and B. Huang, Polymer-Supported Zirconocene Catalyst for Ethylene Polymerization, *Journal of Polymer Science: Part A: Polymer Chemistry*, **37**, 37-46 (1999).

Mortara, S., D. Fregonese, and S. Bresadola, Metallocene derivatives as active supports of olefin polymerization catalysts, *Macromolecular Chemistry and Physics*, **202**, 2630-2633 (2001).

Munoz-Escalona, A., L. Mendez, B. Pena, P. Lafuente, J. Sancho, W. Michiels, G. Hidalgo and M. Fca. Martinez-Nunez, Single-Site Supported Catalysts for Ethylene, In *METALLOCENE TECHNOLOGY in Commercial Applications*, Dr. George M. Benedikt (Ed.), *Plastics Design Library*, (1999).

Musikabhumma, K., T. Uozumi, T. Sano, and K. Soga, Poly(4-vinylpyridine)-supported cationic bis(cyclopentadienyl)zirconocene catalyst: Development of a new simple method

to prepare polymer-supported cationic zirconocene and its application to ethylene polymerization, *Macromolecular Rapid Communications*, **21**, 675-679 (2000).

Nishida, H., T. Uozumi, T. Arai, and K. Soga, Polystyrene-supported metallocene catalysts for olefin polymerizations, *Macromolecular Rapid Communications*, **16**, 821-830 (1995).

Oleshko, V. P., P.A. Crozier, R. D. Cantrell and A. D. Westwood, In-Situ and Ex-Situ Microscopic Study of Gas Phase Propylene Polymerization over a High Activity  $\text{TiCl}_4\text{-MgCl}_2$  Heterogeneous Ziegler-Natta Catalyst, *Macromolecular Rapid Communications*, **22**, 34-40 (2001).

Oleshko, V. P., P.A. Crozier, R. D. Cantrell and A.D. Westwood, In situ real-time environmental TEM of gas phase Ziegler-Natta catalytic polymerization of propylene, *Journal of Electron Microscopy*, **51 (Supplement)**, S27-S39 (2002).

Pahl, M. H. and E. Muschelknautz, Static Mixers and Their Applications, *International Chemical Engineering*, **22**, 197-205 (1982).

Panchenko, V. N., V. A. Zakharov, I. G. Danilova, E. A. Paukshtis, I. I. Zakharov, V. G. Goncharov and A. P. Suknev, Structure and performance of the solid methylaluminoxane at temperatures 20-250°C: Experimental and DFT calculation study, *Journal of Molecular Catalysis. A: Chemical*, **174**, 107-117 (2001).

Pasquet, V. and R. Spitz, Irreversible activation effects in ethylene polymerization, *Die Makromolekulare Chemie*, **194**, 451-461 (1993).

Pater, J. T. M., G. Weickert, and W. P. M. van Swaaij, Optical and Infrared Imaging of Growing Polyolefin Particles, *AIChE Journal*, **49**, 450-464 (2003).

Pietikäinen, P. and J. A. Seppälä, Low molecular weight ethylene/propylene copolymers. Effect of process parameters on copolymerization with homogeneous  $\text{Cp}_2\text{ZrCl}_2$  catalyst, *Macromolecules*, **27**, 1325-1328 (1994).

- Przybyla, C., B. Tesche and G. Fink, Ethylene/hexene copolymerization with the heterogeneous catalyst system  $\text{SiO}_2/\text{MAO}/\text{rac-Me}_2\text{Si}[2\text{-Me-4-Ph-Ind}]_2\text{ZrCl}_2$ : The filter effect, *Macromolecular Rapid Communications*, **20**, 328-332 (1999).
- Qin, Y., T. Tang, Z. Zhao and B. Huang, Ethylene Polymerization with Porous Polystyrene Spheres Supported  $\text{Cp}_2\text{ZrCl}_2$  Catalyst, *Journal of Polymer Science: Part A: Polymer Chemistry*, **41**, 3313-3319 (2003).
- Quijada, R., R. Rojas, R. S. Mauler, G. B. Galland, and R. B. Scipioni, Study of the Effect of the Monomer Pressure on the Copolymerization of Ethylene with 1-Hexene, *Journal of Applied Polymer Science*, **64**, 2567-2574 (1997).
- Reddy, S. S. and S. Sivaram, Homogeneous Metallocene-Methylaluminoxane Catalyst Systems for Ethylene Polymerization, *Progress in Polymer Science*, **20**, 309-367 (1995).
- Ribeiro, M. R., A. Deffieux, and M. F. Portela, Supported Metallocene Complexes for Ethylene and Propylene Polymerizations: Preparation and Activity, *Industrial & Engineering Chemistry Research*, **36**, 1224-1237 (1997).
- Roscoe, S. B., C. Gong, J. M. J. Frechet and J. F. Walzer, Functionalized Polystyrene as a Versatile Support for Olefin Polymerization Catalysts, *Journal of Polymer Science: Part A: Polymer Chemistry*, **38**, 2979-2992 (2000).
- Samson J. J. C., B. van Middelkoop, G. Weickert, and K. R. Westerterp, Gas-Phase Polymerization of propylene with a Highly Active Ziegler-Natta Catalyst, *AIChE J*, **45**, 1548-1558 (1999).
- Schumacher, J. W. and A. V. Borruso, Linear Low-Density Polyethylene (LLDPE) Resins, *Chemical Economics Handbook*, SRI International, California (2002)
- Soares, J. B. P. and A. E. Hamielec, Metallocene/Aluminoxane Catalysts for Olefin Polymerization: A Review, *Polymer Reaction Engineering*, **3**, 131-200 (1995).

Soares, J. B. P. and A. E. Hamielec, Temperature rising elution fractionation of linear polyolefins, *Polymer*, **36**, 1639-1654 (1995).

Soga, K. and M. Kaminaka, Copolymerization of olefins with SiO<sub>2</sub>-supported zirconocene catalysts by common trialkylaluminums, *Makromolekulare Chemie*, **194**, 3499-3504 (1993).

Steinmetz, B., B. Tesche, C. Przybyla, J. Zechlin, and G. Fink, Polypropylene growth on silica-supported metallocene catalysts: A microscopic study to explain kinetic behavior especially in early polymerization stages, *Acta Polymerica*, **48**, 392-399 (1997).

Stork, M., M. Koch, M. Klapper, K. Müllen, H. Gregorius, and U. Rief, Ethylene polymerization using crosslinked polystyrene as support for zirconocene dichloride/methylaluminoxane, *Macromolecular Rapid Communications*, **20**, 210-213 (1999).

Sun, L., C. C. Hsu, and D. W. Bacon, Polymer-supported Ziegler-Natta catalysts. II. Ethylene homo- and copolymerization with TiCl<sub>4</sub>/MgR<sub>2</sub>/Poly(ethylene-*co*-acrylic acid) catalyst, *Journal of Polymer Science: Part A: Polymer Chemistry*, **32**, 2135-2145 (1994).

Tritto, I., C. Meales, M. C. Sacchi and P. Locatelli, Methylaluminoxane: NMR analysis, cryoscopic measurements and cocatalytic ability in ethylene polymerization, *Macromolecular Chemistry and Physics*, **198**, 3963-3977 (1997).

Wang, W., L. Wang, J. Wang, J. Wang, and Z. Ma, Novel Polystyrene-Supported Zirconocene Catalyst for Olefin Polymerization and Its Catalytic Kinetics, *Journal of Polymer Science: Part A: Polymer Chemistry*, **43**, 2650-2656 (2005).

Weickert, G., J. J. Samson, P. Roos, and K. R. Westerterp, Investigation of olefin polymerization with Ziegler-Natta and metallocenes, *DECHEMA Monographs*, **131**, 235-248 (1995).

Wester, T. S. and M. Ystenes, Kinetic studies of the injection of comonomers during polymerization of ethane and propene with MgCl<sub>2</sub>-supported Ziegler-Natta catalysts, *Macromolecular Chemistry and Physics*, **198**, 1623-1648 (1997).

Whiteley, K. S., T. G. Heggs, H. Koch, and W. Immel, Polyolefins, "Ullmann's Encyclopedia of Industrial Chemistry", 6<sup>th</sup> Edition, John Wiley and Sons, Inc. (2002)

Wild, L., T. R. Ryle, D. C. Knobloch, and I. R. Peat, Determination of Branching Distributions in Polyethylene and Ethylene Copolymers, *Journal of Polymer Science: Part B: Polymer Physics*, **20**, 441-455 (1982).

Wu, L., D. T. Lynch, and S. E. Wanke, Kinetics of gas-phase ethylene polymerization with morphology-controlled MgCl<sub>2</sub>-supported TiCl<sub>4</sub> catalyst, *Macromolecules*, **32**, 7990-7998 (1999).

Xu, Z. G., S. Chakravarti, and W. H. Ray, Kinetic study of olefin polymerization with a supported metallocene catalyst. I. Ethylene/propylene copolymerization in gas phase, *Journal of Applied Polymer Science*, **80**, 81-114 (2001).

Ystenes, M., J. L. Eilertsen, J. Liu, M. Ott, E. Rytter and J. A. Stovngeng, Experimental and Theoretical Investigations of the Structure of Methylaluminoxane (MAO) Cocatalysts for Olefin Polymerization, *Journal of Polymer Science: Part A: Polymer Chemistry*, **38**, 3106-3127 (2000).

Zhang, M., Characterization of Commercial Linear Low Density Polyethylenes by TREF, SEC, DSC, and Cross-Fractionation, *M.Sc. Thesis, University of Alberta*, Edmonton, Canada, pp 33-37, (1999).

Zhou, J.-M., N.-H. Li, N.-Y. Bu, D. T. Lynch, and S. E. Wanke, Gas-Phase Ethylene Polymerization over Polymer-Supported Metallocene Catalysts, *Journal of Applied Polymer Science*, **90**, 1319-1330 (2003).

Zöllner, K. and K.-H. Reichert, Video Microscopy for the Examination of Heterogeneous Gas-Phase Polymerization, *Chemical Engineering & Technology*, **25**, 707-710 (2002).

## Appendix A

Summary of details regarding preparation conditions of the supported catalysts are provided in Table A1. The compositions of the catalysts based on the amounts of reagents used (calculated), and the compositions determined by the instrumental neutron activation analysis (INAA measured) are listed in Table A2. The particle size ranges, surface areas by the Brunauer, Emmett and Teller (BET) method and pore sizes by Barrett, Joyner and Halenda (BJH) method of various in-house and commercial polymeric supports used to make the catalysts are given in Table A3.

Table A1: Detailed description of catalyst preparation conditions (continued on next page)

Catalyst	Date Catalyst Prepared	Support	Support Details		Preparation Details								Catalyst recov <sup>d</sup> g
			Mass <sup>1</sup> g	Pretreatment condition	Toluene <sup>2</sup> mL	MAO <sup>3</sup>		Shaking Time <sup>4</sup> h	(n-BuCp) <sub>2</sub> ZrCl <sub>2</sub> Addition			Shaking Time <sup>6</sup> h	
						mL	mmol		mg	mmol	Toluene <sup>5</sup> mL		
TM01	31-Jan-01	60HEMA-1	2.00	85°C, 16 h	10	13	19.6	22.0	44.0	0.109	2, 1	16	2.028
TM02	20-Mar-01	60HEMA-1	2.01	85°C, 16 h	0	17.8	40.1	4.8	41.0	0.101	2, 2	3	4.140
TM03	23-May-02	60HEMA-1	1.43	80°C, 16 h	0	9.4	21.2	4.0	29.0	0.072	1, 1	2.5	2.452
TM04	11-Jun-02	60HEMA-2	2.00	80°C, 16 h	0	13.5	30.4	4.4	40.0	0.099	2, 2, 2	2	2.400
TM05	22-Jun-01	60HEMA-2	1.97	70°C, 16 h	0	8.9 <sup>8</sup>	20.1	3.0	40.0	0.099	3, 3, 3	2	2.400
TM06	7-Jul-01	60HEMA-2	2.00	60°C, 16 h	5	20	30.2	3.1	48.0	0.119	4, 3	3.67	2.050
TM07	13-Jul-01	60HEMA-2	2.10	82°C, 16 h	0	20	30.2	3.2	41.0	0.101	5, 5	3	2.520
TM08	23-Jul-01	60HEMA-3	2.00	67°C, 16 h	0	25	37.7	3.0	40.9	0.101	5, 5	3.03	3.670
TM09	27-Sep-01	60HEMA-4	2.00	60°C, 16 h	5	25	37.7	2.8	44.0	0.109	5, 5	3.83	3.560
TM10	2-Oct-01	60HEMA-4	2.00	60°C, 16 h	0	25	37.7	3.3	45.0	0.111	5, 5	3.17	3.670
TM11	19-Nov-01	HayeSepR-5	2.00	75°C, 16 h	5	20	30.2	3.2	41.0	0.101	5, 5	2.08	3.175
TM12	22-Jan-02	HayeSepR-5	1.50	76°C, 16 h	5	15	22.6	2.1	31.0	0.077	5, 5	3.93	2.143
TM13	8-Apr-02	HayeSepQ-1	2.00	70°C, 16 h	0	20	30.2	2.0	38.0	0.094	5, 5	2.48	3.172
TM14	5-Jun-02	PS/DVB-1	0.51	70°C, 36 h	0	5	7.5	3.0	10.0	0.025	5, 5	3.08	0.735
TM15	25-Jun-02	HayeSepR-1	2.01	70°C, 16 h	0	20	30.2	3.0	39.5	0.098	5, 5	3	3.363
TM16	3-Oct-02	HayeSepR-3	2.00	75°C, 19 h	5	20	30.2	2.0	40.5	0.100	5, 5	4	3.063
TM17	7-Oct-02	HayeSepR-2	2.00	75°C, 19 h	5	20	30.2	2.0	40	0.099	5, 5	2	3.145
TM18A	19-Dec-02	HayeSepR-6	1.00	72°C, 19 h	10	20	30.2	2.0	42	0.104	5, 5	2	1.169
TM18B		HayeSepR-2	1.00										1.738

Table A1: Detailed description of catalyst preparation conditions (continued from last page)

Catalyst	Date Catalyst Prepared	Support	Support Details		Preparation Details								Catalyst recov'd <sup>7</sup> g
			Mass <sup>1</sup> g	Pretreatment condition	Toluene <sup>2</sup> mL	MAO <sup>3</sup>		Shaking Time <sup>4</sup> h	(n-BuCp) <sub>2</sub> ZrCl <sub>2</sub> Addition			Shaking Time <sup>6</sup> h	
						mL	mmol		mg	mmol	Toluene <sup>5</sup> mL		
TM19A	7-Jan-03	HayeSepR-6	1.00	80°C, 23 h	5	20	30.2	2.0	40	0.099	5, 5	2	1.624
TM19B		HayeSepR-2	1.00										1.412
TM20	12-Feb-03	HayeSepR-6	2.00	75°C, 19 h	5	20	30.2	2.0	40.0	0.099	5, 5	2	3.000
TM21	3-Apr-03	HayeSepR-2 <sup>9</sup>	1.34	80°C, 24 h	3	13.5	20.4	2.0	27.0	0.067	3, 3	2	2.101
TM22	25-Apr-03	HayeSepR-2 <sup>10</sup>	1.18	92°C, 20 h	5	11.75	17.7	2.0	23.2	0.057	3, 3	4	1.885

<sup>1</sup> Mass before pretreatment

<sup>2</sup> Volume of toluene used for suspending the support

<sup>3</sup> TM02, TM03, TM04 and TM05 were prepared using MMAO-4 (~6.92 wt% Al)

<sup>4</sup> Contact time of support/cocatalyst suspension on a shaker at ~200 rpm at room temperature

<sup>5</sup> Amounts of toluene used to prepare metallocene solution added to the support/cocatalyst suspension and to wash syringe used to transfer this solution

<sup>6</sup> Contact time of or support/cocatalyst/metallocene suspension on a shaker at ~200 rpm at room temperature

<sup>7</sup> Free flowing catalysts have better recovery (from the preparation flask) than caked ones

<sup>8</sup> Syringe used to transfer MMAO-4 solution washed with 3\*2.5 mL toluene and washing added to flask

<sup>9</sup> Sieved support particles using acetone to collect size range: 250-300 μm

<sup>10</sup> Sieved support particles using anhydrous hexane to collect size range: 300-350 μm

Table A2: Composition of supported catalysts

Catalyst Desig.	Support Mass, g	Total Mass of Reagents g	Amount Catalyst Recovered g	Catalyst Composition					
				Calculated <sup>1</sup>			INAA Measured <sup>2</sup>		
				Al mass%	Zr mass%	Al/Zr Ratio	Al mass%	Zr mass%	Al/Zr Ratio
TM01	2.00	3.18	2.028	16.64	0.31	181	12.9	0.25	176
TM02	2.01	4.58	4.140	23.67	0.20	397	20.1	0.18	382
TM03	1.43	2.79	2.452	20.50	0.23	296	17.6	0.19	306
TM04	2.00	3.96	2.400	20.77	0.23	309	21.2	0.24	301
TM05	1.97	3.27	2.400	16.55	0.27	203	18.2	0.27	229
TM06	2.00	3.80	2.050	21.45	0.28	255	19.6	0.35	191
TM07	2.10	3.89	2.520	20.94	0.24	298	20.1	0.32	212
TM08	2.00	4.23	3.670	24.08	0.22	374	18.9	0.23	275
TM09	2.00	4.23	3.560	24.07	0.23	348	18.3	0.22	282
TM10	2.00	4.23	3.670	24.06	0.24	340	19.7	0.23	285
TM11	2.00	3.79	3.175	21.50	0.24	298	13.8	0.28	168
TM12	1.50	2.84	2.143	21.49	0.25	296	ND <sup>3</sup>	ND <sup>3</sup>	ND <sup>3</sup>
TM13	2.00	3.79	3.172	21.51	0.23	322	13.4	0.21	220
TM14	0.51	0.95	0.735	21.38	0.24	306	16.6	0.12	452
TM15	2.01	3.80	3.363	21.44	0.23	310	15.4	0.23	227
TM16	2.00	3.79	3.063	21.49	0.24	302	15.1	0.23	218
TM17	2.00	3.79	3.145	21.49	0.24	306	13.5	0.23	202
TM18A	1.00	3.79	1.169	21.48	0.25	291	14.3	0.28	174
TM18B	1.00		1.738				14.6	0.27	185
TM19A	1.00	3.79	1.624	21.49	0.24	306	15.1	0.27	189
TM19B	1.00		1.412				14.1	0.27	178
TM20	2.00	3.79	3.000	21.49	0.24	306	15.3	0.25	207
TM21	1.34	2.55	2.101	21.55	0.24	306	13.9	0.24	195
TM22	1.18	2.23	1.885	21.50	0.23	310	14.3	0.24	203

<sup>1</sup> Assumed molar mass of MAO = 58 g/mol and MMAO-4 = 63 g/mol

<sup>2</sup> Only the measured compositions by Instrumental Neutron Activation Analysis (INAA) were used in data analysis and discussion of results

<sup>3</sup> ND – Not detected due to insufficient amount of catalyst to carry out INAA

Table A3: Carriers used for supporting catalysts

Support Designation	Source	Lot number	Composition of Support <sup>1</sup>	Particle Diameter, $\mu\text{m}$	Surface Area, $\text{m}^2/\text{g}$	Pore Volume, $\text{cm}^3/\text{g}$	Pore Radius, $\text{nm}^2$		BET Pretreatment		
							Most Probable	Calculated Average	Temp. $^{\circ}\text{C}$	Time, h	Mass Loss, % <sup>3</sup>
60HEMA-1	Inhouse	PE001128	Poly(60%HEMA/DVB)	78-200	300 <sup>3</sup>	0.7262 <sup>3</sup>	4.3 <sup>4</sup>	4.8 <sup>4</sup>			
60HEMA-2	Inhouse	PE001128	Poly(60%HEMA/DVB)	53-74	48	0.1779	4.1	7.4	125	4	3.5
60HEMA-3	Inhouse	PE010711	Poly(60%HEMA/DVB)	78-200	276	0.6482	4.2	4.7	125	4	4.7
60HEMA-4	Inhouse	PE010920	Poly(60%HEMA/DVB)	200-400	168	0.4339	6.5	5.2	125	4	0.7
PS/DVB-1	Inhouse	PS-0526(9)	Poly(Styrene/DVB)	5	840	1.7963	3 <sup>5</sup>	4.3	125	4	0
HayeSepQ-1	commercial	722	Poly(DVB)	150-180	641	0.7474	3.2	2.3	125	4	0
HayeSepR-1	commercial	302	Poly(DVB/NVP)	600-850	584	1.0123	5.2	3.5	125	4	0
HayeSepR-2	commercial	302	Poly(DVB/NVP)	250-300	619	1.0676	6	3.4	125	4	0
HayeSepR-3	commercial	362	Poly(DVB/NVP)	180-250	656	1.0541	6.2	3.2	125	4	6.4
HayeSepR-4	commercial	377	Poly(DVB/NVP)	150-180	639	1.0576	5.2	3.3	125	4	0
HayeSepR-5	commercial	336	Poly(DVB/NVP)	125-150	696	1.0832	5	3.1	125	4	0.6
HayeSepR-6	commercial	120	Poly(DVB/NVP)	75-90	715	1.1234	2.3	3.1	125	4	0

<sup>1</sup> 60%HEMA: 2-hydroxyethylmethacrylate, 60 mass% initial monomer mix; DVB: divinyl benzene; NVP: *n*-vinyl-2-pyrrolidinone

<sup>2</sup> Most probable pore radius determined from pore size distribution plot and calculated average pore radius =  $2 \cdot (\text{Pore Volume} / \text{Surface Area})$

<sup>3</sup> % Mass Loss =  $100 \cdot [M_{\text{initial}} - M_{\text{final}}] / M_{\text{initial}}$

<sup>4</sup> Estimated values as insufficient amount remained to perform BET analysis

<sup>5</sup> Bimodal pore size distribution

## Appendix B

Details of polymerization conditions and product polymer properties of runs done during the course of this work are listed in chronological order in Table B1. For completeness, inactive catalysts and polymerization runs not discussed in the thesis are also included in Table B1. The molar masses of polymer products determined by gel permeation chromatography (GPC) analyses are given for many of the runs. In the “Comments” column, SEM indicates that scanning electron microscopic analyses of polymer particles were done; and TREF indicates that temperature rising elution fractionation analyses were performed to determine short chain branching.

Table B1: Summary of polymerization run conditions (continued on next page)

Date	Run Number <sup>1</sup>	Catalyst		Scavenger <sup>2</sup>		1-hexene Am't mL	Ethylene Pressure psia	Initial Temp. °C	Run Length h	PE Yield g	Bulk Density g/cm <sup>3</sup>	Molar Mass kg/mol		Comments
		Type	Am't mg	Type <sup>3</sup>	Am't mL							Mn	Mw	
02/01/01	001TM	TM01	100	TIBA	0.30	2.66	206	80	6.20	65.9	0.40			New catalyst
02/05/01	002TM	TM01	101	TIBA	0.50	2.93	213	80	7.28	55.4	0.40			
02/09/01	004TM	TM01	101	TIBA	0.20	2.44	202	80	3.58	2.5	0.39			
02/13/01	005TM	TM01	101	TIBA	0.40	3.02	202	80	8.00	51.7	0.38			
02/16/01	006TM	TM01	80	TEA	0.20	2.83	202	80	6.92	70.8	0.38			
02/20/01	007TM	TM01	86	TEA	0.10	2.67	200	80	4.00	57.8	0.41			
02/21/01	008TM	TM01	88	TEA	0.15	2.62	202	80	4.67	63.8	0.45			
02/23/01	010TM	TM01	88	TEA	0.05	2.79	205	80	1.15	0.4	nd <sup>4</sup>			
02/28/01	012TM	TM01	102	TEA	0.15	2.57	206	80	4.81	39.4	0.39			
03/01/01	013TM	TM01	105	TEA	0.15	2.83	205	80	4.00	42.3	0.42			No salt bed in reactor during run.
03/08/01	016TM	TM01	102	TEA	0.15	2.90	202	80	4.28	73.7	0.37			
03/22/01	019TM	TM02	101	TEA	0.15	3.55	203	80	2.38	94.8	0.40			New catalyst
03/26/01	020TM	TM02	106	TEA	0.15	0	204	80	3.22	71.9	0.36			
03/27/01	021TM	TM02	102	TEA	0.15	3.34	202	80	3.12	110.7	0.42			
03/29/01	023TM	TM02	102	TEA	0.15	3.28	206	80	5.00	170.8	0.33			
04/04/01	024TM	JM54	110	TIBA	0.30	0	200	80	3.44	23.3	0.38			Raised pressure to 300 psia during run.
04/05/01	025TM/HH	TM02	108	TIBA	1.00	0	198	80	4.00	13.1	0.34			
04/06/01	026HH/TM	JM54	103	TIBA	0.51	0	197	80	5.20	6.9	0.33			
04/09/01	027TM	TM02	105	TIBA	0.30	0	203	80	5.00	47.5	0.34	51.7	143.4	
04/11/01	029HH/TM	TM02	107	TIBA	0.30	0	205	80	3.55	29.4	0.33	46.2	139.3	
04/13/01	030TM/HH	TM02	103	TIBA	0.30	0	203	80	1.05	6.5	nd <sup>4</sup>			
04/14/01	041401TMHH	TM02	102	TIBA	0.30	0	203	80	1.00	6.8	0.31			
04/15/01	041501TMHH	TM02	103	TIBA	0.30	0	208	80	1.00	2.5	0.35			
04/19/01	032HH/TM	TM02	100	TIBA	0.30	0	203	80	2.50	25.4	0.27			
04/20/01	033HH/TM	TM02	100	TIBA	0.30	0	202	80	2.50	12.5	0.25			
04/22/01	042201TMHH	TM02	106	TIBA	0.20	0	205	80	1.25	13.5	0.24			
04/23/01	042301TMHH	TM02	107	TIBA	0.10	0	205	80	2.00	56.9	0.27	74.1	169.4	
04/28/01	042801TMHH	TM02	103	TIBA	0.20	0	203	80	4.25	67.6	0.33	64.8	159.4	
04/29/01	042901TMHH	TM02	104	TIBA	0.05	0	203	80	1.00	31.2	0.29	77.3	181.9	

Table B1: Summary of polymerization run conditions (continued from previous page)

Date	Run Number <sup>1</sup>	Catalyst		Scavenger <sup>2</sup>		1-hexene Am't mL	Ethylene Pressure psia	Initial Temp. °C	Run Length h	PE Yield g	Bulk Density g/cm <sup>3</sup>	Molar Mass kg/mol		Comments	
		Type	Am't mg	Type <sup>3</sup>	Am't mL							Mn	Mw		
04/30/01	043001	TMHH	TM02	103	TIBA	trace	0	202	80	1.00	42.5	0.25	72.3	186.1	
05/01/01	050101	TMHH	TM02	103		0	0	202	80	1.00	35.7	0.29	63.1	180.9	
05/02/01	035	TM/HH	TM02	100	TIBA	0.06	0	205	80	2.00	44.5	0.31			
05/03/01	036	TM/HH	TM02	70	TIBA	0.06	2.82	204	80	2.00	83.3	0.21			
05/04/01	050401	TMHH	TM02	72	TIBA	trace	2.80	205	80	1.00	65.9	0.26	73.0	175.7	
05/07/01	037	TM/HH	TM02	72		0	3.09	203	80	1.00	57.8	0.31			
05/08/01	050801	TMHH	TM02	71		0	3.10	209	80	1.00	66.8	0.30			
05/10/01	038	TM	TM02	72	TIBA	0.12	2.89	210	80	1.00	51.3	0.32			
05/11/01	051101	HHTM	TM02	70		0	3.18	205	80	1.00	43.6	0.34			
05/14/01	039	TM/HH	TM02	100		0	0.00	202	80	1.00	27.6	0.32			
05/15/01	040	HH/TM	TM02	72		0	3.02	202	80	1.00	53.5	0.33			
05/16/01	041	HH/TM	JM71	62	TIBA	trace	1.91	200	80	1.00	22.7	0.33			New catalyst
05/29/01	042	TM	TM02	71	TIBA	trace	0	206	80	1.00	15.2	0.26			
05/30/01	043	TM	TM02	71		0	0	200	80	1.00	17.1	0.28			
06/07/01	045	TM	TM02	51		0	3.14	203	80	1.00	17.1	0.35			
06/08/01	046	TM	TM02	72		0	3	200	80	1.00	37.8	0.33			
06/13/01	047	TM	TM04	103		0	0	200	80	1.00	17.6	0.32			New catalyst
06/14/01	048	TM	TM04	71		0	3.12	202	80	1.00	14.7	0.32			
06/15/01	049	TM	JM81	51	TIBA	0.15	5.92	201	80	2.00	27.9	0.40			New catalyst
06/19/01	050	TM	JM81	52	TIBA	trace	5.86	202	80	1.00	28.3	0.48			
06/20/01	051	TM	JM81	71	TIBA	trace	5.48	204	80	1.00	66.7	0.47			
06/21/01	052	TM	JM81	72		0	5.78	203	80	1.00	28.1	0.44			
06/28/01	053	TM	TM05	101	TIBA	trace	0	200	80	1.00	6.6	0.32			New catalyst
06/29/01	054	TM	TM05	104	TIBA	0.1	0	203	80	1.00	9.7	0.35			
07/03/01	055	TM	TM05	104	TIBA	0.1	3.1	200	80	1.00	6.2	0.28			
07/14/01	058	TM	TM07	101	TIBA	trace	0	202	80	1.00	4.6	0.26			New catalyst
07/18/01	059	TM	TM07	99	TIBA	trace	3.42	201	80	1.00	5.6	0.35			
07/19/01	060	TM	TM07	154	TIBA	trace	0	200	80	1.00	4.2	0.32	29.4	134.0	
07/24/01	061	TM	TM08	109	TIBA	trace	0	201	80	1.00	9.7	0.25	42.0	139.2	New catalyst
07/25/01	062	TM	TM08	101	TIBA	trace	3.18	200	80	1.00	33.9	0.30	24.5	88.5	

Table B1: Summary of polymerization run conditions (continued from previous page)

Date	Run Number <sup>1</sup>	Catalyst		Scavenger <sup>2</sup>		1-hexene Am't mL	Ethylene Pressure psia	Initial Temp. °C	Run Length h	PE Yield g	Bulk Density g/cm <sup>3</sup>	Molar Mass kg/mol		Comments
		Type	Am't mg	Type <sup>3</sup>	Am't mL							Mn	Mw	
07/26/01	063TM	TM08	100	TIBA	trace	6.21	200	80	1.00	47.8	0.29	24.5	90.8	Static mixers inserted in coolant channel from this run onwards
09/07/01	064TM	TM08	100	TIBA	trace	6.35	200	80	1.00	38.2	0.28	16.7	71.6	
09/11/01	065TM	TM08	100	TIBA	trace	3.44	202	80	1.00	21.0	0.28	17.6	104.2	
09/12/01	066TM	TM08	100	TIBA	trace	0	200	80	1.00	30.2	0.24	23.4	128.6	
09/24/01	067TM	TM08	102	TIBA	trace	0	200	80	1.00	22.5	0.26	34.6	134.0	
09/25/01	068TM	TM08	102	TIBA	trace	3.59	200	80	1.00	43.9	0.26	29.3	85.9	
09/28/01	069TM	TM09	110	TIBA	trace	0	200	80	1.00	3.7	nd <sup>4</sup>	44.8	175.8	New catalyst
10/01/01	070TM	TM09	110	TIBA	trace	3.07	200	80	1.00	20.9	0.36			
10/02/01	071TM	TM09	110	TIBA	trace	6.11	200	80	1.00	28.9	0.33			
10/03/01	072TM	TM10	110	TIBA	trace	0	200	80	1.00	3.1	nd <sup>4</sup>	23.5	162.7	SEM, New catalyst
10/09/01	073TM	TM10	115	TIBA	trace	3.11	203	80	1.00	39.2	0.37	30.8	87.6	SEM
10/15/01	074TM	TM10	115	TIBA	trace	3.07	102	80	1.00	33.4	0.36	24.5	81.9	SEM
10/16/01	075TM	TM10	115	TIBA	trace	3.09	299	80	1.00	40.5	0.36	35.4	88.1	SEM
10/17/01	076TM	TM10	115	TIBA	trace	3.09	152	80	1.00	31.8	0.39	31.5	89.6	SEM
10/18/01	077TM	TM10	115	TIBA	trace	3.08	252	80	1.00	47.5	0.35	32.3	83.4	SEM
10/19/01	078TM	TM10	115	TIBA	trace	3.22	202	80	1.00	37.5	0.34	34.3	89.7	SEM
10/25/01	079TM	TM10	116	TIBA	trace	3.12	100	80	1.00	24.6	0.34	24.9	82.7	SEM
10/26/01	080TM	TM10	115	TIBA	trace	3.03	200	80	1.00	25.5	0.33	25.0	83.8	
10/31/01	081TM	TM10	115	TIBA	trace	3.02	304	80	1.00	25.6	0.31	29.1	86.0	
11/01/01	082TM	TM10	83	TIBA	trace	3.11	200	80	1.00	28.3	0.37	30.3	88.6	
11/02/01	083TM	TM10	42	TIBA	trace	3.26	201	80	1.00	13.0	0.42	34.4	99.7	Clear & opaque particles with different Mw & Mn
11/07/01	084TM	TM10	115	TIBA	trace	0	205	80	3.00	20.1	0.32	34.1	134.9	Oil at 80°C circ. for T control
11/08/01	085TM	TM10	102	TIBA	trace	3.16	206	80	1.00	43.3	0.33	38.1	93.2	Oil at 80°C circ. for T control
11/09/01	086TM	TM10	53.8	TIBA	trace	3.06	204	80	1.00	27.4	0.37	31.3	87.3	Oil at 80°C circ. for T control
11/15/01	087TM	TM10	151	TIBA	trace	3.18	203	80	1.00	46.4	0.38	34.7	94.2	Oil at 80°C circ. for T control
11/21/01	088TM	TM11	78	TIBA	trace	3.09	200	80	1.00	3.3	nd <sup>4</sup>	10.6	90.0	SEM, New Catalyst, Oil at 80°C circ.
11/22/01	089TM	TM10	151	TIBA	trace	3.15	204	80	1.00	69.1	0.37	32.5	89.6	Oil at 80°C circ. for T control
11/23/01	090TM	TM11	147	TIBA	trace	3.1	200	80	1.00	50.0	0.29	32.2	92.6	SEM, Oil at 80°C circ. for T control

11/28/01	091TM	TM11	100	TIBA	trace	0	201	80	1.00	3.2	0.34	52.1	201.7	SEM, TREF, Oil at 80°C circ.
----------	-------	------	-----	------	-------	---	-----	----	------	-----	------	------	-------	------------------------------

Table B1: Summary of polymerization run conditions (continued from previous page)

Date	Run Number <sup>1</sup>	Catalyst		Scavenger <sup>2</sup>		1-hexene Am't mL	Ethylene Pressure psia	Initial Temp. °C	Run Length h	PE Yield g	Bulk Density g/cm <sup>3</sup>	Molar Mass kg/mol		Comments
		Type	Am't mg	Type <sup>3</sup>	Am't mL							Mn	Mw	
11/29/01	092TM	TM11	100	TIBA	trace	3.11	202	80	1.00	25.3	0.34	30.6	104.6	SEM, Oil at 80°C circ. for T control
11/30/01	093TM	TM11	56	TIBA	trace	3.13	204	80	1.00	24.7	0.32			Oil at 80°C circ. for T control
12/04/01	094TM	TM11	50	TIBA	trace	3.23	204	80	1.00	13.9	0.36			Oil at 80°C circ. for T control
12/05/01	095TM	TM11	150	TIBA	trace	3.32	203	80	1.12	49.7	0.33			Oil at 80°C circ. for T control
12/06/01	096TM	TM11	100	TIBA	trace	3.24	200	80	1.00	39.1	0.32			Oil at 80°C circ. for T control
12/07/01	097TM	TM11	75.6	TIBA	trace	3.21	201	80	1.00	24.0	0.33			Oil at 80°C circ. for T control
12/12/01	098TM	TM11	100	TIBA	trace	3.37	202	80	0.17	3.3	0.30	18.5	133.3	TREF, Oil at 80°C circ. for T control
12/13/01	099TM	TM11	100	TIBA	trace	6	200	80	1.00	31.6	0.39	24.2	93.6	TREF, Oil at 80°C circ. for T control
12/14/01	100TM	TM11	101	TIBA	trace	1.14	200	80	1	27.3	0.36	37.6	102.9	TREF, Oil at 80°C circ. for T control
12/19/01	101TM	TM11	75	TIBA	trace	3.04	205	80	1.15	28.8	0.38	33.2	95.3	SEM
12/20/01	102TM	TM11	76	TIBA	trace	3.01	200	75	1	27.5	0.33	35.2	95.9	
12/21/01	103TM	TM11	75	TIBA	trace	3.12	202	85	1	25.0	0.37	35.7	101.7	SEM
01/04/02	104TM	TM11	75	TIBA	trace	3.39	203	90	1.2	23.8	0.38	29.4	100.2	SEM
01/07/02	105TM	TM11	76	TIBA	trace	3.01	199	70	1	20.7	0.33	34.8	96.8	
01/10/02	106TM	TM11	74	TIBA	trace	3.11	204	80	1	21.0	0.37			
01/23/02	107TM	TM12	103	TIBA	trace	0	200	80	1	3.2	nd <sup>4</sup>			New catalyst
01/24/02	108TM	TM12	99	TIBA	trace	3.24	205	80	2	27.4	0.43			
01/25/02	109TM	TM12	100		0	3.14	202	80	2	7.4	0.41			
01/28/02	110TM	TM12	101	TIBA	0.08	3.14	200	80	2	17.0	0.40			
01/30/02	111TM	TM12	101	TIBA	0.08	3.38	204	80	2	22.4	0.37			
02/06/02	112TM	TM12	102	TIBA	0.08	3.61	200	80	1	4.2	nd <sup>4</sup>			Small amount of air injection
02/07/02	113TM	TM12	101	TIBA	0.08	3.21	208	80	2	19.6	0.38			Small amount of air injection
02/13/02	114TM	TM12	102	TIBA	trace	3.62	203	80	2	26.4	0.40			
02/15/02	115TM	TM12	102	TIBA	0.08	3.53	200	80	2	13.8	0.40			Small amount of air injection
02/20/02	116TM	TM12	100	TIBA	trace	3.53	202	90	2	33.0	0.41			
03/01/02	117TM	TM12	100	TIBA	trace	3.32		80						Run abandoned
03/25/02	118TM	TM12	101	TIBA	trace	3.04	205	80	1	12.4	0.41	34.1	103.2	TREF
03/26/02	119TM	TM12	99	TIBA	trace	3.17	203	80	0.5	3.8	nd <sup>4</sup>	37.8	124.2	TREF
03/27/02	120TM	TM12	101	TIBA	trace	3.08	204	80	0.08	0.3	nd <sup>4</sup>	9.5	93.9	TREF
03/28/02	121TM	TM12	101	TIBA	trace	3.03	202	80	0.25	1.0	nd <sup>4</sup>	25.9	124.8	TREF

Table B1: Summary of polymerization run conditions (continued from previous page)

Date	Run Number <sup>1</sup>	Catalyst		Scavenger <sup>2</sup>		l-hexene Am't mL	Ethylene Pressure psia	Initial Temp. °C	Run Length h	PE Yield g	Bulk Density g/cm <sup>3</sup>	Molar Mass kg/mol		Comments
		Type	Am't mg	Type <sup>3</sup>	Am't mL							Mn	Mw	
04/02/02	122TM	TM12	100	TIBA	trace	2.95	105	80	2	5.0	nd <sup>4</sup>	15.2	80.6	N <sub>2</sub> = 100 psi partial pressure
04/03/02	123TM	TM12	102	TIBA	trace	3.02	205	80	0.15	0.5	nd <sup>4</sup>	19.4	119.7	TREF
04/04/02	124TM	TM12	102	TIBA	trace	3.04	104	80	2	5.6	nd <sup>4</sup>			
04/12/02	125TM	TM13	74.6	TIBA	trace	2.97	205	80	1.05	27.4	0.39			New catalyst
04/16/02	126TM	TM13	75	TIBA	trace	0	206	80	1	7.5	0.30			
04/17/02	127TM	TM13	75	TIBA	trace	3.15	203	80	0.5	17.4	0.39			
04/18/02	128TM	TM13	75	TIBA	trace	3.25	200	80						Run abandoned
04/23/02	129TM	TM13	76	TIBA	trace	3.09	204	80	0.5	23.8	0.40			
04/24/02	130TM	TM13	75	TIBA	trace	3.85	203	80	1	20.3	0.42	21.3	64.5	
04/30/02	131TM	TM13	75	TIBA	trace	3.29	203	80	1	12.0	0.38	22.4	92.3	
05/01/02	132TM	TM13	76	TIBA	trace	6.59	206	80	1	21.4	0.36	22.6	88.3	1-hexene added continuously
05/07/02	133TM	TM13	75	TIBA	trace	6.42	205	80	1	14.8	0.43	15.7	93.7	
05/08/02	134TM	TM13	74	TIBA	trace	7.72	201	80	1.5	25.1	0.41	26.8	87.0	1-hexene added continuously
05/09/02	135TM	TM13	76	TIBA	trace	6.88	206	80	1	18.8	0.41	23.0	93.7	1-hexene added continuously
05/14/02	136TM	TM13	74.5	TIBA	trace	10.2	200	80	2.17	28.8	0.45	19.3	84.7	1-hexene added continuously
05/15/02	137TM	TM13	74	TIBA	trace	0	204	80	1	8.2	0.26	43.7	170.2	
05/21/02	138TM	TM13	74	TIBA	trace	6.42	203	80	1	7.3	0.38	11.0	81.5	1-hexene added continuously
05/22/02	139TM	TM13	75	TIBA	trace	3.08	205	80	1	12.7	0.39	21.3	94.2	
05/23/02	140TM	TM13	74	TIBA	trace	7.17	202	80	1	16.8	0.40	19.9	90.6	1-hexene added continuously
05/29/02	141TM	TM13	74.5	TIBA	trace	8.22	200	80	1	10.9	0.40	14.8	88.2	1-hexene added continuously
06/06/02	142TM	TM14	60	TIBA	trace	0	204	80	1	128.0	0.31	55.0	132.1	New catalyst, 5µm support
06/13/02	143TM	TM14	30	TIBA	trace	0	199	80	1	74.7	0.44	59.3	140.8	
06/14/02	144TM	TM14	20	TIBA	trace	3.78	203	80	1	3.5	nd <sup>4</sup>	30.6	127.5	1-hexene added continuously
06/18/02	145TM	TM14	30.5	TIBA	trace	3.07	200	80	1	1.2	nd <sup>4</sup>	30.0	116.9	
06/19/02	146TM	TM14	31	TIBA	trace	0	200	80	1.03	22.5	0.48	59.7	155.8	
06/20/02	147TM	TM14	41	TIBA	trace	3.1	200	80	1	27.8	0.34	36.6	93.7	
06/25/02	148TM	TM14	40.5	TIBA	trace	8.54	200	80	1.45	60.6	0.43	39.3	97.8	1-hexene added continuously
06/26/02	149TM	TM15	71	TIBA	trace	0	204	80	1.33	0.0	nd <sup>4</sup>			New catalyst
06/27/02	150TM	TM15	116	TIBA	trace	3.54	203	80	1	47.8	0.29	33.2	86.3	Analyzed gas with GC
07/02/02	151TM	TM15	104	TIBA	trace	0	199	80	2	2.1	0.26	36.3	131.3	

Table B1: Summary of polymerization run conditions (continued from previous page)

Date	Run Number <sup>1</sup>	Catalyst		Scavenger <sup>2</sup>		1-hexene Am't mL	Ethylene Pressure psia	Initial Temp. °C	Run Length h	PE Yield g	Bulk Density g/cm <sup>3</sup>	Molar Mass kg/mol		Comments
		Type	Am't mg	Type <sup>3</sup>	Am't mL							Mn	Mw	
07/03/02	152TM	TM15	101	TIBA	0.07	0	203	80	2	8.0	0.33	41.8	143.4	3.4 mL <i>n</i> -heptane in reactor
07/04/02	153TM	TM15	104	TIBA	0.07	0	203	80	2.04	6.9	0.31	52.7	146.2	5.32 mL <i>n</i> -heptane in reactor
07/09/02	154TM	TM15	102	TIBA	0.07	0	203	80	1.95	1.6	0.29			
07/10/02	155TM	TM15	102	TIBA	trace	4.44	202	80	1.05	5.1	0.23	32.5	124.0	1-hexene added continuously
07/11/02	156TM	TM15	103	TIBA	trace	5.03	200	80	1	6.9	0.26	34.8	124.8	1-hexene added continuously
07/18/02	157TM	TM15	119	TIBA	trace	3.53	200	80	1.33	37.1	0.31	35.8	104.8	
07/23/02	158TM	TM15	120	TIBA	trace	5.13	197	80	1.78	10.9	0.24	34.5	117.4	1-hexene added continuously
07/24/02	159TM	TM15	122	TIBA	trace	3.27	200	80	1	4.9	0.28	25.6	125.7	Analyzed gas with GC
07/25/02	160TM	TM15	122	TIBA	trace	3.34	200	80	1	5.8	0.27			
07/30/02	161TM	TM15	120	TIBA	trace	3.97	200	80	1.65	20.9	0.26			
07/31/02	162TM	TM15	120	TIBA	0.1	3.75	202	80	1	41.2	0.28			
08/06/02	163TM	TM15	121	TIBA	0.1	3.83	197	80	1	9.2	0.27			Analyzed gas with GC
08/07/02	164TM	TM15	120	TIBA	0.1	3.13	106	80	1.5	1.9	nd <sup>4</sup>			
08/08/02	165TM	TM15	121	TIBA	0.06	2.01	98.2	80	2.75	3.1	nd <sup>4</sup>			
09/05/02	166TM	TM15	100	TIBA	0.09	4.19	199	80	1	45.7	0.24	45.9	104.4	SEM, Mn & Mw of big particles
09/10/02	167TM	TM15	101	TIBA	0.08	3.84	197	80	1.5	27.1	0.30			Analyzed gas with GC
09/11/02	168TM	TM15	100	TIBA	0.05	3.98	196	80	1	4.3	0.24			Analyzed gas with GC
09/12/02	169TM	TM15	102	TIBA	0.09	3.99	197	80	1	6.0	0.27			Analyzed gas with GC
09/16/02	170TM	TM15	100	TIBA	0.13	4.01	200	80	4	71.8	0.21			No salt bed
09/17/02	171TM	TM15	102	TIBA	0.09	3.92	202	80	1	9.3	0.30			
09/18/02	172TM	TM15	101	TIBA	0.13	3.99	196	80	1	44.7	0.23			
09/19/02	173TM	TM15	102	TIBA	<0.13	3.98	200	80	0.83	12.2	0.32			TIBA injection problem
09/24/02	174TM	TM15	99	TIBA	0.15	4.05	196	80	1	34.0	0.22			
09/25/02	175TM	TM15	101	TIBA	0.15	4.08	202	80	1	34.5	0.22			
09/26/02	176TM	TM15	102		0	4.07	196	80	3	41.7	0.26			TIBA not used
09/27/02	177TM	TM15	103	TIBA	0.06	4.05	197	80	3	72.6	0.27			
10/03/02	178TM	TM15	100	TIBA	0.15	4.04	196	80	1	23.1	0.34			Analyzed gas with GC
10/04/02	179TM	TM16	105	TIBA	0.15	0	206	80	1	3.0	nd <sup>4</sup>			New catalyst
10/08/02	180TM	TM16	103	TIBA	0.15	4.03	200	80	1.75	25.2	0.31			
10/09/02	181TM	TM17	100	TIBA	0.14	4	196	80	1	53.2	0.33			New catalyst

10/11/02	182TM	TM17	107	TIBA	0.1	0	203	80	1	2.9	nd <sup>4</sup>			
----------	-------	------	-----	------	-----	---	-----	----	---	-----	-----------------	--	--	--

Table B1: Summary of polymerization run conditions (continued from previous page)

Date	Run Number <sup>1</sup>	Catalyst		Scavenger <sup>2</sup>		1-hexene Am't mL	Ethylene Pressure psia	Initial Temp. °C	Run Length h	PE Yield g	Bulk Density g/cm <sup>3</sup>	Molar Mass kg/mol		Comments
		Type	Am't mg	Type <sup>3</sup>	Am't mL							Mn	Mw	
10/17/02	183TM	TM17	103	TIBA	0.1	3.95	196	80	1	26.5	0.38			Analyzed gas with GC
10/29/02	184TM	TM17	105	TIBA	0.1	4.01	196	80	1	46.3	0.36			Analyzed gas with GC
10/30/02	185TM	TM17	105	TIBA	0.1	4.01	196	80	1	44.1	0.36			Analyzed gas with GC
10/31/02	186TM	TM17	104	TIBA	0.1	4.03	196	80	1.1	44.6	0.36			Analyzed gas with GC
11/05/02	187TM	TM17	105	TIBA <sup>5</sup>	0.1	4.01	197	80	1	66.1	0.32			Analyzed gas with GC
11/06/02	188TM	TM17	105	TIBA <sup>5</sup>	0.1	0	205	80	1.1	5.3	nd <sup>4</sup>	57.8	224.0	
11/07/02	189TM	TM17	105	TIBA <sup>5</sup>	0.1	19.95	200	80	1.5	106.7	0.36			1-hexene added continuously
11/12/02	190TM	TM17	105	TIBA	0.1	4.08	196	80	1.25	24.6	0.37			Analyzed gas with GC
11/13/02	191TM	TM17	105	TIBA	0.15	4.15	200	80	1	58.3	0.31			Analyzed gas with GC
11/14/02	192TM	TM17	106	TIBA	0.15	4.03	196	80	1	56.6	0.33	33.9	83.5	SEM, Analyzed gas with GC
11/15/02	193TM	TM17	107	TIBA	0.15	10.9	200	80	1	42.5	0.30	32.9	92.8	SEM, 1-hexene added continuously
11/19/02	194TM	TM17	103	TIBA	0.15	4.05	197	90	1.01	48.8	0.38	38.1	94.7	SEM, Analyzed gas with GC
11/20/02	195TM	TM17	105	TIBA	0.15	4.06	198	70	1	36.2	0.26	32.1	83.6	Analyzed gas with GC
11/21/02	196TM	TM17	104	TIBA	0.15	4	197	100	1.5	23.6	0.39	22.6	86.1	SEM, Analyzed gas with GC
11/22/02	197TM	TM17	104	TIBA	0.15	4.02	198	60	1.1	11.3	0.33	35.3	111.4	SEM, Analyzed gas with GC
11/26/02	198TM	TM17	102	TIBA	0.15	3.99	201	80	1	37.3	0.28	33.5	86.3	
11/28/02	199TM	TM17	103	TIBA	0.15	6	293	80	1	82.9	0.32	34.9	82.1	
12/02/02	200TM	TM17	100	TIBA	0.15	7.99	392	80	1.2	52.3	0.33	31.1	83.2	
12/03/02	201TM	TM17	100	TIBA	0.15	6.03	395	80	1.05	55.9	0.32	36.1	85.2	
12/04/02	202TM	TM17	104	TIBA	0.15	6.07	294	80	1	31.1	0.35	25.2	89.9	MW varied with particle type
12/10/02	203TM	TM17	101	TIBA	<0.15	4.03	196	80	1	42.1	0.35	33.0	79.4	Vented after TIBA injection
12/11/02	204TM	TM17	100	TIBA	<0.15	6.07	297	80	1	35.2	0.39	38.0	89.4	Vented after TIBA injection
12/12/02	205TM	TM17	101	TIBA	0.15	6.03	297	80	1	44.7	0.36	35.5	87.1	
12/17/02	206TM	TM17	104	TIBA	0.15	13.9	293	80	1	63.0	0.33	33.2	89.1	1-hexene added continuously
12/18/02	207TM	TM17	101	TIBA	0.15	5.98	298	80	1	78.4	0.33	36.4	82.6	Stirred at 600 rpm
12/19/02	208TM	TM17	103	TIBA	0.15	6.75	293	80	1	78.2	0.32	35.7	81.9	Stirred at 300 rpm
12/24/02	209TM	TM18B	100	TIBA	0.15	4.02	196	80	1.33	2.6	nd <sup>4</sup>	34.7	127.6	New catalyst
12/25/02	210TM	TM18A	100	TIBA	0.15	4.06	196	80	1.02	1.9	nd <sup>4</sup>	42.5	133.4	New catalyst
01/08/03	211TM	TM19A	101	TIBA	0.15	4.06	196	80	1	50.1	0.27	32.5	88.1	New catalyst
01/09/03	212TM	TM19B	101	TIBA	0.15	4.01	198	80	1	23.5	0.30	31.0	90.7	New catalyst

Table B1: Summary of polymerization run conditions (continued from previous page)

Date	Run Number <sup>1</sup>	Catalyst		Scavenger <sup>2</sup>		1-hexene Am't mL	Ethylene Pressure psia	Initial Temp. °C	Run Length h	PE Yield g	Bulk Density g/cm <sup>3</sup>	Molar Mass kg/mol		Comments
		Type	Am't mg	Type <sup>3</sup>	Am't mL							Mn	Mw	
01/10/03	213TM	TM19	102	TIBA	0.15	4.01	201	80	1	48.9	0.23	37.3	89.8	Mixed TM19A&B
01/13/03	214TM	TM19A	104	TIBA	0.15	4.03	196	80	1	81.8	0.29	34.6	85.0	SEM, Stirrer down to 290rpm
01/16/03	215TM	TM19A	104	TIBA	0.15	3.99	198	80	1	79.2	0.35	38.2	93.0	Stirred at 500 rpm
01/17/03	216TM	TM19B	100	TIBA	0.15	3.98	200	80	1	23.8	0.30	35.0	90.2	Stirred at 500 rpm
01/21/03	217TM	TM19A	101	TIBA	0.15	4.01	202	70	1	27.5	0.34	28.9	93.9	SEM, Stirred at 500 rpm
01/22/03	218TM	TM19B	102	TIBA	0.15	3.97	199	70	1	12.9	0.32	28.9	104.9	Stirred at 450 rpm
01/23/03	219TM	TM19A	102	TIBA	0.15	3.97	197	70	1	40.5	0.32	27.1	82.6	Stirred at 450 rpm
01/24/03	220TM	TM19B	101	TIBA	0.15	4.02	196	90	1	25.2	0.33	30.9	87.3	Stirred at 500 rpm
01/28/03	221TM	TM19A	102	TIBA	0.15	0	204	80	1	2.6	nd <sup>4</sup>	30.1	191.8	SEM, Stirred at 500 rpm
01/29/03	222TM	TM19A	104	TIBA	0.15	4.02	296	80	1	29.6	0.32	27.0	84.2	Stirred at 500 rpm
01/30/03	223TM	TM19A	100	TIBA	0.15	4	200	80	1	37.5	0.34	32.6	89.2	Stirred at 500 rpm
01/31/03	224TM	TM19A	101	TIBA	0.15	5.99	193	80	1	44.4	0.40	28.9	86.7	99.4 psia N2
02/03/03	225TM	TM19A	100	TIBA	0.15	4.12	200	80	1	72.7	0.30	34.9	82.3	
02/04/03	226TM	TM19A	102	TIBA	0.15	4.01	196	80	1	79.7	0.28	33.9	82.5	
02/05/03	227TM	TM19B	101	TIBA	0.15	4.02	200	80	1	52.6	0.21	32.9	85.6	
02/06/03	228TM	TM19B	103	TIBA	0.15	4.3	199	70	1	35.9	0.18	33.8	87.8	
02/13/03	229TM	TM20	100	TIBA	0.15	4.05	201	80	1	11.6	0.52	15.2	92.4	New catalyst
02/14/03	230TM	TM20	99	TIBA	0.15	4.01	202	80	1.02	76.4	0.29	32.4	80.5	
02/19/03	231TM	TM20	101	TIBA	0.15	4.14	199	80	1	53.5	0.31	29.8	84.7	
02/20/03	232TM	TM20	100	TIBA	0.15	4.05	197	60	1	13.4	0.35	22.9	101.1	
02/28/03	233TM	TM20	101	TIBA	0.15	4.01	200	60	1	20.7	0.34	23.9	87.7	
03/03/03	234TM	TM20	104	TIBA	0.15	4.01	197	60	1	18.2	0.35	25.6	91.8	
03/06/03	235TM	TM20	101	TIBA	0.15	3.99	197	60	1	17.2	0.38	25.0	91.3	After 2 days of evacuation
03/07/03	236TM	TM20	102	TIBA <sup>5</sup>	0.15	4.05	200	60	2	26.8	0.31	21.7	78.8	
03/12/03	237TM	TM20	104	TIBA <sup>5</sup>	0	3.99	197	60	2.05	18.0	0.40	19.8	85.8	
03/13/03	238TM	TM20	103	TIBA	0.15	3.97	197	60	1	9.1	0.39	19.0	103.4	
03/24/03	239TM	TM20	100	TIBA	0.15	4.01	199	80	1	100.8	0.39	33.9	90.1	SEM
03/25/03	240TM	TM20	101	TIBA	0.15	4.03	198	80	0.03	nd <sup>4</sup>	nd <sup>4</sup>	8.1	88.7	SEM, 2 min run
03/26/03	241TM	TM20	100	TIBA	0.15	4.02	198	80	0.07	nd <sup>4</sup>	nd <sup>4</sup>	10.7	114.3	SEM, 4 min run
03/27/03	242TM	TM20	102	TIBA	0.15	4.02	198	80	0.25	9.5	0.32	17.7	112.8	SEM, 15 min run

Table B1: Summary of polymerization run conditions (continued from previous page)

Date	Run Number <sup>1</sup>	Catalyst		Scavenger <sup>2</sup>		1-hexene Am't mL	Ethylene Pressure psia	Initial Temp. °C	Run Length h	PE Yield g	Bulk Density g/cm <sup>3</sup>	Molar Mass kg/mol		Comments
		Type	Am't mg	Type <sup>3</sup>	Am't mL							Mn	Mw	
03/28/03	243TM	TM20	103	TIBA	0.15	4.02	197	80	0.17	5.0	0.32	15.4	120.0	SEM, 10 min run
04/07/03	244TM	TM21	102	TIBA	0.15	4.04	196	80	1.02	nd <sup>4</sup>	nd <sup>4</sup>	21.1	127.2	SEM, New catalyst-inactive
04/08/03	245TM	TM21	101	TIBA	0.15	4.15	198	90	1	nd <sup>4</sup>	nd <sup>4</sup>	12.5	82.9	New catalyst-inactive
04/09/03	246TM	TM20	101	TIBA	0.15	4.61	198	70	1	20.1	0.39	20.3	94.6	SEM
04/10/03	247TM	TM20	106	TIBA	0.15	4.18	200	70	0.07	nd <sup>4</sup>	nd <sup>4</sup>	8.2	71.1	SEM, 4 min run
04/28/03	248TM	TM22	101	TIBA	0.15	4.03	196	80	1	32.7	0.30	32.0	81.8	SEM, New catalyst
04/29/03	249TM	TM22	100	TIBA	0.15	4	198	80	0.03	0.3	nd <sup>4</sup>	7.3	72.5	SEM, 2 min run
05/01/03	250TM	TM22	102	TIBA	0.15	4.02	196	80	0.17	1.6	nd <sup>4</sup>	13.2	103.6	SEM, 10 min run
05/02/03	251TM	TM22	101	TIBA	0.15	3.96	200	80	0.07	0.5	nd <sup>4</sup>	10.0	76.2	SEM, 4 min run
05/09/03	252TM	TM22	104	TIBA	0.15	4	197	80	0.25	4.8	0.23	33.5	126.7	SEM, 15 min run
05/13/03	253TM	TM22	103	TIBA	0.15	4.03	201	70	1	36.1	0.23	33.4	87.5	SEM, New C2H4 cylinder
05/14/03	254TM	TM22	99	TIBA	0.15	4.03	196	70	0.03	0.2	nd <sup>4</sup>	7.0	49.5	SEM, 2 min run
05/21/03	255TM	TM22	102	TIBA	0.15	3.99	196	70	0.25	3.8	0.22	31.1	144.0	SEM, 15 min run
05/22/03	256TM	TM22	102	TIBA	0.15	4.01	196	70	0.17	2.2	0.23	23.3	133.6	SEM, 10 min run
05/23/03	257TM	TM22	103	TIBA	0.15	3.99	197	70	0.07	0.4	nd <sup>4</sup>	9.9	57.7	SEM, 4 min run
05/28/03	258TM	TM22	102	TIBA	0.15	0	201	80	0.5	1.7	0.43	77.2	239.2	SEM, 30 min run
06/20/03	259TM	TM22	102	TIBA	0.15	0	202	80	0.03	0.2	nd <sup>4</sup>	96.2	242.9	SEM, 2 min run
07/18/03	260TM	TM22	101	TIBA	0.15	0	205	80	0.17	0.6	nd <sup>4</sup>	91.6	263.2	SEM, 10 min run
07/24/03	261TM	TM22	110	TIBA	0.15	6.8	193	80	1.03	26.2	0.39	10.3	81.3	SEM,
07/31/03	262TM	TM22	105	TIBA	0.15	7.98	192	80	1	9.8	0.39	14.0	93.3	SEM

<sup>1</sup> Run numbers of all runs performed shown chronologically inclusive of failed runs; some early runs numbers with "HH" done with Hassan Hammawa

<sup>2</sup> Amount of scavenger in reactor during polymerization shown; trace = scavenger removed from reactor by evacuation before polymerization

<sup>3</sup> Types of scavengers used: TEA = Triethyl aluminum, TIBA = Tri-isobutyl aluminum

<sup>4</sup> nd – not determined due to insufficient amount of polymer

<sup>5</sup> 1ml MAO solution (10 mass%) added to salt bed